21333-6016-RU-00

FINAL REPORT

STUDY OF THE RELATION BETWEEN Pc 3 MICROPULSATIONS AND MAGNETOSHEATH FLUCTUATIONS AND FOR THE MULTISATELLITE MULTIMEASUREMENT INVESTIGATION OF EARTH'S BOW SHOCK

Prepared for

National Aeronautics and Space Administration
Washington, D.C.

Contract NASW-2398

by

Eugene W. Greenstadt

Space Sciences Department
TRW Systems Group

July 1974

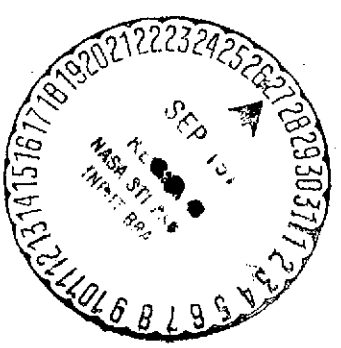

Space Sciences Department

TRW Systems Group
One Space Park
Redondo Beach, California 90278

(NASA-CR-140183) STUDY OF THE RELATION BETWEEN Pc 3 MICROPULSATIONS AND MAGNETOSHEATH FLUCTUATIONS AND FOR THE MULTISATELLITE MULTIMEASUREMENT (TRW Systems Group) 143 p HC $4.75 CSCL 03B

N74-35235

Unclas
G3/30 17105

21333-6016-RU-00

FINAL REPORT

STUDY OF THE RELATION BETWEEN Pc 3 MICROPULSATIONS AND MAGNETOSHEATH FLUCTUATIONS AND FOR THE MULTISATELLITE MULTIMEASUREMENT INVESTIGATION OF EARTH'S BOW SHOCK

Prepared for

National Aeronautics and Space Administration
Washington, D.C.

Contract NASW-2398

by

Eugene W. Greenstadt

Space Sciences Department
TRW Systems Group

July 1974

Space Sciences Department

TRW Systems Group
One Space Park
Redondo Beach, California 90278

TABLE OF CONTENTS

	Page
INTRODUCTION	1
BACKGROUND	1
Purpose	1
Micropulsations	1
Shock Structure	2
OBJECTIVES AND APPROACH	2
RESULTS	4
Micropulsations	4
Shock Structure	12
COMMENTARY	16
RECOMMENDATIONS	18
REFERENCES	19
APPENDIX A. Program Listing	
APPENDIX B. The Upstream Escape of Energized Solar Wind Protons from the Bow Shock	
APPENDIX C. Structure of the Terrestrial Bow Shock	
APPENDIX D. Structure of the Quasi-Perpendicular, Laminar Bow Shock	

INTRODUCTION

This is the last quarterly, and annual summary report on the subject contract for the year July 1973 - July 1974. In the ensuing sections, the background of the study is synopsized, the year's objectives described, and the results summarized. Details of newly-completed results are attached as appendices, which make up the bulk of the report. Following the summary of results, a short commentary and a recommendations section complete the document.

BACKGROUND

Purpose. The existing program (NASW-2398) has basically a twofold purpose. First, to test the validity of a suggested model according to which Pc 3 micropulsations are excited by magnetosheath field (and plasma) fluctuations arising in the oblique structure of the subsolar bow shock; second to continue and expand a previous study of the influence of solar wind plasma parameters, particularly ambient field direction, on local bow structure.

Micropulsations. Certain micropulsations, especially Pc 3 (period range 10-45 sec), have shown strong correlation of their various characteristics with solar wind features. These correlations, together with the results on field-dependent shock and sheath structure obtained by the present investigator, led to his suggesting a mechanism whereby the interplanetary field $\underset{\sim}{B}_{SW}$ should strongly influence the excitation of Pc 3 at the magnetopause when it aligns itself with solar wind velocity $\underset{\sim}{V}_{SW}$, thus causing large amplitude waves at the subsolar point of the shcok. The waves should be conveyed to the magnetopause by the pattern of solar wind flow in the magnetosheath. Additional

factors expected to contribute to the postulated model are thermal-to-field energy ratio β and solar wind mach number M.

Shock Structure. Collisionless plasma shock structure is determined in all scale lengths by the three plasma parameters, or, more precisely, the three classes of plasma parameters β, M, and θ_{nB}, denoting the thermal-to-field energy ratio, mach number, and field-to-shock normal angle, respectively (Tidman and Krall, 1971). We say clsses of parameters because different constituents of the plasma may have different β's and different wavemodes may have separate M's, some dependent in turn on θ_{nB}. A full description of shock-structural processes can be arrived at with multiple satellite measurements only if the effect of each of the relevant parameters can be isolated.

This study has emphasized the use of simultaneous data from two or more spacecraft and, recently, from multiple diagnostics, to evaluate the geometrical factor θ_{nB}, or, more precisely in some cases, its B-X equivalent, and the principal plasma parameters.

OBJECTIVES AND APPROACH

In broad terms, the aim of the past year's effort has been, first, to find data that confirm or confute the investigator's suggestion that Pc 3 micropulsations are excited by shock-generated oscillations, and, second, to advance the study of shock and magnetosheath structure in general by taking advantage of the numerous instances in which simultaneous data from two or more spacecraft have been recorded near the bow shock. More specific objectives have been tailored to the opportunities that have become available from time to time to make meaningful headway in a complicated investigation requiring cooperation by other, sometimes many, researchers.

The micropulsation side of the investigation began with two specific objectives: 1. to continue seeking verification of the postulated model by visual inspection of Explorer 35, Inuvik, and Tungsten records for a particular interval in 1969, and 2. to move toward a more mechanical, objective, and detailed method of evaluating solar-wind surface relationships to establish a physical link underlying the relationships that might emerge. At the outset it was believed that visual verification (or contradiction) of the model would eventually provide at least a satisfactory beginning and a guide to further analysis. By the end of the year, it had been decided that reliance on visual evaluation of micropulsation recordings, even by experts, was subjective and unreliable and should probably be abandoned. The new specific objective was creation of a computer program that would transform large quantities of interplanetary field data into the appropriate variables and plot these on optional time scales for eventual comparison with any accessible micropulsation data in spectral form, beginning with a set of records being prepared by John Olson at the University of Alberta.

The shock-structure aspect of the investigation started out to examine the effect on the bow shock of various plasma parameters and to seek some explanation for the success of l_p in predicting quasi-parallel structure with $p = 1.6$ (Greenstadt, 1972). Largely through collaboration with V. Formisano the examination of parameter-dependent structure has been extremely successful, and the year ended with a major program underway to catalogue shock morphology and to produce detailed documentation on each identifiable structural form, using OGO 5's high resolution, multidiagnostic data as the principal source of shock observations. The study of l_p geometry, meanwhile, produced a first-

order view of the geometrical context in which protons reflected from, and energized by, the shock can escape upstream.

RESULTS

Micropulsations

Preliminary Visual Surveys. Hourly averages of HEOS 1 interplanetary field and plasma parameters were obtained for some selected intervals in 1969 from V. Formisano. The appropriate geometrical field quantities, θ_{nB}, $\cos \theta_{nB}$, were computed from these where necessary and compared with micropulsation spectrograms taken at Inuvik, a presumably ideal auroral zone station, and six other stations, during a fifteen-day interval of December 69. The spectrograms were obtained from R. R. Heacock of the Geophysical Institute at the University of Alaska.

The results were disappointing, for no apparent correlation was found. The results were also puzzling, however, since a paper was given at the September 73 Kyoto meeting by Nourry and Watanabe asserting not only that they have confirmed Troitskaya's published result, which was consistent with the model of the present investigator, but that their correlation was one-for-one. Moreover, their micropulsation station was not even at auroral latitudes, where Pc 3 should be most apparent, according to postulate.

Several possible explanations of the above discrepancy came to mind. The two most important were: (1) contrary to the investigators' expectation, auroral latitudes are not the best for seeking the postulated correlation, and (2) the spectrograms, recorded on a scale most suitable for exhibiting shorter period pulsations (Pi 1), simply did not display Pc 3 events properly, if at all.

Reprocessing the Inuvik records by Heacock reinforced the suspicion that his sonograms complicated rather than simplified the initial correlation effort being attempted. Three versions of the same sonograms differing only in their processing technique produced three apparently different Pc 3 behaviorisms. Further development of recording technique would be required before the College records could be routinely applied to this correlation study.

Meanwhile, a visual evaluation of UCLA's Tungsten induction coil records for 1-15 December 69 was made (in collaboration with Carlene Arthur and Bob McPherron), and a statistical summary obtained. Subjectively, there did appear to be a class of pulsations sometimes in the Pc 3, sometimes in the Pc 4 range, whose appearance was correlated with solar wind field-flow alignment. The latter was also evaluated visually from Explorer 35 interplanetary field records. The statistical summary verified part of this correlation: Pc 4 definitely occurred preferentially when the field-flow angle θ_{VB}, approximated in practice by θ_{XB}, was close to zero. Seventy percent of the hours when Pc 4 were detected, the field $\underset{\sim}{B}_{SW}$ was oriented within 36°.7 of both the ecliptic plane and the solar azimuth. Latitude and longitudes of $\underset{\sim}{B}_{SW}$ jointly within this limit correspond to conditions for irregular, quasi-parallel shock structure at the subsolar point of the bow shock. Half the Pc 4 hours corresponded to θ_{XB} within 18°.4 of the solar azimuth.

Figure 1 summarizes the results projected onto the ecliptic plane, with solar and antisolar field directions combined. Each graph represents, for one pulsation condition, the fraction of measured directions of $\underset{\sim}{B}_{SW}$ that fell in various sectors during hours in which the condition applied. At upper left, the angular distribution of all measurements shows the usual stream angle preference. At upper right, the distribution of measurements for which Pc 3-4

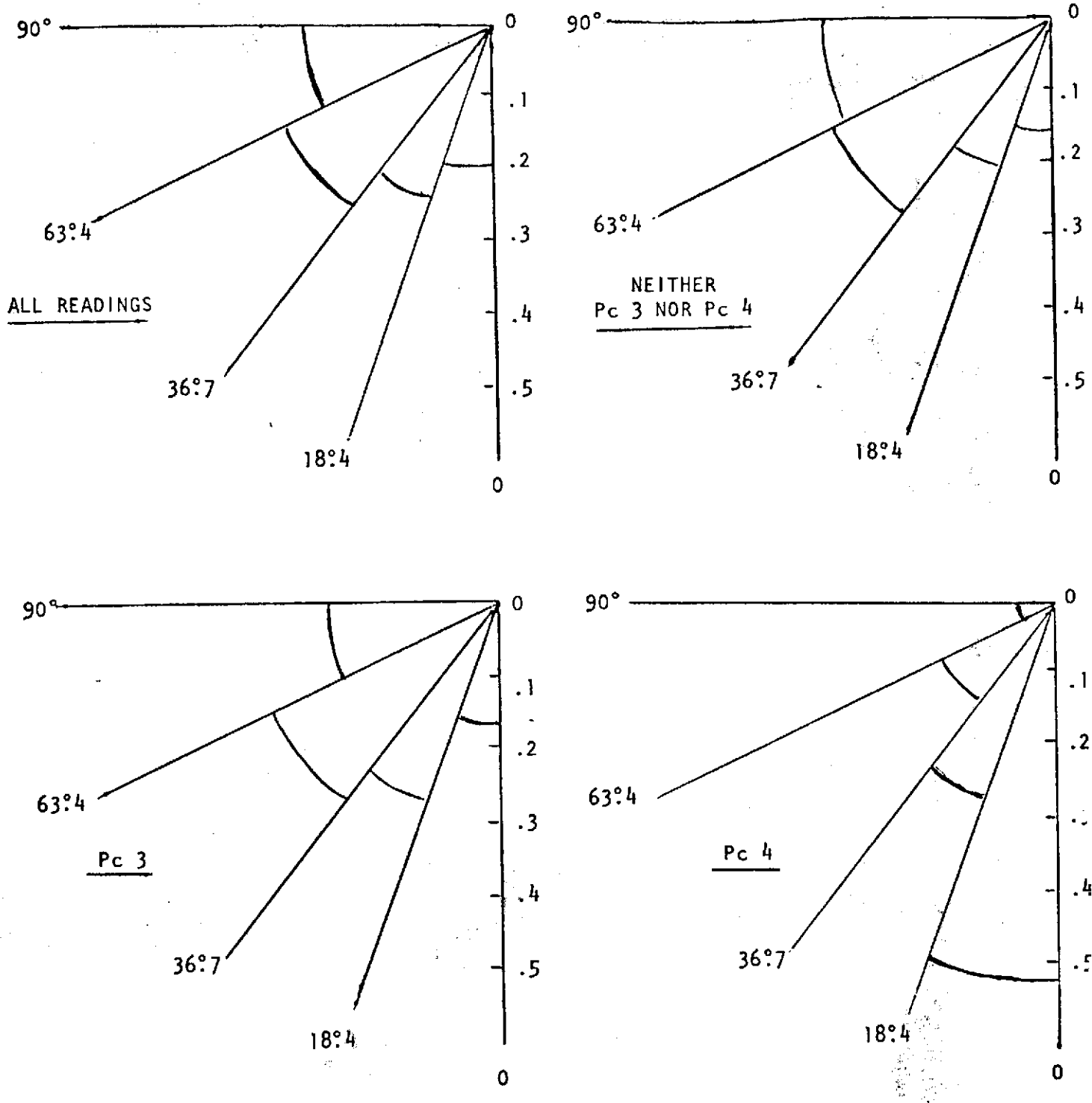

Figure 1. Angular distributions of the ecliptic projection of $\underset{\sim}{B}_{SW}$ for various Pc 3,4 conditions.

were absent, was deficient in the 0-18°.4 and 18°.4-36°.7 sectors and somewhat excessive in the 36°.7-63°.4 and 63°.4-90° sectors, with respect to the distribution of all measurements. At lower left, the distribution for Pc 3 hours was slightly excessive in the sectors from 18°.4 to 63°.4 and deficient elsewhere; this result is not obviously significant, but is at best consistent with a result claimed by Bol'shakova and Troitskaya (1968). At lower right, measurements in the 0-18°.4 sector were grossly in excess and in the 63°.4-90° sector grossly deficient in readings during hours when Pc 4 occurred.

Another version of some of the results of visual comparison with Tungsten is shown in Figure 2. The first three-dimensional construction in 2(a) portrays the distribution in solid angle, divided as already described, in which $\underset{\sim}{B}_{SW}$ fell during Pc 4 events. The radial length of each angular block represents the fraction of hours of observation of Pc 4 during which the solid angle of the block was occupied by $\underset{\sim}{B}_{SW}$ during some part of the hour. The second construction, 2(b), is the same type of representation for hours during which neither Pc 3 nor Pc 4 occurred. The strong preference of Pc 4 for hours when θ_{XB} lay close to 0°, and the equally-strong avoidance of $\theta_{XB} < 36°.7$ when Pc 3-4 were absent are clear in the figure.

The statistical summary and visual examination of the Tungsten data suggested, in line with the Russian results and the recent Canadian observations of Nourry and Watanabe (1973), that there is a pulsation phenomenon of variable period strongly associated with certain interplanetary field directions. The periods of the phenomenon span the accepted division between Pc 3 and Pc 4 at T = 45 seconds. In the Pc 4 range ($45 \leq T \leq 150$ sec), the phenomenon is reasonably isolated, but in the Pc 3 range, the phenomenon is confounded with, and often overshadowed by, other types of oscillations, most notably Pi 2.

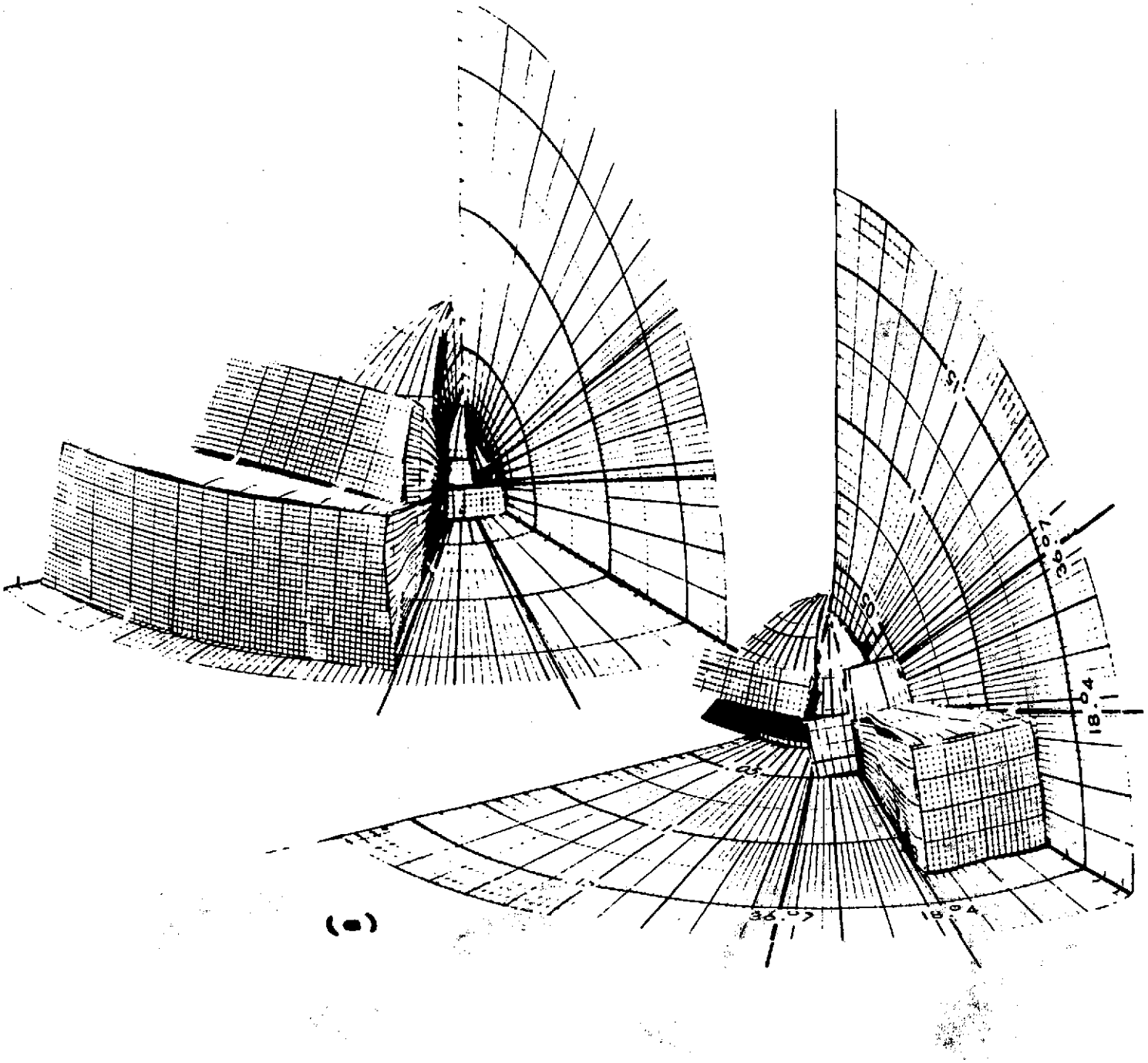

Figure 2. Distributions of northward θ_{XB} for (a) Pc 4 and (b) neither Pc 3 nor Pc 4.

Visual evaluations of this phenomenon become very unreliable in the Pc 3 range.

Preliminary printed versions of the Nourry and Watanabe data were received and examined, and the Russian publications were reviewed once again. It appears tentatively that the Soviet and Canadian results are completely compatible with the model of Pc generation proposed by this investigator. The evidence tends to be anecdotal, however, or, at best, incompletely documented. Pc 1 spectrograms from Borok, a commonly-cited Russian observatory, have been published, showing the Russian capability with f-t technique, but it is not clear whether these, or only visual judgments of Pc 3-4 occurrence were applied in the Soviet work. Although statistical compatibility is not proof of the model itself, it was decided to continue to seek a more solid correlative foundation in this program before attempting to explore any physical details of the model. However, it was concluded that suitable methods of mechanizing and objectivizing the correlation sought here had become unavoidable. The effort of this study was therefore redoubled to obtain an entirely independent demonstration with more sophisticated techniques than have hitherto been applied.

Computer Program for Spectral Correlation. The best demonstration of the correlation central to the model of this study should be provided by examination of a long interval (weeks to months) of data in which interplanetary field orientation in suitable graphic representation is compared with concurrent micropulsation spectrograms (f-t plots) on the same time scale. Production of suitable magnetic field plots requires a computer programming and running effort. A magnetic tape for a selected test interval was obtained from NASA/ARC. The tape contains the "sequence averages" from the ARC

Explorer 35 magnetometer. The test interval was determined in consultation with John Olson of the University of Alberta (Edmonton), who is in the process of reducing micropulsation data to suitable format. The comparison of spacecraft with surface data is intended to span the last four months of 1969, when the Canadian chain of stations operated by Edmunton provided good time and latitude coverage. Since the UCLA station at Tungsten also operated during this interval, the potential for a comprehensive examination of the relationship under study is good.

As this is written, an initial version of the computer program for handling Explorer 35 magnetic field tapes to produce appropriate plots at TRW is essentially debugged, while a program for preparation of spectograms from Canadian micropulsation tapes is in about the same condition. Figure 3 shows a three-hour test version of part of the plotted output of our routine, compared with a micropulsation record from Tungsten (courtesy UCLA) on the same time scale. Time-scale matching is one of the options of the TRW program. The two curves at the top are cos θ_{XB} and θ_{XB}, as marked, with low θ_{XB}, i.e., favorable θ_{XB} at the top of the graph. A burst, or sequence of bursts, of pulsations of about 120-sec period (Pc 4 range) appear in approximate coincidence with rotations of $\underset{\sim}{B}_{SW}$ from 10-20° to about 50°. Unfortunately, this is exactly the opposite of the correlation we seek and of the reported results of Bol'shakova and Troitskaya (1968) and Nourry and Watanabe (1974). We have no explanation for this outcome at present, but we note that the local time at Tungsten is dawn rather than noon, when such pulsations usually appear. Also, the true rotation of $\underset{\sim}{B}_{SW}$ was southward, so the oscillations on the surface are undoubtedly substorm-associated. The figure demonstrates well that we now have the capability of producing our own anecdotes. It also illustrates clearly

REPRODUCIBILITY OF THE
ORIGINAL PAGE IS POOR

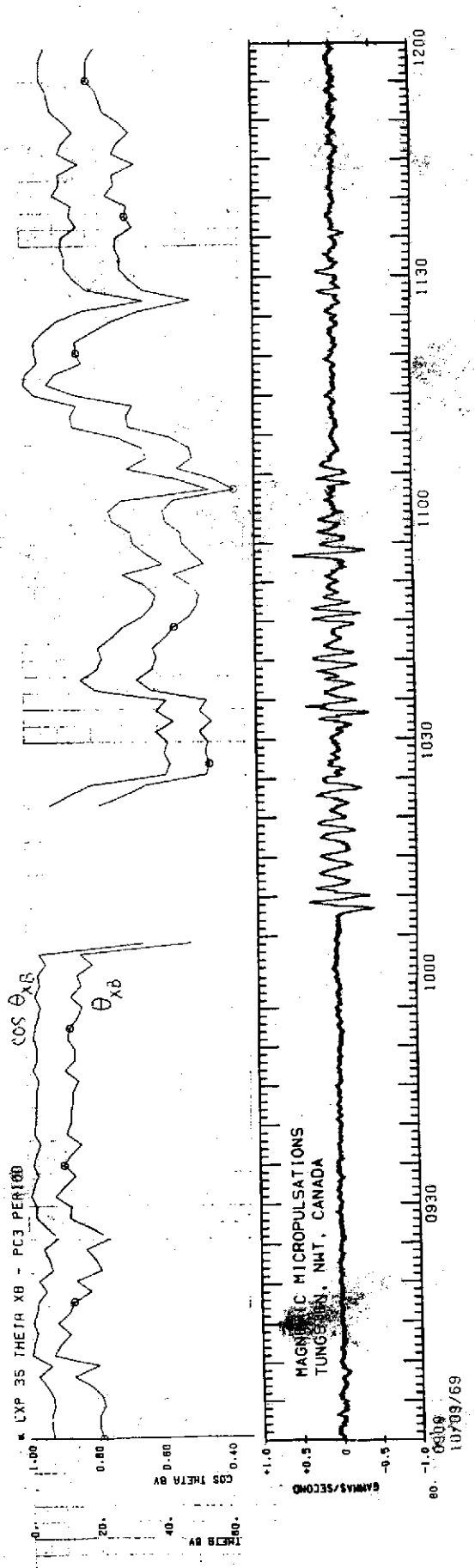

Figure 3. Partial output of TRW preliminary program for θ_{XB}, compared with 3-hour micropulsation record.

the type of result that supplies grounds for our conviction that a suitable long-term, objectivized approach to the micropulsation study is essential.

A listing of the preliminary TRW program is attached as Appendix A. Our routine will compute several specialized functions, but the program has been written in such a way as to facilitate later use of interplanetary field readings from the same Explorer data tapes in computing a variety of quantities related to bow shock and magnetosheath structure, none of which would have justified the rather complex program by themselves.

Shock Structure

Geometry. An important task in following up earlier work on the response of the bow shock to local field geometry (Greenstadt, 1972a,b) has been to discover the reason that propagation of precursor effects upstream from the shock apparently occurs consistently along $\underset{\sim}{B}_{SW}$ at a speed $u_{\parallel} \approx 1.6\ V_{SW}$. Northrop and Birmingham (1973) accepted the premise that $p \equiv 1.6$ was independent of position on the shock and derived the improbable result that $u_{\parallel}$ would then be constant, i.e., independent of V_{SW}. It seems more likely that p does not vary strongly with position, and that limited early experimental work has simply not picked up the variation, but this has yet to be demonstrated.

There is more than one precursor effect (Appendix B). The effect referred to above consists of decasecond waves propagating downstream as a result of excitation by some other precursor agency. It is not known whether the long period waves are coupled to a dominant category of reflected protons or simply represent a dominant frequency range most easily excited. It is known that reflected protons are found at many energies with $u_{\parallel} \neq 1.6$ (Asbridge

et al., 1968; Lin et al., 1974). In their recent paper, Lin et al. have given arguments why they believe 100 Kev-reflected protons are accelerated en route upstream rather than in the shock proper. Their conclusion would tend to support the notion that protons come out of the shock itself in a narrower range of energies, possibly concentrated around $(1.6\ V_{SW})^{\frac{1}{p}}$.

An attempt was made by this investigator to discover whether the geometrical relationship of the shock to reflected protons of finite pitch angle places restrictions on their energies that would tend to select those with $p \approx 1.6$ for escape upstream. The attempt was unsuccessful for an interesting reason. There turned out to be at least two free geometric parameters, leaving p essentially unconstrained. An unexpected result has followed: protons of large energy (30-100 Kev) and large pitch angle (70°), such as those commonly encountered by Lin et al., can escape the shock upstream when the angle made by $\underset{\sim}{B}_{SW}$ with the local shock normal is about 50°, the value at which upstream waves typically are generated. It thus appears that the particles detected by Lin et al. could have come directly from the bow shock as far as the credibility of their escape is concerned, although the process of their creation is still undetermined.

An explanation of, and report on, the above calculation was prepared for presentation at the Neil Brice Memorial Symposium "The Magnetospheres of Earth and Jupiter," and given in Frascati in May. It is attached as Appendix B. A more extensive inquiry into the geometry of reflected particles is planned.

Laminar Shocks. A comprehensive study of the quasi-perpendicular laminar shocks of 12 February 1969 was completed after addition of several new sections. A draft of a final report on these events is attached as Appendix D.

Especially interesting among the newly-added results is the detailed display of ELF noise juxtaposed on the shock's magnetic profile and the new method of computing instantaneous shock velocity from the standing wave period (Figure 6 and Table 2 and Appendix 2 of Appendix D).

Parametric Profiles of the Bow Shock. A collaboration was opened a year ago among V. Formisano, C. T. Russell, M. Neugebauer, F. L. Scarf, and this investigator for the purpose of compiling and studying plasma diagnostics recorded simultaneously by OGO 5 and HEOS 1 under differing solar wind conditions during bow shock crossings by OGO 5. We have succeeded in isolating over a dozen distinct combinations of M, β, and θ_{nB} and have made significant progress in determining the effect of each of these parameters on each of several plasma diagnostics measured in the shock. We are also in the process of merging the shock-structural classification schemes of Greenstadt et al. (1970b) and Formisano and Hedgecock (1973a) into a single comprehensive framework. A summary of some of the core results of this project is contained in Appendix C, a paper given recently at the Third Solar Wind Conference in Asilomar. The bulk of the program is incomplete, but a compendium of shock profiles is presently being prepared and should be available before the end of the year.

Quasi-Parallel Shock Structure. A case of prolonged, concurrent observation of quasi-parallel ("pulsation") shock structure by OGO 5 and HEOS 1 occurred on 14 February 1969. The situation is similar to the one reported earlier that led to identification of the pulsation shock phenomenon (Greenstadt et al., 1970a, but with the addition this time of substantially-improved diagnostic coverage. Initial examination of the data has verified the extreme thickness of the pulsation, or quasi-parallel structure, and revealed an

apparently distinct plasma particle distribution associated with this class of shock. A description of this preliminary result is part of Appendix

Reports

The following report was published during the year July 73 - July 74.

Greenstadt, E. W., Oblique Structure of Jupiter's Bow Shock, J. Geophys. Res., 78, 5813, 1974.

A report was prepared and delivered orally by R. W. Fredricks at the Summer Advanced Studies Institute, "Earth's Particles and Fields," Sheffield, England, August 13-24, 1973:

Greenstadt, E. W., and R. W. Fredricks, Plasma Instability Modes Related to the Earth's Bow Shock.

The report is scheduled to be published in the Institute Proceedings.

An informal presentation of shock structure results was given at the joing USA/USSR Bi-Lateral Working Group Meeting on Collisionless Shock Waves held in November at NASA Goddard Space Flight Center.

Three more reports have been completed:

Greenstadt, E. W., Structure of the Terrestrial Bow Shock, presented to the Third Solar Wind Conference held at Pacific Grove, California, 25-29 March 1974. To be published in the Conference Proceedings.

Greenstadt, E. W., C. T. Russell, F. L. Scarf, V. Formisano, and M. Neugebauer, Structure of the Quasi-Perpendicular, Laminar Bow Shock, prepared for J. Geophys. Res.

Greenstadt, E. W., The Upstream Escape of Energized Solar Wind Protons from the Bow Shock, Presented at the Neil Brice Memorial Symposium, "The Magnetospheres of Earth and Jupiter," Frascati, Italy, May 1974. To be published in the Proceedings.

COMMENTARY

Correlative Results of Other Investigators

This is an appropriate time and communication in which to note briefly the research context in which our shock investigation now finds itself.

The revival of interest in the bow shock, and its upstream effects on the solar wind, which seemed to be developing a year ago has been realized. Research on the shock as a plasma, rather than fluid-like, phenomenon is beginning to flourish, partly through fresh attention by European investigators. A selection of specific results bearing directly on this program are listed below:

Formisano et al. (1973a) distinguished statistically between Maxwellian and non-Maxwellian proton distributions in the magnetosheath, dependent on mach number and angle θ_{nB}.

Formisano et al. (1973b) studied fluid parameters across the shock and bow shock velocities as functions of M, β, and θ_{nB}.

Formisano and Hedgecock (1973a) developed a structural classification scheme for the bow shock, parametized by M, β, and θ_{nB}.

Formisano and Hedgecock (1973b) described the bimodal proton distribution found in the quasi-perpendicular, turbulent shock structure (see Appendix C).

Northrop and Birmingham (1973) examined the implications of a position (θ_{nB})-independent upstream wave parameter p = 1.6 on the critical angle of upstream wave appearance.

Olson and Holzer (1974) made a statistical study of the wave and spectral structure of the bow shock, finding relatively little local time dependence of structure at search coil frequencies ($f > .1$ Hz), but they were without information on M or β. The role of β in the generation of magnetic noise is now better understood (Appendix C).

R. D. Auer (unpublished preprint) has found the apparent plasma bow shock position of quasi-parallel bow shocks to be earthward of their quasi-perpendicular counterparts. He has also found that a more marked statistical symmetry between dawn and dusk structures should have prevailed during the HEOS 2 data interval than during the interval examined by Greenstadt (1973).

Feldman et al. (1973) attributed the reversal of heat-flux anisotropy of electrons upstream from the bow shock to their shock origin when the solar wind field was appropriately oriented.

Lin et al. (1974), in the first direct observation of reflected protons since the short paper by Scarf et al. (1970), described the commonplace observation of protons in the 30-100 Kev energy range.

Finally, the two most exciting new results are the observation of an apparent quasi-parallel shock structure at Venus by Mariner 10 (Ness et al., 1974), consistent with a similar interpretation of the Mariner 5 record by this investigator (Greenstadt, 1970), and the tentative compatibility of the Pioneer 10 measurements with the predicted shock structure at Jupiter (Greenstadt, 1973; Ed Smith, personal discussion).

All the foregoing developments draw on results from this program or its preliminary phases.

RECOMMENDATIONS

Micropulsations. It is recommended that efforts to objectivize the reduction and analysis of micropulsation data be supported and expanded. Techniques of display such as the frequency-time contour plots coming out of UCLA (Arthur et al., 1973) should be encouraged for the entire Pc 3-4 spectral range. Quite beyond the current or planned application that this investigation seeks to make of such displays, the eventual use of micropulsation indices as diagnostics of solar wind and magnetosheath conditions will certainly require such techniques, which are expensive and inadequately funded at present. Development of micropulsation diagnostics ought to be a major goal of the International Magnetospheric Study (IMS), but such development will not occur without sustained effort in this direction. It is urgently recommended that a working panel be created to encourage at the very least a uniform micropulsation recording method and schedule among a suitably-selected set of stations as part of the IMS preparations.

Shock Structure. It is recommended that efforts be continued to exploit the earth's bow shock as a source of collisionless plasma phenomenology. The earth's interaction region is nicely representative of the interaction regions of other planets and is subject to such a wide range of incident plasma parameters as to provide almost universal coverage of the variety of collisionless phenomena for which experimental data are needed. Moreover, there seem to be plenty of opportunities to acquire new results through analysis of existing data.

REFERENCES

Arthur, C. W., R. L. McPherron, and P. J. Coleman, Jr., Micropulsations in the morning sector, 1, Ground observations of 10- to 45-second waves, Tungsten, Northwest Territories, Canada, J. Geophys. Res., 78, 8180, 1973.

Asbridge, J. R., S. J. Bame, and I. B. Strong, Outward flow of protons from the earth's bow shock, J. Geophys. Res., 73, 5777, 1968.

Bol'shakova, O. V., and V. A. Troitskaya, Relation of the interplanetary magnetic field direction to the system of stable oscillations, Dokl. Akad. Nauk SSSR, 180, 4, 1968.

Feldman, W. C., J. R. Asbridge, S. J. Bame, and M. D. Montgomery, Solar wind heat transport in the vicinity of the earth's bow shock, J. Geophys. Res., 78, 3697, 1973.

Formisano, V., and P. C. Hedgecock, Solar wind interaction with the earth's magnetic field, 3. On the earth's bow shock structure, J. Geophys. Res., 78, 3745, 1973a.

Formisano V., and P. C. Hedgecock, On the structure of the turbulent bow shock, J. Geophys. Res., 78, 6522, 1973b.

Formisano, V., G. Moreno, F. Palmiotto, and P. C. Hedgecock, Solar wind interaction with the earth's magnetic field, 1. Magnetosheath, J. Geophys. Res., 78, 3714, 1973a.

Formisano, V., P. C. Hedgecock, G. Moreno, F. Palmiotto, and J. Chao, Solar wind interaction with the earth's magnetic field, 2. The magnetohydrodynamic bow shock, J. Geophys. Res., 78, 3731, 1973b.

Greenstadt, E. W., Binary index for assessing local bow shock obliquity, J. Geophys. Res., 77, 5467, 1972.

Greenstadt, E. W., Statistics of bow shock nonuniformity, J. Geophys. Res., 78, 2331, 1973a.

Greenstadt, E. W., Oblique structure of Jupiter's bow shock, J. Geophys. Res., 78, 5813, 1973b.

Greenstadt, E. W., I. M. Green, G. T. Inouye, D. S. Colburn, J. H. Binsack, and E. F. Lyon, Dual satellite observations of the earth's bow shock, 1, The thick pulsation shock, Cosmic Electrodyn., 1, 100, 1970a.

Greenstadt, E. W., I. M. Green, G. T. Inouye, D. S. Colburn, J. H. Binsack, and E. F. Lyon, Dual satellite observations of the earth's bow shock, 3. Field-determined shock structure, Cosmic Electrodyn., 1, 316, 1970b.

Greenstadt, E. W., Dependence of shock structure at Venus and Mars on orientation of the interplanetary magnetic field, Cosmic Electrodyn., 1, 380, 1970c.

Lin, R. P., C. -I. Meng, and K. A. Anderson, 30- to 100-keV protons upstream from the earth's bow shock, J. Geophys. Res., 79, 489, 1974.

Ness, N. F., K. W. Behannon, R. P. Lepping, Y. C. Whang, and K. H. Schatten, Magnetic field observations near Venus: Preliminary results from Mariner 10, Science, 183, 1301, 1974.

Northrop, T. G., and T. J. Birmingham, On Greenstadt's binary index criterion, J. Geophys. Res., 78, 2308, 1973.

Nourry G., and T. Watanabe, Geomagnetic micropulsations and interplanetary magnetic field, Abstract, EOS, 54, 1179, 1973.

Olson, J. V., and R. E. Holzer, On the local time dependence of the bow shock wave structure, J. Geophys. Res., 79, 939, 1974.

Scarf, F. L., W. R. Fredricks, L. A. Frank, C. T. Russell, P. J. Coleman, Jr., and M. Neugebauer, Direct correlations of large amplitude waves with suprathermal protons in the upstream solar wind, J. Geophys. Res., 75, 7316, 1970.

Tidman, D. A., and N. A. Krall, Shock Waves in Collisionless Plasmas, John Wiley-Interscience, New York, 1971.

APPENDIX A

PROGRAM LISTING

REPRODUCIBILITY OF THE
ORIGINAL PAGE IS POOR


```
      PROGRAM E35BXP(INPUT,TAPE5=INPUT,TAPE6,OUTPUT,TAPE7=OUTPUT,TAPE8,
     1               TAPE50)
C
C PROGRAM E35BXP - J.S. BURGESS FOR EXPLORER 35 SEQUENCE AVERAGES.
C E35BXP USES SUBROUTINE E35DRV TO MERGE THE AMES COC EXPLORER 35
C SEQUENCE AVERAGE TAPE WITH SELECTED TIME INTERVALS AND THEN COMPUTES -
C
C       THBV - THE ANGLE THETA BV BETWEEN INTERPLANETARY FIELD BSW AND
C              THE X(SE) AXIS. (IT IS ASSUMED X IS PARALLEL TO V(SW))
C      TBVCS - THE COSINE OF THETA BV (THBV).
C     TPCBSW - THE MICROPULSATION PERIOD = 160/BSW ACCORDING TO THE
C              RUSSIAN EXPERIMENTAL RESULT.
C     TCYBSW - THE PROTON CYCLOTRON PERIOD IN THE SOLAR WIND ACCORDING
C              TO TCYBSW = TPCBSW/2.44.
C
C INTERPLANETARY FIELD HAS MAGNITUDE BSW, LATITUDE LAMBDAB = BLMB, AND
C LONGITUDE PHIB.
C
      COMMON/PLOTIN/NSECIN,NFIRST,NAFTER,ITIC
      COMMON/DATOUT/NEWDAT(26,60),IDUM
      COMMON/XHEAD/NTAPE,NFOT,NYEAR,COMENT(8)
      COMMON/XTINT/NINT,NFILE,NRECORD,NDAY1,NHOUR1,NMIN1,NDAY2,NHOUR2,
     1             NMIN2,ISTART,IEND,IERROR,NF,NR,IFEMP
      COMMON/OPTION/LISTOP,NPLOTOP,NPLTSAV
      COMMON/XTIM/IDAY(60),ITIM(60),INSTRT,INEND,LSEQSAV
      COMMON/DARRAY/INDEX,TIM(500),NSEQ(500),LDAY(500),LHRMN(500),
     1              LSEC(500),BSW(500),TPCBSW(500),TCYBSW(500),
     2              BLMB(500),PHIB(500),TBVCS(500),THBV(500),COMBAC,
     3              TOPLOT,NSEQSAV,ISGAP,ISGAPSV,MTIMSAV
      COMMON/CONS/RADEG
      LOGICAL COMBAC,TOPLOT,ISGAP,ISGAPSV
      DATA RADEG/57.2957795/
C NCODE IS THE PRINCIPAL DIRECTIVE FROM E35DRV TO E35BXP.
C NOTE - NCODE = 1 MEANS THERE IS NEW DATA FOR PROCESSING.
C      - NCODE = 2 MEANS THERE IS SOME NEW DATA FOR PROCESSING AND THE
C        END OF THE INTERVAL HAS BEEN DETECTED, SO WRAP IT UP.
C      - NCODE = 3 MEANS THERE IS NO NEW DATA FOR PROCESSING AND THE END
C        HAS BEEN DETECTED, SO WRAP IT UP (ANNOTATE, ETC.).
C      - NCODE = 4 MEANS ABNORMAL TERMINATION - EOF REACHED ON TAPE6.
C      - NCODE = 5 MEANS NORMAL TERMINATION - EOF REACHED ON TAPE5.
C
```

```
C SECTION 1 - INITIALIZATION.
C
      CALL E35DRV(1,NCODE)
      CALL BXPLST(1)
C
C SECTION 2 - BEGINNING OF A NEW TIME INTERVAL.
C
  150 CONTINUE
C DIRECT E35DRV TO READ A NEW TIME INTERVAL.
      CALL E35DRV(2,NCODE)
C IF NCODE = 5 THEN IT IS TIME FOR NORMAL TERMINATION.
      IF(NCODE.EQ.5)GO TO 2000
C WRITE TIME INTERVAL VALUES ON DATA LISTING.
      CALL BXPLST(2)
C IF IERROR = 1 THE INTERVAL WILL BE USED.
      IF(IERROR.EQ.1)GO TO 400
      NPLOTOP = 1
C IF NPLTSAV = 3 ANNOTATION IS REQUIRED ON PLOT OF PREVIOUS INTERVAL.
      IF(NPLTSAV.EQ.3)CALL BXPPLT(3)
      GO TO 150
C DIRECT E35DRV TO POSITION TAPE AND READ FIRST DATA RECORD.
  400 CONTINUE
      IF(NPLTSAV.EQ.3.AND.NPLOTOP.EQ.1)410,420
  410 CALL BXPPLT(3)
      NPLTSAV = NPLOTOP
  420 CALL E35DRV(3,NCODE)
      GO TO(500,500,150,2000)NCODE
C
C SECTION 3 - PROCESS FIRST RECORD OF GOOD DATA.
C
  500 CONTINUE
      ISGAP = .TRUE.
C IF NPLOTOP = 1 THERE WILL BE NO PLOT MADE OF THIS INTERVAL.
      IF(NPLOTOP.EQ.1)GO TO 550
C IF NPLTSAV = 3 THE PRESENT PLOT WILL CONNECT TO THE PREVIOUS PLOT.
      IF(NPLTSAV.EQ.3)510,520
  510 ISGAP = .FALSE.
      GO TO 560
C INITIALIZE PLOT AND SAVE BEGIN TIME.
  520 MTIMSAV = ISTART
      CALL BXPPLT(1)
```

REPRODUCIBILITY OF THE ORIGINAL PAGE IS POOR

REPRODUCIBILITY OF THE ORIGINAL PAGE IS POOR

```
C RESET TIME GAP CHECK (SEQUENCE NUMBER IS USED FOR THIS).
  550 NSEQSAV = NEWDAT(1,INSTRT) - 1
C RESET COUNTER FOR DATA ARRAYS.
  560 INDEX = 0
      GO TO(600,800)NCODE
C
C SECTION 4 - PROCESSING FOR NORMAL DATA FLOW (IN MIDDLE OF INTERVAL).
C
  600 CONTINUE
      CALL CALARR
C IS IT TIME TO PLOT AND/OR LIST.
      IF(TOPLOT)610,700
  610 CONTINUE
      IF(NPLOTOP.NE.1)CALL BXPPLT(2)
      IF(LISTOP.EQ.1)CALL BXPLST(3)
      INDEX = 0
C IS THERE MORE DATA TO PROCESS.
      IF(COMBAC)GO TO 600
C DIRECT E35DRV TO READ A NEW DATA RECORD.
  700 CONTINUE
      CALL E35DRV(4,NCODE)
      GO TO(600,800,900,900)NCODE
C
C SECTION 5 - PROCESS DATA AT END OF INTERVAL AND PLOT AND/OR LIST IT
C             AND WRAP UP THIS INTERVAL.
C
  800 CONTINUE
      CALL CALARR
      IF(NPLOTOP.EQ.1)GO TO 850
      CALL BXPPLT(2)
      IF(COMBAC)850,820
  820 IF(NPLOTOP.EQ.3)GO TO 850
C ANNOTATE TIME ON PLOT.
      CALL BXPPLT(3)
  850 CONTINUE
      IF(LISTOP.EQ.1)CALL BXPLST(3)
C IT IS POSSIBLE THAT THERE IS STILL MORE DATA TO PROCESS.
      IF(COMBAC)870,150
  870 INDEX = 0
      GO TO 800
C
```

```
C SECTION 6 - END OF INTERVAL AND NO NEW DATA TO PROCESS, SO PLOT AND/OR
C             LIST ANY DATA LEFT IN ARRAYS AND WRAP UP THIS INTERVAL.
C
  900 CONTINUE
      IF(NPLOTOP.EQ.1)GO TO 950
      IF(INDEX.NE.0)CALL BXPPLT(2)
      CALL BXPPLT(3)
  950 IF(LISTOP.NE.1)GO TO 970
      IF(INDEX.GT.0)CALL BXPLST(3)
C WAS EOF REACHED ON THE TAPE (TAPE6).
  970 IF(NCODE.EQ.4)GO TO 2000
      GO TO 150
C
C SECTION 7 - TERMINATION.
 2000 CONTINUE
C TERMINATE PLOT TAPE.
      CALL BXPPLT(4)
      IF(NCODE.EQ.4)2010,2020
 2010 CALL BXPLST(4)
      STOP
 2020 CALL BXPLST(5)
      STOP
      END
"
      SUBROUTINE CALARR
C
C SUBROUTINE CALARR - J.S. BURGESS FOR EXPLORER 35 CDC SEQUENCE AVE.
C CALARR CALCULATES AND FILLS ARRAYS OF DATA FOR MAIN PROGRAM ESSEXP.1J
C TAKES FROM 1-60 SETS OF UNPACKED EXPLORER 35 SEQUENCES AVERAGES,
C CALCULATES NECESSARY QUANTITIES, CHECKS FOR TIME GAPS, AND DECIDES
C WHETHER IT IS TIME TO PLOT OR RETURN FOR MORE DATA.
C
      COMMON/CONS/RADEG
      COMMON/DATOUT/NEWDAT(26,60),IDUM
      COMMON/XTIM/IDAY(60),ITIM(60),INSERT,INEND,LSECSAV,
      COMMON/OPTION/LISTOP,NPLOTOP,NPLTSAV
      COMMON/OARRAY/INDEX,TIM(500),NSEQ(500),LDAY(500),LHRMN(500),
     1              LSEC(500),BSW(500),TPCBSW(500),TCYBSW(500),
     2              BLMB(500),PHIB(500),TBVCS(500),THBV(500),COMBAC,
     3              TOPLOT,NSEQSAV,ISGAP,ISGAPSV,MTIMSAV
      LOGICAL COMBAC,TOPLOT,ISGAP,ISGAPSV
```

REPRODUCIBILITY OF THE ORIGINAL PAGE IS POOR

REPRODUCIBILITY OF THE
ORIGINAL PAGE IS POOR


```
C
C SECTION 1 - PROCESS DATA.
C
C NOTE - TOPLOT = .TRUE. MEANS IT IS TIME TO PLOT EITHER BECAUSE A TIME
C        GAP IS DETECTED OR THE ARRAYS ARE FULL.
C NOTE - COMBAC = .TRUE. MEANS THAT AFTER PLOTTING CALARR MUST BE CALLED
C        AGAIN TO FINISH PROCESSING DATA REMAINING.
C NOTE - ISGAP = .TRUE. MEANS THAT THERE IS A TIME GAP AND THE PRESENT
C        SET OF DATA TO BE PLOTTED WILL NOT BE JOINED TO PREVIOUS DATA.
C NOTE - ISGAPSV SAVES VALUE OF ISGAP FOR BXPPLT.
      TOPLOT = .FALSE.
      COMBAC = .FALSE.
      DO 500 I=INSTRT,INEND
C CHECK FOR TIME GAP AND SEQUENCE RECYCLE.
      IF((NEWDAT(1,I)-NSEQSAV).EQ.1)GO TO 300
      IF(NEWDAT(1,I).EQ.1.AND.NSEQSAV.EQ.999999)GO TO 300
C MAKE SURE THAT ARRAY IS NON-EMPTY BEFORE GOING TO PLOT.
      IF(INDEX.NE.0)GO TO 700
      ISGAP = .TRUE.
C MAKE CALCULATIONS. INDEX COUNTS CONSECUTIVE DATA POINTS.
  300 INDEX = INDEX + 1
      TIM(INDEX) = ITIM(I)
      IF(LISTOP.EQ.2)GO TO 400
      NSEQ(INDEX) = NEWDAT(1,I)
      LDAY(INDEX) = IDAY(I)
      IHRMN = 100*NEWDAT(3,I) + NEWDAT(4,I)
      CALL IFILIN(4,IHRMN,LHRMN(INDEX),MXER)
      CALL IFILIN(2,NEWDAT(5,I),LSEC(INDEX),MXER)
  400 CONTINUE
      IF(NEWDAT(6,I).NE.9999.AND.NEWDAT(6,I).NE.0)GO TO 410
C SET BAD POINTS TO FLAG VALUE
      BSW(INDEX) = 5000.
      TPCBSW(INDEX) = 5000.
      TCYBSW(INDEX) = 5000.
      GO TO 415
  410 CONTINUE
      BSW(INDEX) = NEWDAT(6,I)/10.
      TPCBSW(INDEX) = 160./BSW(INDEX)
      TCYBSW(INDEX) = TPCBSW(INDEX)/2.44
  415 IF(NEWDAT(21,I).NE.9999)GO TO 420
      BLMB(INDEX) = 5000.
```

```
      GO TO 425
  420 BLMB(INDEX) = NEWDAT(21,I)/10.
  425 IF(NEWDAT(22,I).NE.9999)GO TO 430
      PHIB(INDEX) = 5000.
      GO TO 435
  430 PHIB(INDEX) = NEWDAT(22,I)/10.
  435 IF(PHIB(INDEX).LT.5000..AND.BLMB(INDEX).LT.5000.)GO TO 450
      TBVCS(INDEX) = 5000.
      THBV(INDEX) = 5000.
      GO TO 475
  450 TBVCS(INDEX) = ABS(COS(BLMB(INDEX)/RADEG)*COS(PHIB(INDEX)/RADEG))
      THBV(INDEX) = ACOS(TBVCS(INDEX))*RADEG
  475 CONTINUE
C SAVE PREVIOUS SEQUENCE NUMBER AND CHECK TO SEE IF ARRAYS ARE FULL.
      NSEQSAV = NEWDAT(1,I)
      IF(INDEX.EQ.500)GO TO 600
  500 CONTINUE
C IF IT GETS HERE IT IS TIME TO RETURN FOR MORE DATA.
      ISGAPSV = ISGAP
      RETURN
C
C SECTION 2 - MAKE PLOT AND RETURN FOR MORE PROCESSING DECISIONS.
C
C PART 1 - THE ARRAYS ARE FILLED.
  600 CONTINUE
      ISGAPSV = ISGAP
      ISGAP = .FALSE.
      IF(I.LT.INEND)COMBAC = .TRUE.
      TOPLOT = .TRUE.
      INSTRT = I+1
      RETURN
C
C PART 2 - THERE IS A TIME GAP.
  700 CONTINUE
      ISGAPSV = ISGAP
      ISGAP = .TRUE.
      COMBAC = .TRUE.
      TOPLOT = .TRUE.
      INSTRT = I
      NSEQSAV = NEWDAT(1,INSTRT) = I
      RETURN
```

```
      END
"                                                                    "
      SUBROUTINE BXPLST(JCODE)
C
C SUBROUTINE BXPLST - J.S. BURGESS FOR EXPLORER 35 CDC SEQUENCE AVE.
C BXPLST IS A DATA LISTING SUBROUTINE FOR MAIN PROGRAM E35BXP. IT
C PROVIDES A COMPLETE DATA LISTING FOR ANY TIME INTERVAL THAT HAS THE
C LIST OPTION ON (LISTOP=1). IT ALSO PROVIDES A LIST OF ALL TIME
C INTERVALS IN A PARTICULAR RUN REGARDLESS OF THE LIST OPTION.
C
      COMMON/XHEAD/NTAPE,NFOT,NYEAR,COMENT(8)
      COMMON/XTINT/NINT,NFILE,NRECORD,NDAY1,NHOUR1,NMIN1,NDAY2,NHOUR2,
     1             NMIN2,ISTART,IEND,IERROR,NF,NR,IFEMP
      COMMON/DARRAY/INDEX,TIM(500),NSEQ(500),LDAY(500),LHRMN(500),
     1              LSEC(500),BSW(500),TPCBSW(500),TCYBSW(500),
     2              BLMB(500),PHIB(500),TBVCS(500),THBV(500),COMBAC,
     3              TOPLOT,NSEQSAV,ISGAP,ISGAPSV,MTIMSAV
      DIMENSION TITLE(4),TGP(2)
      DATA TITLE/40H*** EXPLORER 35 THETA XB, PC3 PERIOD ***/
      DATA TGP/20H***** TIME GAP *****/
      LOGICAL ISGAPSV
      GO TO(100,200,300,1000,2000)JCODE
C
C SECTION 1 - WRITE TITLE PAGE
C
  100 CONTINUE
      WRITE(8,10)TITLE,NTAPE,COMENT
   10 FORMAT(1H1////10X,4A10/10X,*TAPE NUMBER -*,I6//10X,8A10)
      RETURN
C
C SECTION 2 - WRITE TIME INTERVAL VALUES OR AN ERROR MESSAGE
C
  200 CONTINUE
      WRITE(8,20)TITLE,NINT
   20 FORMAT(1H1,4A10//25H    * TIME INTERVAL NUMBER,I4)
C NOTE - IERROR = 1 MEANS THAT EVERYTHING IS OK.
      IF(IERROR.EQ.1)GO TO 250
      WRITE(8,30)
   30 FORMAT(///10X,*THIS INTERVAL WAS SKIPPED BECAUSE OF AN ERROR.*//
     1          10X,*SEE MONITOR LISTING FOR ERROR INFORMATION.*)
      RETURN
```

```
C WRITE OUT TIME INTERVAL VALUES.
C NOTE - LINE COUNTS PRINT LINES FOR PAGE EJECT DECISION.
C NOTE - LDAYSAV SAVES THE LAST DAY USED IN DATE PRINTOUT.
  250 CONTINUE
      LINE = 100
      LDAYSAV = -100
      CALL XDATE(NDAY1,NYEAR,MTH1,JDAY1)
      CALL IFILIN(2,JDAY1,KDAY1,MXER)
      CALL XDATE(NDAY2,NYEAR,MTH2,JDAY2)
      CALL IFILIN(2,JDAY2,KDAY2,MXER)
      WRITE(8,40)MTH1,KDAY1,NYEAR,NDAY1,NHOUR1,NMIN1,
     1           MTH2,KDAY2,NYEAR,NDAY2,NHOUR2,NMIN2
   40 FORMAT(//10X,*FROM*,I3,1H/,A2,1H/,I2,* (DAY*,I4,*)  HR*,I3,*  MIN*
     1,I3/10X,*  TO*,I3,1H/,A2,1H/,I2,* (DAY*,I4,*)  HR*,I3,*  MIN*,I3)
      RETURN
C
C SECTION 3 - DATA PRINTOUT FOR LISTOP = 1. PRINT OUT THE DATA ARRAYS.
C
  300 CONTINUE
      IF(LINE.EQ.100.OR..NOT.ISGAPSV)GO TO 310
C WRITE TIME GAP LINE
      WRITE(8,45)TGP,TGP
   45 FORMAT(14X,2A10,17X,2A10)
      LINE = LINE + 1
  310 DO 400 I=1,INDEX
C CHECK TO SEE IF NEW DATE IS REQUIRED.
      IF(LDAYSAV.EQ.LDAY(I))GO TO 320
      LDAYSAV = LDAY(I)
      CALL XDATE(LDAY(I),NYEAR,MON,MDAY)
      CALL IFILIN(2,MON,LMON,MXER)
      CALL IFILIN(2,MDAY,LMDAY,MXER)
      IF(LINE.GT.36)GO TO 330
      WRITE(8,50)LMON,LMDAY,NYEAR,LDAYSAV
   50 FORMAT(/2X,A2,1H/,A2,1H/,I2,*  DAY*,I4/)
      LINE = LINE + 3
      GO TO 350
C MAKE DECISION TO EJECT PAGE AND PRINT HEADING.
  320 IF(LINE.LT.40)GO TO 350
  330 WRITE(8,60)LMON,LMDAY,NYEAR,LDAYSAV,TITLE
   60 FORMAT(1H1,1X,A2,1H/,A2,1H/,I2,*  DAY*,I4,3X,4A10//*  SEQUENCE  HR
     1MN SC       BSW   LAMBDAB    PHIB   THBVCOS   THETABV       TPCBSW   TCYC
```

```
     2BSW*/)
      LINE = 4
C PRINT ONE LINE OF DATA
  350 CONTINUE
      WRITE(8,70)NSEQ(I),LHRMN(I),LSEC(I),BSW(I),BLMB(I),PHIB(I),
     1           TBVCS(I),THBV(I),TPCBSW(I),TCYBSW(I)
   70 FORMAT(1X,I8,3X,A4,1X,A2,1X,3F8.1,F8.3,F9.1,4X,F8.1,F9.1)
      LINE = LINE + 1
  400 CONTINUE
      RETURN
C
C SECTION 4 - TERMINATION
C
 1000 CONTINUE
      WRITE(8,80)
   80 FORMAT(1H1///43H *** ABNORMAL TERMINATION - SEE MONITOR ***)
      RETURN
 2000 CONTINUE
      WRITE(8,90)
   90 FORMAT(1H1///19H *** END OF JOB ***)
      RETURN
      END
"
      SUBROUTINE BXPPLT(MCODE)
C
C SUBROUTINE BXPPLT - J.S. BURGESS FOR EXPLORER 35 SEQUENCE AVERAGES.
C BXPPLT IS THE PLOT SUBROUTINE FOR E35BXP. VALUES OF THBV, TBVCS,
C TPCBSW, AND TCYBSW (SEE E35BXP) ARE PLOTTED AS A FUNCTION OF TIME.
C BXPPLT USES THE TRW PLOT EXECUTIVE SUBROUTINE CCP FOR THE CAL-COMP.
C AT PRESENT, THIS PROGRAM WILL NOT PLOT ACROSS THE END OF THE YEAR.
C
      COMMON/XHEAD/NTAPE,NFOT,NYEAR,COMENT(8)
      COMMON/PLOTIN/NSECIN,NFIRST,NAFTER,ITIC
      COMMON/DARRAY/INDEX,TIM(500),NSEQ(500),LDAY(500),LHRMN(500),
     1              LSEC(500),BSW(500),TPCBSW(500),TCYBSW(500),
     2              BLMB(500),PHIB(500),TBVCS(500),THBV(500),COMBAC,
     3              TOPLOT,NSEQSAV,ISGAP,ISGAPSV,MTIMSAV
      DIMENSION PTITLE(3),F1(8),F2(7),F3(2),F4(1),YTIC(1500)
      LOGICAL ISGAPSV
      DATA YTHBV,DTHBV,YTBVCS,DTBVCS,YTPCSOV,DTPCSOV,YTCYBSW,DTCYBSW
     1    / 200., -20.,  -1.0,   0.2,    0.0,    20.,    0.0,    20./
```

```
      DATA PTITLE/30H* EXP 35 THETA XB - PC3 PERIOD/
      DATA F1,F2,F3,F4/6*10H           ,12H    THETA BV,
     1                  5*10H          ,12HCOS THETA BV,
     2                    10H          ,10HTPC SOVIET,
     3                                  10H  TCYCBSW /
C
C NOTE - MCODE = 1 MEANS A NEW PLOT WILL BE SET UP.
C      - MCODE = 2 MEANS GO PLOT DATA.
C      - MCODE = 3 MEANS PLOT TIC MARKS AND ANNOTATE TIME ON PLOT.
C      - MCODE = 4 MEANS TERMINATE THE PLOT TAPE (TAPE50).
C
      GO TO(100,200,300,400)MCODE
C
C SECTION 1 - MCODE=1 - SETUP FOR A NEW PLOT.
C
  100 CONTINUE
      ISECIN = NSECIN
      IFIRST = NFIRST*60
      IAFTER = NAFTER*60
      NTIC = ITIC*60
C GET START TIME (LEFT CORNER) OF PLOT FOR GIVEN TIME INTERVAL.
      CALL MOVBAC(ISECIN,MTIMSAV,ITSTART,NSET)
      XTSTART = ITSTART
      XSECIN = ISECIN
C GET SYMBOL FREQUENCY.
      NSYM = .025*XSECIN + .5
C CALL CCP SETUP ENTRANCE.
      CALL CCP(1,  2,XTSTART,XSECIN,TIM,0,4,
     1           YTHBV,  DTHBV,  4,NSYM,  THBV,
     2          YTBVCS, DTBVCS,  0,   1, TBVCS,
     3         YTPCSOV,DTPCSOV, 45,NSYM,TPCBSW,
     4         YTCYBSW,DTCYBSW,  0,   1,TCYBSW,  30,PTITLE, 0, 0,
     5         72,F1,  62,F2,  20,F3,  10,F4)
      RETURN
C
C SECTION 2 - MCODE=2 - PLOT DATA.
C
  200 CONTINUE
      ICONECT = 0
      IF(ISGAPSV)ICONECT=1
C CALL CCP DATA ENTRANCE TO PLOT.
```

```
      CALL CCP(2,INDEX,ICONECT)
C SAVE TIME OF LAST POINT PLOTTED EACH TIME.
      ITRIGHT = TIM(INDEX) + .5
      RETURN
C
C SECTION 3 - MCODE=3 - PLOT TIC MARKS AND ANNOTATE TIME FOR THE WHOLE
C             PLOT. THIS IS THE END OF THIS PLOT.
C
  300 CONTINUE
C GET TOTAL NUMBER OF TIC MARKS AND ANNOTATIONS AND ALSO GET THE RIGHT-
C    MOST TIME (ITRIGHT) ON THE PLOT FRAME.
      LTIMSUM = ITSTART + IFIRST
      ITIMSUM = ITRIGHT - LTIMSUM
      NUMBER = ITIMSUM/IAFTER
      ITRIGHT = LTIMSUM + NUMBER*IAFTER
      IF(MOD(ITIMSUM,IAFTER).NE.0)310,320
  310 NUMBER = NUMBER + 2
      ITRIGHT = ITRIGHT + IAFTER
      GO TO 330
  320 NUMBER = NUMBER + 1
  330 NUMTIC = (ITRIGHT - ITSTART)/NTIC + 1
      IF(NUMTIC.GT.1500)NUMTIC = 1500
      DO 340 J=1,NUMTIC
  340 YTIC(J) = 0.0
      XRIGHT = ITRIGHT
      XTIC = -NTIC
C CALL CCP PARAMETER REDEFINE ENTRANCE TO SET UP TIC MARK PLOT.
      CALL CCP(-1, 2,XTSTART,XSECIN,XRIGHT,XTIC,1,0.0,100.,13,1,YTIC,
     1          0,0,0,0,0,0)
      CALL CCP(2,NUMTIC,1)
C FINISH TIC MARK LINE TO LEFT CORNER IF NECESSARY.
      IF(LTIMSUM.EQ.ITSTART)GO TO 350
      XTIC = -XTIC
      CALL CCP(-1, 2,XTSTART,XSECIN,XTSTART,XTIC,1,0.0,100.,13,1,YTIC,
     1          0,0,0,0,0,0)
      CALL CCP(2,1,0)
C
C ANNOTATE TIME ON PLOT (CCP ANNOTATION ENTRANCE).
C
  350 CONTINUE
      MDAYSAV = 0
```

```
      DO 390 I=1,NUMBER
      TOTSEC = LTIMSUM - ITSTART
      IDIS = (TOTSEC/XSECIN)*100. - 26. + .5
      CALL TIMCON(3,IFER,LTIMSUM,MDAY,MHR,MIN,MSEC,MIL)
      IF(MDAYSAV.EQ.MDAY)GO TO 370
      MDAYSAV = MDAY
C GET NEW DATE.
      CALL XDATE(MDAY,NYEAR,MONTH,MDY)
      CALL IFILIN(2,MONTH,MNTH,IXER)
      CALL IFILIN(2,MDY,LDY,IXER)
      ENCODE(8,10,DATE)MNTH,LDY,NYEAR
   10 FORMAT(A2,1H/,A2,1H/,I2)
C ANNOTATE NEW DATE - MO/DA/YR.
      CALL CCP(3,IDIS,5,.15,8,DATE)
  370 CONTINUE
      MHRMN = 100*MHR + MIN
      CALL IFILIN(4,MHRMN,KHRMN,IXER)
C ANNOTATE TIME - HRMN.
      CALL CCP(3,IDIS,30,.15,4,KHRMN)
      LTIMSUM = LTIMSUM + IAFTER
  390 CONTINUE
C CALL CCP CLEAN-UP ENTRANCE.
      CALL CCP(5,999999)
      RETURN
C
C SECTION 4 - MCODE=4 - TERMINATE PLOT TAPE.
C
  400 CONTINUE
      CALL CCP(6)
      RETURN
      END
"                                                                    "
      SUBROUTINE MOVBAC(ISECIN,MTIMSAV,ITSTART,NSET)
C
C SUBROUTINE MOVBAC - J.S. BURGESS FOR EXPLORER 35 SEQUENCE AVERAGES.
C MOVBAC CALCULATES THE START OF THE TIME AXIS ON THE CAL-COMP PLOT TO
C   THE NEAREST  10 MIN  IF    300.LE.ISECIN.LT. 1800 SEC/INCH,
C   THE NEAREST   1 HOUR  IF   1800.LE.ISECIN.LT.10800 SEC/INCH,
C   THE NEAREST   6 HOURS IF  10800.LE.ISECIN.LE.64800 SEC/INCH.
C IN THIS WAY THE TIME INTERVAL CAN BEGIN ANYWHERE, BUT THE PLOT WILL
C ALWAYS BEGIN ON SOME CONVENIENT MULTIPLE OF WHOLE MINUTES.
```

```
C MOVBAC IS CALLED FROM THE E35 PLOT EXECUTIVE SUBROUTINE, BXPPLT.
C
      DIMENSION LIMIT(2),NDIV(3)
      DATA LIMIT/1800,10800/
      DATA NDIV/600,3600,21600/
C FIND THE SET OF TIME INCREMENTS THAT CONTAINS ISECIN.
      DO 200 I=1,2
      IF(ISECIN.LT.LIMIT(I))GO TO 220
  200 CONTINUE
      I=3
C GET TIME OF LEFT CORNER OF PLOT (ITSTART)
  220 ITSTART = (MTIMSAV/NDIV(I))*NDIV(I)
      NSET = I
      RETURN
      END
"
      SUBROUTINE E35DRV(ICODE,NCODE)
C
C SUBROUTINE E35DRV - J.S. BURGESS FOR EXPLORER 35 CDC SEQUENCE AVE.
C E35DRV IS THE EXPLORER 35 CDC TAPE DRIVER PROGRAM. IT MERGES THE TAPE
C WITH SELECTED TIME INTERVALS. IN GENERAL IT READS A TIME INTERVAL,
C POSITIONS THE TAPE AND LOCATES THE START TIME, AND THEN RETURNS DATA
C RECORD BY RECORD TO A MAIN CALLING PROGRAM UNTIL THE INTERVAL HAS
C BEEN SATISFIED. A LIST OF RECORDS SUPPLIED FOR EACH INTERVAL IS
C RECORDED BY E35MON. CARD INPUT IS TAPE5, THE CDC TAPE IS TAPE6, AND
C THE MONITOR IS TAPE7. SEE E35DRV WRITE-UP FOR INSTRUCTIONS.
C
      COMMON/PLOTIN/NSECIN,NFIRST,NAFTER,ITIC
      COMMON/DATIN/INDATA(8,60)
      COMMON/DATOUT/NEWDAT(26,60),IDUM
      COMMON/XHEAD/NTAPE,NFOT,NYEAR,COMENT(8)
      COMMON/XTINT/NINT,NFILE,NRECORD,NDAY1,NHOUR1,NMIN1,NDAY2,NHOUR2,
     1             NMIN2,ISTART,IEND,IERROR,NF,NR,IFEMP
      COMMON/OPTION/LISTOP,NPLOTOP,NPLTSAV
      COMMON/XTIM/IDAY(60),ITIM(60),INSTRT,INEND,LSEQSAV
      DATA COMENT/8*10H**********/
      DATA LISTOP,NPLOTOP,NSECIN,NFIRST,NAFTER,ITIC/2,1,300,0,60,10/
      NAMELIST/HEADER/NTAPE,NFOT,NYEAR,COMENT
      NAMELIST/TIMINT/NINT,NFILE,NRECORD,NDAY1,NHOUR1,NMIN1,NDAY2,NHOUR2
     1               ,NMIN2,NYEAR,LISTOP,NPLOTOP,NSECIN,NFIRST,NAFTER,
     2                ITIC
```

```
C  ICODE MUST BE SUPPLIED BY THE CALLING PROGRAM TO DIRECT E35DRV.
      GO TO(200,300,400,500)ICODE
C
C  SECTION 1 - ICODE=1 - INITIALIZATION - READ HEADER CARD, WRITE TITLE
C              PAGE ON MONITOR, INITIALIZE RECORD AND FILE COUNTERS.
C
  200 CONTINUE
      CALL NMLEOF
      NCODE = 0
      REWIND 6
      READ(5,HEADER)
      CALL E35MON(1)
      NR = 0
      NF = 1
      RETURN
C
C  SECTION 2 - ICODE=2 - READ TIME INTERVALS AND CHECK.
C
  300 CONTINUE
      NPLTSAV = NPLOTOP
      LISTOP = 2
      NPLOTOP = 1
      LSEQSAV = 0
      READ(5,TIMINT)
      IF(EOF,5)2000,320
  320 CONTINUE
      CALL INTCHK
      CALL E35MON(2)
      RETURN
C
C  SECTION 3 - ICODE=3 - POSITION TAPE TO FILE AND RECORD CONTAINING
C              START OF INTERVAL AND READ FIRST GOOD RECORD(SEE SEC.4).
C
  400 CONTINUE
C FIND FILE.
      IF(NFILE.EQ.NF)GO TO 450
      CALL SKIPF(6,NFILE-NF)
      NR = 0
      NF = NFILE
  450 IFSAME = 1
      IF(NRECORD.EQ.NR)460,470
```

```
C IF IT GETS HERE THE RECORD HAS ALREADY BEEN READ.
  460 IFSAME = 2
      GO TO 610
C FIND RECORD.
  470 LRECORD = NRECORD - 1
      IF(LRECORD.EQ.NR)GO TO 500
      MX = LRECORD - NR
      DO 490 LX=1,MX
  490 READ(6)
      NR = LRECORD
C
C SECTION 4 - ICODE=4 - READ NEXT DATA RECORD, UNPACK AND SCAN TIMES.
C
  500 CONTINUE
      NR = NR + 1
      READ TAPE6,INDATA
      IF(EOF,6)510,600
  510 NF = NF + 1
      IF(NF.GT.NFDT)GO TO 1000
      NR = 0
      GO TO 500
C UNPACK DATA AND SEARCH FOR DATA TIMES CONTAINED IN INTERVAL.
  600 CONTINUE
      CALL UNPKEX
  610 CALL TIMEND(IFSAME,IFEMP,ISTART,IEND,NCODE)
      CALL E35MON(3,NCODE)
      IF(IFEMP.NE.3)GO TO 500
      RETURN
C
C SECTION 5 - TERMINATION
C
C NOTE - NCODE = 4 MEANS ABNORMAL TERMINATION - EOF REACHED ON TAPE6.
C        NCODE = 5 MEANS NORMAL TERMINATION - EOF REACHED ON TAPE5.
C
 1000 CONTINUE
      REWIND 6
      CALL E35MON(4)
      NCODE = 4
      RETURN
 2000 CONTINUE
      REWIND 6
```

```
      CALL E35MON(5)
      NCODE = 5
      RETURN
      END
"                                                                    "
      SUBROUTINE INTCHK
C
C SUBROUTINE INTCHK - J.S. BURGESS FOR EXPLORER 35 SEQUENCE AVE.
C INTCHK DOES ROUTINE CHECKING FO TIME INTERVAL INPUT FOR E35DRV,
C THE EXPLORER 35 CDC TAPE DRIVER SUBROUTINE. IT RETURNS THE STATUS
C OF THE INPUT DATA THROUGH THE PARAMETER IERROR. ERROR MESSAGES
C CAN BE FOUND IN THE SUBROUTINE E35MON. INTCHK ALSO CALCULATES
C START AND STOP TIMES OF THE INTERVAL IN TOTAL SECONDS.
C
      COMMON/PLOTIN/NSECIN,NFIRST,NAFTER,ITIC
      COMMON/XHEAD/NTAPE,NFOT,NYEAR,COMENT(8)
      COMMON/XTINT/NINT,NFILE,NRECORD,NDAY1,NHOUR1,NMIN1,NDAY2,NHOUR2,
     I             NMIN2,ISTART,IEND,IERROR,NF,NR,IFEMP
      COMMON/OPTION/LISTOP,NPLOTOP,NPLTSAV
C CHECK OPTION VALUES.
      IF(LISTOP.EQ.1.OR.LISTOP.EQ.2)100,120
  100 IF(NPLOTOP.GT.0.AND.NPLOTOP.LE.3)150,120
  120 IERROR = 7
      RETURN
C CHECK VALUE OF NFILE (FILE CONTAINING START TIME OF THE INTERVAL).
  150 IF(NFILE.LE.NFOT)GO TO 160
      IERROR = 6
      RETURN
C CHECK POSITION OF TAPE RELATIVE TO NFILE (NF IS CURRENT POSITION).
  160 IF(NFILE.GE.NF)GO TO 170
      IERROR = 4
      RETURN
C CHECK POSITION OF TAPE RELATIVE TO NRECORD (IF NFILE=NF).
  170 IF(NFILE.NE.NF)GO TO 180
      IF(NRECORD.GE.NR)GO TO 180
      IERROR = 5
      RETURN
C CALCULATE START AND STOP TIMES OF TIME INTERVAL IN TOTAL SECONDS.
  180 CONTINUE
      CALL TIMCON(-3,IFER,ISTART,NDAY1,NHOUR1,NMIN1,0)
      CALL TIMCON(-3,IFER,IEND,NDAY2,NHOUR2,NMIN2,0)
```

```
C MAKE SURE START TIME IS LESS THAN STOP TIME.
      IF(IEND.GT.ISTART)GO TO 190
      IERROR = 3
      RETURN
C MAKE SURE TIMES ARE IN RANGE OF YEAR.
  190 NSCINYR = 31536000
      IF(MOD(NYEAR,4).EQ.0)NSCINYR=31622400
      IF(IEND.LT.NSCINYR)GO TO 200
      IERROR = 2
      RETURN
C ARE THERE PLOT VALUES TO CHECK.
  200 IF(NPLOTOP.NE.1)GO TO 300
      NSECIN = 0
      NFIRST = 0
      NAFTER = 0
      ITIC   = 0
      GO TO 1000
  300 IF(NPLTSAV.EQ.3)GO TO 345
C CHECK RANGE OF TIME INCREMENT PER INCH VALUE.
      IF(NSECIN.GE.300.AND.NSECIN.LE.64800)GO TO 310
      IERROR = 8
      RETURN
C CHECK RANGE OF FIRST ANNOTATION INCREMENT.
  310 IF(NFIRST.GE.0.AND.NFIRST.LE.1440)GO TO 320
      IERROR = 9
      RETURN
C CHECK RANGE OF FOLLOWING ANNOTATION INCREMENT.
  320 IF(NAFTER.GE.5.AND.NAFTER.LE.25920)GO TO 330
      IERROR = 10
      RETURN
C CHECK TIC MARK INCREMENT VALUE.
  330 IF(ITIC.GT.0.AND.MOD(NAFTER,ITIC).EQ.0)GO TO 340
  335 IERROR = 11
      RETURN
  340 NSTART = ISTART
  345 ITIMTOT = IEND - NSTART + NAFTER*60
      IF(ITIMTOT/(ITIC*60).GT.1500)GO TO 335
C EVERYTHING APPEARS TO BE OK.
 1000 IERROR = 1
      RETURN
      END
```

```
      SUBROUTINE E35MON(LCODE,NCODE)
C
C SUBROUTINE E35MON - J.S. BURGESS FOR EXPLORER 35 CDC SEQUENCE AVE.
C E35MON IS A LISTING SUBROUTINE CALLED FROM E35DRV, THE EXPLORER 35
C CDC TAPE DRIVER PROGRAM. THE PRIMARY FUNCTION OF E35MON IS TO MAKE
C A LISTING OF ALL RECORDS ACCEPTED BY E35DRV AS VALID INPUT FOR THE
C CURRENT TIME INTERVAL. IT ALSO LISTS VALUES OF INTERVAL INPUT AND
C WRITES VARIOUS ERROR MESSAGES.
C
      COMMON/PLOTIN/NSECIN,NFIRST,NAFTER,ITIC
      COMMON/XHEAD/NTAPE,NFOT,NYEAR,COMENT(8)
      COMMON/XTINT/NINT,NFILE,NRECORD,NDAY1,NHOUR1,NMIN1,NDAY2,NHOUR2,
     1             NMIN2,ISTART,IEND,IERROR,NF,NR,IFEMP
      COMMON/OPTION/LISTOP,NPLOTOP,NPLTSAV
      COMMON/DATOUT/NEWDAT(26,60),IDUM
      COMMON/XTIM/IDAY(60),ITIM(60),INSTRT,INEND,LSEQSAV
      DIMENSION ERRMES(3,11),ERRIND(2),MLERR(3,2)
      DATA ERRIND/10H0*********,10H0* ERROR */
      DATA ERRMES/30H*** OK ****** OK ****** OK ***,
     1            30HTIME IS OUT OF RANGE OF YEAR. ,
     2            30HTIME 2 IS LESS THAN TIME 1.   ,
     3            30HTAPE POSITION IS PAST NFILE.  ,
     4            30HTAPE POSITION IS PAST NRECORD.,
     5            30HNFILE IS GREATER THAN NFOT.   ,
     6            30HOPTION VALUE IS OUT OF RANGE. ,
     7            30HNSECIN IS OUT OF RANGE.       ,
     8            30HNFIRST IS OUT OF RANGE.       ,
     9            30HNAFTER IS OUT OF RANGE.       ,
     A            30HITIC IS NOT ACCEPTABLE.       /
      DATA MLERR/30H***** OVERLAP OR NO TIME MATCH,
     1           30H***** RECORD HAS ALL BAD TIMES/
      GO TO(100,200,200,1000,2000)LCODE
C
C SECTION 1 - WRITE TITLE PAGE.
C
  100 CONTINUE
      WRITE(7,10)NTAPE,NFOT,NYEAR,COMENT
   10 FORMAT(1H1////10X,32H**** E35DRV MONITOR LISTING ****
     1            //15X,        *TAPE NUMBER -*,I7
     2            //15X,        *NUMBER OF FILES -*,I3
```

BEST PRODUCIBILITY OF THE ORIGINAL PAGE IS POOR

```
     3              //15X,        *YEAR OF DATA =*,I6//10X,8A10)
      LINE = 100
      RETURN
C
C SECTION 2 - WRITE PAGE HEADING.
C
  200 CONTINUE
      IF(LINE.LT.40)GO TO(100,300,400)LCODE
      LINE = 2
      WRITE(7,20)
   20 FORMAT(1H1,* INT FILE REC  START-SEQUENCE DAY HR MN SC  END-SEQUEN
     1CE   DAY HR MN SC NCODE     ISTART    TIME1     TIME2      IEND*/)
      GO TO(100,300,400)LCODE
C
C SECTION 3 - WRITE TIME INTERVAL VALUES AND ANY ERROR MESSAGE.
C
  300 CONTINUE
      IER = 1
      IF(IERROR.GT.1)IER = 2
      WRITE(7,30)ERRIND(IER),NINT,NFILE,NRECORD,NDAY1,NHOUR1,NMIN1,
     1           NDAY2,NHOUR2,NMIN2,NYEAR,LISTOP,NPLOTOP,NPLTSAV,
     2           (ERRMES(LM,IERROR),LM=1,3),IERROR,NSECIN,NFIRST,NAFTER,
     3           ITIC
   30 FORMAT(A10,I5,* NFILE=*,I3,* NRECORD=*,I4,1H,,I5,2I4,1X,I5,2I4,
     1       *  NYEAR=*,I5,1H,,3I3,1X,3A10,I5/16X,*NSECIN=*,I9,1H,,
     2       *  NFIRST=*,I9,1H,,*  NAFTER=*,I9,1H,,*  ITIC=*,I9)
      LINE = LINE + 3
      RETURN
C
C SECTION 4 - WRITE ONE MONITOR LINE OR ERROR MESSAGE.
C
  400 CONTINUE
      LINE = LINE + 1
      IF(IFEMP.EQ.3)GO TO 450
      WRITE(7,35)NINT,NF,NR,(MLERR(LM,IFEMP),LM=1,3)
   35 FORMAT(1X,2I4,I5,2X,3A10)
      RETURN
  450 CONTINUE
      IF(NCODE.EQ.3)GO TO 500
      WRITE(7,40)NINT,NF,NR,INSTRT,NEWDAT(1,INSTRT),IDAY(INSTRT),
     1           NEWDAT(3,INSTRT),NEWDAT(4,INSTRT),NEWDAT(5,INSTRT),
```

```
     2             INEND,NEWDAT(1,INEND),IDAY(INEND),NEWDAT(3,INEND),
     3             NEWDAT(4,INEND),NEWDAT(5,INEND),NCODE,ISTART,
     4             ITIM(INSTRT),ITIM(INEND),IEND
  40 FORMAT(1X,2I4,I5,2(*  S(*,I2,*)=*,I7,I5,3I3),I4,3X,4I10)
     RETURN
 500 CONTINUE
     WRITE(7,50)NINT,NF,NR
  50 FORMAT(1X,2I4,I5,2X,*ALL OF THIS RECORD PAST END OF INTERVAL*)
     RETURN
C
C SECTION 5 - WRITE TERMINATION MESSAGE.
C
1000 CONTINUE
     WRITE(7,60)NINT,NF
  60 FORMAT(1H1///* ABNORMAL TERMINATION*/* END OF TAPE REACHED IN INTE
    IRVAL NO.*,I4/* NF =*,I4)
     RETURN
2000 CONTINUE
     WRITE(7,70)
  70 FORMAT(1H1///* NORMAL TERMINATION*)
     RETURN
     END
"                                                                    "
     SUBROUTINE TIMEND(IFSAME,IFEMP,ISTART,IEND,NCODE)
C
C SUBROUTINE TIMEND - J.S. BURGESS FOR EXPLORER 35 SEQUENCE AVE.
C TIMEND IS CALLED FROM E35DRV TO DETERMINE THE FIRST (INSTRT) AND
C LAST (INEND) SEQUENCES (FROM A DATA RECORD OF 60 SEQUENCES) THAT ARE
C CONTAINED IN THE CURRENT TIME INTERVAL. TIMEND ALSO REMOVES OVERLAP,
C CALCULATES EACH TIME IN TOTAL SECONDS, GETS ACTUAL DAY OF YEAR, AND
C DETERMINES IF THE END OF THE TIME INTERVAL HAS BEEN REACHED.
C
     COMMON/DATOUT/NEWDAT(26,60),IDUM
     COMMON/XTIM/IDAY(60),ITIM(60),INSTRT,INEND,LSEQSAV
C NOTE - IFSAME = 1 MEANS RECORD CHECK AND TIME CALCULATIONS MUST BE
C          MADE FOR THE CURRENT DATA RECORD.
C        - IFSAME = 2 MEANS THAT A NEW TIME INTERVAL BEGINS IN THE SAME
C          RECORD JUST PROCESSED BY TIMEND, SO SKIP SECTION 1.
     GO TO(100,400)IFSAME
C
C SECTION 1 - TIME CALCULATIONS.
```

ORIGINAL PAGE IS POOR

```
C
  100 CONTINUE
C FIND LAST GOOD TIME IN RECORD.
      DO 200 I=1,60
      IF(NEWDAT(1,61-I).EQ.999999.AND.NEWDAT(5,61-I).EQ.0)GO TO 200
      GO TO 210
  200 CONTINUE
C NOTE - IFEMP = 2 MEANS NO GOOD TIMES. RETURN FOR NEW RECORD.
      IFEMP = 2
      RETURN
  210 LASTIM = 61-I
C ELIMINATE OVERLAP AT END OF RECORD.
      IF(LASTIM.LT.2)GO TO 290
      DO 250 I=2,LASTIM
      IF(NEWDAT(1,I).GT.NEWDAT(1,I-1))GO TO 250
      IF(NEWDAT(1,I).LT.1000.AND.NEWDAT(1,I-1).GT.999000)250,270
  250 CONTINUE
      GO TO 290
  270 LASTIM = I-1
  290 CONTINUE
C GET ACTUAL DAY OF YEAR AND CALCULATE SEQUENCE TIMES IN TOTAL SECONDS.
      DO 300 I=1,LASTIM
      IDAY(I) = NEWDAT(2,I) + 1
      CALL TIMCON(-3,IFER,ITIM(I),IDAY(I),NEWDAT(3,I),NEWDAT(4,I),NEWDAT
     1(5,I))
  300 CONTINUE
      GO TO 410
C
C SECTION 2 - DETERMINE INSTRT AND INEND
C
  400 CONTINUE
      IFSAME = 1
C NOTE - IFEMP = 3 MEANS EVERYTHING IS OK.
  410 IFEMP = 3
C FIND FIRST SEQUENCE TIME IN TIME INTERVAL.
      DO 500 I=1,LASTIM
      IF(NEWDAT(1,I).GT.LSEQSAV)GO TO 490
      IF(NEWDAT(1,I).LT.1000.AND.LSEQSAV.GT.999000)490,500
  490 IF(ITIM(I).GE.ISTART)GO TO 510
  500 CONTINUE
C NOTE - IFEMP = 1 MEANS ALL OF TIMES IN RECORD ARE BEFORE THE START OF
```

```
C          THE CURRENT TIME INTERVAL. RETURN FOR A NEW RECORD.
      IFEMP = 1
      RETURN
  510 INSTRT = I
      MTIMFIX = LASTIM+1-INSTRT
      ILASTIM = LASTIM+1
C FIND LAST SEQUENCE TIME IN TIME INTERVAL.
      DO 600 I=1,MTIMFIX
      IF(ITIM(ILASTIM-I).LE.IEND)GO TO 610
  600 CONTINUE
C NOTE - NCODE = 3 MEANS THAT ALL SEQUENCE TIMES ARE BEYOND THE END TIME
C          OF THE CURRENT TIME INTERVAL. THEREFORE, THE END HAS BEEN
C          REACHED AND THERE IS NO NEW DATA FOR PROCESSING.
      NCODE = 3
      RETURN
  610 INEND = ILASTIM-I
      IF(INEND.LT.LASTIM.OR.ITIM(INEND).EQ.IEND)620,630
C NOTE - NCODE = 2 MEANS THAT THE END OF THE TIME INTERVAL HAS BEEN
C          DETECTED, BUT THERE IS SOME NEW DATA FOR PROCESSING.
  620 NCODE = 2
      RETURN
C NOTE - NCODE = 1 MEANS THERE IS NEW DATA FOR PROCESSING AND THE END
C          OF THE TIME INTERVAL HAS NOT BEEN DETECTED.
  630 NCODE = 1
      LSEQSAV = NEWDAT(I,INEND)
      RETURN
      END
```

CARD COUNT 889

APPENDIX B

THE UPSTREAM ESCAPE OF ENERGIZED SOLAR WIND PROTONS FROM THE BOW SHOCK

21333-6014-RU-00

THE UPSTREAM ESCAPE OF ENERGIZED SOLAR WIND PROTONS FROM THE BOW SHOCK

by

Eugene W. Greenstadt

Space Sciences Department
TRW Systems Group

Presented at

The Neil Brice Memorial Symposium
Magnetospheres of Earth and Jupiter
Frascati, Italy
28 May-1 June 1974

May 1974

Space Sciences Department

TRW Systems Group
One Space Park
Redondo Beach, California 90278

THE UPSTREAM ESCAPE OF ENERGIZED SOLAR WIND PROTONS FROM THE BOW SHOCK

by

Eugene W. Greenstadt

Space Sciences Department
TRW Systems Group
Redondo Beach, California 90278

ABSTRACT

Protons of energies up to 100 Kev have been consistently observed traveling upwind from the bow shock in the solar wind. The conditions determined by the geometry of escape are defined and the resulting restrictions on pitch angles and total energies are computed. It is found that backstreaming protons of observed total energies are compatible with typical angles of the upstream-wave region boundary but that geometrical conditions alone do not select the boundary angle. It is also found that the high energies of 30-100 Kev, the 100 Kev cutoff, and the pitch angles of 60°-90° reported recently by Lin, Meng, and Anderson are compatible with the conditions imposed by escape geometry.

INTRODUCTION

A constellation of field and particle precursors has been identified upstream from the earth's bow shock. Backstreaming 2-7 keV protons (Asbridge et al., 1968; Scarf et al., 1970) and electrons (Anderson, 1969; Feldman et al., 1973) have been identified directly, and an association between backstreaming protons and electric and hydromagnetic precursor waves has been found emperically (Scarf et al., 1971; Fredricks et al., 1972) and explored theoretically (Fredricks et al., 1971; Barnes, 1970; Fredricks, 1974). In addition, the coincident occurrence of hydromagnetic precursors, "pulsation," or relation, shock structure, and quasi-parallel field orientation has been documented (Greenstadt et al., 1970a; Greenstadt, 1972b), and it has been concluded that the longest-period hydromagnetic precursors could not have propagated upstream from the shock, but must have been generated upstream by some other agency and swept downstream with the solar wind (Greenstadt et al., 1970b; Fairfield, 1969). Finally, it has been shown that protons reflected from the bow shock should be accelerated by the interplanetary electric field, seen in the shock frame, to energies comparable to those observed by plasma experiments (Sonnerup, 1969). These energies correspond to particles traveling along $\underline{B}$ at velocities comparable to the rate at which locally-excited hydromagnetic precursor waves appear to progress upstream (Greenstadt et al., 1970b).

Despite the seemingly tight logic by which the foregoing results might be taken to imply that quasi-parallel geometry, reflected particles, hydromagnetic precursors, and relaxation shocks are all aspects of the same phenomenon, the circle has never been closed experimentally: for example, no report has been

published showing protons of the proper velocity component along $\underset{\sim}{B}$ being observed simultaneously with precursor waves progressing upstream at the same rate in the appropriate magnetic geometry. Even statistical data on the energies of reflected ions or the rates of precursor progression as functions of location of the point of origin on the bow shock are unreported. Recently, some difficulty in connecting upstream waves with particles has developed out of the systematic observation of backstreaming protons with parallel velocity components and total energies much too high to be associated with the usual long-period upstream waves (Lin et al., 1974). Thus, there is need for a fresh effort to examine the relationship between reverse flowing protons, upstream waves, shock structure, and reflected-particle energization.

This report sets forth an initial attack on a fairly straightforward part of the problem: To what extent does the geometry of individual particle motion alone select among reflected particles those that can escape upstream and those that cannot?

In the following paragraphs, the geometry of escape is described and some simple numerical examples are worked out for a few special cases. It is found that finite pitch angles are compatible with, and, indeed, necessary to produce experimentally-observed particle energies for protons moving along $\underset{\sim}{B}$ at typical wave generation advance rates or, equivalently, for protons appearing upstream on field lines making specified maximal angles with the local shock normal. It is found that geometrical restrictions do not select particles with any particular parallel speed and thus do not explain the observed upstream wave cutoff at field-normal angles of about 50° and, consequently, do not single out any particular group of particles responsible for upstream wave generation.

Somewhat surprisingly, protons with rather high energies and pitch angles can escape the shock at only marginally quasi-parallel field orientations (i.e., $\theta_{nB} \approx 50°$), if they have quite moderate speeds parallel to $\underset{\sim}{B}$.

Frequent reference is made in the text, for purposes of example, to the "Vela-Explorer case." By this is meant the only instance in which the upstream wave progression rate has been measured at a specific location on the shock (Greenstadt et al., 1970b).

THE GEOMETRY OF ESCAPE

Assumptions, Conventions, and Definitions

For simplicity, we place ourselves exclusively in the ecliptic plane so that we have an observation point on the ecliptic outside the shock. Solar wind velocity and field vectors $\underset{\sim}{V}_{SW}$ and $\underset{\sim}{B}_{SW}$ are assumed in the ecliptic, and we deal with the shock locally only as a plane whose unit normal lies in the ecliptic. It is convenient to work with dimensionless ratios and at the same time not unreasonable to suppose that reflected particle velocities are proportional to the solar wind velocity, so we dimension all velocities and energies by reference to V_{SW}, and adopt the convention that the projection $u_{\parallel}$ of a reflected particle's velocity on $\underset{\sim}{B}_{SW}$ is a product of some scalar p and V_{SW}, i.e., $u_{\parallel} = pV_{SW}$. Thermal velocities can also be written as a fraction of V_{SW}, should they need to be taken into account. If the particle also has a velocity $u_{\perp}$ perpendicular to $\underset{\sim}{B}_{SW}$, we shall set $u_{\perp} \equiv PV_{SW}$ and note that $u_{\parallel}$ is the guiding center velocity in the plasma frame and the particle has pitch angle $\alpha = \arctan \frac{u_{\perp}}{u_{\parallel}} = \arctan P/p$, also in the plasma (solar wind) frame.

The left side of Figure 1 defines a set of quantities to be used in this report. The curve represents the ecliptic intersection of the bow shock; $\underset{\sim}{n}$

is the local normal at a point located at angle θ_{XR} from the sun-earth line (X-axis). The shock is taken to be symmetric about the X axis and is given by $Y^2 = .331\left[(X-75.25)^2 - 3686\right]$. This is a symmetrized version of Fairfield's (1971) average shock used in an earlier paper (Greenstadt, 1972a). The right panel of Figure 1 is a plot of θ_{Xn} vs θ_{XR} for the dawn side of the given symmetric shock. It will be useful to refer to Figure 1 in reading the following analysis.

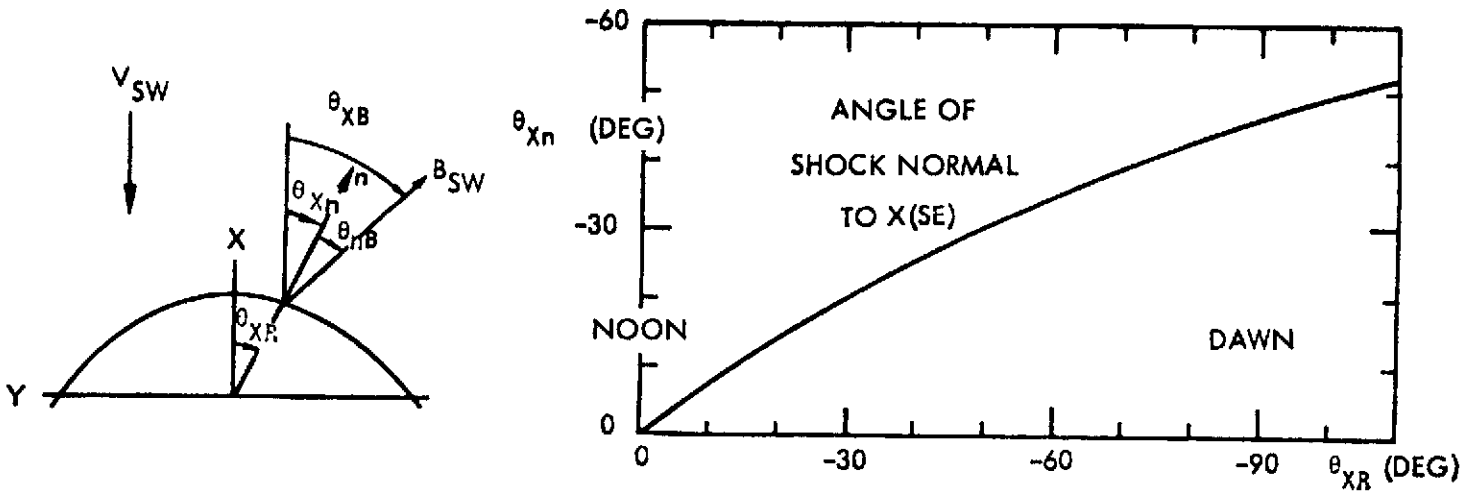

Figure 1

Negligible Pitch Angle

If a reflected proton travels in the ecliptic exactly along $\underset{\sim}{B}_{SW}$, then P = 0 and its velocity $\underset{\sim}{V}_r$ as measured by a satellite sensor in the bow shock's frame is $\underset{\sim}{V}_r = pV_{SW}\hat{\underset{\sim}{B}}_{SW} + \underset{\sim}{V}_{SW} = pV_{SW}\,(\cos\theta_{XB}, -\sin\theta_{XB}, 0) + V_{SW}(-1,0,0) = V_{SW}(p\cos\theta_{XB} - 1, -p\sin\theta_{XB}, 0)$. Its energy ratio is $E_r/E_{SW} = p^2 + 1 - 2p\cdot\cos\theta_{XB}$. The numerical result for the Vela-Explorer case (Greenstadt et al., 1970b) is instructive: There, at the time the upstream wave advance rate was

measured, $\theta_{XB} = 58°.5$. Figure 2 shows E_r/E_{SW} as a function of p for this angle. The value p = 1.6 found there would correspond to $E_r/E_{SW} = 1.8$ if reflected particles were responsible for the appearance of the waves. This is appreciably lower than energy ratios of backstreaming protons measured by Vela (Asbridge et al., 1968) or furnished by equation (5) of Sonnerup (1969), which gives $E_r/E_{SW} = 3.25$ when evaluated at $\psi = 58°.5$, $\phi = 21°.5$, $\delta = 1/2$, $\mu = \gamma = 0$. In the notation of this report, $\psi = \theta_{XB}$, $\phi = \theta_{Xn}$, $\psi - \phi = \theta_{nB}$.

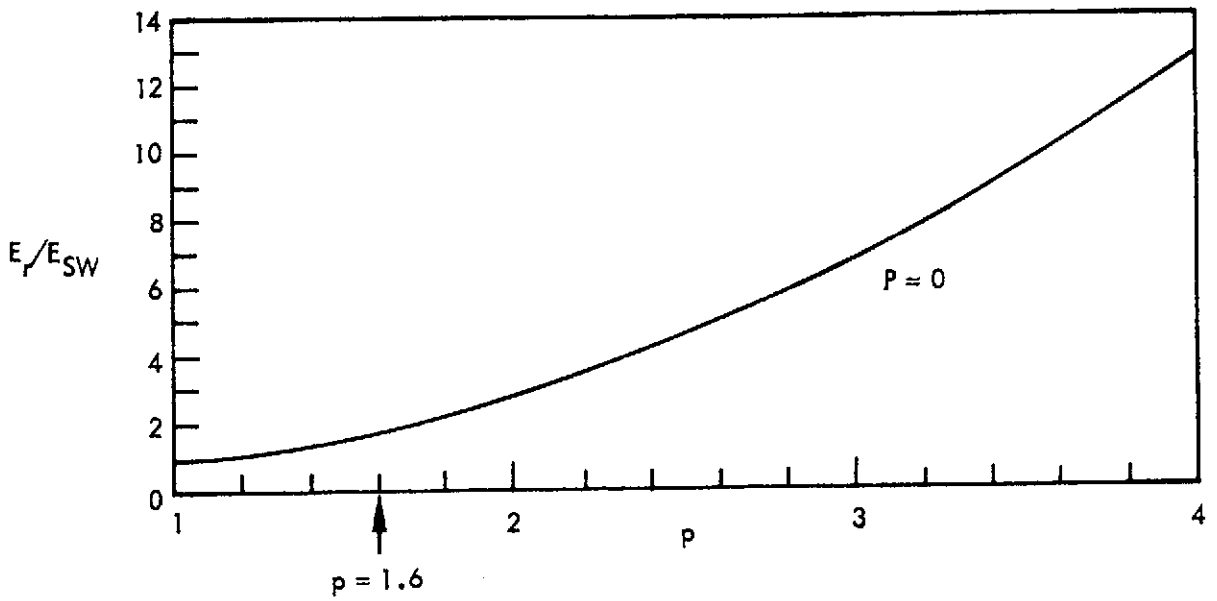

Figure 2

These comparisons suggest that P = 0 is a poor approximation to use. The relative positions of shock and satellite in the dual satellite case and the cases reported by Asbridge et al. are unknown, however, so direct comparison is impossible. Nevertheless, a simple geometric generalization confirms the indication that $P \neq 0$ if upstream waves and protons are tightly bound to each other. Figure 3 displays E_r/E_{SW} for P = 0 at various positions

along the ecliptic profile of the shock in the western hemisphere, at what, judging by statistics of upstream wave and pulsation shock geometry, should be an improbably high cutoff angle, $\theta_{nB} = 60°$. Position on the shock is designated by θ_{XR} (see Figure 1). A high cutoff angle tilts the field toward the antisolar direction, raising the total energy sensed by a sun-oriented detector for particles traveling along $\underset{\sim}{B}_{SW}$. We see in Figure 3 that not until near the dawn meridian ($\theta_{XR} = -60°$), and only with $p \gtrsim 1.9$, does E_r/E_{SW} equal 5 for $\theta_{nB} = 60°$. The morning measurements reported by Vela were taken at about this position and found $E_r/E_{SW} \approx 5$, which would be compatible with such a combination, i.e., $\theta_{XR} \simeq -60°$, $\theta_{nB} = 60°$, $p = 1.9$, $P = 0$, but would be too high for any $p < 1.9$, or $\theta_{nB} < 60°$. If we assume morning-afternoon symmetry when backstreaming protons are detected in the afternoon quadrant, then one of the Vela cases, at $\theta_{XR} = 53°$, gave a value $E_r/E_{SW} \approx 6.5$ much too high for $\theta_{nB} < 60°$ or $p \lesssim 2.3$. The limited statistic on p, which has been fairly effective at correlating quasiparallel structure when $p = 1.6$, and the more extensive statistic on upstream wave cutoff, which usually occurs at $40° \lesssim \theta_{nB} \lesssim 50°$, suggest that the observed reflected proton energies were above those allowed by the calculation of Figure 3, and cannot have been produced by particles traveling parallel to $\underset{\sim}{B}_{SW}$ only. It would follow that $P \neq 0$. This suggestion is virtually certified by the recent work of Lin et al. (1974) describing backstreaming protons with high pitch angles and E_r/E_{SW} up to 100 Kev forward of the bow shock at $\theta_{nB} \approx 45°$. We shall return to this observation later.

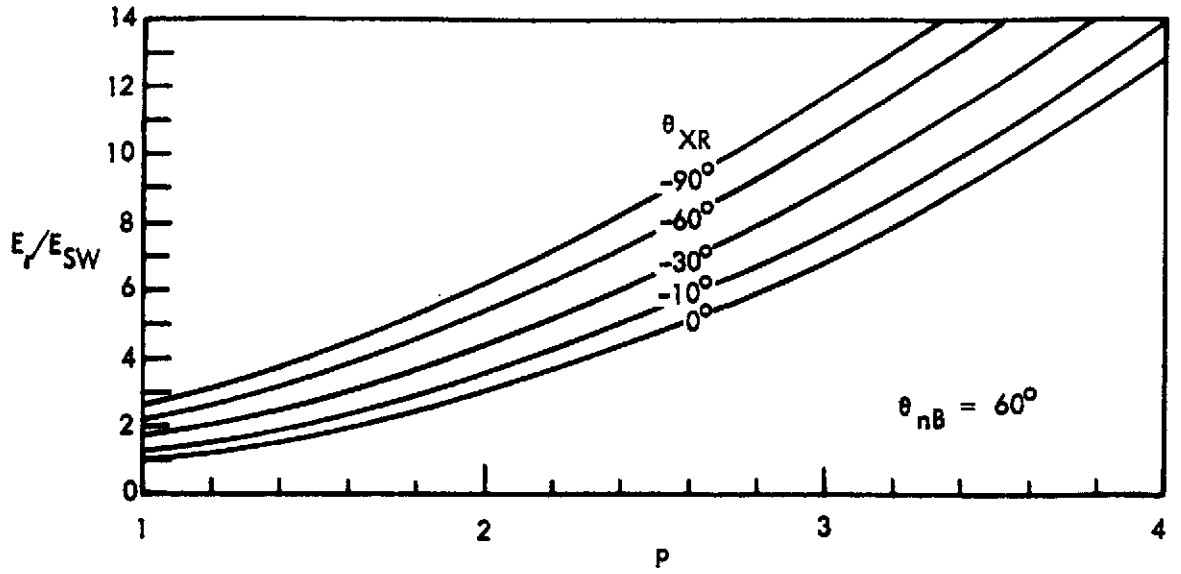

Figure 3

So far, we have simply rummaged in the available data for some empirical support for what must anyway be an intuitively incontroversial notion: reflected particles are unlikely to leave the shock exclusively at zero pitch angle in the plasma frame. The general case, $P \neq 0$, can be developed, however, by building on the geometric foundation already set forth.

Finite Pitch Angle

New terms used in the following paragraphs are defined in Figure 4. The ecliptic plane contains $\underset{\sim}{X}$, $\underset{\sim}{Y}$, $\underset{\sim}{B}$, $\underset{\sim}{B}_{\perp}$, and $\underset{\sim}{n}$, and $\underset{\sim}{Z}$ is the usual ecliptic pole. The solar wind impacts the shock at velocity $\underset{\sim}{V}_{SW}$ along $-\underset{\sim}{X}$. The insert shows the common $XYBB_{\perp}n$ plane looking down in the direction of negative $\underset{\sim}{Z}$. We are interested in a proton whose trajectory, given by the vector $\underset{\sim}{S}$ from the origin, follows a spiral along $\underset{\sim}{B}$ away from the shock, as depicted. Its guiding center has speed $u_{\parallel} = pV_{SW}$, and its Larmor radius is $a_c = u_{\perp}/\omega_c = PV_{SW}/\omega_c$. We shall enhance the clarity of the ensuing discussion by treating

the unshocked plasma as if at rest at zero temperature, so the shock, moving upward along $\underset{\sim}{n}$ at speed $V_{SW} \cos \theta_{Xn}$, encounters protons at rest, some of which are picked up by the shock, accelerated, and emitted, like our test particle, at phase ϕ and time $t = 0$. These protons spiral up $\underset{\sim}{B}_{SW}$ with the shock in pursuit. Phase angle ϕ is defined as 0 when $\underset{\sim}{u}_{\perp}$ is parallel to $\hat{\underset{\sim}{B}}_{\perp}$, i.e., when the reflected proton escapes the shock at $\underset{\sim}{S}(X,Y,Z) = (0,0,a_c)$.

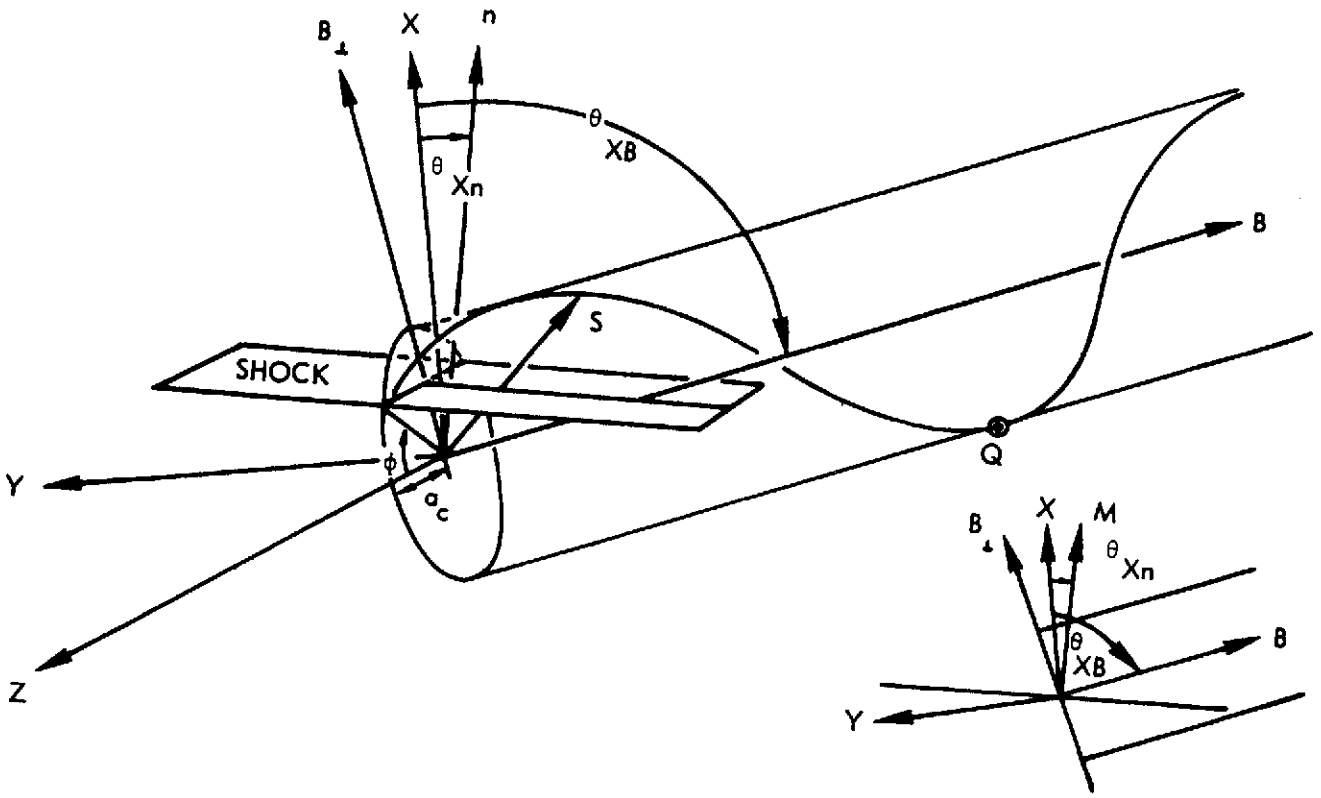

Figure 4

We are interested in those protons that are not overtaken by the shock after they begin their corkscrew journey away from it. These are the particles that will be detected far upstream and with which we continue to

assume that upstream waves are associated. The condition for "free escape" is $\underset{\sim}{S}\cdot\underset{\sim}{n} > V_{SW}t \cos \theta_{Xn}$ for all $t > 0$. Note that a proton is most vulnerable to recapture when it circles around to the "bottom" of its spiral the first time ($\phi + \omega_c t \approx 2\pi$), shown as point Q in Figure 4. It should be intuitive that only some ratios P/p will permit free escape. It is less obvious that phase ϕ at $t = 0$ strongly influences the acceptable range of P/p. If $S_n \equiv \underset{\sim}{S}\cdot\underset{\sim}{n}$, the condition previously stated can be written $S_n(t) - S_n(0) > V_{SW}t \cos \theta_{Xn}$, which, when expanded, yields the inequality:

$$P \sin \theta_{nB} \frac{\sin (\omega_c t+\phi) - \sin \phi}{\omega_c t} + (p \cos \theta_{nB} - \cos \theta_{Xn}) > 0 \ . \qquad (1)$$

Combinations of p, P, and ϕ which satisfy this relation for all t define the free escape particles. Actually, the above expression places a maximum limit on $P/p > 0$ for each value of t, but since the inequality must be satisfied for all t, there is a least such maximum limit for any given ϕ.

NUMERICAL EXAMPLES

The Observed Case p = 1.6

To make the foregoing result more concrete, we turn again to the Vela-Explorer dual satellite example where $\theta_{nB} = 37°$, $\theta_{Xn} = 21°.5$, $\theta_{XB} = 58°.5$, and $p = 1.6$. Figure 5 shows a vector velocity diagram on a polar plot of P vs ϕ for these parameters. The length of each arrow indicates the greatest relative velocity $P = u_{\perp}/V_{SW}$ a proton may have to escape the shock if it emerges at $t = 0$ at the phase position represented by the tail end of the arrow. In the figure, we are looking backward along $\underset{\sim}{B}_{SW}$ at the projection of the proton's Larmor circle on a plane perpendicular to $\underset{\sim}{B}_{SW}$; arrows are placed at 30° phase increments.

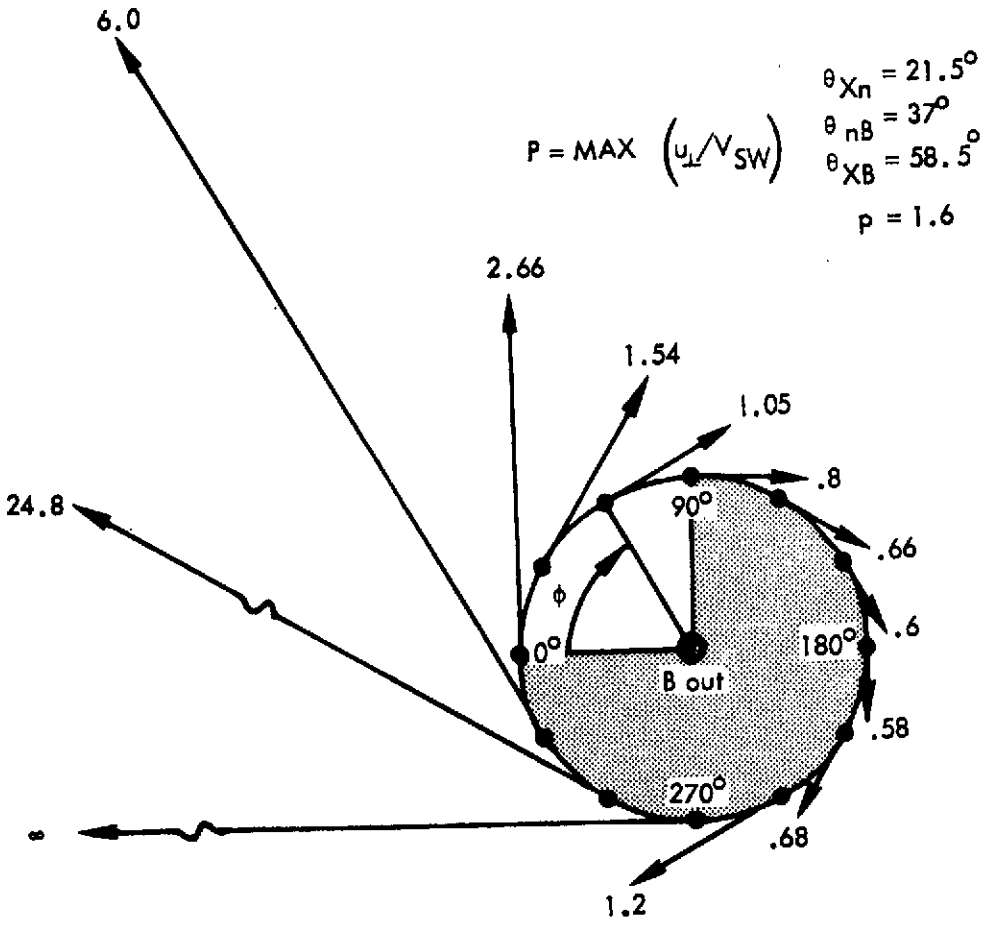

Figure 5

The computation summarized in Figure 5 allows a wide range of possible maximum P for arbitrary ϕ. The outcome can be narrowed significantly, however, by reasoning that a stationary proton, initially captured, according to assumption, by the shock at relative normal speed $V_{SW} \cos \theta_{Xn}$, will enter the shock layer at $\phi = 180°$ and emerge after one-half to one cyclotron orbit at $0° \lesssim \phi \lesssim 90°$. Subject to this argument, P would take on values up to about 2.7.

The energy ratio of a reflected proton of finite pitch angle measured by a directionally-sensitive detector, and its direction of arrival, will depend on the phase ϕ_D of the spiralling particle at its instant of detection and on the angle θ_{XB} the interplanetary field makes with the solar wind flow (along X):

$$E_r/E_{SW} = p^2 + P^2 + 1 - 2\ (p \cos \theta_{XB} + P \cos \phi_D \sin \theta_{XB}).$$

If ϕ_D is 0 when the proton is at the sunward extreme of its Larmor spiral, the highest value of E_r/E_{SW} is achieved when $\phi_D = \pi$, and the lowest when $\phi_D = 0$. Figure 6 shows the behavior of the maximum and minimum of E_r/E_{SW} vs p for $\phi_D = \pi$ and 0, respectively, when P takes on its maximum values of 2.66 and .8 at $\phi = 0°$ and 90°. The P = 0 result of Figure 2 is repeated as the dashed curve, for comparison. Obviously, introduction of the limiting P value for reflected protons raises appreciably the possible measured energy of escaping particles over that permitted when P = 0. In fact, at p = 1.6 there is no difficulty in providing backstreaming protons of energy 6 kev or more (such as those recorded by Vela) for $\phi_D = \pi$, $\phi = 0°$. One may interpolate visually to appreciate that the same is true for a range of $\phi_D < \pi$, $\phi > 0°$ as well.

The Subsolar Point

Another specialized case of considerably more general interest is illustrated in Figure 7. Here, the curves represent the maximal detectable energy ratio E_r/E_{SW} (at $\phi_D = \pi$) of protons reflected from the subsolar point of the shock ($\theta_{XR} = \theta_{Xn} = 0$) and traveling along $\underset{\sim}{B}_{SW}$ at the forward edge of the upstream particle (= wave?) region. Exit phases $\phi = 0$ and 90°, with three possible cutoff angles θ_{nB} for each phase, are shown. To clarify the interpretation of Figure 7 by specific example, suppose a satellite-borne proton detector is located in the ecliptic upstream from the bow shock, westward and

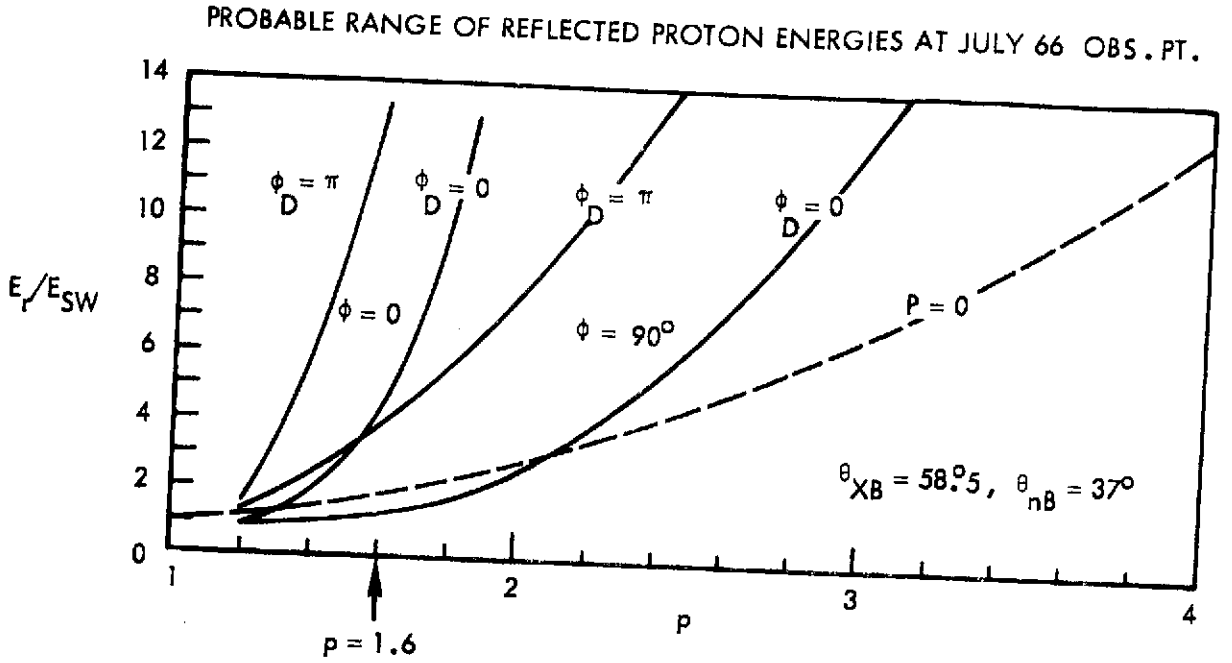

Figure 6

forward of the subsolar point, and the interplanetary field, which has been perpendicular to the solar wind flow thereby cutting off all reflected particles, rotates suddenly to a stream angle of 50°, connecting the satellite to the subsolar point. Then reflected protons barely emerging from the shock at $\phi = 90°$ with $u_{||}/V_{SW} = p = 1.6$, after completing three-quarters of a cyclotron rotation in the shock layer, will be permitted to arrive at the satellite with total energies up to $E_r = 1.6\ E_{SW}$. Alternatively, imagine the satellite moving antisunward in the same upstream region and first encountering the edge of the precursor zone when $\theta_{nB} = 50°$; at that point protons will be detected with $u_{||} = 1.6\ V_{SW}$ and $E_r/E_{SW} \leq 1.6$. It is an assumption that an accompanying magnetometer would first detect upstream waves at the same time.

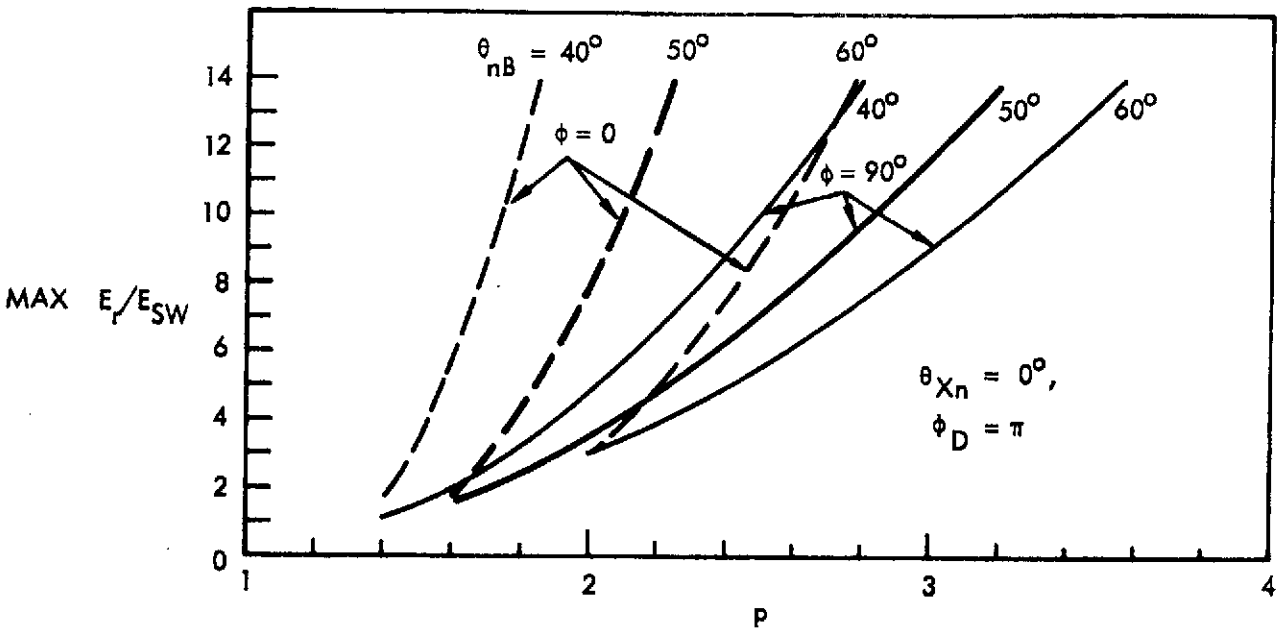

Figure 7

High Energy (30-70 KeV) Protons

Another example provides some interesting numbers. We refer to the insert at the upper left of Figure 8. Imagine a proton detector in the ecliptic upstream on the morning side of the shock at the forward edge of the precursor region (circled point), and suppose that the field angle θ_{nB} corresponding to that boundary of the forward region is 40° to 50° at the subsolar point (where the shock normal is parallel to the X axis). Then, for escape angles ϕ = 0° and 90° at the subsolar point, our formulas for P and E_r/E_{SW} give the maximal energy ratios vs p shown in the curves in the main part of Figure 8. The figure states, for example, that a proton can leave the subsolar shock at ϕ = 0°, travel along $\underset{\sim}{B}_{SW}$ at 40° to the normal, with parallel component (guiding center velocity) $u_{||} = 3\ V_{SW}$, and escape upstream with energy as high as E_r = 100 E_{SW}. A bulk velocity of the solar wind corresponding to 1 Kev would imply

E_r = 100 Kev. Such an example would provide the high energy particles found by Lin et al. (1974) without invoking any acceleration enroute. The shaded region of Figure 8 denotes the width of the 30 to 100 Kev energy channel of the Lin et al. experiment, for a 1 Kev solar wind. We see that, for p = 5, which was at the extreme of the distribution Lin et al. found, even a proton barely escaping at $\phi = 90°$ with the field at 50° to the normal could have total energy high enough to be recorded in their 30-100 Kev channel. The shapes and ranges of the curves suggest that a preference for escape angle of intermediate $\phi \approx 45°$ could easily explain both the consistency with which the 30-100 Kev channel was occupied for moderate p and the apparent absence of protons above 100 Kev even at high p.

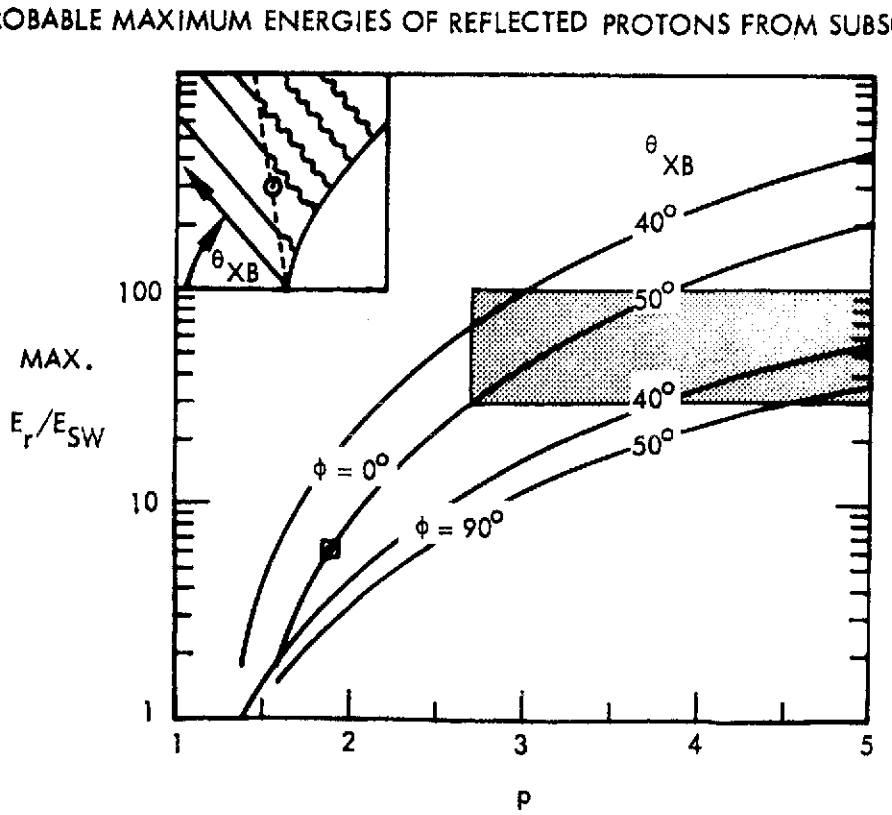

Figure 8

DISCUSSION

The geometry of escape and the numerical examples described above demonstrate that protons can leave the bow shock and travel upstream with almost arbitrary energy, given only the appropriate p, θ_{Xn}, θ_{nB}, and ϕ, and can satisfy observation with very reasonable selection of values for these parameters. However, we do not know the correct values of p or θ_{nB}, even at the subsolar point, or, in any event, do not know that we know, nor do we know the acceleration mechanism.

The foregoing calculations regarding high energy protons cannot therefore be used as evidence that such particles are produced at the bow shock, but only that, if produced, they can escape upstream with the characteristics already observed. The maximal energy ratio yielded at the subsolar point by Sonnerup's (1969) formula for protons energized by the interplanetary electric field is approximately 6.7 at $\theta_{nB} = 50°$ (setting his $\delta = 1/2$, $\mu = \gamma = 0$). In Figure 8, this would correspond, for $\phi = 90°$, to p = 1.9 (square point) and, incidentally, to P ≈ 1.9. Clearly, if the interplanetary electric field is all there is to work with and p is about as small at the subsolar point as it is on the midmorning flank, where p ≈ 1.6, the protons of Lin *et al.* cannot be explained without invoking some upstream energization process, as those authors do.

But consider the following: the entire preceding exposition has treated only cold particles encountering the shock at relative speed V_{SW} and leaving it with combinations of p, P, θ_{nB}, ϕ, etc. rendering them capable of perfect escape. But what of those that don't satisfy the inequality (1)? Are they all retained or recaptured by the shock? What happens, for instance, to a proton that emerges, say, at $\phi = 60°$ with P = 2 when p = 1.6 (see Figure 5)?

It seems reasonable that some particles will encounter the shock two or more times, accelerating each time and compounding their total energy until it reaches a high level. A proton of 30 Kev has observed velocity of only about 5.5 V_{SW} for a 1 Kev solar wind. This does not seem impossible to achieve by multiple reflection when a double reflection may multiply the original relative velocity by, say a factor of 2.56 (= 1.6^2), especially remembering the character of quasi-parallel shocks with their large amplitude pulsations and irregular boundaries. The question of whether energization by multiple reflection in quasi-parallel turbulent waves should be designated as a shock process or an upstream process may thus be only semantic. It is this author's provisional belief that most if not all of the acceleration responsible for the high energies detected by Lin et al. occurs close to the nominal shock although some may be technically "upstream." The only apparent difficulty is providing the proper ratio of $P/p \approx \sqrt{5.5} = 2.3$ for such reflected protons.

The provision of adequate P/p by the physics of shock reflection, the introduction of finite temperature, and the representation of three-dimensional reflection in the curved bow shock are left for future analysis.

CONCLUSION

The first-order calculations described in this report support three conclusions:

1. The geometry of escape does not by itself select from all possible backstreaming protons a particular group that would necessarily leave the shock at $\theta_{nB} \approx 50°$, i.e., with $u_{||} \approx 1.6\ V_{SW}$.

2. The geometry of escape does, however, permit backstreaming protons to leave the shock at $40° \lesssim \theta_{nB} \lesssim 60°$, with $1.5 \lesssim u_{\parallel}/V_{SW} \lesssim 2$ and a wide range of total energies comparable to those observed, i.e., $2 \lesssim E_r \lesssim 10$ keV.

3. The geometry of escape permits backstreaming protons of 30-100 keV to leave the subsolar region of the shock at $\theta_{nB} = 50°$ with $2 \lesssim u_{\parallel}/V_{SW} \lesssim 5$, hence with large pitch angles.

The first two conclusions above imply that the connection between upstream particles and waves should be found in the selectivity of either the shock acceleration process itself, the growth rate of the appropriate instability in the solar wind, or the dispersion characteristics of the wavemode. We close by noting that it seems intuitive that for a given θ_{nB}, the larger the shock radius of curvature, i.e., the less convex it is locally, the more likely a particle will undergo multiple reflection before free escape upstream. Higher energies should therefore be expected for particles upstream from interplanetary shocks, and from Jupiter's bow shock than from the earth's. Such particles have been observed (Armstrong et al., 1970; Simpson et al., 1974), and the acceleration of protons to relativistic energies by multiple reflection in interplanetary shocks has been developed theoretically by Sarris and Van Allen (1974).

ACKNOWLEDGMENT

The material presented in this report was funded by the National Aeronautics and Space Administration under Contract NASW-2398.

REFERENCES

Anderson, K. A., Energetic electrons of terrestrial origin behind the bow shock and upstream in the solar wind, J. Geophys. Res., 74, 95, 1969.

Armstrong, T. P., S. M. Krimigis, and K. W. Behannon, Proton fluxes at 300 keV associated with propagating interplanetary shock waves, J. Geophys. Res., 75, 5980, 1970.

Asbridge, J. R., S. J. Bame, and I. B. Strong, Outward flow of protons from the earth's bow shock, J. Geophys. Res., 73, 5777, 1968.

Barnes, A., Theory of generation of bow-shock-associated hydromagnetic waves in the upstream interplanetary medium, Cosmic Electrodyn., 1, 90, 1970.

Fairfield, D. H., Bow shock associated waves observed in the far upstream interplanetary medium, J. Geophys. Res., 74, 3541, 1969.

Feldman, W. C., J. R. Asbridge, S. J. Bame, and M. D. Montgomery, Solar wind heat transport in the vicinity of the earth's bow shock, J. Geophys. Res., 78, 3697, 1973.

Fredricks, R. W., F. L. Scarf, and L. A. Frank, Nonthermal electrons and high-frequency waves in the upstream solar wind, 2. Analysis and interpretation, J. Geophys. Res., 76, 6691, 1971.

Fredricks, R. W., F. L. Scarf, and I. M. Green, Distributions of electron plasma oscillations upstream from the earth's bow shock, J. Geophys. Res., 77, 1300, 1972.

Greenstadt, E. W., Binary index for assessing local bow shock obliquity, J. Geophys. Res., 77, 5467, 1972a.

Greenstadt, E. W., Observation of nonuniform structure of the earth's bow shock correlated with interplanetary field orientation, J. Geophys. Res., 77, 1729, 1972b.

Greenstadt, E. W., I. M. Green, G. T. Inouye, D. S. Colburn, J. H. Binsack, and E. F. Lyon, Dual satellite observation of the earth's bow shock, 1. The thick pulsation shock, Cosmic Electrodyn., 1, 160, 1970a.

Greenstadt, E. W., I. M. Green, G. T. Inouye, D. S. Colburn, J. H. Binsack, and E. F. Lyon, Dual satellite observation of the earth's bow shock, 2. Field-aligned upstream waves, Cosmic Electrodyn., 1, 279, 1970b.

Lin, R. P., C.-I. Meng, and K. A. Anderson, 30- to 100-keV protons upstream from the earth's bow shock, J. Geophys. Res., 79, 489, 1974.

Sarris, E. T., and J. A. Van Allen, Effects of interplanetary shock waves on energetic charged particles, Univ. of Iowa Report 74-4, January 1974.

Scarf, F. L., R. W. Fredricks, L. A. Frank, C. T. Russell, P. J. Coleman, Jr., and M. Neugebauer, Direct correlations of large amplitude waves with suprathermal protons in the upstream solar wind, J. Geophys. Res., 75, 7316, 1970.

Scarf, F. L., R. W. Fredricks, L. A. Frank, and M. Neugebauer, Nonthermal electrons and high-frequency waves in the upstream solar wind, 1. Observations, J. Geophys. Res., 76, 5162, 1971.

Simpson, J. A., D. Hamilton, G. Lentz, R. B. McKibben, A. Mogro-Campero, M. Perkins, K. R. Pyle, and A. J. Tuzzolino, Protons and electrons in Jupiter's magnetic field: results from the University of Chicago experiment on Pioneer 10, Science, 183, 306, 1974.

Sonnerup, B. U. O., Acceleration of particles reflected at a shock front, J. Geophys. Res., 74, 1301, 1969.

APPENDIX C

STRUCTURE OF THE TERRESTRIAL BOW SHOCK

21333-6013-RO-00

STRUCTURE OF THE TERRESTRIAL BOW SHOCK

by

Eugene W. Greenstadt

Space Sciences Department

TRW Systems Group
Redondo Beach, California 90278

May 1974

Prepared for
publication in

Proceedings of the Asilomar Solar Wind Conference

Asilomar, California
25-29 March 1974

Space Sciences Department

TRW Systems Group
One Space Park
Redondo Beach, California 90278

STRUCTURE OF THE TERRESTRIAL BOW SHOCK

Eugene W. Greenstadt

Space Sciences Department
TRW Systems Group
One Space Park
Redondo Beach, California 90278

ABSTRACT

An extensive examination of bow shock morphology has progressed to a point where distinctions in shock structure, as sensed by a variety of diagnostics, can be correlated with M, β, and θ_{nB} in the solar wind. Shock structures are now designated quasi-perpendicular or quasi-parallel, and laminar, quasi-laminar, quasi-turbulent, or turbulent, depending on the ambient parameters set. For quasi-perpendicular geometry, electromagnetic turbulence, as detected by magnetic sensors, increases with β, independent of M. Irregularity of the shock transition layer and plasma wave noise in the layer increase with M, independent of β. For quasi-parallel geometry, the shock layer broadens and breaks up, showing strongly periodic components at the lowest frequencies, limited levels of plasma wave noise, and marked precursor effects. The parallel shock produces a hybrid average ion spectrum characteristic of neither solar wind nor magnetosheath. The shock is summarized as a complex plasma system in the solar wind.

STRUCTURE OF THE TERRESTRIAL BOW SHOCK

Eugene W. Greenstadt

Space Sciences Department
TRW Systems Group
One Space Park
Redondo Beach, California 90278

INTRODUCTION

A persistent objective among researchers concerned with the solar wind-magnetosphere interaction region has been to study the intricacies of collisionless plasma shocks. Two interrelated questions are at the heart of the issues raised by shock investigations:

1. What processes limit the steepening of the waves composing the shock by dissipating flow energy, thus preventing the superposed waves from forming a discontinuity of infinite amplitude?

2. What processes heat the streaming ions, giving them a jump in temperature across the shock?

Answers to these questions are known not to be unique but to depend on various qualities of the flowing plasma in which the shock forms. The qualities most important to determination of shock processes are apparently defined by combinations of three quantities: Alfvénic or magnetosonic mach number M_A or M_{MS}, ratio of thermal to magnetic field energy β, and angle θ_{nB} between the shock normal and the magnetic field vector in the unshocked plasma flow. The importance of these quantities is illustrated, for example, by a property dependent on M: when M is very low ($\gtrsim 1$), ion heating is negligible and question 2 hardly arises, while when M is high (≈ 5), ion heating is appreciable and indeed exceeds electron heating.

For reference, these quantities are defined here as follows: $M_A = V_1/C_{A1}$, $M_{MS} = V_1/(C_{A1}^2 + C_{S1}^2)^{1/2}$, $\beta = 8\pi N_1 k(T_{i1} + T_{e1})/B_1^2$, $\theta_{nB} = \arccos(\underset{\sim}{B}_1 \cdot \underset{\sim}{n}/|B_1|)$, where C_A and C_S are Alfvénic and sonic velocities, N denotes

density, $\underset{\sim}{n}$ the shock normal, $\underset{\sim}{B}$ the magnetic field, T_i and T_e the ion and electron temperatures, and subscript 1 refers to the unshocked (upstream) plasma.

Isolation of the effects associated with each of these quantities is the first step in moving toward answers to the questions posed. This has been achieved in part in the laboratory, but always within certain inherent experimental limitations, such as the presence of chamber walls. The earth's bow shock parameter separation is just now becoming a reality through the use of high resolution data sampling and simultaneous measurements by two spacecraft and by groups of related diagnostics. An extensive case by case study of the bow shock based on isolation of the various parameters is in progress by V. Formisano, C. T. Russell, F. L. Scarf, M. Neugebauer, and the present author. This report synopsizes the early results of the investigation using data principally from OGO 5 and HEOS 1. The main result is successful isolation of shock structures by parameter set and correlated diagnostic behavior. We shall first modify the existing shock structural nomenclature to suit the results of spacecraft observations and to provide the terminology needed in the remainder of the paper. We then display a few examples of shock morphology for a wide range of plasma states, as seen with various diagnostics. We summarize by describing the bow shock as a system in the solar wind, note its advantages as an object of shock investigation, and close by listing a few aims of future study.

CLASSIFICATION AND NOMENCLATURE

Existing Classifications. The classification scheme for shock structures with which most workers are familiar arises out of laboratory experience (Paul, 1971) and theoretical idealization (Tidman and Krall, 1971). There are two main divisions for magnetic shocks, by which we mean those in which the flowing plasma includes a magnetic field. These divisions are Perpendicular and Oblique, as defined in Figure 1a. The Perpendicular is actually a narrowly-

defined case in which θ_{nB} is almost exactly 90°. More precisely, the restriction on this division is that the complement of $\theta_{nB} \lesssim \arctan \sqrt{\frac{m_-}{m_+}}$ which means that $\underset{\sim}{B}$ must be within 1°.3 of tangency to the shock "surface." The latter division, Oblique, is intended to include every other θ_{nB}, with the possible exception of the parallel shock when $\theta_{nB} = 0°$. The question marks designate the range of θ_{nB} essentially unexplored.

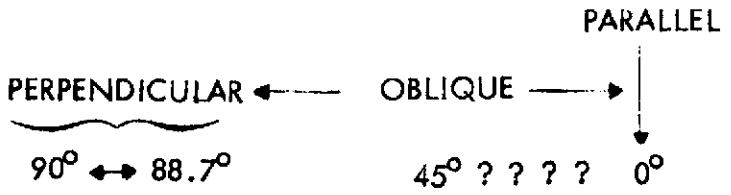

Figure 1a

Perpendicular Class. Most experimental work has dealt with perpendicular shocks, which are further subdivided into parameter ranges of β and M as shown in Figure 1b. M_c denotes a "critical" mach number which is in turn dependent on β. In low-β shocks the magnetic field dominates the internal (thermal) disorder of the plasma. At low M, resistivity and/or dispersion limit shock steepening up to M_c, and the shock has a thin ramp profile. Above M_c resistivity and/or dispersion are inadequate, and an effective viscosity is needed to provide additional dissipation. The shock then broadens, and reflected ions form a foot ahead of the main shock ramp. The resistive critical value $M_c = M_A^*$ lies roughly between 2.3 and 2.7, tending to decrease with rising β. In ultra high-β shocks, thermal disorder dominates the field, perpendicularity becomes moot, and the structural distinction between subcritical and supercritical shocks loses identity probably because of the reduction of M_c to very low values between 1.0 and 2.0 (see reference to Figure 1c below). A useful experimenter's review has been given by Paul (1969).

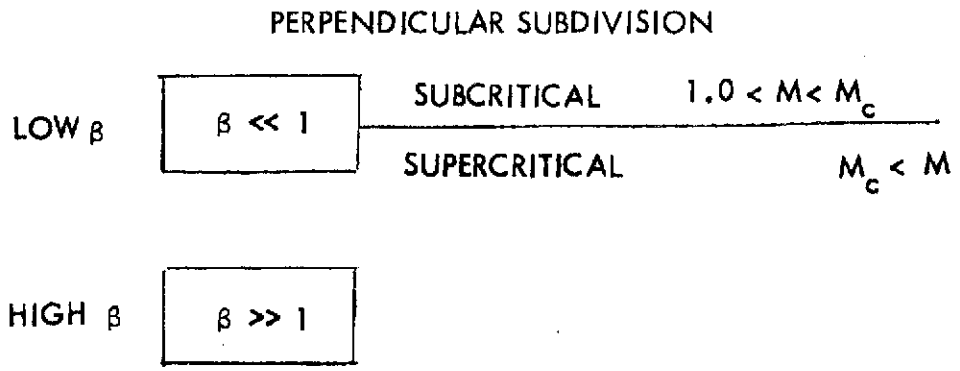

Figure 1b

Oblique Class. Experimental work with oblique shocks (Robson, 1969) has been confined almost entirely to the range $45° \lesssim \theta_{nB} \lesssim 90°$, a limitation important to the revised classification with which this paper will be concerned. In general, oblique shocks preserve the subcritical/supercritical subdivision of perpendicular shocks insofar as resistive/viscous dissipation is concerned, but add to the structure a large amplitude, damped whistler wave standing upstream from the main ramp at low M and downstream at high M while losing the supercritical "foot" of reflected ions. The ions presumably escape upstream along the field. Another feature of oblique shocks is an additional dependence of M_c on θ_{nB} as well as on β. A typical dependence has been computed from theory by Drummond and Robson (1969) and is displayed for a few parameter combinations in Figure 1c. The shaded section of the figure denotes the values of θ_{nB} incompletely studied in the laboratory. The figure shows that M_c, in this case M_A^*, diminishes with decreasing θ_{nB} and increasing β until the parameter distinction between subcritical and supercritical structure almost vanishes for parallel shocks with $\beta \gtrsim 1$, where M_A^* is close to 1.0, the minimal M for having any shock at all. In other words, at the extreme lower right of the panel virtually all structures ought to be supercritical with respect to M_A^*, with viscosity as the necessary dissipation mechanism taking over when resistivity no longer suffices. Dispersion can also limit shock steepening for $M > M_A^*$,

however, with viscosity not taking over until a higher critical value is reached. The elevation of M_c by dispersion is indicated for cold plasma (β=0) at 90° and 45° by the arrows at the left of the lower panel. The result of this elevation is to widen the "subcritical" range of M, making observation of low-M shocks easier. Wave breaking occurs at a still higher critical number.

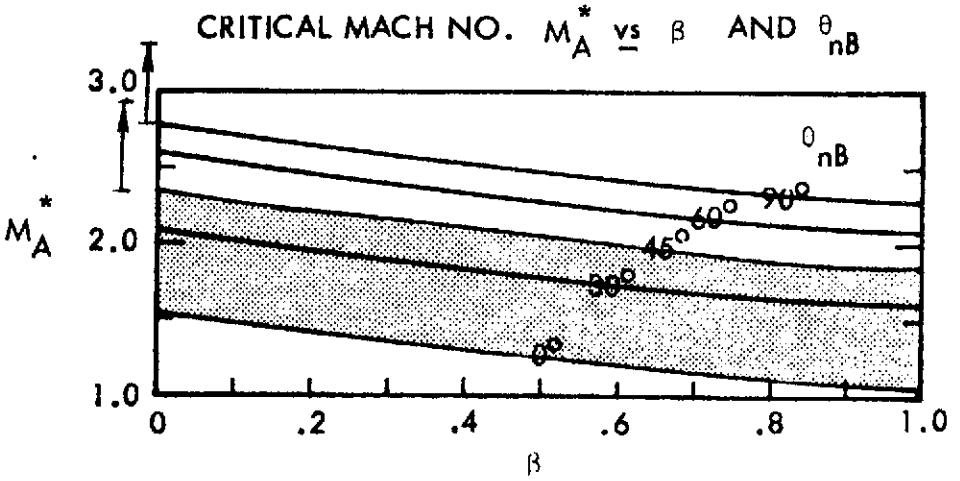

$M = M_A^*$ WHEN $V_2 = C_{S2}$

Figure 1c

The relationships depicted in Figure 1c seem to be in fair agreement with laboratory observation for $88° \gtrsim \theta_{nB} \gtrsim 45°$. Although the remaining range of θ_{nB} has been extended to about 30° at high β experimentally (Robson, 1969), it is more accessible and actually common, in the earth's bow shock.

Revised Classification. The chart of Figure 2 introduces the classification and nomenclature that will be used in this report. There are still two main divisions in this scheme. Together, they encompass the very wide range of θ_{nB} hitherto called "oblique" plus two extreme classes, perpendicular and parallel, defined as before. These last two are simply special cases observed

much less frequently in space than the others. The two principal divisions, quasi-perpendicular and quasi-parallel, memorialize the empirically-determined distinction in magnetic structure that depends on whether the upstream field in the unshocked plasma is greater or less than about 45°. Physically, the division probably separates those cases in which the upstream field prohibits or permits the shock to communicate its presence to the oncoming plasma with sufficient energy to "preoscillate" the field, "prescatter" the approaching ions and, by feedback of these effects, modify its own structure through wave amplification (McKenzie and Westphal, 1968) or other process. Note that the "quasiparallel" class covers just the range of θ_{nB} unfamiliar in the laboratory and corresponds to the "pulsation" shocks described by Greenstadt et al. (1970); its observational range of identification has been almost entirely the contribution of satellite measurements.

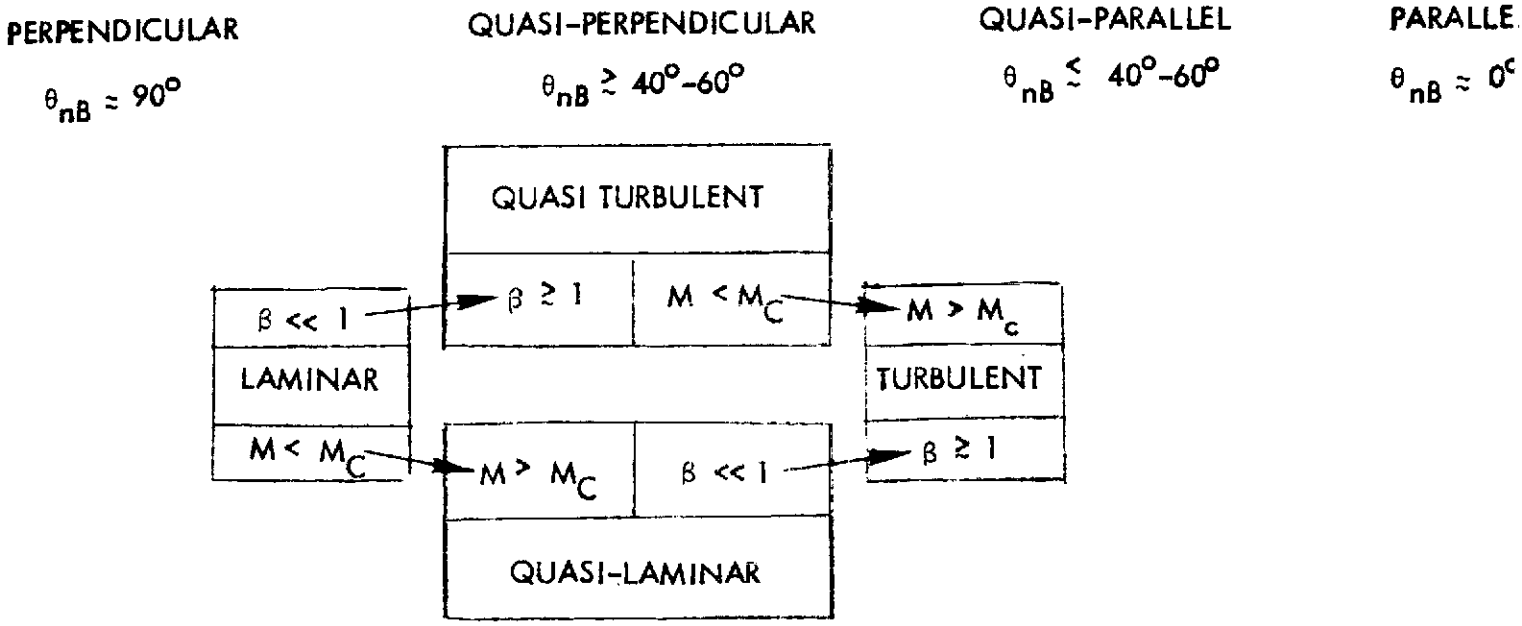

Figure 2

Each of the main classes may be subdivided according to various combinations of β and M. The subdivisions are shown in the chart under the quasi-perpendicular heading. Cold plasma at subcritical mach number is represented by the laminar designation at the left, hot plasma at supercritical mach number is represented by the turbulent designation at right. The upper and lower subclasses define two routes from simplicity to complexity of shock structure. One, called quasi-laminar, results when a cold solar wind flows supercritically; the second, called quasi-turbulent, results when a hot solar wind flows subcritically. Criticality is used here as a general term without specification of what kind. Spacecraft results so far make a distinction only of M_c less than or greater than about 3.0. The transitions in form are assumed to be smooth as far as β is concerned, there being no critical value of this quantity.

The scheme of the figure is a blend of observation and speculation, as not all designated categories have been observed in detail. It is anticipated from the M_c-β-θ_{nB} dependence of Figure 1c that the subdivisions should become increasingly indistinct or inapplicable in progressing from perpendicular to parallel geometry. Certainly they should be increasingly difficult to record as the range of subcritical M shrinks. Up to now, results have been consistent with anticipation in that the quasi-perpendicular category has provided the most complete documentation. In the sequel, it should be remembered that the chart of Figure 2 does not exhaust the ways in which shock morphology can be described. For example, the shock does communicate upstream for some angles $\theta_{nB} \gtrsim 45°$ by reflecting electrons rather than protons, creating a region of small amplitude upstream waves of frequency about 1 Hz. Also, ratios T_e/T_i or N_α/N_p may be important in differentiating certain shock structures. The possibility of overlapping classification schemes should be kept in mind.

BOW SHOCK MORPHOLOGY

Quasi-Perpendicular Structures. Figure 3 displays four multidiagnostic profiles of the quasi-perpendicular bow shock according to the scheme of Figure 2, but with specific values $M_c = 3$, $\beta = .1$ defining the subclasses at the center. These values follow the empirical divisions of Formisano and Hedgecock (1973b). We shall see that suitable plasma diagnostics follow these divisions. The left and top examples were obtained at 1.15 sec/sample, the botton and right examples at .144 sec/sample. All are from observations by OGO 5 instruments, with upstream parameters checked against HEOS measurements, and free-stream magnetosonic mach number used throughout.

The laminar shock at left is magnetically monotonic and virtually free of macroscopic and microscopic turbulence. One cycle of a very small wave, probably a standing whistler, is visible just at the foot of the ramp. The uncalibrated output of the Lockheed light ion spectrometer, below the field profile, shows the presence of thermalized protons in the sheath behind the trailing edge of the ramp. Next below, the 560 Hz channel of the TRW plasma wave detector registers electrostatic noise up to a few millivolts/meter in the ramp and just outside in the small standing wave. Below the plasma wave panel, four channels of the x-axis of the JPL/UCLA search coil, uncalibrated, show a region of magnetic noise up to about 100 Hz centered on the midramp of the shock.

When β and M are both elevated above their "laminar" values, the monotonic nature of the ramp disappears, a clear foot develops, and macroscopic turbulence is evident both ahead of and behind the principal leading gradient. All of these features are apparent at the right of Figure 3. Also, in contrast to the laminar profile, the turbulent shock at right shows numerous bursts of electromagnetic noise at frequencies up to and including 1 kHz,

with higher activity in various channels upstream and downstream. The symbol X10 indicates that the search coil data were recorded at 10 times higher sensitivity than where the symbol is absent. This noise was also present deeper in the magnetosheath. In this case, the plasma (electric) wave noise in the 560 Hz channel reaches about 50 millivolt/meter. The Lockheed spectrometer records the scattering of protons behind the outermost irreversible field gradient.

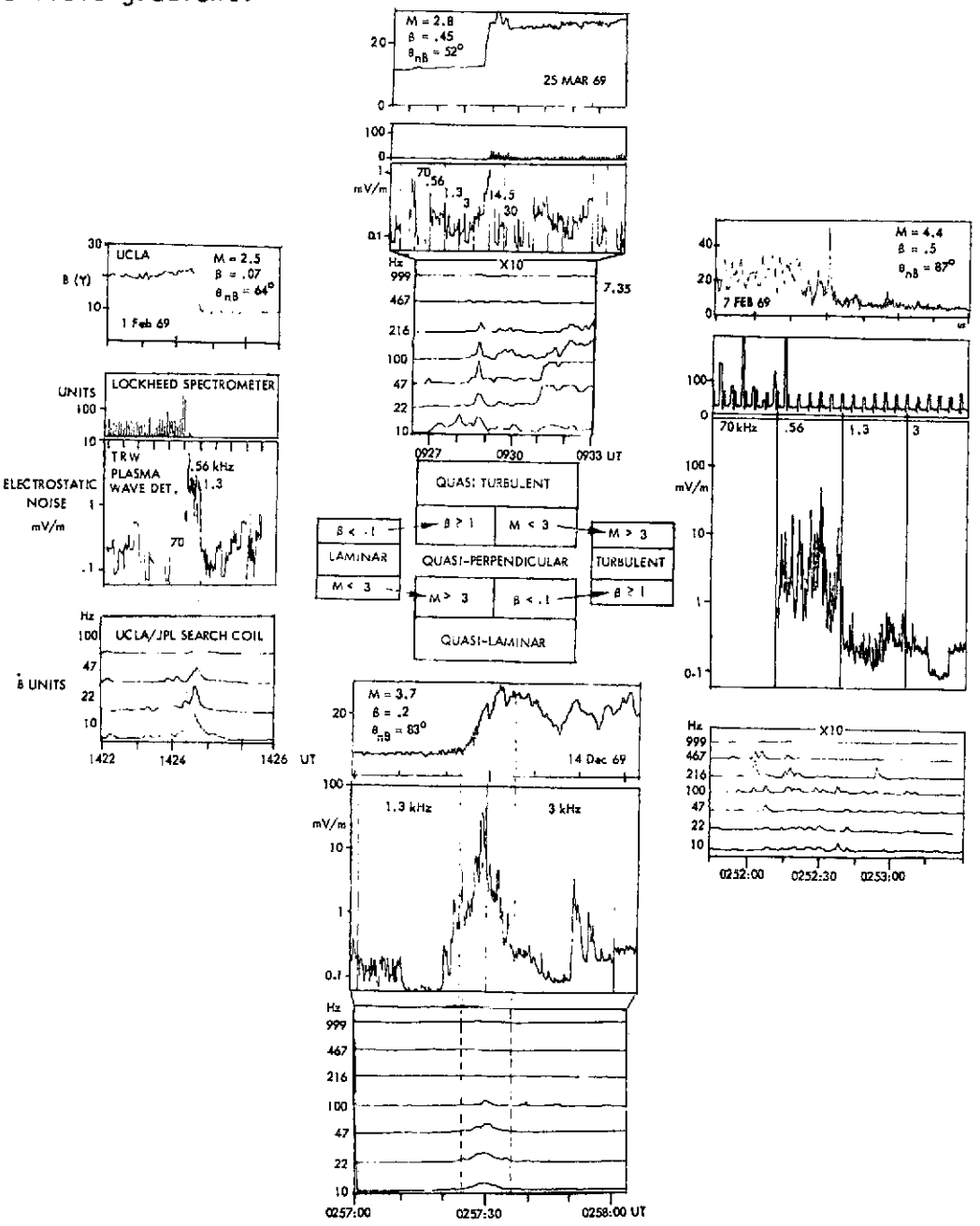

Figure 3

If β is raised, but M remains low (subcritical), the macrostructure of the shock remains largely indistinguishable from that of the laminar case. The quasi-turbulent example at top center shows a monotonic ramp and perhaps a modest increase in fluctuation level just behind the ramp. The other diagnostics applied to the quasi-turbulent case reveal a distinction from the laminar shock not apparent in the magnetic field profile. Electromagnetic noise occurs at higher frequencies and amplitudes (X10) than in the laminar case, even up to 1 kHz, and is not confined to the ramp, but remains intense downstream in the sheath. Electrostatic noise does not reach above 1 mv/m in this case. The electric wave frequency sampled, 7 kHz, is not the best frequency with which to observe the shock with this diagnostic, but the electrostatic profile is representative, anyway; such low noise levels are typical of quasi-turbulent shocks observed in any of the lower frequency channels. Proton thermalization occurs at the rear of the ramp, as in the laminar case.

We look finally at the quasi-laminar example, at the bottom center, which illustrates the result of the mach number rising above 3 while β remains low. The ramp remains monotonic but the waves created in oblique shocks by dispersion in the plasma appear downstream. The magnetic noise occurs only in and around the ramp, as in the laminar case, but intense plasma wave noise up to tens of millivolts per meter appear, as in the turbulent structure. Particle data were unavailable in this case.

The foregoing examples illustrate the dependence of shock structure interpretation on the diagnostic employed and the interleaving of similarities and differences among the various subclasses. Magnetic noise, always present up to the local ion plasma frequency, is confined to the immediate neighborhood of the shock ramp in laminar and quasi-laminar cases, but persists in the sheath in quasi-turbulent and turbulent cases. Plasma wave noise, also always present in

the ramp, remains below a few millivolts per meter in laminar and quasi-turbulent shocks, but rises an order of magnitude higher in quasi-laminar and turbulent shocks.

The physical meaning of these distinctions is clarified to some degree by consulting another diagnostic. Post-shock ion spectra in the magnetosheath were not available from OGO 5, but a statistical study of HEOS data by Formisano et al (1973) revealed that downstream proton spectra were Maxwellian when $M \lesssim 3$. while they had a high energy tail when $M \gtrsim 3$. In detailed studies of particle behavior inside the shock transition, Montgomery et al (1970) and Formisano and Hedgecock (1973a) have shown that double-peaked distributions appear within the turbulent shock structure, the second peak occurring above the solar wind bulk velocity at about 2-4 V_{sw}. The change in proton distribution through the early part of the shock reported by Montgomery et al (1970) is shown in Figure 4a. The double distributions of Formisano and Hedgecock (1973a) are shown in Figure 4b in relation to the simultaneously-measured magnetic field shock profile. The field indicated a shock encounter in which the shock retreated from the satellite (HEOS) before it was fully crossed. The solar wind spectrum at the left was obtained a few minutes before the shock was engaged; the two bimodal spectra are positioned approximately at the times they were recorded.

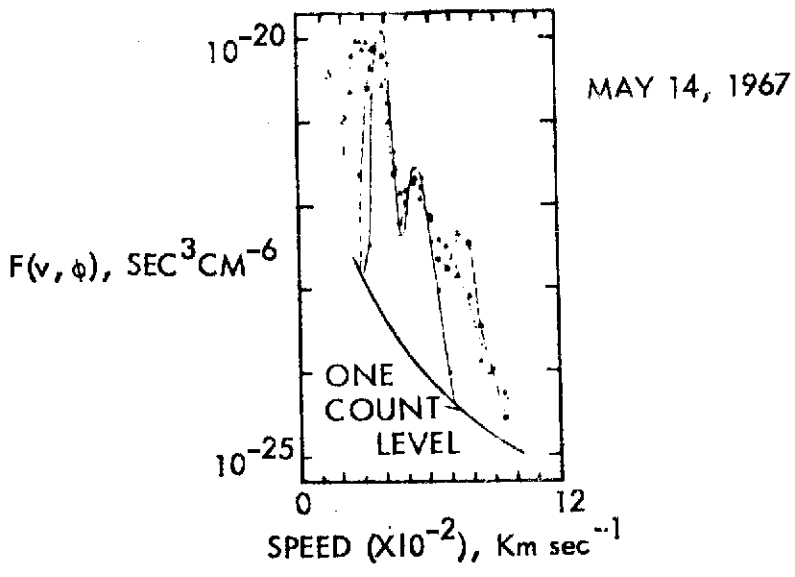

Figure 4a

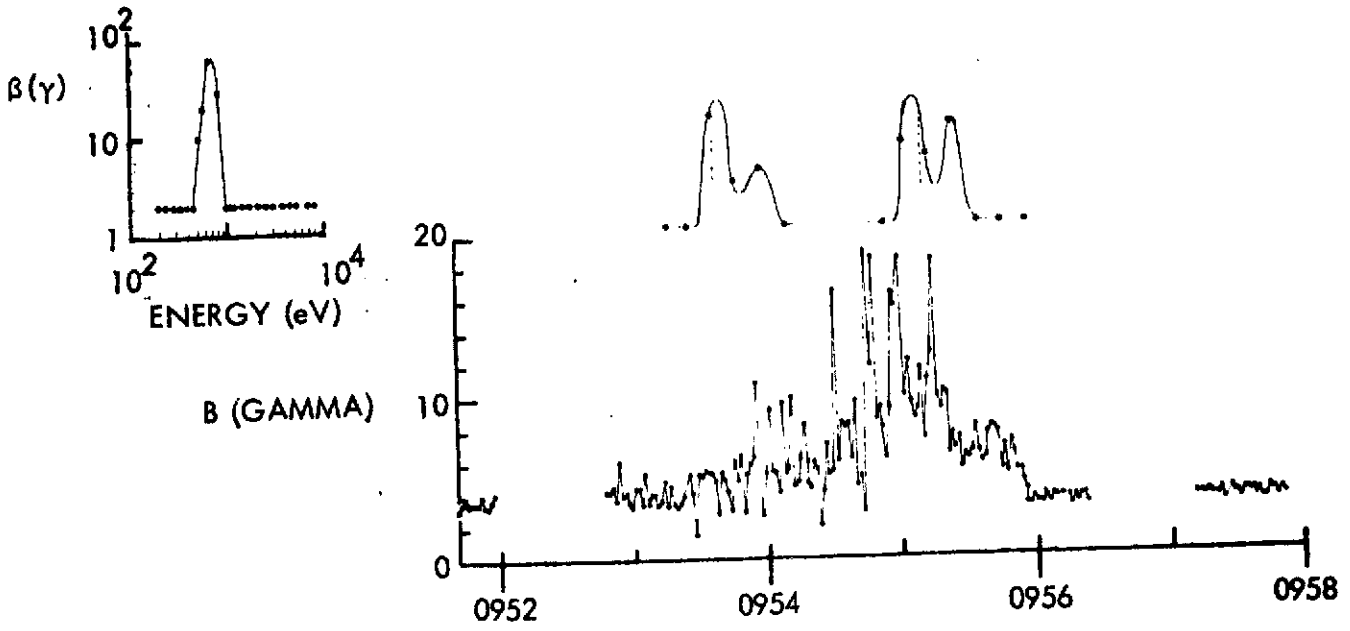

Figure 4b

The bimodal distribution immediately suggests the presence of bulk velocity protons reflected by the shock and energized by the interplanetary electric field through the process described by Sonnerup (1969). Counterstreaming protons are central to the idea that viscosity takes over to limit shock steepening above M_c where resistivity becomes inadequate. The bimodal distribution, together with the electron heating known to develop early in the ramp (Montgomery et al., 1970; Neugebauer et al., 1971), which in turn elevates T_e/T_p, provides a medium favorable to plasma instability, possibly leading to a subshock, finally resulting in high postshock proton temperature, characterized by a non-Maxwellian energy distribution with a high energy tail.

These findings round out the distinctions among the subclasses and their likely physical bases. Quasi-laminar and turbulent shocks are supercritical, in some sense, are characterized by high levels of electrostatic and electromagnetic activity, probably associated with a viscous subshock. Downstream

the bimodal distribution of the shock is smoothed to form a visibly-skewed ion spectrum. Laminar and quasi-turbulent shocks are subcritical, lack the conditions presumed to be associated with a subshock, especially high electrostatic noise, are limited by anomalous resistivity and dispersion only, and produce cool ion spectra downstream, with relatively little detectable deviation from Maxwellian distributions. The persistent magnetic noise of the quasi-turbulent shock is a feature consistently associated with its high thermal noise level and high-β plasma upstream.

Observe that in no quasi-perpendicular case are any regular, undamped, long period upstream waves present, but that very small fluctuations at about 1 Hz are visible ahead of the shock in three examples, those of 1, 7, and 14 February.

Quasi-Parallel Structures. The quasi-parallel structures collected so far have included no quasi-turbulent case. Figure 5 is therefore deficient in this subclass. Also, chance has produced only one transient laminar case. Nevertheless the laminar example at the left of the figure illustrates clearly, by comparison with Figure 4, the upstream activity produced by even borderline quasi-parallel $\theta_{nB} \approx 45°$. The monotonicity of the magnetic ramp has been destroyed, as in the irregular turbulent, quasi-perpendicular cases, but with an important difference: the precursor waves forward of the final average field elevation of 0640:30 are of appreciable amplitude and show the strong near-periodicity, in this case $T \approx 20$ sec, often observed far upstream on field lines connected to the shock (Fairfield, 1969). The regularity of the field in the sheath before 0640 UT appears to have been associated with a quasi-perpendicular upstream field orientation which became quasi-parallel at 1640.

The quasi-laminar example at bottom center of Figure 5 is formally on the borderline between quasi-laminar and turbulent as far as β is concerned,

but since β-determined changes are continuous anyway, it has been placed by virtue of its diagnostic combination in the quasi-laminar category. The alternation between large amplitude "pulsations" and upstream waves typical of quasi-parallel structures (Greenstadt et al., 1970) is evident in the figure. Observe that this example was recorded at the low resolution 1.15 sec/sample rate. The section shown is 28 minutes long in contrast to the minute-and-a-half view of the "irregular" turbulent shock of Figure 4. Moreover, this example is of a relatively subdued section taken near the solar wind end of a structure that was observed for over an hour by two satellites, one more than an earth radius behind the other. It is quite likely that this is actually an example of a parallel shock within the accuracy of estimation of θ_{nB}.

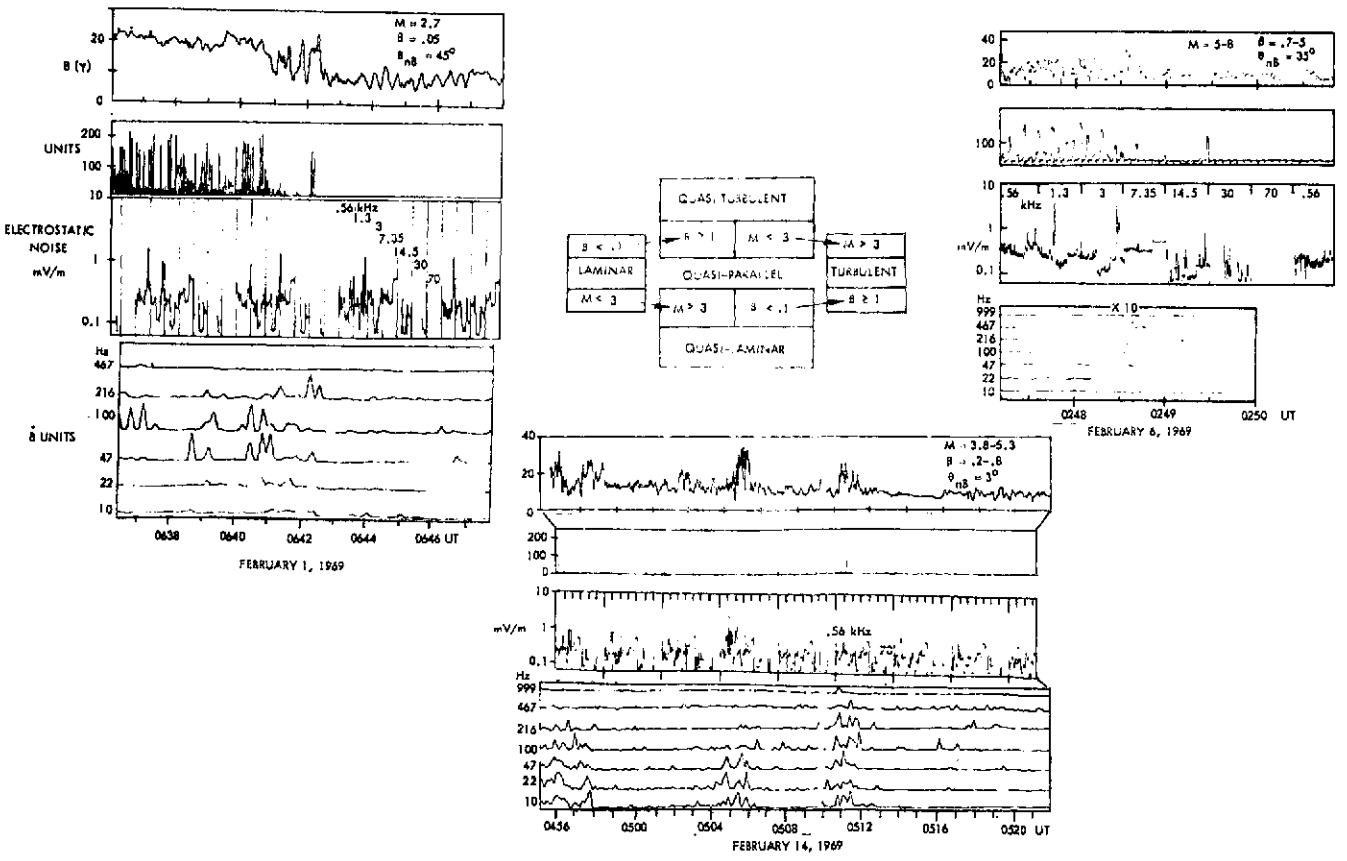

Figure 5

A shock that is definitely quasi-parallel and definitely turbulent is shown in the last example at the right in considerably greater detail. Here, at .144 sec/sample, we see the total absence of any regularity in what appears to be the shock at 0248:40. We also see both short and long period waves upstream, the latter having peak-to-peak amplitudes equal to the average field level. Bursts of damped waves appear at the leading edges of the longer-period upstream waves.

The other diagnostics displayed for the quasi-parallel shocks are informative. The figure shows the same format of electrostatic, electromagnetic, and proton scatter data used earlier. The irregularity of the magnetic profiles is clearly shared by the other measurements, but one phenomenon is particularly striking: intense electrostatic noise is absent just where it is notable in quasi-perpendicular shocks, namely in quasi-laminar and turbulent cases. Magnetic noise, as detected by the search coil, occurs at high amplitude only in the turbulent case. The expanded diagnostic picture of the quasi-parallel, turbulent shock emphatically confirms the observation that high electrostatic noise levels are absent in quasi-parallel structures. To complete the picture, we recall that the statistical analysis by Formisano et al. (1973a) gave only Maxwellian distributions in the sheath when upstream waves were detected, under presumably quasi-parallel geometry, regardless of M or β.

14 February 1969. Further examination of the essentially parallel shock of 14 February provides some evidence of conditions in a well-developed pulsation region. Figure 6 shows an overall view of the shock as seen concurrently by both HEOS 1 and OGO 5 magnetometers, when the satellites occupied the relative position seen in the figure at the top. The extremely active shock structure,

which coincided with $I_p = 1$ conditions (Greenstadt, 1972a), as shown in the small inserts above the field profiles, was at least 1 R_e thick. The figure incidentally demonstrates the difficulty of obtaining reliable upstream plasma parameters for the parallel shock, even with two spacecraft. Plasma data obtained by OGO 5 before and after the large field excursions yielded β and M associated with either the quasi-laminar or the turbulent subclass.

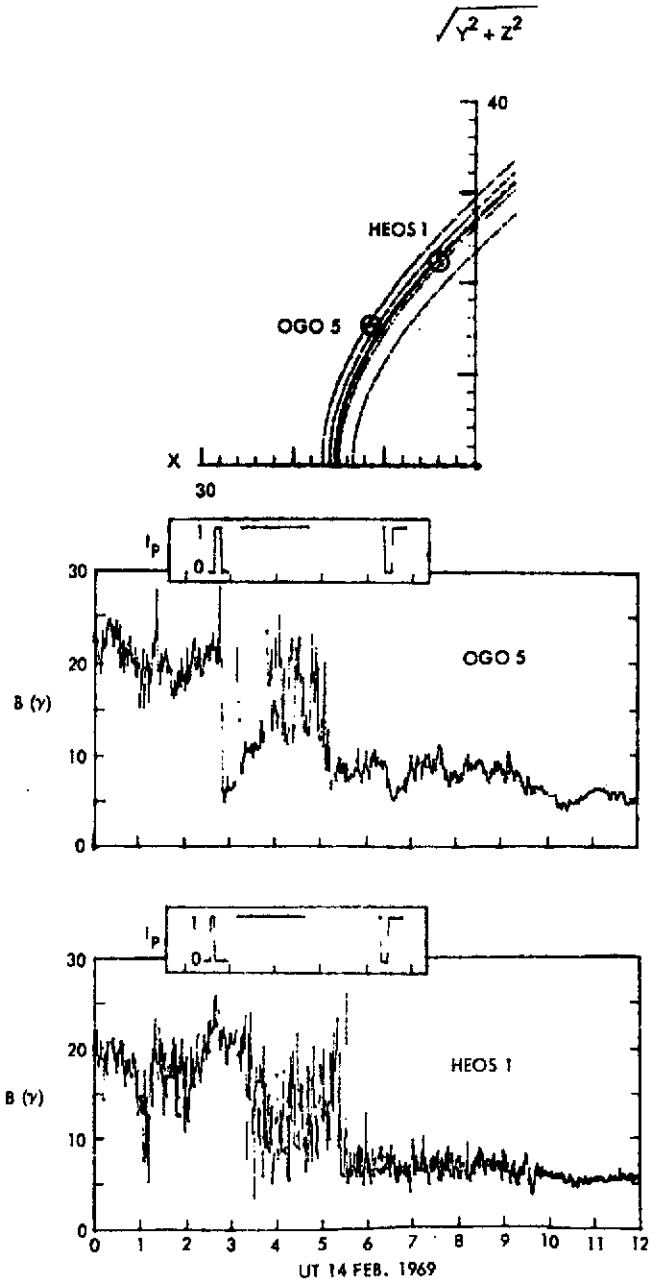

Figure 6

A detail of the magnetic field behavior at OGO obtained in the center of the pulsation structure at 1.15 sec/sample is shown in Figure 7. Above the sample are shown three contrasting ion spectra taken from HEOS 1 data. The solar wind spectrum was averaged from several distributions upstream from the shock. The magnetosheath spectrum is an average composite of several such distributions collected downstream from the shock before the quasi-parallel structure was encountered. The pulsation spectrum is the average of all distributions recorded while HEOS was in the pulsation structure. This spectrum clearly shows the plasma energy peak at the bulk energy of the solar wind but with a lower maximum and a broadened, hotter distribution. It appears, then, that the ions were severely scattered but the flow was not visibly retarded by the large amplitude magnetic waves of the parallel structure. This structure therefore offers some ambiguity as to whether it existed "upstream" or "downstream" of the "shock": it was thermally downstream, but dynamically upstream as far as slowing the bulk flow was concerned.

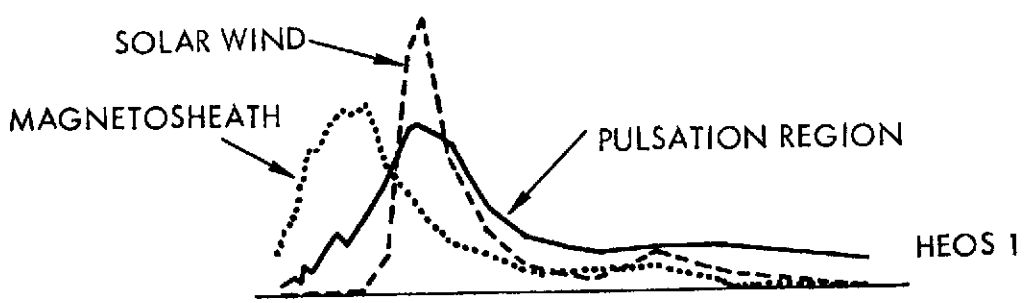

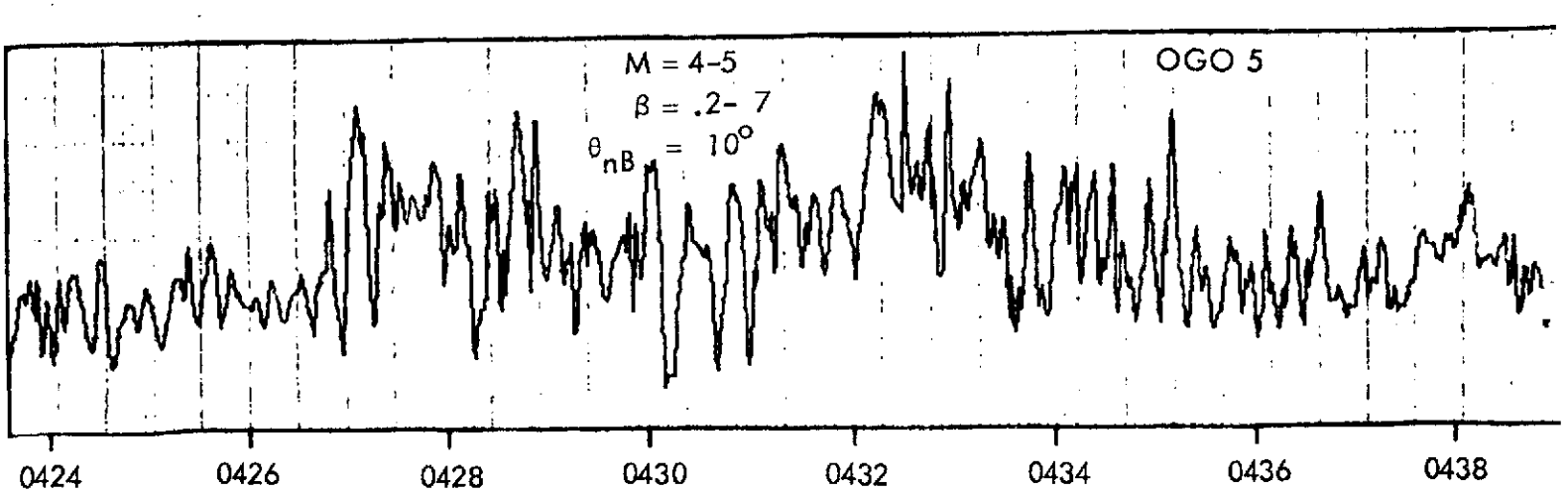

Figure 7

The foregoing result suggests the qualitative inference that to the extent that quasi-parallel structure may be regarded as upstream from some eventual average field and velocity jump, the plasma parameters delivered to the jump could be significantly different from those naively computed far upstream in the unaffected solar wind, and could put the shock in a different subclass, or in even more than one subclass simultaneously.

Venus Bow Shock. The character of Mariner 5's encounter with the Venus interaction region was interpreted earlier as consistent with the quasi-perpendicular/quasi-parallel division discussed here (Greenstadt, 1970). The fresh results from Mariner 10's recent flyby of Venus reconfirm this interpretation and the applicability of earth-derived shock analyses to neighboring planets. The characteristics associated with a thick, well-developed quasi-parallel shock, probably turbulent, are evident on early examination of the data (Ness et al., 1974), and the experimenters point out that such an interpretation is compatible with the average stream angle field direction in the ecliptic in the morning quadrant, discernible before a time gap in their Figure 4, and with the position of the Mariner crossing near the dawn meridian. It is also consistent with the quietude of the field after the time gap, when the field had apparently changed to the afternoon quadrant, preventing the familiar precursor region from reaching the spacecraft. It will be important, in further analysis, however, to bear in mind that the recorded structure could signify an ultra-high-β electrostatic shock, if the plasma temperature proves to have been very high.

DISCUSSION

Communication with the Solar Wind. The foregoing remark about an anticipated precursor region at Venus serves as a reminder that a planetary bow shock, in particular the earth's, is not an isolated, self-contained phenomenon

affecting only a tight region around the magnetosphere through which an insignificant tube of solar wind flux passes. From a space researcher's viewpoint, the bow shock must be regarded as the principal entity inside a large volume of solar wind with which it communicates. Downstream, the shock sends a heated, decelerated, and deflected solar wind it has prepared to flow around the magnetosphere. The field in this magnetosheath flow carries significant information from the shock. Its direction with respect to the magnetospheric field at the magnetopause may differ from what it had been upstream and may initiate or cancel a substorm by virtue of its refracted orientation. Large amplitude oscillations associated with quasi-parallel structure may reach the magnetopause and stimulate the magnetosphere, setting up resonant oscillations detectable at the surface as micropulsations. A model for such an excitation has been proposed by Greenstadt (1972b) and appears to be consistent with observation (Bolshakova and Troitskaya, 1968; Nourry and Watanabe, 1973). Upstream, the shock radiates waves and reflects protons and electrons of considerable enrgy (Asbridge et al., 1968; Feldman et al., 1973; Lin et al., 1974), which in turn stimulate upstream waves that forewarn the solar wind of the obstacle in its path. The low-frequency upstream wave region mapped out statistically by Fairfield (1969) is well known, and a plasma wave region has also been described (Fredricks et al., 1972). The intimate, apparently 1-for-1 association of long period upstream waves with what we here designate as quasi-parallel structure, has been documented by Greenstadt et al. (1970), and related by statistical inference to Maxwellian ion distributions downstream by Formisano et al. (1973).

The Bow Shock System. Figure 8 synopsizes the key elements of what should be regarded as the bow shock system. The shock itself is divided broadly into quasi-parallel and quasi-perpendicular regions, shown here in an ecliptic view for a nominal 45° stream angle. The precursor region is di-

$$\tan \theta_{XS\pm} = \frac{p_{\pm} \sin \theta_{XB}}{p_{\pm} \cos \theta_{XB} - 1}$$

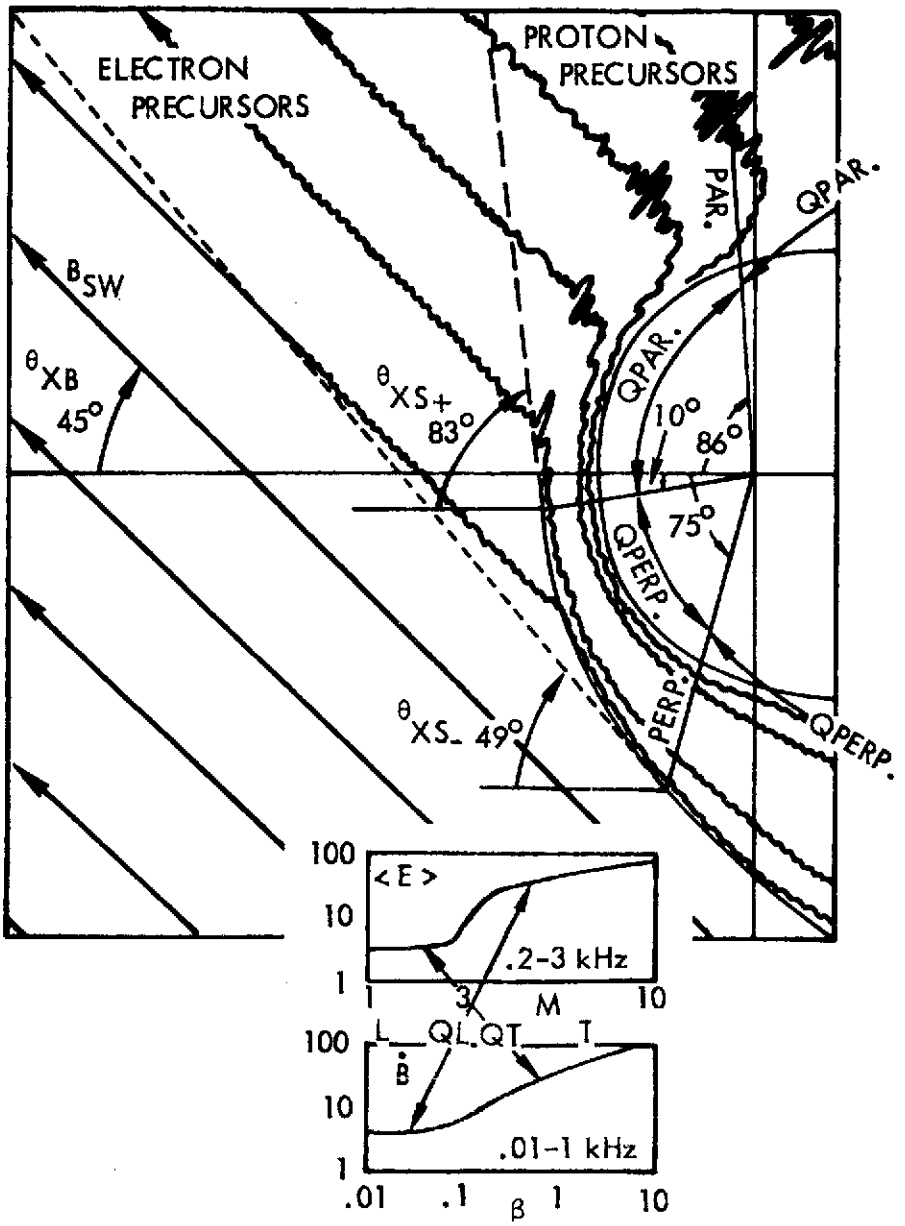

Figure 8

vided into two parts. An advance region of electron precursors consists of reflected electrons, plasma waves at the local electron plasma or upper hybrid frequency (generally in the 15-30 kHz range, Fredricks et al., 1972), accompanying magnetic waves in the same range, and very possibly small amplitude waves around 1 Hz, at least close to the shock. A less extensive region of proton precursors consists of reflected protons of energies up to as much as 100 keV, low frequency waves of tens of seconds period in a spacecraft frame, and the features of the electron precursor region as well. The formula at the top gives the means of estimating the forward boundaries of the two precursor regions, shown as dashed lines in the figure. In the equation, p represents the speed, as a multiple of V_{SW}, with which the appropriate reflected particle moves upstream along the field while the field is carried downwind. The angles indicated here, 83° and 49°, were obtained by setting $p_+ = 1.6$, a value found by the author to work well for predicting long period upstream waves and quasi-parallel structures, and $p_- = 10$, a value roughly compatible, for a 400-Km/sec solar wind, with the 4000 Km/sec ($\sim 10\ V_{SW}$) electron velocity cited in a report on reflected electrons by Feldman et al. (1973). Actually, both electrons and protons are reflected with a spectrum of velocities. Electrons, in particular, are hot and not well represented by a single velocity.

The insert at the bottom synopsizes qualitatively the empirical behavior of electric and magnetic noise in the quasi-perpendicular shock as functions of M and β. When both parameters are low, both noise levels are low and the shock is clearly laminar (L); when M rises above about 3 but β remains very low, the electric noise increases dramatically; the shock is quasi-laminar (QL). In the opposite case, when M remains low but β approaches 1, the mag-

netic noise increases in a more or less continuous fashion; the shock becomes quasi-turbulent (QT). When M and β are both high, the shock is turbulent (T); it is electrostatically and magnetically noisy and the sheath is magnetically noisy.

When similar parameter divisions are applied to the quasi-parallel structure, the shock is found to be low in electrostatic noise regardless of β or M, although the magnetic noise seems to rise with β as in quasi-perpendicular shocks.

CONCLUSION

The new data from which examples of bow shock structure were drawn for this report will be described in detail and discussed in greater depth in a series of papers now being prepared by the researchers named earlier. The overall result will be to bring the study of collisionless plasma shocks by means of spacecraft techniques up to and, in some respects, ahead of the prevailing level of laboratory and theoretical investigation. This paper is concluded therefore by outlining a few of the remaining goals to be pursued in seeking improved understanding of processes in the bow shock. These are:

1. Precise separation of structures differentiated by refined definitions of critical mach number.

2. Identification of the mechanisms responsible for the bimodal proton distribution, the viscous subshock, and thermalization of the ions.

3. Exact identification of the processes responsible for generation of the proton precursor waves.

4. Determination of the means by which reflected particles are energized and released upstream and the proportions in which they are divided into reflected and transmitted subspectra.

5. Differentiation of the roles of particle reflection, wave amplification, and wave breaking in the development of quasi-parallel structures.

Anyone interested in plasma processes can enlarge this list. The important point, however, is that none of the objectives listed seems impossible to achieve even with existing spacecraft data, and all should be reached when the HMD satellites go into operation.

ACKNOWLEDGMENT

Results described in this report were funded in part by the National Aeronautics and Space Administration under Contract NASW-2398.

REFERENCES

Asbridge, J. R., S. J. Bame, and I. B. Strong, Outward flow of protons from the earth's bow shock, J. Geophys. Res., 73, 5777, 1968.

Bol'shakova, O. V., and V. A. Troitskaya, Relation of the interplanetary magnetic field direction to the system of stable oscillations, Dokl. Akad. Nauk SSSR, 180, 4, 1968.

Drummond, Wm. E., and A. E. Robson, Oblique collisionless shock waves in plasma, DASA Report 2520, September 1969.

Fairfield, D. H., Bow shock associated waves observed in the far upstream interplanetary medium, J. Geophys. Res., 74, 3541, 1969.

Feldman, W. C., J. R. Asbridge, S. J. Bame, and M. D. Montgomary, Solar wind heat transport in the vicinity of the earth's bow shock, J. Geophys. Res., 78, 3697, 1973.

Formisano, V., and P. C. Hedgecock, On the structure of the turbulent bow shock, J. Geophys. Res., 78, 6522, 1973a.

Formisano, V., and P. C. Hedgecock, Solar wind interaction with the earth's magnetic field, 3. On the earth's bow shock structure, J. Geophys. Res., 78, 3745, 1973b.

Formisano V., G. Moreno, F. Palmiotto, and P. C. Hedgecock, Solar wind interaction with the earth's magnetic field, 1. Magnetosheath, J. Geophys. Res., 78, 3714, 1973.

Fredricks, R. W., Scarf, F. L., and Green, I. M., Distributions of electron plasma oscillations upstream from the earth's bow shock, J. Geophys. Res., 77, 1300, 1972.

Greenstadt, E. W., Binary Index for assessing local bow shock obliquity, J. Geophys. Res., 77, 5467, 1972a.

Greenstadt, E. W., Field-determined oscillations in the magnetosheath as possible source of medium-period, daytime micropulsations, Proc. of Conf. on Solar Terrestrial Relations, Univ. of Calgary, 515, April 1972b.

Greenstadt, E. W., Dependence of shock structure at Venus and Mars on orientation of the interplanetary magnetic field, Cosmic Electrodyn., 1, 380, 1970.

Greenstadt, E. W., I. M. Green, G. T. Inouye, D. S. Colburn, J. H. Binsack, and E. F. Lyon, Dual satellite observation of the earth's bow shock, 1. The thick pulsation shock, Cosmic Electrodyn., 1, 160, 1970.

Lin, R. P., C. -I. Meng, and K. A. Anderson, 30- to 100-keV protons upstream from the earth's bow shock, J. Geophys. Res., 79, 489, 1974.

McKenzie, J. F., and Westphal, K. O., Interaction of linear waves with oblique shock waves, Phys. Fluids, 11, 2350, 1968.

Montgomery, M. D., J. R. Asbridge, and S. J. Bame, Vela 4 plasma observations near the earth's bow shock, J. Geophys. Res., 75, 1217, 1970.

Ness, N. F., K. W. Behannon, R. P. Lepping, Y. C. Whang, and K. H. Schatten, Magnetic field observations near Venus: Preliminary results from Mariner 10, Science, 183, 1301, 1974.

Neugebauer, M., C. T. Russell, and J. V. Olson, Correlated observations of electrons and magnetic fields at the earth's bow shock, J. Geophys. Res., 76, 4366, 1971.

Nourry, G., and T. Watanabe, Geomagnetic micropulsations and interplanetary magnetic field, Abstract, EOS, 54, 1179, 1973.

Paul, J. W. M., Collisionless shocks, Cosmic Plasma Physics, edited by K. Schindler, Plenum., New York, 1971.

Paul., J. W. M., Review of experimental studies of collisionless shocks propagating perpendicular to a magnetic field, Spec. Publ. 51, p 97, ESRO, Frascati, Italy, 1969.

Robson, A. E., Experiments on oblique shock waves, Spec. Publ. 51, p 159, ESRO Frascati, Italy, 1969.

Sonnerup, B. U. O., Acceleration of particles reflected at a shock front, J. Geophys. Res., 74, 1301, 1969.

Tidman, D. A., and N. A. Krall, Shock Waves in Collisionless Plasmas, John Wiley-Interscience., New York, 1971.

APPENDIX D

STRUCTURE OF THE QUASI-PERPENDICULAR, LAMINAR BOW SHOCK

21333-6015-RU-00

STRUCTURE OF THE QUASI-PERPENDICULAR, LAMINAR BOW SHOCK

by

E. W. Greenstadt, C. T. Russell*, F. L. Scarf,
V. Formisano†, and M. Neugebauer[1]

May 1974

*Institute of Geophysics & Planetary Physics, University of California, Los Angeles, California 90024

†CNR-LPS "Laboratorio Plasma Spazio", 00044 Frascati, Italy

[1]Jet Propulsion Laboratory, Pasadena, California 91103

Space Sciences Department
TRW Systems Group
One Space Park
Redondo Beach, California 90278

ABSTRACT

The earth's bow shock was observed several times at high resolution on 12 February 69 by an array of OGO 5 field and plasma instruments under unusual circumstances: The field was at large angle to the local shock normal, the solar wind parameters M and β were both low enough to ensure laminar shock structures, upstream parameters were verified by complementary measurements by HEOS 1, and approximate shock velocities were available by virtue of elapsed time observations obtained with the two satellites. It was found that the low $M(\lesssim 2.5)$ and $\beta(<< 1)$ and high $\theta_{nB}(\gtrsim 65°)$ produced oblique, laminar shock profiles as expected from theory, with marginal or vanishing upstream standing whistlers probably damped by drift or other plasma wave instability. The whistler mode appeared to dominate the electromagnetic spectrum. The laminar shock ramp thickness was several hundred kilometers and equal to 2-4 c/ω_{pi}. Composition of the shock as an accumulation of near-standing waves and an evidently reproducible varying flux pattern was discernible. Electron thermalization occurred early in, or just before, the magnetic ramp, while proton thermalization occurred late in the ramp. Instantaneous shock velocities derived from the standing whistler wavelength were consistent with average velocities derived from the elapsed-time estimates and were as high as 200 Km/sec.

INTRODUCTION

One of the major applications of the study of particles and fields in space is to the physics of collisionless plasmas in general, and to collisionless shocks in particular. Shock phenomena are difficult to scale in the laboratory and notoriously complex to represent in theory. A principal reason for their theoretical complexity is the number of independent parameters that can affect shock structure and shock dissipation processes. The contribution of satellite measurements to the experimental study of collisionless shocks lies in the opportunity to obtain repeated, high resolution observations of the earth's bow shock, which is constantly available for examination, for a wide range of instantaneous parameter sets.

Naturally, the most advantageous use of satellite data is in illuminating shock structures under complicated conditions least accessible to laboratory and theoretical attacks. However, spacecraft shock observations are not without their limitations too, the most blatant of which is the need for simultaneous measurements by at least two vehicles, one of which must define the parameter set under investigation through measurement upstream in the continuously-changing solar wind. A second, not much less serious, limitation is the need for reliable estimates of bow shock velocities, for the shock is seldom stationary in the spacecraft frame, and without its velocity, its dimensions may not be correctly inferred, especially when complex structure prevails. A third limitation lies in the difficulty of finding comprehensive plasma instrumentation on a single spacecraft.

In view of these restrictions, it is not inappropriate to seek first a comprehensive characterization of the bow shock in its simplest phases, which

are already fairly well understood theoretically, for cases where all or most of these limitations can be overcome. We regard this as a necessary step to more advanced analysis of the bow shock under conditions where fresh ground will have to be broken. In this report we therefore describe several observations of the bow shock in a single day, 12 February 1969, when the important parameters M and β were very low for many hours and θ_{nB} was oblique, but made a large angle with the local shock normal. The parameter combination $M \lesssim 3$, $\beta << 1$ corresponds to the so-called "laminar" shock in which "fields and particle distributions change coherently through the shock," as discussed by Tidman and Krall (1971), i.e., large scale turbulence is absent and small scale microturbulence, if it exists, "does not destroy the ordered appearance of the transition layer."

Geometrically, we describe the situation of our shocks as "quasi-perpendicular," meaning numerically that $50° \lesssim \theta_{nB} \lesssim 88°$, where θ_{nB} is the angle between solar wind field $\underset{\sim}{B}$ and the local shock normal. The term quasi-perpendicular is used to designate that range of oblique θ_{nB} in which the shock retains its essentially monotonic character and is readily identifiable in the data (Greenstadt et al., 1970; Fairfield, 1974; Greenstadt, 1974).

We define M as the magnetosonic mach number $M \equiv M_{MS} = V_{SW} \cos \theta_{xn} / (C_A^2 + C_S^2)^{1/2}$, and $\beta = 8\pi Nk(T_p+T_e)/B^2$, where V_{SW} and B are the solar wind speed and magnetic induction, θ_{xn} is the assumed angle between V_{SW} and local shock normal $\underset{\sim}{n}$ (X is the solar ecliptic X-axis), C_A and C_S are the Alfvénic and sonic velocities, N is the plasma density, and T_p and T_e are the proton and electron temperatures of the solar wind. We assume, since electron temperatures were not measured, that $T_e = 1.5 \times 10^5$°K. For the cases to be described here, β varied between .035 and .23, but remained below .1 in all

but one instance. Under these circumstances, M_{MS} is essentially identical to the Alfvén mach number M_A, since $C_S \ll C_A$. In our cases, $M_A \lesssim 2.4$.

This communication, then, gives the first detailed picture of the bow shock in what should be its simplest, laminar form. The shock crossings we display were the first for which velocities were estimated directly by elapsed time observations of shock motion between two satellites (Greenstadt et al., 1972), and therefore the first for which direct estimates of shock thickness could be made. We have assembled a comprehensive, although still imperfect, set of plasma diagnostics in order to discern the various stages of plasma alteration through the shock and the wave noise that accompanied them. In the following sections, we describe the data, calling attention to numerous details, some of which may assume additional importance in future analyses of laminar or other shocks, and we discuss some of the most significant characteristics of the wave structure in and around the shock transition layer. We include an analysis of the whistler precursor that leads to an independent confirmation of the elapsed-time velocities, and introduce thereby a new technique for computing instantaneous shock velocity when upstream standing waves are detected.

MEASUREMENTS

The data shown here were obtained by the TRW plasma wave detector of OGO 5, the triaxial fluxgate magnetometers of OGO 5 (UCLA) and HEOS 1 (Imperial College), and the JPL plasma analyzer, Lockheed light ion spectrometer, University of London Langmuir probe, and UCLA/JPL search coils of OGO 5. The OGO 5 instruments provided the high resolution records of the shock at sampling intervals of 1.15 and .144 sec/sample, corresponding to 1 and 8 kilobit/sec telemetry rates.

The field and particle instrumentation of OGO 5 and HEOS 1 that provided data for this report are described by Bonetti et al. (1969), Hedgecock (1970), Crook et al. (1969), Snare and Benjamin (1966), Harris and Sharp (1969), and Neugebauer (1970). In using data from the University of London Langmuir Probe, we rely here only on relative changes in the raw signature of its energy sweep.

Magnetic field measurements are direct vector recordings of ambient induction, with the HEOS-1 data used to adjust the absolute bias levels of the OGO-5 readings, the latter having been subject to intermittent spacecraft interference. Plasma wave measurements were generally represented by the field strength in a broadband channel covering the range 1 to 22 kHz, with most of the shock noise probably contributed by signals between a few hundred Hz and 2 kHz. The broadband channel was sampled for 1.15 sec every 9.216 sec, and the wave amplitude level is given in terms of the wideband electric field strength for a broad noise spectrum. Electromagnetic wave noise is represented by the equivalent level of white noise over the bandwidth of each channel of the UCLA/JPL search coils. The JPL plasma analyzer provided plasma flux readings and upstream velocity and density parameters in the solar wind. These quantities were lost once OGO entered the shock because the analyzer looked only in a fixed direction toward the sun. Proton thermalization and diversion of solar wind protons in directions away from that of normal flow were detected by the Lockheed spectrometer, after the shock was entered, since this instrument looked only in a direction across the solar wind stream. Electron behavior was monitored by noting the slope of the electron distribution registered by the London probe, in which a high energy component appeared when electrons were thermalized (scattered) by the shock process. These last two measurements are represented here by relative changes in uncalibrated telemetry units.

Measurement imprecision contributed partially to the uncertainties of numbers quoted in this communication. Raw measurements of individual magnetic field components were accurate to 0.5γ (5×10^{-6} gauss) or better, and field angles based on them to 5° or less. VLF electric field strengths were measured to within a factor of two because the wideband output of only one of the triaxial electric antennas was monitored. Another source of uncertainty of numbers quoted here lay in the separations of the various satellites from each other in space and in the uncontrolled constitution of the solar wind. It has been assumed that the solar wind was not perfectly uniform over the distances between OGO 5 and the other spacecraft and that what near-uniformity there was, was not instantaneous. The ranges of some parameter values given in the next section reflect uncertainties arising from the unknown degree of non-uniformity in the solar wind and from delays of up to 15 or 20 minutes between OGO 5 and the other spacecraft. The chief uncertainties were contributed by solar wind density and magnetic field variability. Ranges of magnetic field direction mean that the field was varying in orientation on a scale comparable to the expected intersatellite delay. It must be remembered throughout this report that neither the aberration nor the instantaneous angles of solar wind flow were taken into account in any computation, so that all quantities dependent on direction of the shock normal or the flow contain uncertainties of up to several degrees. It was decided that comparable, unrecoverable uncertainties in the shock-normal model and inherent in temporal field variation would have vitiated the "accuracy" implied by incorporating average flow direction in estimates of instantaneous quantities.

In addition to the data illustrated in this report, plasma and magnetic field parameters for the unshocked solar wind were obtained from plasma analy-

zers on HEOS 1 (Univ. of Rome) and Explorer 33 (MIT) and from the magnetometer of Explorer 35 (NASA/ARC).

OBSERVATIONS

General. The center panel of Figure 1 displays the magnitude of ambient $\underset{\sim}{B}$ recorded for 20 hours by HEOS 1 and OGO 5. Low values are for the solar wind, high values for the magnetosheath. HEOS was the more distant of the two, so as the shock moved outward and inward past the two spacecraft, HEOS was always in the solar wind outside the magnetosheath when the shock crossed OGO. The crossings numbered 1 through 4 are those for which average shock velocities were obtained in an earlier study (Greenstadt et al., 1972).

In the central panel, the HEOS field data are represented by 48-second samples, the OGO data by 1-minute averages. In the five separate panels surrounding the central one, the OGO data are represented by 1.15-sec samples. In the top four inserts, the step-like, almost noise-free appearance of the shock in the averages and at the 48-sec sample interval is seen to have been preserved at resolution 48 times higher than that of the HEOS graph at center. There are small differences between the first shock signature and the other three, namely in the presence or absence of upstream waves. These differences will be discussed later. The bottom panel in Figure 1 shows the pair of crossings 7 and 8, which were no longer strictly laminar, but turbulent and, in the case of crossing 8, perhaps multigradient as well. The shock front of crossing 7 was as sharp as those of the earlier crossings, but there was a small foot ahead of it and appreciable noise behind it. The change may have

been caused by a rise in β or in the mach number closer to the critical value, which is assumed to have been between 2.5 and 3.0. A sudden rotation of the interplanetary field toward the shock normal at 1750 was responsible for the additional complexity of crossing 8. These last two shock observations of the day serve to show the extreme simplicity of the earlier laminar shock profiles chosen for this study.

Dimensions. The upper half of Table 1 lists the salient quantities pertaining to the dimensions and local geometry of shock crossings 1 through 4. Measured dimensions are at the left, derived theoretical quantities at the right of the vertical division. Ramp thickness ΔS is the product $\overline{V}_{SS}\Delta t$, where Δt is the observed rise time of the ramp and $\overline{V}_{SS}$ is the average velocity of normal shock motion between OGO and HEOS positions in the spacecraft frame: positive indicates outward, negative inward, shock motion. V_{SH} is the velocity of the shock relative to the solar wind velocity component along the shock normal. Angle θ_{nB} is the angle between solar wind field vector B_{SW} and the local normal to the assumed rotationally-symmetric hyperbolic bow shock surface at OGO 5. The right-hand columns give M_A, proton inertial length c/ω_{pi}, and the ratio of ΔS to this last quantity. The inertial length was computed from HEOS 1 and Explorer 33 plasma data and HEOS 1 magnetometer data; the ranges of c/ω_{pi} express uncertainties in n_i.

The ramp thickness could also be related to the cyclotron radius of the bulk flow component across the field in the shock. However, the cyclotron radius was of the same order as c/ω_{pi} in the cases described here, so no useful distinction could be made by displaying it separately, and we have chosen to compare ΔS with c/ω_{pi} only.

In the θ_{nB} column, the table shows that at crossing 1, B_{SW} was 25° away from the perpendicular orientation, while at crossing 4, it was very close to perpendicular. In all but the third case, the ramp thickness was a small multiple of c/ω_{pi}, as listed. The third case is included for completeness, but we do not regard its listed velocity $\overline{V}_{SS}$ as reliable for reasons discussed below; hence, quantities derived from V_{SS} are not useful.

Details at High Resolution. Further details of the laminar shock were resolved in observations at a still higher sampling rate. Figure 2 displays the pair of crossings numbered 5 and 6, which were observed when OGO 5 was operating at its 8-kilobit telemetry rate. The magnitude and the three components of the magnetic field in spacecraft coordinates are shown. Magnetic field samples were .144-sec apart, which was adequate to provide some 67 measurement points in the ramp alone in case 6. The two shock profiles are very similar, there being only two significant distinctions between them, namely, that at the second shock a set of tiny waves is visible in the foot and some wavelike steps are more pronounced in the ramp. (In the following discussion the term "waves" is used to describe ultra low frequency electromagnetic noise measured by the magnetometer; the terms "plasma waves" or "electric field waves" are used to describe electromagnetic or electrostatic oscillations measured in various channels by the plasma wave electric field antenna.) The magnitude and all components are equally "laminar." Each of the two shock signatures exhibits a "plume" consisting of five distinct waves, or pulses, at the top of its main field jump, seen in B, and its principal component, B_y, and each has a "dome" of average field higher than was found a few tens of seconds

further downstream The domes seem to have been about one-and-a-half to two times the duration of the plumes. The waves of the plumes were evidently stationary in the respective shock frames, so they were propagating upstream in the solar wind plasma at 300 to 400 Km/sec.

The time-dimensions of the high-resolution shocks of Figure 2 are characterized in the figure by three quantities: first, the duration of the ramp, defined as the time between the first point at which the field rises above the level of small preshock maxima and the last point at which the field is below the level of small postshock minima; second, the duration of the plume; third the sum of ramp and plume. In Table 1, Δt denotes the duration of the ramp. This quantity was chosen as the only common quantity reasonably identifiable in shocks 1 through 4, where plumes would not have been resolvable, as well as in 5 and 6. Thus the Δt entered for shocks 1 through 4 in Table 1 is not the time from base to peak, but is the interval from the beginning of the steep field gradient to the level of the post-gradient minima, going in the direction from solar wind to magnetosheath.

The period of the average pulse in the plume at 1325 was 1.26 sec; the period of the average pulse in the plume at 1355 was 1.03 sec. The sums of ramp and plume duration were 10.3 seconds in both cases. The "steps" in the 1355 ramp were 1 to 1.5 seconds long, and the small oscillations in the foot averaged .4 sec. If we take the period of the average step in the ramp and pulse in the plume to be 1.2 sec, the ratios of durations of: foot wave to plume (or ramp) wave to ramp to total structure (ramp and plume) are 1/3/13/25 for the 1355 UT shock. Thus, the total structure from the base of the gradient to the end of distinguishable individual waves (the sheath end of the plume) appeared to be composed of some eight or nine waves or steps of a little over

1-second period each, half of them in the ramp and half in the plume; this was preceded by a precursor comprised of a few cycles of a damped standing wave (to be discussed later) and an eight-sec train of very small amplitude oscillations of about .4 sec average period. The small oscillations in the foot are close to the digitization level of the instrument, and form a somewhat irregular pattern in which groups of waves less than 0.14-sec period were just resolved in the raw data.

As the center panel of Figure 1 shows, there was a gap in HEOS data when the shock crossings of hour 13 (Figure 2) were observed by OGO. Consequently no average shock velocities could be determined for these events, so translation of periods and durations into thicknesses and wavelengths could not be made directly. However, we note that the ramp duration of case 4 is comparable to that of cases 5 and 6 and we reason as follows: the correct conversion of times to distances actually requires not an average shock velocity but an instantaneous velocity at the moment of crossing. Of the four measured average velocities, the last one, at 1628, is the closest to a true instantaneous velocity because the elapsed time from which it was calculated was the shortest of the four, leaving the least margin for discrepancy between average and instantaneous speeds. Also, an instantaneous velocity of some 100 Km/sec has been determined independently for the shock's crossing of HEOS at about 1627 UT as it was on its way toward OGO (Formisano et al., 1973).

If the structure of the laminar shock is assumed to have been essentially the same for crossings 4, 5, 6, and 7, then the ramp thickness for crossings 5 and 6 should have been about 2-3 c/ω_{pi}. This value is indicated in parenthesis in the last column in the lower half of Table 1. From this multiple of c/ω_{pi}, inferred values of ΔS, hypothetical V_{SH}, V_{SS}, and M_A were calculated for

cases 5, 6, and 7. These are also indicated by parentheses in Table 1. Based on the above argument that short elapsed times should reduce discrepancies between average and instantaneous shock speeds, cases 1 and 2 have good approximations to true instantaneous velocity, although not as good as case 4, while case 3's estimate is poor, which is why it was discounted in an earlier remark. The derived velocities for cases 5, 6, and 7 are therefore compatible with those of the most reliable of the first four cases of the table.

We recognize that θ_{nB} was not the same in case 4 as it was in cases 5 and 6, and that our thickness estimate could be affected. Appreciable broadening of the shock ramp may have occurred with decreasing θ_{nB}. If significant thickening had occurred, 400 Km would be an underestimate for ΔS in cases 5 and 6. Doubling ΔS, for example, would in turn raise the inferred V_{SH} in case 5 to 200 Km/sec, a speed at or above a statistical extreme found by Formisano et al. (1973). Substantial thickening was therefore not ruled out, and will be supported in a later section (Table 2). Very large ΔS, for $73° \leq \theta_{nB} \leq 80°$, would, however, have been incompatible with the value of ΔS found for case 2.

Shock broadening by field obliquity did clearly take effect when θ_n fell in the range 65°-70°. An example is illustrated by case 1. Figure 3 shows a comparison of the field and plasma wave profiles of crossings 1 and 3. At crossing 3, the shock encounter was sudden and the plasma wave noise consisted of a well defined noise peak at the field gradient; at crossing 1, a set of waves had developed ahead of the shock and the region of plasma wave noise was broadened to coincide with the waves, probably indicating preshock electron thermalization or reflection. The electric field noise appeared to increase with increasing wave amplitude as the main gradient was approached.

Still Further Details: Plasma Modifications in the Shock. The laminar structure and high resolution of the 1325-1355 shock crossings combined to offer an unusually uncluttered picture of the sequence of plasma changes across the shock gradient. These changes are shown in Figure 4. At the bottom, the field magnitude graph of Figure 3 is repeated for reference, with the range of estimated c/ω_{pi} thicknesses noted. Above the field is the plasma flux profile from the JPL Faraday Cup. Recall that this analyzer maintained a fixed view toward the sun; absence of flux inside the magnetosheath signifies deflection of flow outside the acceptance angle of the instrument, as at left and right edges, respectively, in the figure. We shall discuss the sequence of events in Figure 4 always from solar wind to magnetosheath, regardless of the actual order of observation. In the left panel, the flux underwent some small fluctuations as the shock was approached, then began a series of major oscillations just as the ramp started, and finally reappeared at a very low level behind the shock (the instrument was turned off at the top of the ramp and beginning of the plume). In the right panel, the same sequence was repeated with two exceptions: there appears to have been a gradual decline in average flux in the foot just outside the ramp, and the flux never entirely disappeared behind the ramp. The pattern of major oscillations was evidently a fixed characteristic of the laminar shock structure, as the numbered maxima and minima in the two panels elucidate. The first minimum in each case occurred before, and highest maximum after, midramp. Examination of plasma spectra indicates that the bulk solar wind velocity was still essentially unaffected at the time of the highest maximum, so this peak represents a density increase in the sheathside half of the shock ramp. The preramp, or early ramp, decrease in flux, on the other hand, was the result of a change

in flow direction. The sequence of observable flux events in the laminar shock, then, was early deflection of flow, strong variations in density, and essentially unreduced bulk velocity through most of the field ramp until the flow was redirected and the flux so diminished at the head of the ramp that plasma parameters could no longer be determined. The density variations included a rise to a density above that of the unshocked solar wind.

The third and fourth graphs from the bottom of Figure 4 illustrate the relative thermal behavior of solar wind electrons and protons, in uncalibrated telemetry units. In both panels magnetosheath electron spectra are clearly distinguishable from solar wind electron spectra by their rather flat distribution when the Langmuir probe sweep analyzed the higher electron energies (right-hand side of each sample curve). The shaded portions of the electron retardation curves indicate the difference between those spectra and the unaffected solar wind distribution measured upstream several minutes outside the shock. The electron measurements of both panels show that slight changes in electron energy distribution occurred outside the shock ahead of the ramp. The right panel shows that significant enhancement at high energy took place in the first half of the ramp; the left panel shows that full thermalization had not occurred by the end of the ramp and beginning of the plume; the right panel shows that full thermalization did occur by the end of the plume. Electron acceleration on the upstream side of the shock has previously been observed by Montgomery et al. (1970) and by Neugebauer et al. (1971) in their study of five non-laminar oblique shocks.

The Lockheed light ion spectrometer peers in a direction not aligned with the sun and is therefore a detector of thermalization and flow deflection, sensing only the protons that move in directions across the original direction

of flow. For brevity, we shall designate appearances of particles in this instrument as "heating" or "thermalization." The left panel, then, shows that by midramp no proton thermalization whatever was apparent; the right panel shows that some proton heating could have occurred after midramp; both panels show that the protons were deflected and/or thermalized by midplume. There is an ambiguity between the panels in properly associating proton heating with the flux pattern, but it appears that initial deflections of the ions occurred in conjunction with the high density spike or its forward edge.

Above the proton graph, the fifth and sixth strips depict the electric field noise recorded by the TRW plasma wave detector (PWD). The PWD, which cycled through its frequency channels at a relatively slow pace, was not in any of the more favorable channels ($\leq$ 3 kHz; Fredricks et al., 1970) during either crossing in Figure 4, as the fifth strip shows. Nevertheless, it is evident that sporadic elevated noise levels, even at 7 and 14 kHz, accompanied the shock ramp. In particular, a well-defined spike of 7 kHz noise was recorded at midramp simultaneously with the forward edge of the major density elevation in the left panel, and a noise jump at 14 kHz was detected at the analogous point of the right panel

The subcommutated PWD data in the sixth strip are somewhat more informative. We see that in both panels the 200 Hz channel recorded increases in noise level outside the ramp where the electrons were already affected by the presence of the shock, and that the 200 Hz noise was considerably elevated where partial thermalization of the electrons was taking place, both early and late, in the ramp. Noise in this channel persisted longer behind the shock in the right than in the left panel. There is no obvious association of electrostatic noise with proton effects, but this could have been easily missed with the PWD's incomplete frequency-time coverage. Special purpose, i.e., wideband, PWD data were not recorded on 12 February.

Electromagnetic Noise. The crossings of cases 5 and 6, as witnessed by one axis of the OGO 5 search coils, are shown in Figure 5, with the field magnitude profile repeated at the bottom for reference. Individual channel center-frequencies are identified in the vertical center column, between the two panels. In this figure, the very small-amplitude, damped standing waves barely discernible in front of the shock have been marked by a dottec curve near the bottom, just above the plot of B. These will be discussed further in a later paragraph.

We see that EM wave noise began upstream from the ramp (in one or more of the five lowest frequency channels) concurrently with the appearance of the tiny, standing waves ahead of the shock, and continued through the ramp. This upstream noise had an upper frequency cutoff somewhere between 216 and 467 Hz: this is the range in which the electron cyclotron frequency, f_{ce} = 252 Hz, fell at that time. We take it that the upstream data represent whistler mode noise arising in the shock and propagating at angles less than 60° to $\underset{\sim}{B}$, since the high frequency whistler cutoff is already reduced to 216 Hz and 100 Hz for propagation at 30° and 60° to $\underset{\sim}{B}$, respectively. Along the shock normal, i.e., at 75°, the cutoff was only 62 Hz. The small standing waves were simply the appropriate component of the whistler spectrum, at about 1 to 2 Hz, matching the solar wind velocity along the local normal. The steps in the ramp and the waves of the plume may then have been whistlers just below the standing wave frequency, or with decreasing $d\omega/dk$ as discussed by Tidman and Krall (1971, p 22).

Another perspective of the search coil data, in physical units, helps to clarify the EM noise behavior. Figure 6(a) shows a three-dimensional repre-

sentation of the history of one-axis magnetic wave power spectra through the shock crossing of 1355. Selected spectra, constructed from the seven-channel data of Figure 5 are shown on a common time scale with a sampled version of the field magnitude plotted obliquely on an arbitrary baseline. The entire array of spectra is 38.6 seconds long, with adjacent spectra .69 sec apart. Some spectra were omitted where they essentially duplicated those adjacent to them. The small circles designate the 100 Hz channels of the spectra as a guide to the eye in following wave behavior between $f_{ce} \cos \theta_{nB}$ and f_{ce}. Conversion to physical units of spectral density was based on assumed white noise across each frequency channel bandwidth.

As the figure shows, field noise grew rapidly just as, but definitely before, the shock ramp was approached, and decayed again rapidly behind the ramp. The pattern of 100 Hz noise illustrates well the generation of whistlers in the forward edge of the shock ramp, their propagation upstream along $\underset{\sim}{B}$, and their rapid damping in the solar wind. The 100 Hz noise reached its peak power at the foot of the ramp, suggesting propagation along the shock or, more probably, along $\underset{\sim}{B}$, which is only 15° from the tangent. The (b) insert at the lower right of the figure details the 216 and 467 Hz noise patterns through the ramp. The 216 Hz noise, just below the upstream whistler cutoff at $f_{ce} = 252$ Hz, appears within what must have been the 30° cone of propagation for that frequency. Moreover, the whistlers must have been severely damped along $\underset{\sim}{B}$, or they would have reached the detector earlier, having traveled laterally from a more distant point on the shock. The 467 Hz noise, which could not have propagated in any direction in the solar wind, peaked in the ramp behind the 216 Hz peak, only after the elevation in B raised the electron cyclotron frequency.

To summarize, we may imagine two typical "antenna patterns" of whistler mode waves propagating from the shock preferentially along $\underset{\sim}{B}$, one pattern ahead of the forward edge of the shock ramp, the other behind it. As the shock approached the satellite, the search coils moved through the various phase velocity "layers" of the upstream pattern, each frequency channel being affected as it entered the corresponding propagation cone, at $f_{ce} \cos \theta$. Behind the ramp, the satellite moved through the second pattern in reverse order, but with elevated f_{ce} affecting channels of higher frequency. The mode was effectively damped both upstream and downstream in distances on the order of the ramp thickness. Toward the rear of the ramp, changes in n, B, and T evidently allowed higher frequencies up to and above 1 kHz to propagate.

The Upstream Waves of Crossing 1. Simple geometrical properties of the standing waves can be obtained. As the OGO 5 panel in the center of Figure 1 shows, crossing number 1 into the sheath was immediately proceeded by a crossing out of the sheath. The two crossings were very similar to one another in profile, with one the reverse of the other. The field components spanning the two crossings are shown in Figure 7, in rectangular spacecraft coordinates, in which the X-Y plane approximates the shock plane. The mean interplanetary field, measured by HEOS and Explorer 35, was very steady, except for a slight shift in direction, seen just before the 0049 crossing in the X and Y components of the OGO 5 data. Angle θ_{Bn} was $\approx 74°$ at the time of crossing; before the shift, about half a minute earlier, it was 64°-66° (Table 1).

Outstanding features of these crossings were the damped wavetrains appearing both times in the solar wind ahead of the shock. There are about six identifiable cycles associated with each crossing, the first set averaging about 8 seconds per cycle, the second about 11.5 sec per cycle. The appearance of

the waves certainly suggests that they were standing in the shock frame. The ratios of ramp duration to average wave period are .9 and 1.1 in the two cases, so the wavetrain precursor seems to have been moving with the shock. No elapsed time velocity estimate is available for the first set, but the 55 Km/sec found for the 0049 crossing (Table 1) gives an average wavelength λ of 630 Km.

In Figure 7, the wave perturbation lies in the X-Y plane, i.e., in a plane approximately parallel to the local shock surface. The polarization diagrams for the two wave sets are shown at the top of Figure 8; the senses of rotation of the two sets are opposite in the spacecraft frame. The sketch at the bottom of Figure 8 depicts the common standing wave perturbation in three dimensions relative to the local shock. The wave is polarized in the sense of a whistler propagating along the outward normal. Since it is standing in the shock frame, its phase velocity in the solar wind plasma is some 470 Km/sec.

DISCUSSION

The details of the laminar shock described above can be used to make some quantitative tests for consistency of the measurements with theory. Ideally, one would like to have high resolution proton and electron spectra through the shock transition layer, including the ramp, to define completely the behavior of the particles. Particle data of such fine resolution were unavailable, however, so our discussion is confined to some selected items involving wave behavior. Since whistler mode waves played a large role in these laminar shocks, we concentrated on these.

Standing Waves. The oblique (not necessarily laminar) shock in the laboratory and in theory is typically depicted as having a damped, standing

whistler precursor at both subcritical and supercritical mach numbers, with the last preshock cycle often of amplitude comparable to that of the final shock gradient (Robson, 1969; Tidman and Krall, 1971). Yet of the seven shock profiles shown in this paper, only three, the pair in Figure 7 (including case number 1) and number 7 of Figure 1, show any clear wavelike oscillations in the foot of the shock, and those are of small amplitude. Only one demonstrable standing wave occurred, in case 1, if we regard the prior crossing of 0045 (Figure 6) as simply another view of the same shock under the same conditions at essentially the same time. A barely-discernible example, of very small amplitude, was associated with the crossing pair of Figure 5. Thus, it appears that stationary whistler precursors are rare for quasi-perpendicular, laminar shocks and do not appear or barely appear when $\theta_{Bn} \gtrsim 70°$ (case 7 may not even have been laminar). Examination of other laminar crossings at high bit rates, not shown here, support this inference. We note that a sequence of non-laminar shocks with a particularly long whistler precursor studied by Holzer et al. (1972) revealed no waves which were phase-standing in the solar wind flow.

The marginal appearance of upstream standing precursors in these laminar shocks is explainable. A stationary whistler precursor must satisfy the following conditions to exist: 1) Its phase velocity must equal the solar wind velocity; 2) its group velocity must exceed the solar wind velocity; 3) it must be stable at finite amplitude. When we use the term velocity, we always mean the component of velocity along the local shock normal. Whistler phase velocities depend on B, N, and θ_{nB}, and typically exceed the solar wind velocity for a range of frequencies, as depicted by Smith et al., 1967; and Scarf et al., 1968. Their examples for average conditions were essentially similar to the solid curves of Figure 9, in which are plotted the whistler phase velocity dependences for the

conditions that prevailed for our cases 1 and 4. The pairs of curves take into account the possible ranges of phase velocities V_ϕ allowed by the limit over which N and θ_{nB} might have occurred within measurement uncertainties. For each case the applicable velocity vs frequency curve lay somewhere between the extremes. The high frequency cutoff in each case is at $f/f_{ce} = \cos \theta_{nB}$ rather than $f = f_{ce}$, as in parallel propagation (where $\cos \theta_{nB} = 1$). The frequencies at which whistlers would stand along the shock normal occur where the phase velocity curves cross the corresponding shock velocity lines V_{SH}. There are two such crossings for each curve that has $V_\phi > V_{SH}$, but we have noted only the lower frequency crossing in each case. The circles near the apex of the curves mark the frequencies below which the group velocities V_g exceed the phase velocities; these critical frequencies are located at $f/f_{ce} = \frac{1}{2} \cos \theta_{nB}$. Hence, $V_\phi = V_{SH} < V_g$ only at the lower standing frequencies, where applicable. The algebraic relations underlying Figure 8 are outlined in Appendix 1.

The message of Figure 9 is that in case 1, whistlers can propagate upstream for a wide range of frequencies and will be stationary for some value f between 1.9×10^{-3} f_{ce} and 5×10^{-3} f_{ce}, while in case 4, values of N and θ_{nB} may have prevailed for which $V_\phi < V_{SH}$ for all frequencies, with no standing wave possible. Since case 1 (together with its companion in Figure 7) was the only one in which a significant standing wave was observed, the phase (and group) velocity criterion seems to explain the difference between the case 1 and 4 profiles.

In all the remaining cases except case 7, the phase velocity curves were similar to those of case 1. Case 7 was similar to case 4. Standing wave precursors should therefore have been the rule rather than the exception on the basis that, at some frequency, $V_\phi = V_{SH} < V_g$ in five out of seven observations. However, favorable velocity considerations do not by themselves guarantee the existence of waves of measurable amplitude nor do they provide any guidance as

to what upstream amplitudes should be. Waves of finite amplitude present finite field gradients to the upstream solar wind flow and can therefore cause finite currents large enough to generate their own signatures in the plasma, i.e., currents associated with field gradients tend to generate plasma instabilities which may in turn damp the waves.

The general criterion for development of instability is that the drift velocity responsible for the current exceed the plasma thermal velocity w_T. The threshold value at which $V_D \gtrsim w_T$ is proportional to the product of $\Delta B/B$ and either β^{-1} or $\beta^{-1/2}$, depending on the scale length involved. A convenient tabulation of several instability modes related to the bow shock has been assembled, together with suitable references, by Greenstadt and Fredricks (1973), who show that on the c/ω_{pi} scale, instabilities arise when $\Delta B/B \gtrsim A\beta^{1/2}$, where A is a constant depending on the mode invoked. The key fact is that low β is conducive to microinstability growth for a given $\Delta B/B$, and $\beta_i << .1$ on 12 February 1969. The drift instability, for example, requires $\Delta B/B \gtrsim \beta_i^{1/2}$ on the c/ω_{pi} scale length ($A \simeq 1$). For $\beta_i = .01$, $\beta_i^{1/2} = .1$, so that at the time of case 2, a wave with $\Delta B \geq .1B = .1(9) = .9\ \gamma$ would have been sufficient to trigger this mode. Formisano et al. (1971) have given values of $\beta_i = .002$ to $.004$ early on the 12th, so the drift mode requirement may have been satisfied even by tiny waves of amplitude $\simeq .5\ \gamma$. Certainly, where small standing waves of 1 to 2 γ amplitude did appear, in case 1, they were accompanied by doppler-shifted plasma wave noise of unknown frequency recorded in the broadband channel (Figure 3). In nonlaminar cases of high β examined by the authors, profiles with at least one large amplitude wave outside the shock have been noted.

In sum: in four cases, 2, 3, 4, and 6, where phase and group velocity considerations would in principal have permitted upstream standing whistler waves, the dispersive wavelength could have been less than the dissipative scale length and waves could have been damped by easily triggered plasma instabilities; in three cases, 1, 4, and 7, where the dispersive wavelength may have exceeded the dissipative scale length, only one, case 1, occurred when upstream whistler propagation was unambiguously permitted, and in that one case, only small waves appeared, which were accompanied by plasma wave noise possibly generated by the waves themselves in a condition of extremely low β_i. The present observational profiles of low mach number shocks with no standing precursors and considerable magnetic noise is substantially similar to the results of the AVCO laboratory experiment (Pugh and Patrick, 1967; Patrick and Pugh, 1969), which also obtained thicknesses of (2-4) c/ω_{pi}.

Velocity Estimates from Standing Wavelength. Since in oblique shocks, the standing whistler wavelength must necessarily be related to the shock velocity as well as to the ambient plasma parameters, it is possible to use the wavelength, L_d, to estimate the local, instantaneous shock velocity V_{SS} in the plasma frame. The procedure for doing so is described in Appendix 2. We have applied equation (4) of Appendix 2 to three cases in which standing waves were in evidence, case 1 (0049 UT), and cases 5 and 6 (1325, 1355 UT). The outline of the small waves ahead of the shock in cases 5 and 6 was indicated in Figure 5.

The results of estimating V_{SS} from L_d are shown in Table 2, along with some useful data for comparison. The first five columns of the table give the case number, time, estimated average standing wave period T_{wave} in the spacecraft frame, density N, and velocity V_{SS} in the spacecraft frame. Equation (4) (Appendix 2) was evaluated for the extremes of the density range, N = 1 and 2.

The equation is capable, of course, of yielding up to four real solutions, but only for N = 2 in case 5 did it actually do so. Only real solutions of reasonable magnitude are shown in the table. In case 5, density N = 1 gave no real solution at all. The sixth column of Table 2 repeats $\overline{V}_{SS}$ from Table 1. In case 1, the solution V_{SS} for N = 1 is very close to $\overline{V}_{SS}$, giving remarkably good agreement between the instantaneous and average velocities, estimated by entirely independent methods. It will be recalled that the crossings of cases 5 and 6 were not observed by both spacecraft, so $\overline{V}_{SS}$ (Table 1) had to be approximated in an indirect way, assuming ramp thickness as a suitable multiple of c/ω_{pi} (parentheses in the table). Nevertheless, in case 6, the lower end of the range of estimated $\overline{V}_{SS}$ is very close to V_{SS}. In case 5, the instantaneous and average velocities are not in agreement numerically, but the higher instantaneous speed is consistent with the higher estimated range of average speed.

The next two columns give the wave-derived shock ramp thickness $\Delta S_w = V_{SS}\Delta t$, computed from V_{SS}, the ramp time of Table 1, and the ratio of ΔS_w to c/ω_{pi}. The earlier inference that shock thickness is a small multiple of c/ω_{pi} is supported, although it appears that a range of 2-4 or 2-5 would be better for $\Delta S/c/\omega_{pi}$ than 2-3. The last two columns of the table display $L_d = V_{SS}T_{wave}$ and the ratio $\Delta S/T_{wave}$, showing $\Delta S \gtrsim T_{wave}$, i.e., the ramp length is on the order of the dispersive length or a little longer. It would follow that the dissipative length for the electrons ought to be less than, or about equal to, T_{wave}, and the wave noise (Figures 3, 5) and electron heating profiles (Figure 4) are compatible with such an inference.

The bottom entry in Table 2 shows the thickness and dispersion lengths for case 4, for comparison with the cases just discussed. This case had the

most reliable average velocity. Ratio $\Delta S/c/\omega_{pi}$ is reasonably compatible with the others, but $\Delta S/L_d$ is appreciably larger and perhaps even very much larger than in the other cases. Here, L_d was computed from expression (1) of Appendix 2, since no upstream waves were visible. The high values of $\Delta S/L_d$ are precisely what would be expected for the absence of detectable waves and the nearly perpendicular θ_{nB}: the standing wavetrain was swallowed up by the ramp because the wavelength exceeded the dissipation length.

Ion Acoustic Waves. An argument was given in an earlier paragraph that upstream whistlers were damped by wavemodes easily excited at low β. The drift instability was selected as an example of a suitable mode, but the ion acoustic mode might also have been chosen. We therefore show separately here that this mode was highly improbable, using the dimensions estimated in this report.

The condition for generation of ion acoustic noise is that the electron drift velocity $V_d \approx \Delta B/2\Delta S\mu_o Ne$ (mks units) exceed the sound speed $w_T = (kT_e/m_i)^{1/2}$ in the ramp, where ΔB is the jump in B over distance ΔS. In our case 1 (0049 UT), we take $\Delta B \approx 17\ \gamma$ (Figure 3), $\Delta S = 660$ Km (Table 2) at N = 1, and we assume T_e, which tends to be largely constant in the solar wind, $\approx 1.5 \times 10^{5}$°K. The measured value of T_i was about 6×10^{3}°K. Then $V_d/w_T \approx .08/35 << 1$. which falls far short of the threshold for generation of ion noise. This value, based on an assumed T_e in the solar wind, is undoubtedly too high in the ramp, because the early preferential heating of electrons (Figure 4) would have raised T_e and w_T there, thus lowering V_d/w_T. Although our value of T_e was only assumed, it is highly improbable that $V_d/w_T \geq 1$, since this would require T_e to have been less than $\left(\frac{.08}{35}\right)^2 \times 1.5 \times 10^5 = .78$°K, according to the expressions above. It therefore seems certain that ion acoustic noise was not responsible for the plasma waves surrounding the shock

in cases 1 and 3 (Figure 3), 5 and 6 (Figure 4), and the other laminar cases, not illustrated, where similar electric oscillations occurred. This improbability does not necessarily mean the drift instability was a contributor to the noise. More sophisticated apparatus, or perhaps further analysis, will be needed to distinguish the correct wavemode.

CONCLUSION

The structure of the earth's bow shock for low β, low M upwind plasma conditions in local quasi-perpendicular geometry when $65° \lesssim \theta_{nB} \lesssim 88°$ is indeed laminar in the sense that macroscopic turbulence is absent from the magnetic field profile and particle thermalizations evidently occur in an orderly way. The electrons are heated first over a relatively broad region including both precursor and ramp, and the protons are heated in a relatively narrow region somewhere between the middle and end of the magnetic ramp. The shock magnetic profile is 2-4 c/ω_{pi} thick and corresponds well to the form expected from laboratory and theoretical results for oblique shocks at low β, where upstream standing whistlers are heavily damped.

Whistler waves propagating within their frequency-dependent phase-velocity cones around B are a significant constituent of the electromagnetic spectrum in the shock and its precursor up to the local electron cyclotron frequency. Indeed the precursor itself is simply the whistler whose phase velocity equals the normal component of solar wind velocity in the shock frame. The shock (magnetic) ramp itself appears to be composed of damped whistlers near the standing wave frequency, and the times at which whistlers were detected at all observed frequencies coincided in our cases with the region in which small waves or steps were clearly visible in the magnetic record, the region consisting of precursor, ramp, and plume.

Electric plasma waves occur in the laminar shock and its precursor. In one of our cases, noise at 7 kHz was concentrated at midramp, probably where proton thermalization began and the solar wind flux underwent some fluctuations. These fluctuations of the plasma flux appeared to form a pattern characteristic of the shock, probably related to density gradients and current sheets in the shock transition layer.

The measured period of standing precursor whistlers can be used to obtain a reliable instantaneous bow shock velocity in the spacecraft frame, if the upstream plasma parameters, as well as the field, are known. The method for obtaining the shock velocity should work equally well for any quasi-perpendicular (oblique) shock, whether it is laminar or not, as long as the stationary upstream waves are discernible.

ACKNOWLEDGMENTS

Numerous discussions with R. W. Fredricks, T. G. Northrop, and A. E. Robson were valuable in preparing this report, which was funded by the National Aeroanutics and Space Administration under Contracts NASW-2398, NGR 05-007-004, NASW-2513, and NAS7-100. We thank Drs. G. Sharp, K. Harris, and K. Norman for allowing us to display and discuss their low energy proton and electron data.

REFERENCES

Bonetti, A., G. Moreno, S. Cantarano, A. Egidi, R. Marconero, F. Palutan, and G. Pizzella, Solar wind observations with ESRO satellite HEOS 1 in December 1968, Nuovo Cimento, 64B, 307, 1969.

Crook, G. M., F. L. Scarf, R. W. Fredricks, I. M. Green, and P. Lukas, The OGO 5 plasma wave detector: Instrumentation and in-flight operation, IEEE Trans. Geosci. Electron., GE-7, 120, 1969.

Fairfield, D. H., Whistler waves observed upstream from collisionless shocks, J. Geophys. Res., 79, 1368, 1974.

Formisano, V., P. C. Hedgecock, G. Moreno, J. Sear, and D. Bollea, Observations of earth's bow shock for low mach numbers, Planet. Space Sci., 19, 1519, 1971.

Formisano, V., P. C. Hedgecock, G. Moreno, F. Palmiotto, and J. Chao, Solar wind interaction with the earth's magnetic field, 2. The magnetohydrodynamic bow shock, J. Geophys. Res., 78, 3731, 1973b.

Fredricks, R. W., G. M. Crook, C. F. Kennel, I. M. Green, F. L. Scarf, P. J. Coleman, Jr., and C. T. Russell, OGO 5 observations of electrostatic turbulence in bow shock magnetic structures, J. Geophys. Res., 75, 3751, 1970.

Greenstadt, E. W., I. M. Green, G. T. Inouye, D. S. Colburn, J. H. Binsack, and E. F. Lyon, Dual satellite observation of the earth's bow shock, 1. The thick pulsation shock, Cosmic Electrodyn., 1, 160, 1970.

Greenstadt, E. W., P. C. Hedgecock, and C. T. Russell, Large-scale coherence and high velocities of the earth's bow shock on February 12, 1969, J. Geophys. Res., 77, 1116, 1972.

Greenstadt, E. W., Structure of the terrestrial bow shock, paper presented at Third Solar Wind Conference, Asilomar, March 1974.

Greenstadt, E. W., and R. W. Fredricks, Plasma instability modes related to the earth's bow shock, Magnetospheric Physics, ed. by B. M. McCormac, D. Reidel, Dordrecht, Holland, 355, 1974.

Harris, K. K., and G. W. Sharp, OGO 5 ion spectrometer, IEEE Trans. Geosci. Electron., GE-7, 93, 1969.

Hedgecock, P. C., The solar particle event of February 25, 1969, in Intercorrelated Satellite Observations Related to Solar Events, edited by V. Manno and D. E. Page, D. Reidel, Dordrecht, Netherlands, 419, 1970.

Holzer, R. E., T. G. Northrop, J. V. Olson, and C. T. Russell, Study of waves in the earth's bow shock, J. Geophys. Res., 77, 2264, 1972.

Montgomery, M. D., J. R. Asbridge, and S. J. Bame, Vela 4 plasma observations near the earth's bow shock, J. Geophys. Res., 75, 1217, 1970.

Morton, K. W., Finite-amplitude compression waves in a collision-free plasma, Phys. Fluids, 7, 1801, 1964.

Neugebauer, M., Initial deceleration of solar-wind positive ions in the earth's bow shock, J. Geophys. Res., 75, 717, 1970.

Neugebauer, M., C. T. Russell, J. V. Olson, Correlated observations of electrons and magnetic fields at the earth's bow shock, J. Geophys. Res., 76, 4366, 1971.

Patrick, R. M., and E. R. Pugh, Laboratory study of turbulence in collision-free shocks, Phys. Fluids, 12, 366, 1969

Pugh, E. R., and R. M. Patrick, Plasma wind tunnel studies of collision-free flows and shocks, Phys. Fluids, 10, 2579, 1967.

Robson, A. E., Experiments on oblique shock waves, Spec. Publ. 51, ESRO, Frascati, Italy, 159, 1969.

Scarf, F. L., G. M. Crook, I. M. Green, and P. F. Virobik, Initial results of the Pioneer 8 VLF electric field experiment, J. Geophys. Res., 73, 6665, 1968.

Smith, E. J., R. H. Holzer, M. G. McLeod, and C. T. Russell, Magnetic noise in the magnetosheath in the frequency range 3-300 Hz, J. Geophys. Res., 72, 4803-4813, 1967.

Snare, R. C., and C. R. Benjamin, Magnetic field instrument for the OGO-E spacecraft, IEEE Trans. Nucl. Sci., NS-13, 6, 1966.

Stix, T. H., The Theory of Plasma Waves, McGraw-Hill, New York, 1962.

Tidman, D. A., and N. A. Krall, Shock Waves in Collisionless Plasmas, John Wiley-Interscience, New York, 1971.

Table 1. Shock Thicknesses

Time (UT)	Δt (Sec)	$\overline{V}_{SS}$ (KM/Sec)	ΔS (Km)	n (cm^{-3})	B (γ)	V_{SH} (Km/Sec)	θ_{Bn} (Deg)	M_A	c/ω_{pi} (Km)	$\Delta S/c/\omega_{pi}$
1) 0049	13	55	720	1-2	13.5	430	64-66 74	1.5-2.1	160-230	3.1-4.5
2) 0215	4.6	-49	226	1-2.5	13.0	326	73-80	1.2-1.8	143-230	1.0-1.6
3) 0223	9.2	11	101	1-2.5	12.5	387	75-79	1.4-2.2	143-230	.4-.7
4) 1628	4	-100	400	1-2	7.5	273	84-88	1.7-2.4	160-230	1.7-2.5
5) 1325	4	-(80-120)	(320-480)	1-2	9.0	-(242-282)	75	(1.2-2.0)	160-230	(2-3)
6) 1355	5.15	(62-93)	(320-480)	1-2	9.0	(424-455)	75	(2.2-3.3)	160-230	(2-3)
7) 1741	6	(43-115)	(260-690)	1-3	7.5	(443-515)	77-85	(2.7-5.5)	130-230	(2-3)
8) 1752		No single ramp defined					47-66			

Table 2. Shock Velocities from Standing Wavelength

$$V_{SS}^4 + (2nV_{SW}\cos\theta_{Vn})V_{SS}^3 + (V_{SW}^2\cos^2\theta_{Vn} - C_A^2)V_{SS}^2 - \left(\frac{2\pi C_A}{T}\cos\theta_{Bn}\frac{c}{\omega_{pi}}\right)^2 = 0$$

$$L_d = \frac{2\pi\cos\theta_{Bn}}{\sqrt{M_A^2-1}}\quad\frac{c}{\omega_{pi}}$$

Case	Time	T_{wave}(sec)	n	V_{SS}(Km/sec)	$\overline{V}_{SS}$(Km/sec)	ΔS_W(Km)	$\Delta S_W/\frac{c}{\omega_{pi}}$	L_d	$\Delta S/L_d$
1	0049	11.5	1	51	55	663	2.9-4.6	587	1.13
			2	23		299	1.3-2.1	265	1.13
5	1325	4.0	1	-561		2244	9.8-14.0	2244	1.0
			2	-502		2008	8.7-12.6	2008	1.0
				-21/	-(60-120)	868	3.8-5.4(2-3)	868	1.0
				-30		120	.5-.75	120	1.0
6	1355	3.1	1	62.4	(62-93)	321	1.4-2(2-3)	193	1.7
			2	32.0		165	.71-1.0	100	1.7
						ΔS	$\Delta S/c/\omega_{pi}$		
4	1628				-100	400	1.7-2.5	16-110	3.6-25

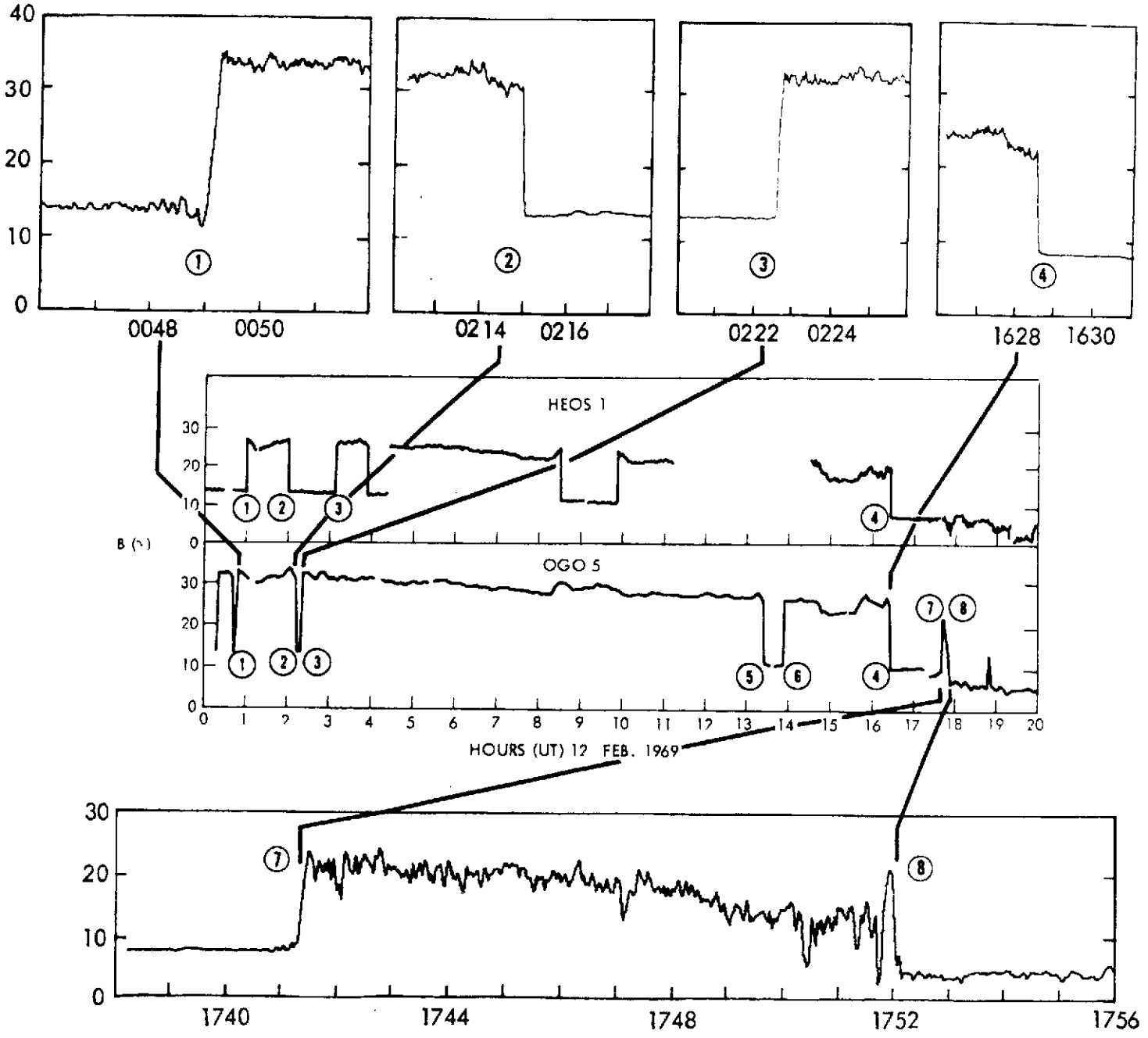

Figure 1. Summary view of the shock-crossing sequence of 12 February 1969. The circled numbers designated case numbers discussed in the text.

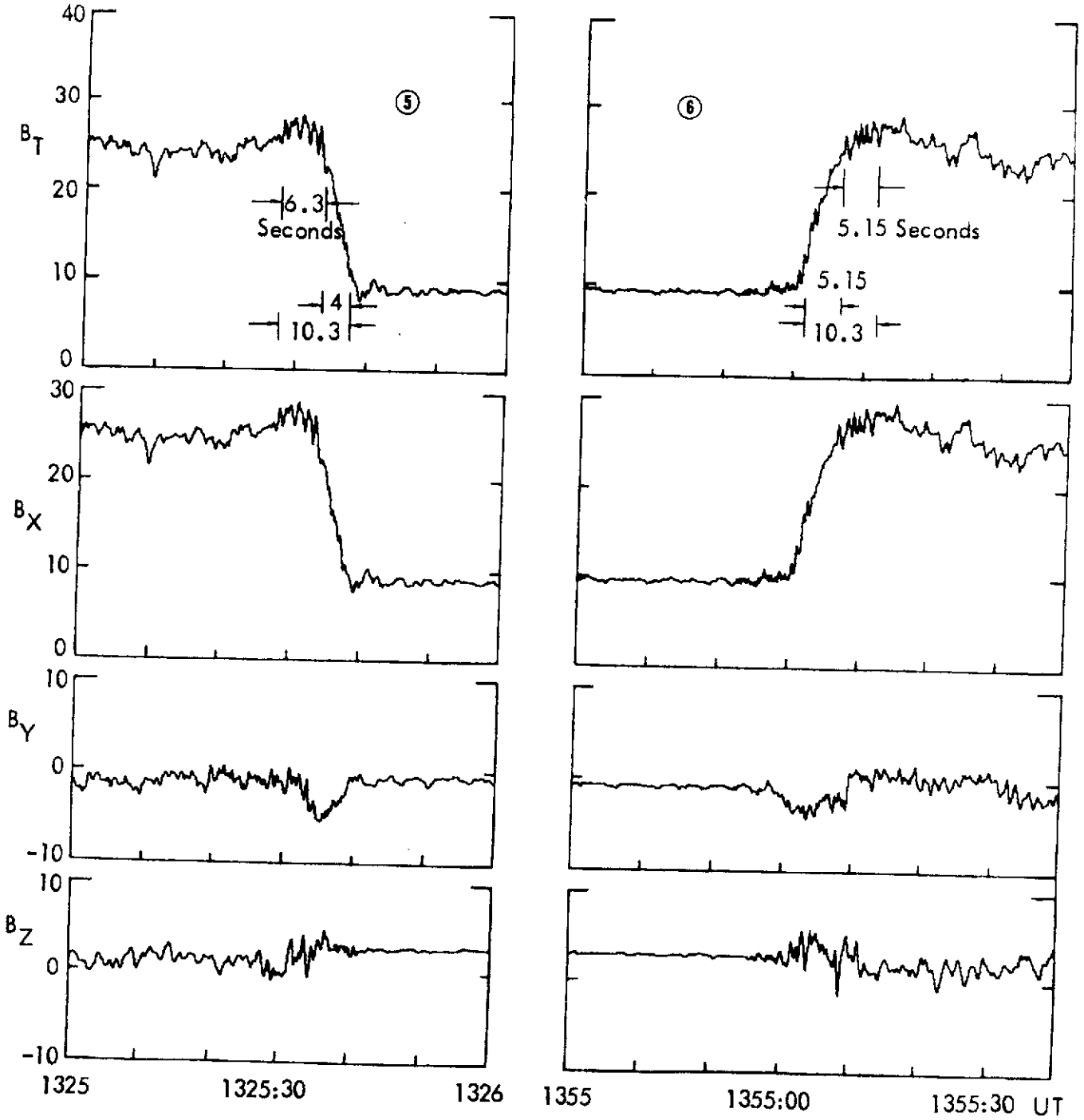

Figure 2. Two adjacent magnetic profiles of the laminar shock at high resolution: .144 sec/sample.

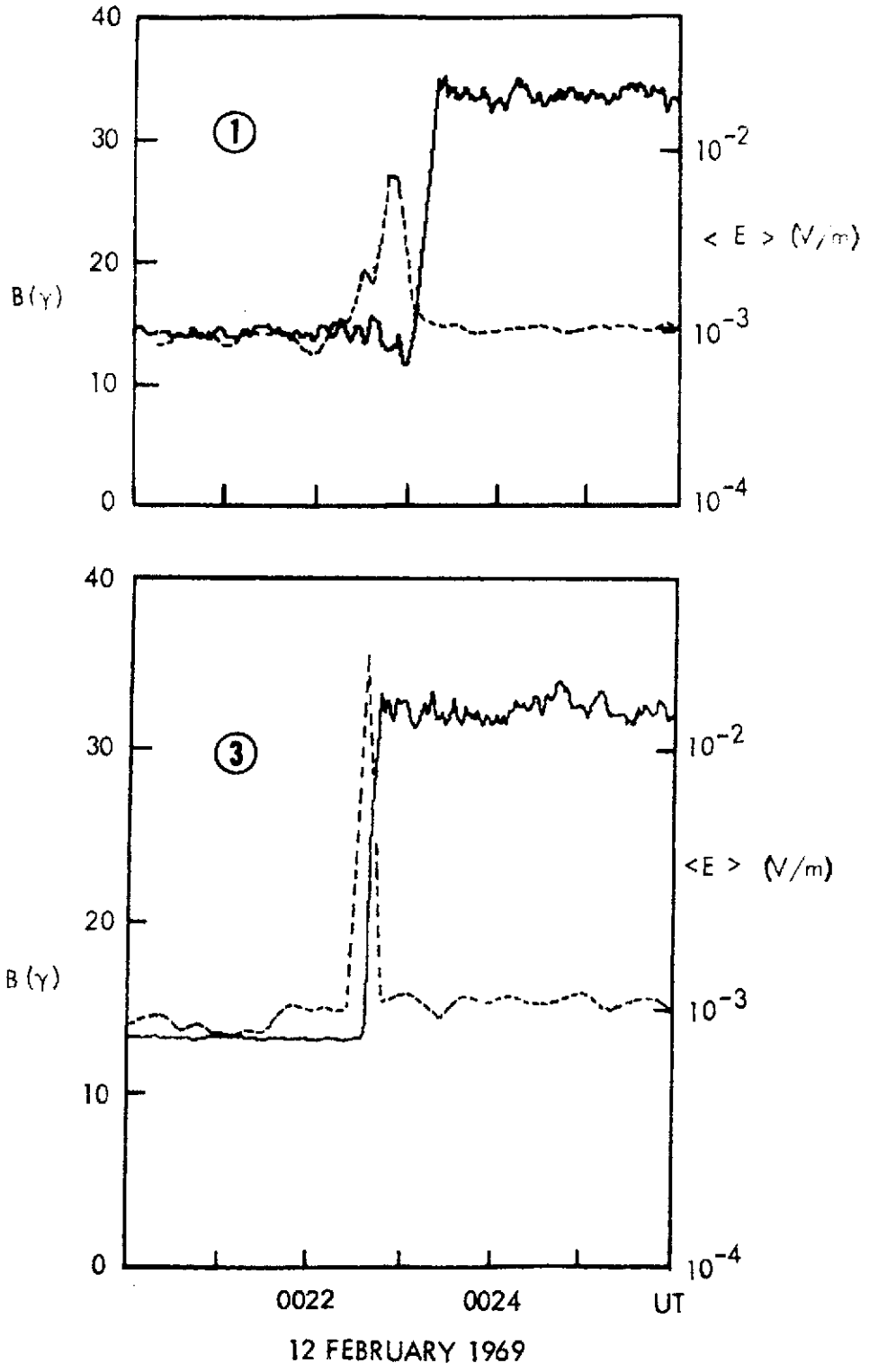

Figure 3. Two profiles of the laminar shock at a resolution of 1.15 sec/sample, with differing field-normal angle θ_{nB}. At $\theta_{nB} \approx 65°$, upper panel, the shock exhibits damped precursor oscillations with a correspondingly broadened region of plasma wave noise (dashed curve). At $\theta_{nB} \approx 78°$, the waves vanish and the electric noise is narrowed to the shock ramp.

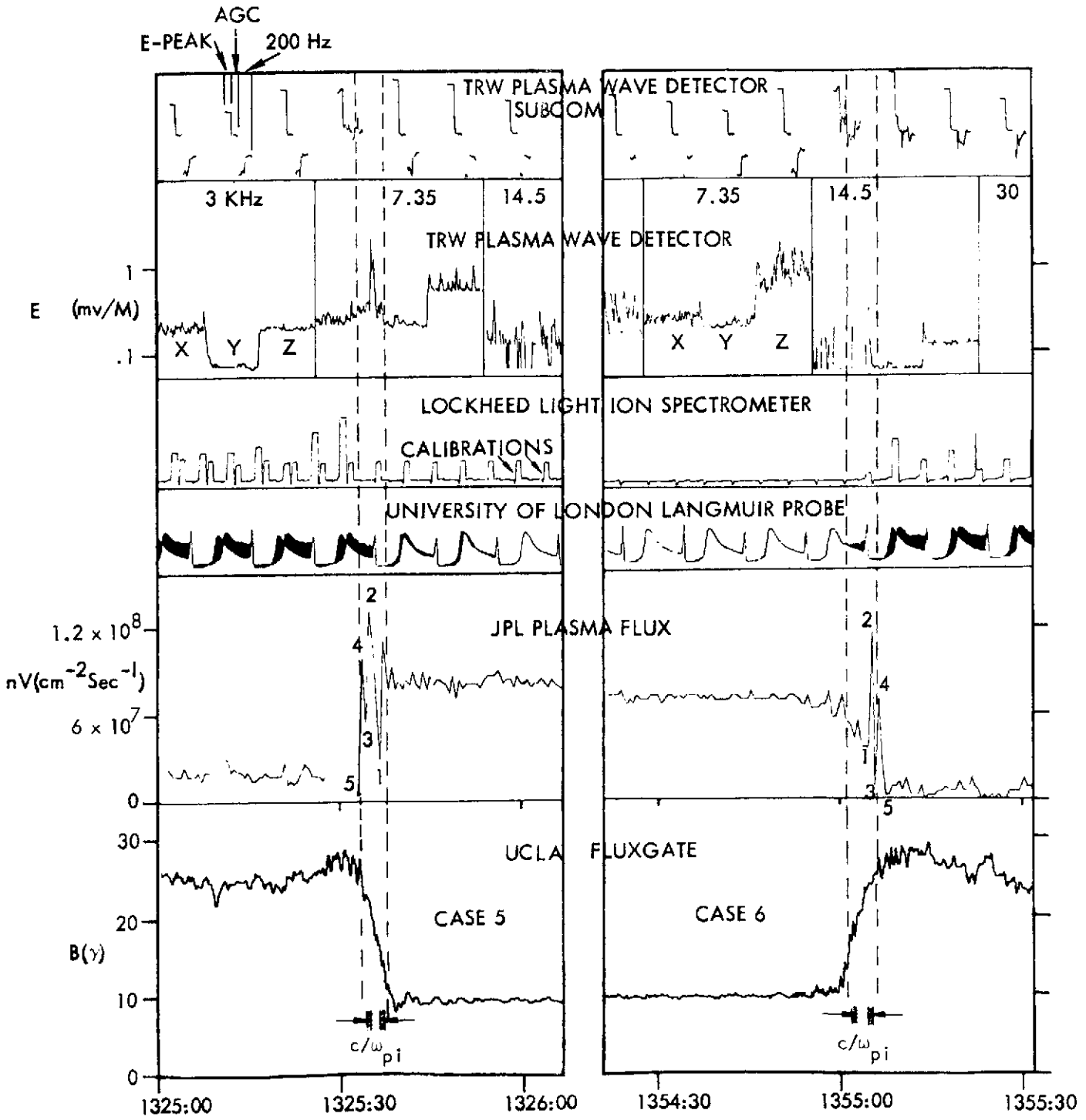

Figure 4. Multi-diagnostic view of the high-resolution crossings.

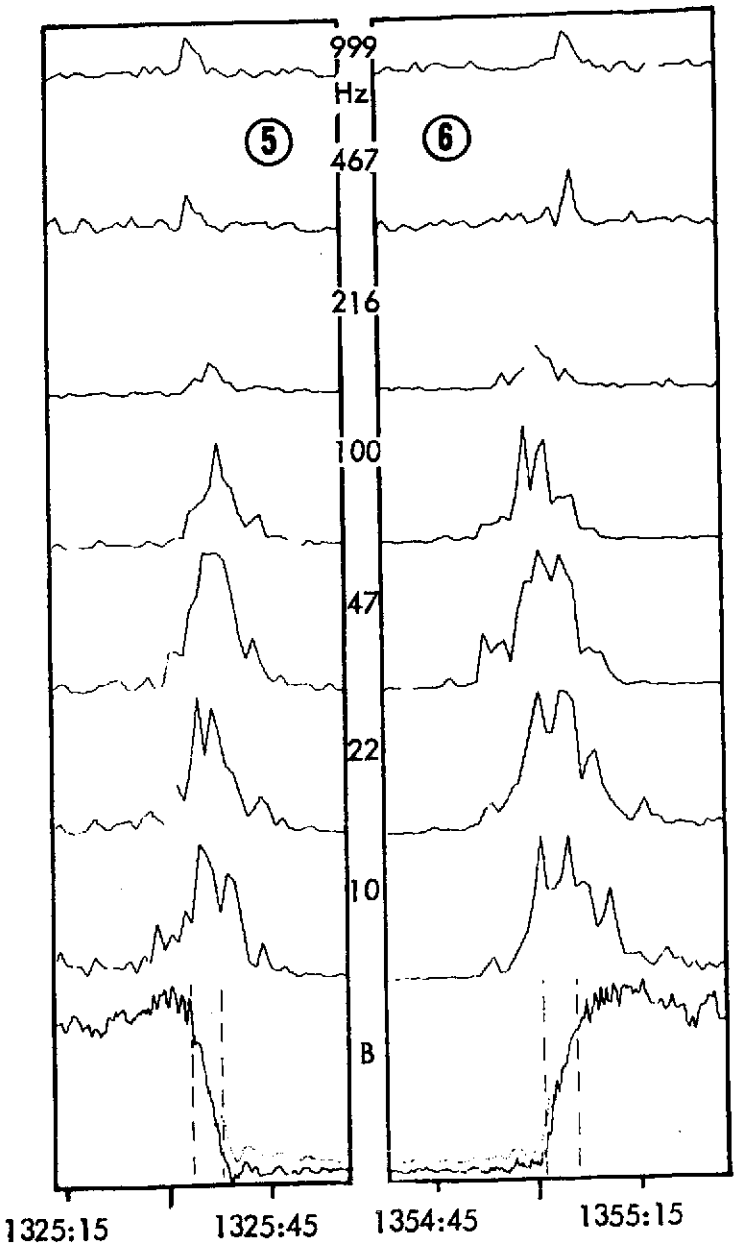

Figure 5. Multi-channel view of the high-resolution crossings as recorded by the X-axis loop of the B ELF search coils.

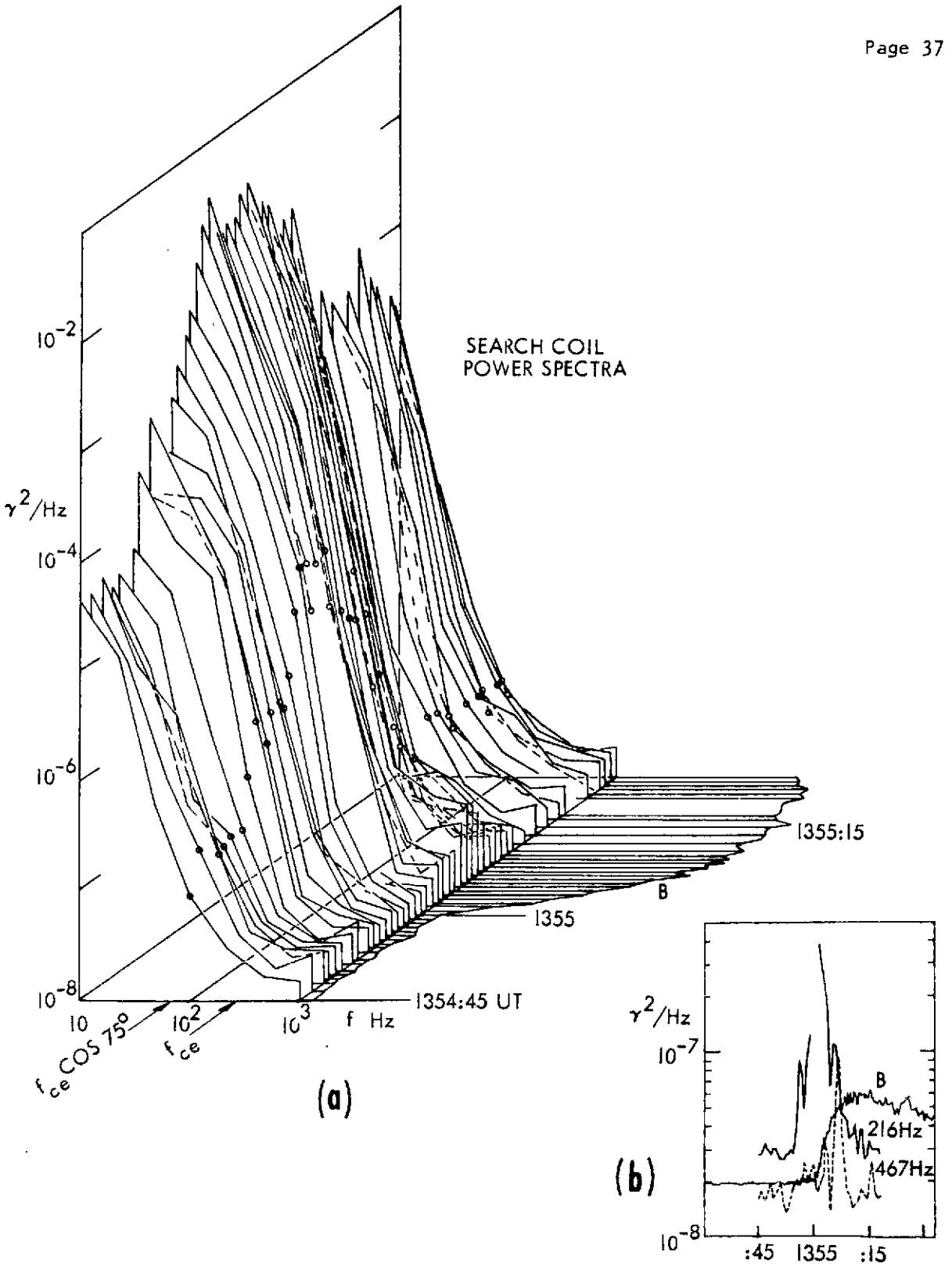

Figure 6. (a) ELF power spectra accompanying the high-resolution crossing of 1355 UT. (b) Behavior of the ELF 216 Hz channel, below, and the 467 Hz channel, above, f_{ce} in the solar wind as the ramp was crossed.

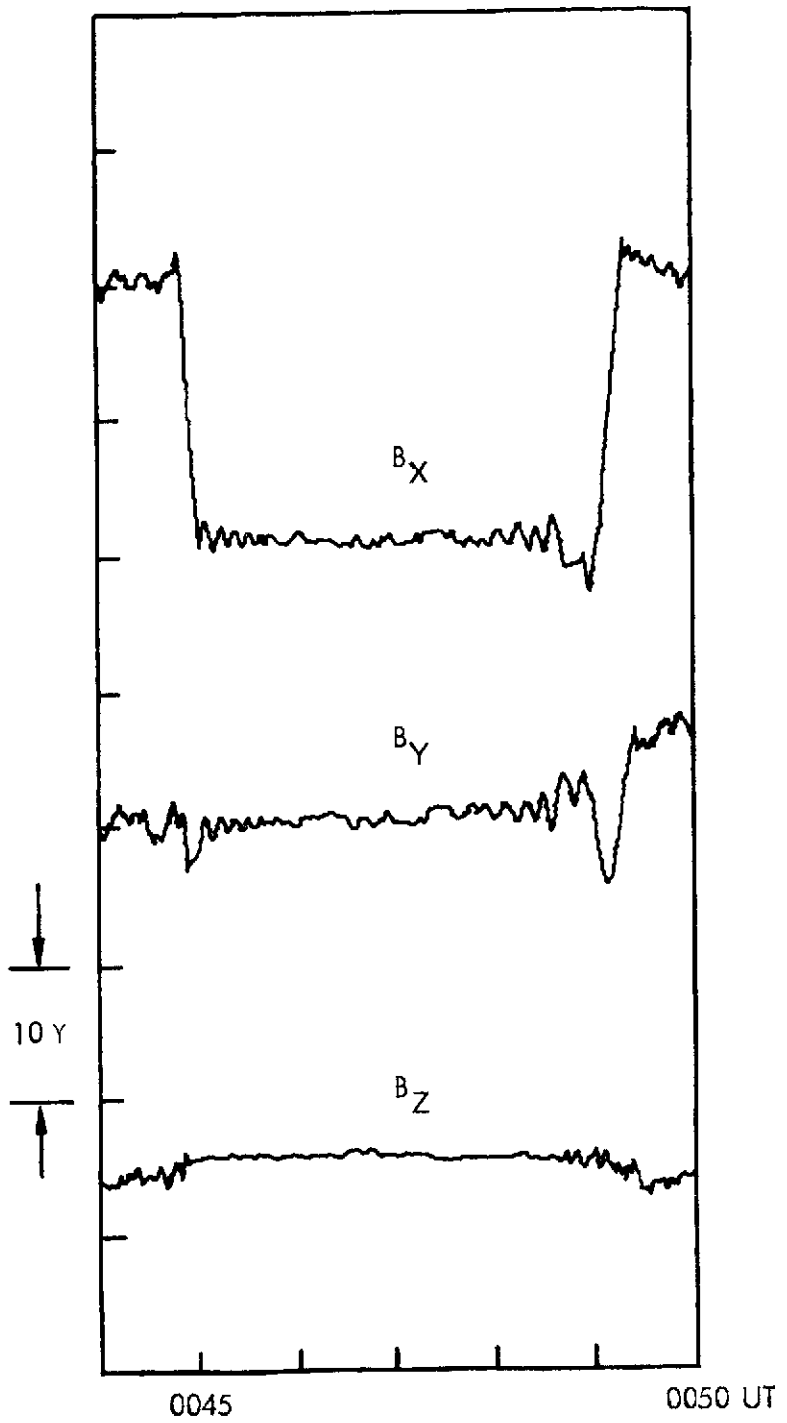

Figure 7. A pair of adjacent shock crossings showing stationary upstream wave structure.

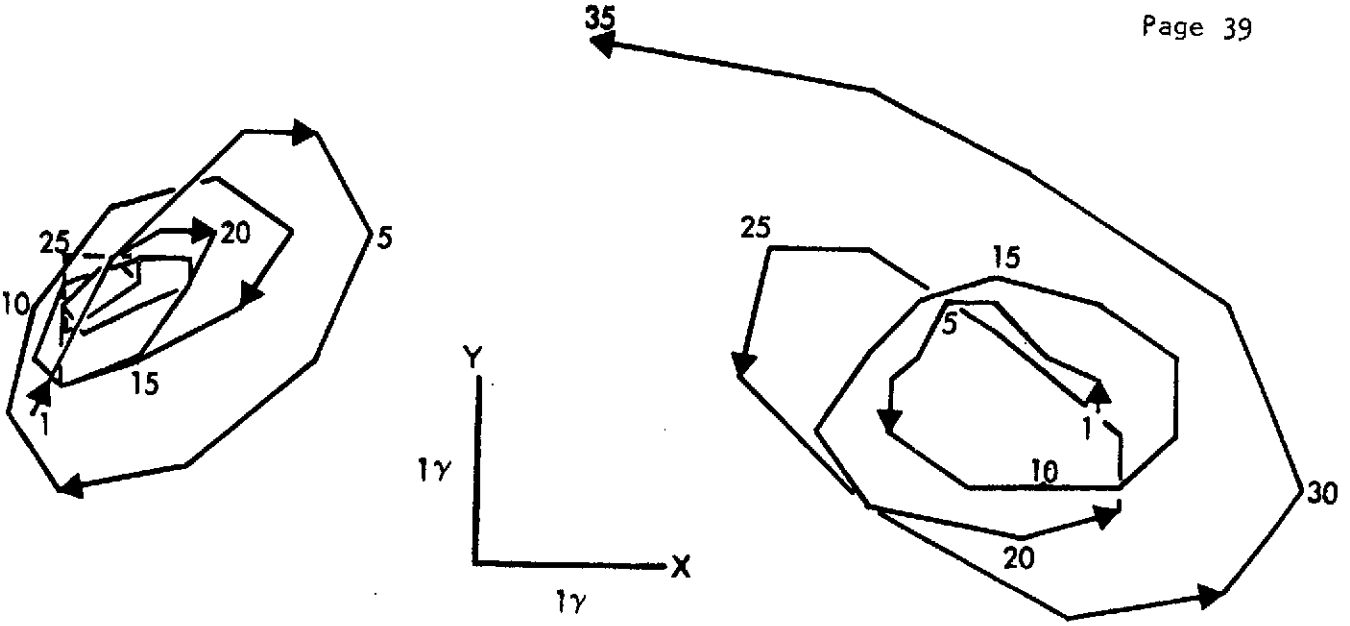

0044:50-0045:43

0047:48.5-0048:27.7

(a)

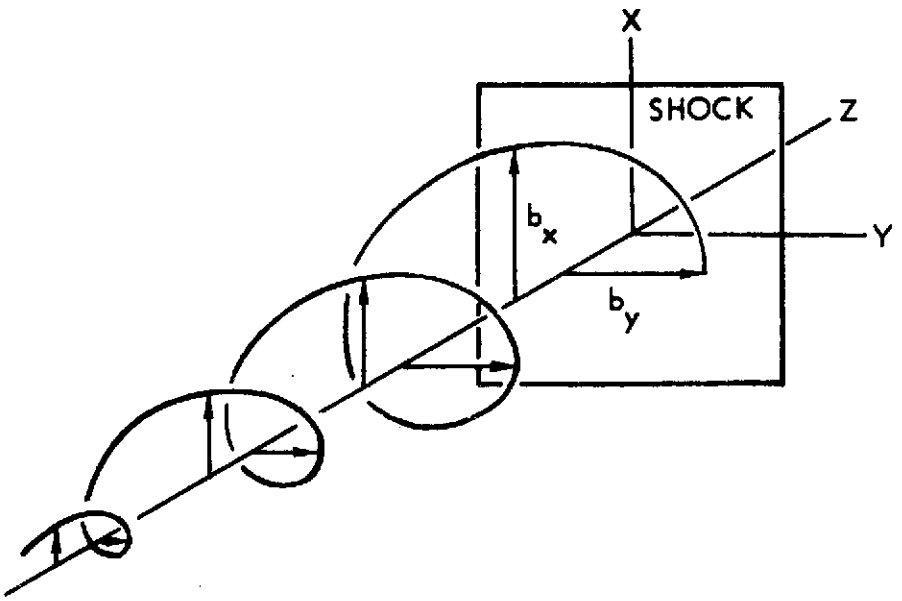

(b)

Figure 8. Whistler polarization characteristics of the stationary precursors of Figure 7; (a) individual polar diagrams of the perturbation vectors in an approximate shock plane; (b) conceptualization of the common whistler-wave polarization of the two precursors along the approximate shock normal. The average upstream field is about 25° from the shock plane, with its sensor inward.

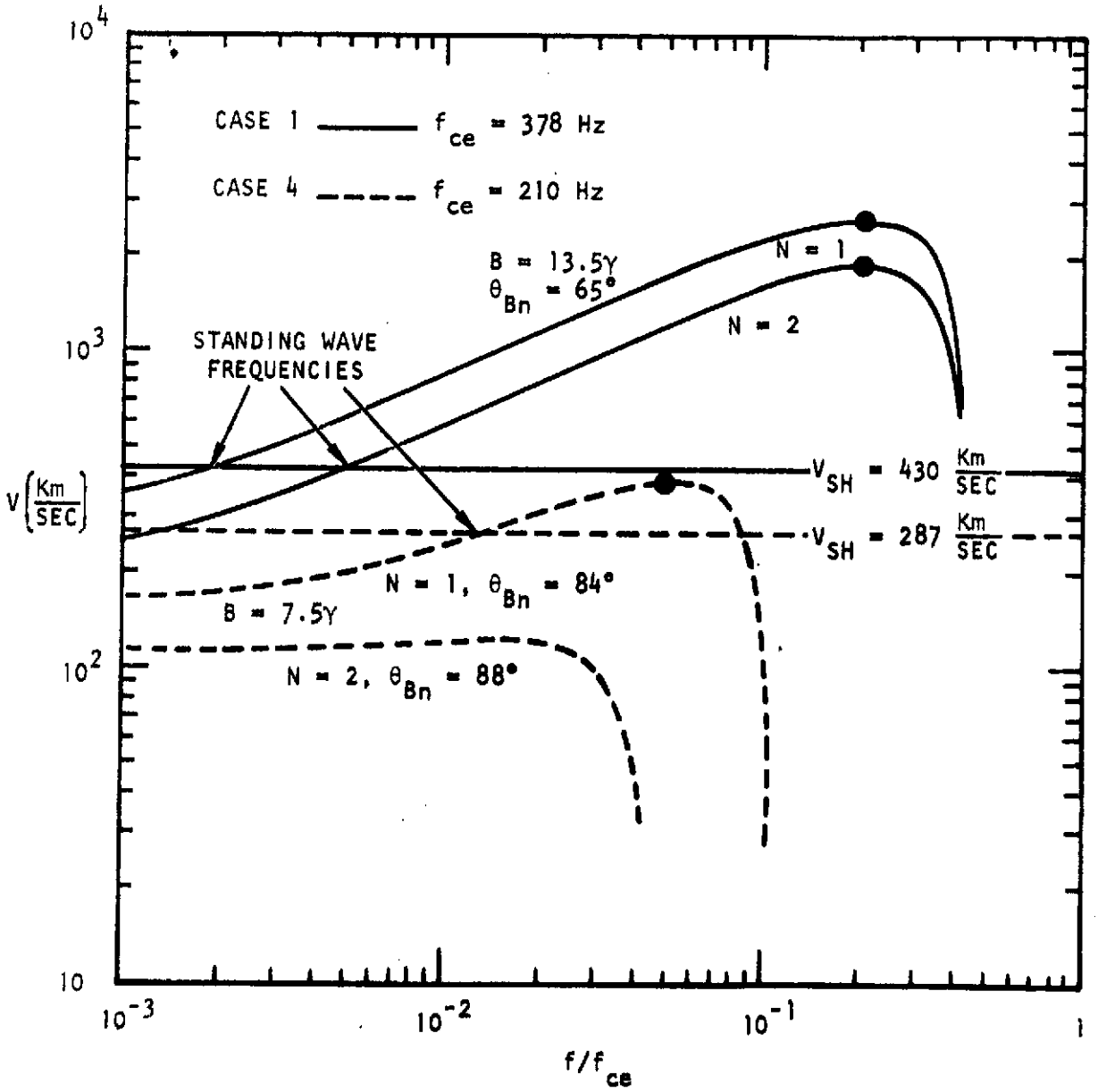

Figure 9. Phase velocity vs frequency for the whistler mode (Appleton-Hartree cold-plasma approximation) in the solar wind in cases 1 (solid curves) and 4 (dashed curves).

APPENDIX 1

WHISTLER PHASE AND GROUP VELOCITIES

The curves in Figure 8 of the text are based on the Appleton-Hartree, quasi-longitudinal dispersion relation for cold plasma, justified here by the low β_i, laminar conditions that prevailed for these observations. We refer particularly to the QL-R expression of equation (50) of Stix (1962, p 40), with the factors 1 and ω_{pi} neglected, so $\alpha = \omega_{pe}^2/\omega^2$ and

$$n^2 = \frac{k^2c^2}{\omega^2} = \frac{c^2}{u_n^2} = \frac{-\omega_{pe}^2}{\omega(\omega-\omega_{ce}\cos\theta_{nB})} = \frac{-f_{pe}^2}{f(f-f_{ce}\cos\theta_{nB})} \quad .$$

As the notation indicates, we are interested in phase velocity u_n upstream along the local shock normal at angle θ_{nB} to the interplanetary field. For any angle θ to $\underset{\sim}{B}$ the group velocity vector $\underset{\sim}{u}_g$ is given by $\underset{\sim}{u}_g \equiv \frac{d\omega}{d\underset{\sim}{k}} = \underset{\sim}{k}\frac{\partial\omega}{\partial k} + \underset{\sim}{\theta}\frac{1}{k}\frac{\partial\omega}{\partial\theta}$, but along $\underset{\sim}{n} = \underset{\sim}{k}$, $u_{gn} \equiv \underset{\sim}{u}_g \cdot \underset{\sim}{n} = \underset{\sim}{u}_g \cdot \underset{\sim}{k} = \frac{\partial\omega}{\partial k}$. When evaluated algebraically from the expression given above for $u_n \equiv \frac{\omega}{k}$, $u_{gn} = -2\,u_n \frac{f_{pe}^2 u_n}{c^2k^2f_{ce}\cos\theta_{nB}}$. Elimination of $k(= 2\pi f/u_n)$ and some algebraic excercise ultimately yield

$$u_{gn} = 2\,u_n\,(1 - f/f_{ce}\cos\theta_{nB}) \quad ,$$

hence $u_{gn}/u_n > 1$ when $f < \frac{1}{2} f_{ce}\cos\theta_{nB}$, i.e., whistler mode waves can advance upstream along n only for frequencies less than half the electron cutoff frequency in the normal direction.

APPENDIX II

BOW SHOCK VELOCITY DERIVED FROM STANDING WHISTLER WAVELENGTH

For laminar, oblique shocks, the wavelength λ_d, or L_d, of the whistler wave standing upstream in the unshocked plasma is given by the formula

$$L_d = \frac{2\pi \cos \theta_{Bn}}{\sqrt{M_A^2 - 1}} \frac{c}{\omega_{pl}} , \tag{1}$$

where L_d is measured along the shock normal (Morton, 1964). If V_{SS} is the shock speed in the spacecraft frame, the apparent period of the standing wave as it moves with the shock along the shock normal is

$$T_d = L_d / V_{SS} . \tag{2}$$

If spacecraft motion, seldom more than about 1 Km/sec along the bow shock normal, is neglected, then the local velocity V_{SH} of the shock with respect to the ambient plasma is

$$V_{SH} = V_{SW} \cos \theta_{vn} + V_{SS}, \tag{3}$$

where θ_{vn} is the angle between the local normal and solar velocity V_{SW}, and V_{SS} is defined as positive outward from the earth, i.e., positive when it increases the velocity of the shock relative to the solar wind. The local Alfvén mach number is given by

$$M_A = V_{SH} / C_A ,$$

where C_A is the upstream Alfvén velocity. Combination of all the above expressions yields the 4th degree equation in V_{SS},

$$V_{SS}^4 + (2V_{SW}\cos\theta_{vn})V_{SS}^3 + (V_{SW}^2\cos^2\theta_{vn} - C_A^2)V_{SS}^2 - \left(\frac{2\pi C_A \cos\theta_{nB}}{T_d}\frac{c}{\omega_{pi}}\right)^2 = 0 \quad (4)$$

This equation may have more than one real root, necessitating some independent criterion for selecting the one most probably correct. The measurements necessary to obtain V_{SS} are $\underset{\sim}{B}_{SW}$ (for B and θ_{Bn}), N_{SW}, and V_{SW}, all upstream. In addition, a local normal $\underset{\sim}{n}$ must be estimated from a model shock surface to obtain θ_{nB}.

INTRODUCTION

This is the last quarterly, and annual summary report on the subject contract for the year July 1973 - July 1974. In the ensuing sections, the background of the study is synopsized, the year's objectives described, and the results summarized. Details of newly-completed results are attached as appendices, which make up the bulk of the report. Following the summary of results, a short commentary and a recommendations section complete the document.

BACKGROUND

Purpose. The existing program (NASW-2398) has basically a twofold purpose. First, to test the validity of a suggested model according to which Pc 3 micropulsations are excited by magnetosheath field (and plasma) fluctuations arising in the oblique structure of the subsolar bow shock; second to continue and expand a previous study of the influence of solar wind plasma parameters, particularly ambient field direction, on local bow structure.

Micropulsations. Certain micropulsations, especially Pc 3 (period range 10-45 sec), have shown strong correlation of their various characteristics with solar wind features. These correlations, together with the results on field-dependent shock and sheath structure obtained by the present investigator, led to his suggesting a mechanism whereby the interplanetary field $\underset{\sim}{B}_{SW}$ should strongly influence the excitation of Pc 3 at the magnetopause when it aligns itself with solar wind velocity $\underset{\sim}{V}_{SW}$, thus causing large amplitude waves at the subsolar point of the shcok. The waves should be conveyed to the magnetopause by the pattern of solar wind flow in the magnetosheath. Additional

factors expected to contribute to the postulated model are thermal-to-field energy ratio β and solar wind mach number M.

Shock Structure. Collisionless plasma shock structure is determined in all scale lengths by the three plasma parameters, or, more precisely, the three classes of plasma parameters β, M, and θ_{nB}, denoting the thermal-to-field energy ratio, mach number, and field-to-shock normal angle, respectively (Tidman and Krall, 1971). We say clsses of parameters because different constituents of the plasma may have different β's and different wavemodes may have separate M's, some dependent in turn on θ_{nB}. A full description of shock-structural processes can be arrived at with multiple satellite measurements only if the effect of each of the relevant parameters can be isolated.

This study has emphasized the use of simultaneous data from two or more spacecraft and, recently, from multiple diagnostics, to evaluate the geometrical factor θ_{nB}, or, more precisely in some cases, its B-X equivalent, and the principal plasma parameters.

OBJECTIVES AND APPROACH

In broad terms, the aim of the past year's effort has been, first, to find data that confirm or confute the investigator's suggestion that Pc 3 micropulsations are excited by shock-generated oscillations, and, second, to advance the study of shock and magnetosheath structure in general by taking advantage of the numerous instances in which simultaneous data from two or more spacecraft have been recorded near the bow shock. More specific objectives have been tailored to the opportunities that have become available from time to time to make meaningful headway in a complicated investigation requiring cooperation by other, sometimes many, researchers.

The micropulsation side of the investigation began with two specific objectives: 1. to continue seeking verification of the postulated model by visual inspection of Explorer 35, Inuvik, and Tungsten records for a particular interval in 1969, and 2. to move toward a more mechanical, objective, and detailed method of evaluating solar-wind surface relationships to establish a physical link underlying the relationships that might emerge. At the outset it was believed that visual verification (or contradiction) of the model would eventually provide at least a satisfactory beginning and a guide to further analysis. By the end of the year, it had been decided that reliance on visual evaluation of micropulsation recordings, even by experts, was subjective and unreliable and should probably be abandoned. The new specific objective was creation of a computer program that would transform large quantities of interplanetary field data into the appropriate variables and plot these on optional time scales for eventual comparison with any accessible micropulsation data in spectral form, beginning with a set of records being prepared by John Olson at the University of Alberta.

The shock-structure aspect of the investigation started out to examine the effect on the bow shock of various plasma parameters and to seek some explanation for the success of l_p in predicting quasi-parallel structure with $p = 1.6$ (Greenstadt, 1972). Largely through collaboration with V. Formisano the examination of parameter-dependent structure has been extremely successful, and the year ended with a major program underway to catalogue shock morphology and to produce detailed documentation on each identifiable structural form, using OGO 5's high resolution, multidiagnostic data as the principal source of shock observations. The study of l_p geometry, meanwhile, produced a first-

order view of the geometrical context in which protons reflected from, and energized by, the shock can escape upstream.

RESULTS

Micropulsations

Preliminary Visual Surveys. Hourly averages of HEOS I interplanetary field and plasma parameters were obtained for some selected intervals in 1969 from V. Formisano. The appropriate geometrical field quantities, θ_{nB}, $\cos \theta_{nB}$, were computed from these where necessary and compared with micropulsation spectrograms taken at Inuvik, a presumably ideal auroral zone station, and six other stations, during a fifteen-day interval of December 69. The spectrograms were obtained from R. R. Heacock of the Geophysical Institute at the University of Alaska.

The results were disappointing, for no apparent correlation was found. The results were also puzzling, however, since a paper was given at the September 73 Kyoto meeting by Nourry and Watanabe asserting not only that they have confirmed Troitskaya's published result, which was consistent with the model of the present investigator, but that their correlation was one-for-one. Moreover, their micropulsation station was not even at auroral latitudes, where Pc 3 should be most apparent, according to postulate.

Several possible explanations of the above discrepancy came to mind. The two most important were: (1) contrary to the investigators' expectation, auroral latitudes are not the best for seeking the postulated correlation, and (2) the spectrograms, recorded on a scale most suitable for exhibiting shorter period pulsations (Pi 1), simply did not display Pc 3 events properly, if at all.

Reprocessing the Inuvik records by Heacock reinforced the suspicion that his sonograms complicated rather than simplified the initial correlation effort being attempted. Three versions of the same sonograms differing only in their processing technique produced three apparently different Pc 3 behaviorisms. Further development of recording technique would be required before the College records could be routinely applied to this correlation study.

Meanwhile, a visual evaluation of UCLA's Tungsten induction coil records for 1-15 December 69 was made (in collaboration with Carlene Arthur and Bob McPherron), and a statistical summary obtained. Subjectively, there did appear to be a class of pulsations sometimes in the Pc 3, sometimes in the Pc 4 range, whose appearance was correlated with solar wind field-flow alignment. The latter was also evaluated visually from Explorer 35 interplanetary field records. The statistical summary verified part of this correlation: Pc 4 definitely occurred preferentially when the field-flow angle θ_{VB}, approximated in practice by θ_{XB}, was close to zero. Seventy percent of the hours when Pc 4 were detected, the field $\underset{\sim}{B}_{SW}$ was oriented within 36°.7 of both the ecliptic plane and the solar azimuth. Latitude and longitudes of $\underset{\sim}{B}_{SW}$ jointly within this limit correspond to conditions for irregular, quasi-parallel shock structure at the subsolar point of the bow shock. Half the Pc 4 hours corresponded to θ_{XB} within 18°.4 of the solar azimuth.

Figure 1 summarizes the results projected onto the ecliptic plane, with solar and antisolar field directions combined. Each graph represents, for one pulsation condition, the fraction of measured directions of $\underset{\sim}{B}_{SW}$ that fell in various sectors during hours in which the condition applied. At upper left, the angular distribution of all measurements shows the usual stream angle preference. At upper right, the distribution of measurements for which Pc 3-4

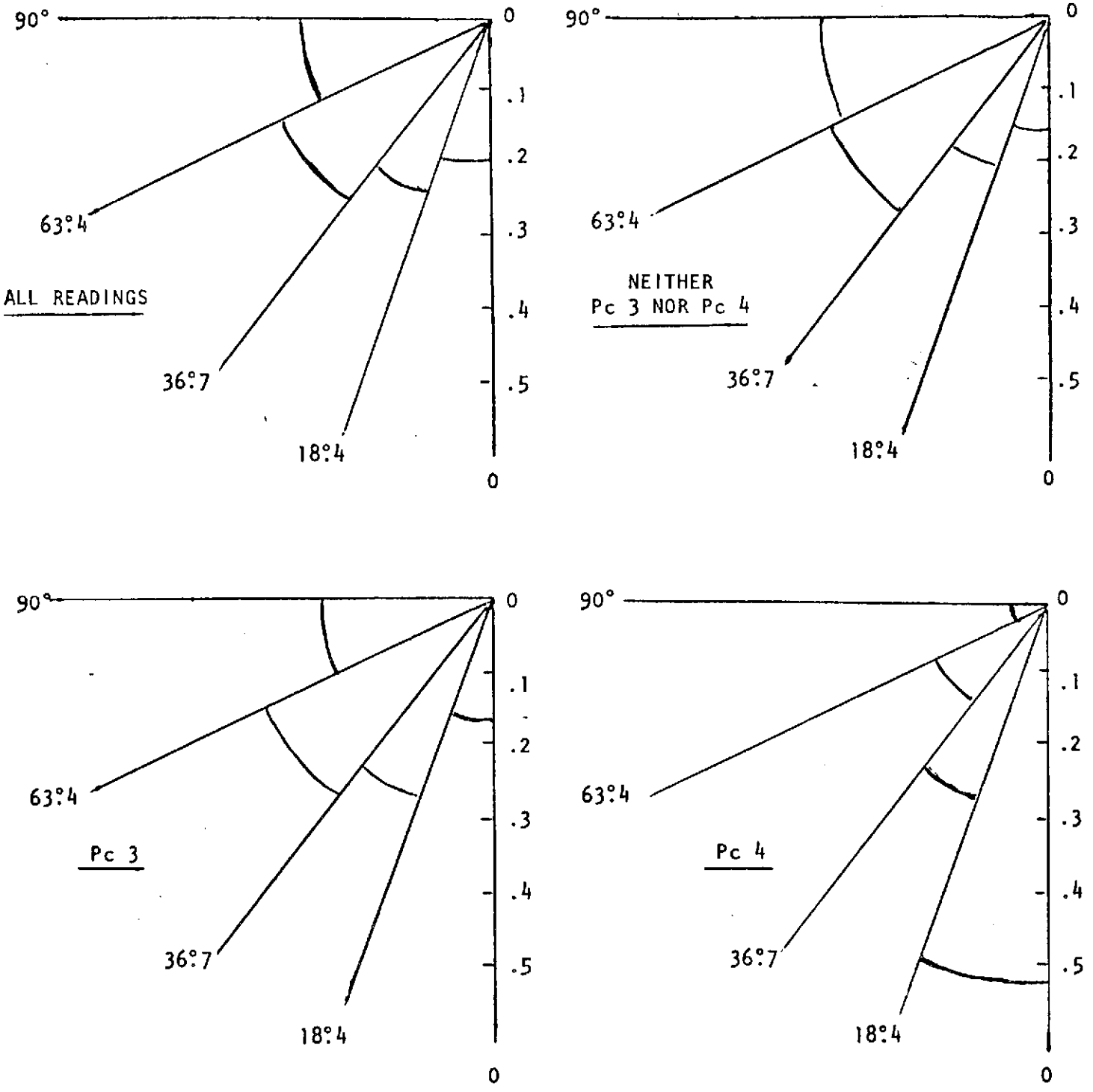

Figure 1. Angular distributions of the ecliptic projection of $\underset{\sim}{B}_{SW}$ for various Pc 3,4 conditions.

were absent, was deficient in the 0-18°.4 and 18°.4-36°.7 sectors and somewhat excessive in the 36°.7-63°.4 and 63°.4-90° sectors, with respect to the distribution of all measurements. At lower left, the distribution for Pc 3 hours was slightly excessive in the sectors from 18°.4 to 63°.4 and deficient elsewhere; this result is not obviously significant, but is at best consistent with a result claimed by Bol'shakova and Troitskaya (1968). At lower right, measurements in the 0-18°.4 sector were grossly in excess and in the 63°.4-90° sector grossly deficient in readings during hours when Pc 4 occurred.

Another version of some of the results of visual comparison with Tungsten is shown in Figure 2. The first three-dimensional construction in 2(a) portrays the distribution in solid angle, divided as already described, in which $\underset{\sim}{B}_{SW}$ fell during Pc 4 events. The radial length of each angular block represents the fraction of hours of observation of Pc 4 during which the solid angle of the block was occupied by $\underset{\sim}{B}_{SW}$ during some part of the hour. The second construction, 2(b), is the same type of representation for hours during which neither Pc 3 nor Pc 4 occurred. The strong preference of Pc 4 for hours when θ_{XB} lay close to 0°, and the equally-strong avoidance of $\theta_{XB} < 36°.7$ when Pc 3-4 were absent are clear in the figure.

The statistical summary and visual examination of the Tungsten data suggested, in line with the Russian results and the recent Canadian observations of Nourry and Watanabe (1973), that there is a pulsation phenomenon of variable period strongly associated with certain interplanetary field directions. The periods of the phenomenon span the accepted division between Pc 3 and Pc 4 at T = 45 seconds. In the Pc 4 range ($45 \leq T \leq 150$ sec), the phenomenon is reasonably isolated, but in the Pc 3 range, the phenomenon is confounded with, and often overshadowed by, other types of oscillations, most notably Pi 2.

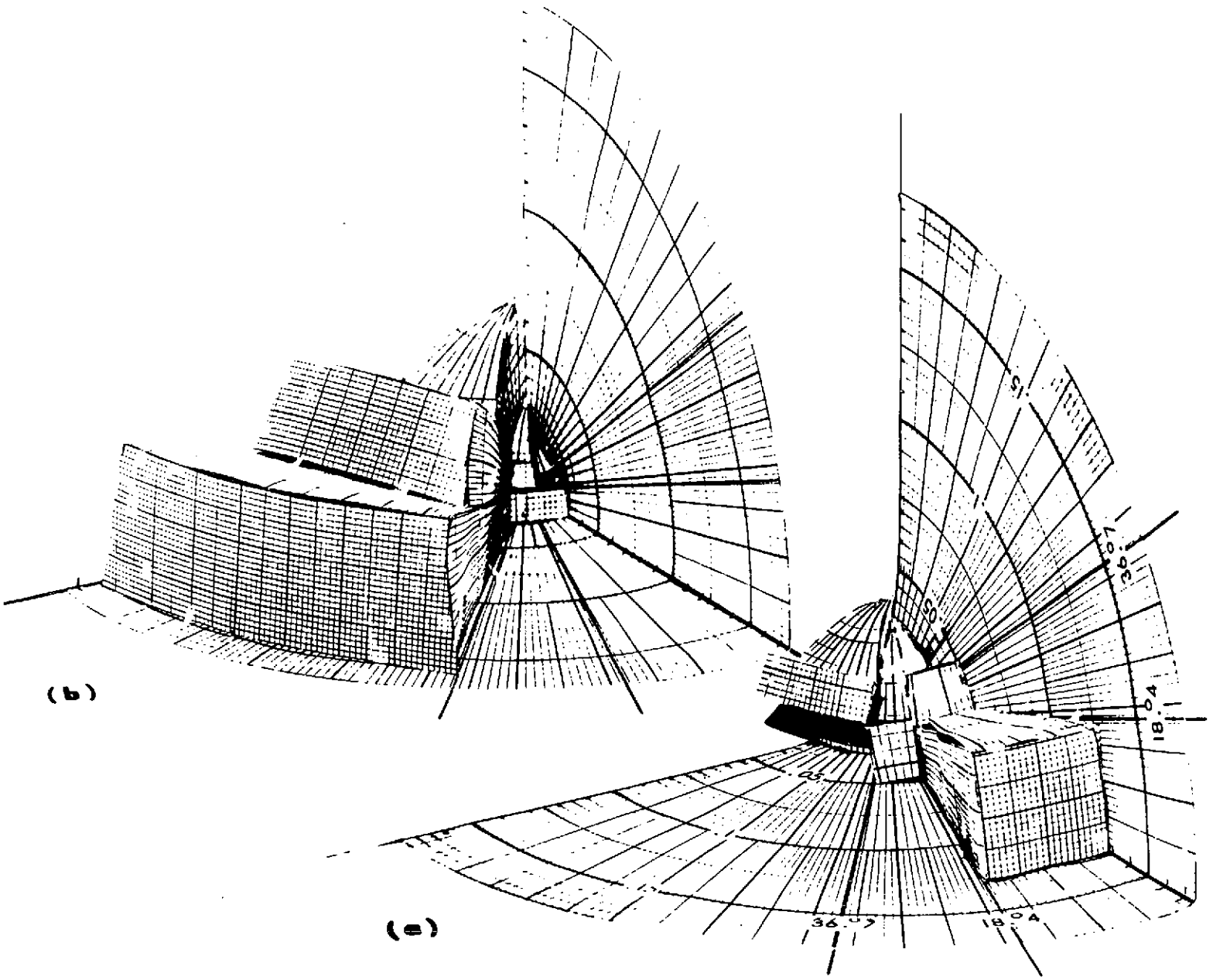

Figure 2. Distributions of northward θ_{XB} for (a) Pc 4 and (b) neither Pc 3 nor Pc 4.

Visual evaluations of this phenomenon become very unreliable in the Pc 3 range.

Preliminary printed versions of the Nourry and Watanabe data were received and examined, and the Russian publications were reviewed once again. It appears tentatively that the Soviet and Canadian results are completely compatible with the model of Pc generation proposed by this investigator. The evidence tends to be anecdotal, however, or, at best, incompletely documented. Pc 1 spectrograms from Borok, a commonly-cited Russian observatory, have been published, showing the Russian capability with f-t technique, but it is not clear whether these, or only visual judgments of Pc 3-4 occurrence were applied in the Soviet work. Although statistical compatibility is not proof of the model itself, it was decided to continue to seek a more solid correlative foundation in this program before attempting to explore any physical details of the model. However, it was concluded that suitable methods of mechanizing and objectivizing the correlation sought here had become unavoidable. The effort of this study was therefore redoubled to obtain an entirely independent demonstration with more sophisticated techniques than have hitherto been applied.

Computer Program for Spectral Correlation. The best demonstration of the correlation central to the model of this study should be provided by examination of a long interval (weeks to months) of data in which interplanetary field orientation in suitable graphic representation is compared with concurrent micropulsation spectrograms (f-t plots) on the same time scale. Production of suitable magnetic field plots requires a computer programming and running effort. A magnetic tape for a selected test interval was obtained from NASA/ARC. The tape contains the "sequence averages" from the ARC

Explorer 35 magnetometer. The test interval was determined in consultation with John Olson of the University of Alberta (Edmonton), who is in the process of reducing micropulsation data to suitable format. The comparison of spacecraft with surface data is intended to span the last four months of 1969, when the Canadian chain of stations operated by Edmunton provided good time and latitude coverage. Since the UCLA station at Tungsten also operated during this interval, the potential for a comprehensive examination of the relationship under study is good.

As this is written, an initial version of the computer program for handling Explorer 35 magnetic field tapes to produce appropriate plots at TRW is essentially debugged, while a program for preparation of spectograms from Canadian micropulsation tapes is in about the same condition. Figure 3 shows a three-hour test version of part of the plotted output of our routine, compared with a micropulsation record from Tungsten (courtesy UCLA) on the same time scale. Time-scale matching is one of the options of the TRW program. The two curves at the top are cos θ_{XB} and θ_{XB}, as marked, with low θ_{XB}, i.e., favorable θ_{XB} at the top of the graph. A burst, or sequence of bursts, of pulsations of about 120-sec period (Pc 4 range) appear in approximate coincidence with rotations of $\underset{\sim}{B}_{SW}$ from 10-20° to about 50°. Unfortunately, this is exactly the opposite of the correlation we seek and of the reported results of Bol'shakova and Troitskaya (1968) and Nourry and Watanabe (1974). We have no explanation for this outcome at present, but we note that the local time at Tungsten is dawn rather than noon, when such pulsations usually appear. Also, the true rotation of $\underset{\sim}{B}_{SW}$ was southward, so the oscillations on the surface are undoubtedly substorm-associated. The figure demonstrates well that we now have the capability of producing our own anecdotes. It also illustrates clearly

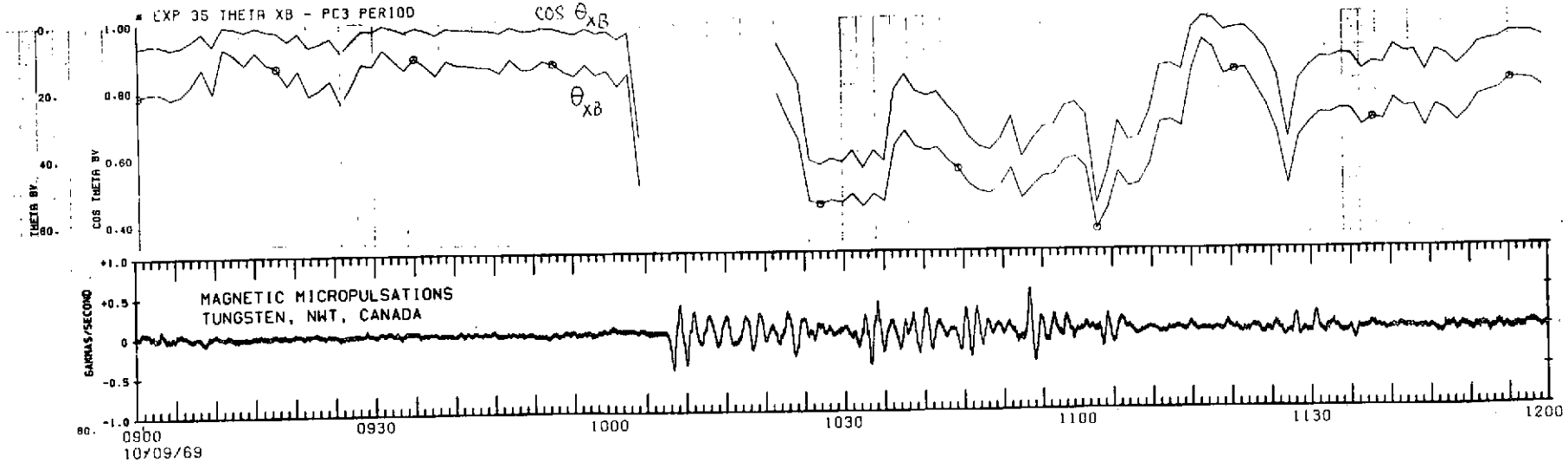

Figure 3. Partial output of TRW preliminary program for θ_{XB}, compared with 3-hour micropulsation record.

the type of result that supplies grounds for our conviction that a suitable long-term, objectivized approach to the micropulsation study is essential.

A listing of the preliminary TRW program is attached as Appendix A. Our routine will compute several specialized functions, but the program has been written in such a way as to facilitate later use of interplanetary field readings from the same Explorer data tapes in computing a variety of quantities related to bow shock and magnetosheath structure, none of which would have justified the rather complex program by themselves.

Shock Structure

Geometry. An important task in following up earlier work on the response of the bow shock to local field geometry (Greenstadt, 1972a,b) has been to discover the reason that propagation of precursor effects upstream from the shock apparently occurs consistently along $\underset{\sim}{B}_{SW}$ at a speed $u_{\|} \approx 1.6\ V_{SW}$. Northrop and Birmingham (1973) accepted the premise that $p \equiv 1.6$ was independent of position on the shock and derived the improbable result that $u_{\|}$ would then be constant, i.e., independent of V_{SW}. It seems more likely that p does not vary strongly with position, and that limited early experimental work has simply not picked up the variation, but this has yet to be demonstrated.

There is more than one precursor effect (Appendix B). The effect referred to above consists of decasecond waves propagating downstream as a result of excitation by some other precursor agency. It is not known whether the long period waves are coupled to a dominant category of reflected protons or simply represent a dominant frequency range most easily excited. It is known that reflected protons are found at many energies with $u_{\|} \neq 1.6$ (Asbridge

et al., 1968; Lin et al., 1974). In their recent paper, Lin et al. have given arguments why they believe 100 Kev-reflected protons are accelerated en route upstream rather than in the shock proper. Their conclusion would tend to support the notion that protons come out of the shock itself in a narrower range of energies, possibly concentrated around $(1.6\ V_{SW})^2$.

An attempt was made by this investigator to discover whether the geometrical relationship of the shock to reflected protons of finite pitch angle places restrictions on their energies that would tend to select those with $p \approx 1.6$ for escape upstream. The attempt was unsuccessful for an interesting reason. There turned out to be at least two free geometric parameters, leaving p essentially unconstrained. An unexpected result has followed: protons of large energy (30-100 Kev) and large pitch angle (70°), such as those commonly encountered by Lin et al., can escape the shock upstream when the angle made by $\underset{\sim}{B}_{SW}$ with the local shock normal is about 50°, the value at which upstream waves typically are generated. It thus appears that the particles detected by Lin et al. could have come directly from the bow shock as far as the credibility of their escape is concerned, although the process of their creation is still undetermined.

An explanation of, and report on, the above calculation was prepared for presentation at the Neil Brice Memorial Symposium "The Magnetospheres of Earth and Jupiter," and given in Frascati in May. It is attached as Appendix B. A more extensive inquiry into the geometry of reflected particles is planned.

Laminar Shocks. A comprehensive study of the quasi-perpendicular laminar shocks of 12 February 1969 was completed after addition of several new sections. A draft of a final report on these events is attached as Appendix D.

Especially interesting among the newly-added results is the detailed display of ELF noise juxtaposed on the shock's magnetic profile and the new method of computing instantaneous shock velocity from the standing wave period (Figure 6 and Table 2 and Appendix 2 of Appendix D).

Parametric Profiles of the Bow Shock. A collaboration was opened a year ago among V. Formisano, C. T. Russell, M. Neugebauer, F. L. Scarf, and this investigator for the purpose of compiling and studying plasma diagnostics recorded simultaneously by OGO 5 and HEOS 1 under differing solar wind conditions during bow shock crossings by OGO 5. We have succeeded in isolating over a dozen distinct combinations of M, β, and θ_{nB} and have made significant progress in determining the effect of each of these parameters on each of several plasma diagnostics measured in the shock. We are also in the process of merging the shock-structural classification schemes of Greenstadt et al. (1970b) and Formisano and Hedgecock (1973a) into a single comprehensive framework. A summary of some of the core results of this project is contained in Appendix C, a paper given recently at the Third Solar Wind Conference in Asilomar. The bulk of the program is incomplete, but a compendium of shock profiles is presently being prepared and should be available before the end of the year.

Quasi-Parallel Shock Structure. A case of prolonged, concurrent observation of quasi-parallel ("pulsation") shock structure by OGO 5 and HEOS 1 occurred on 14 February 1969. The situation is similar to the one reported earlier that led to identification of the pulsation shock phenomenon (Greenstadt et al., 1970a, but with the addition this time of substantially-improved diagnostic coverage. Initial examination of the data has verified the extreme thickness of the pulsation, or quasi-parallel structure, and revealed an

apparently distinct plasma particle distribution associated with this class of shock. A description of this preliminary result is part of Appendix

Reports

The following report was published during the year July 73 - July 74.

Greenstadt, E. W., Oblique Structure of Jupiter's Bow Shock, J. Geophys. Res., 78, 5813, 1974.

A report was prepared and delivered orally by R. W. Fredricks at the Summer Advanced Studies Institute, "Earth's Particles and Fields," Sheffield, England, August 13-24, 1973:

Greenstadt, E. W., and R. W. Fredricks, Plasma Instability Modes Related to the Earth's Bow Shock.

The report is scheduled to be published in the Institute Proceedings.

An informal presentation of shock structure results was given at the joing USA/USSR Bi-Lateral Working Group Meeting on Collisionless Shock Waves held in November at NASA Goddard Space Flight Center.

Three more reports have been completed:

Greenstadt, E. W., Structure of the Terrestrial Bow Shock, presented to the Third Solar Wind Conference held at Pacific Grove, California, 25-29 March 1974. To be published in the Conference Proceedings.

Greenstadt, E. W., C. T. Russell, F. L. Scarf, V. Formisano, and M. Neugebauer, Structure of the Quasi-Perpendicular, Laminar Bow Shock, prepared for J. Geophys. Res.

Greenstadt, E. W., The Upstream Escape of Energized Solar Wind Protons from the Bow Shock, Presented at the Neil Brice Memorial Symposium, "The Magnetospheres of Earth and Jupiter," Frascati, Italy, May 1974. To be published in the Proceedings.

COMMENTARY

Correlative Results of Other Investigators

This is an appropriate time and communication in which to note briefly the research context in which our shock investigation now finds itself.

The revival of interest in the bow shock, and its upstream effects on the solar wind, which seemed to be developing a year ago has been realized. Research on the shock as a plasma, rather than fluid-like, phenomenon is beginning to flourish, partly through fresh attention by European investigators. A selection of specific results bearing directly on this program are listed below:

Formisano et al. (1973a) distinguished statistically between Maxwellian and non-Maxwellian proton distributions in the magnetosheath, dependent on mach number and angle θ_{nB}.

Formisano et al. (1973b) studied fluid parameters across the shock and bow shock velocities as functions of M, β, and θ_{nB}.

Formisano and Hedgecock (1973a) developed a structural classification scheme for the bow shock, parametized by M, β, and θ_{nB}.

Formisano and Hedgecock (1973b) described the bimodal proton distribution found in the quasi-perpendicular, turbulent shock structure (see Appendix C).

Northrop and Birmingham (1973) examined the implications of a position (θ_{nB})-independent upstream wave parameter p = 1.6 on the critical angle of upstream wave appearance.

Olson and Holzer (1974) made a statistical study of the wave and spectral structure of the bow shock, finding relatively little local time dependence of structure at search coil frequencies ($f > .1$ Hz), but they were without information on M or β. The role of β in the generation of magnetic noise is now better understood (Appendix C).

R. D. Auer (unpublished preprint) has found the apparent plasma bow shock position of quasi-parallel bow shocks to be earthward of their quasi-perpendicular counterparts. He has also found that a more marked statistical symmetry between dawn and dusk structures should have prevailed during the HEOS 2 data interval than during the interval examined by Greenstadt (1973).

Feldman et al. (1973) attributed the reversal of heat-flux anisotropy of electrons upstream from the bow shock to their shock origin when the solar wind field was appropriately oriented.

Lin et al. (1974), in the first direct observation of reflected protons since the short paper by Scarf et al. (1970), described the commonplace observation of protons in the 30-100 Kev energy range.

Finally, the two most exciting new results are the observation of an apparent quasi-parallel shock structure at Venus by Mariner 10 (Ness et al., 1974), consistent with a similar interpretation of the Mariner 5 record by this investigator (Greenstadt, 1970), and the tentative compatibility of the Pioneer 10 measurements with the predicted shock structure at Jupiter (Greenstadt, 1973; Ed Smith, personal discussion).

All the foregoing developments draw on results from this program or its preliminary phases.

RECOMMENDATIONS

Micropulsations. It is recommended that efforts to objectivize the reduction and analysis of micropulsation data be supported and expanded. Techniques of display such as the frequency-time contour plots coming out of UCLA (Arthur et al., 1973) should be encouraged for the entire Pc 3-4 spectral range. Quite beyond the current or planned application that this investigation seeks to make of such displays, the eventual use of micropulsation indices as diagnostics of solar wind and magnetosheath conditions will certainly require such techniques, which are expensive and inadequately funded at present. Development of micropulsation diagnostics ought to be a major goal of the International Magnetospheric Study (IMS), but such development will not occur without sustained effort in this direction. It is urgently recommended that a working panel be created to encourage at the very least a uniform micropulsation recording method and schedule among a suitably-selected set of stations as part of the IMS preparations.

Shock Structure. It is recommended that efforts be continued to exploit the earth's bow shock as a source of collisionless plasma phenomenology. The earth's interaction region is nicely representative of the interaction regions of other planets and is subject to such a wide range of incident plasma parameters as to provide almost universal coverage of the variety of collisionless phenomena for which experimental data are needed. Moreover, there seem to be plenty of opportunities to acquire new results through analysis of existing data.

REFERENCES

Arthur, C. W., R. L. McPherron, and P. J. Coleman, Jr., Micropulsations in the morning sector, 1, Ground observations of 10- to 45-second waves, Tungsten, Northwest Territories, Canada, J. Geophys. Res., 78, 8180, 1973.

Asbridge, J. R., S. J. Bame, and I. B. Strong, Outward flow of protons from the earth's bow shock, J. Geophys. Res., 73, 5777, 1968.

Bol'shakova, O. V., and V. A. Troitskaya, Relation of the interplanetary magnetic field direction to the system of stable oscillations, Dokl. Akad. Nauk SSSR, 180, 4, 1968.

Feldman, W. C., J. R. Asbridge, S. J. Bame, and M. D. Montgomery, Solar wind heat transport in the vicinity of the earth's bow shock, J. Geophys. Res., 78, 3697, 1973.

Formisano, V., and P. C. Hedgecock, Solar wind interaction with the earth's magnetic field, 3. On the earth's bow shock structure, J. Geophys. Res., 78, 3745, 1973a.

Formisano V., and P. C. Hedgecock, On the structure of the turbulent bow shock, J. Geophys. Res., 78, 6522, 1973b.

Formisano, V., G. Moreno, F. Palmiotto, and P. C. Hedgecock, Solar wind interaction with the earth's magnetic field, 1. Magnetosheath, J. Geophys. Res., 78, 3714, 1973a.

Formisano, V., P. C. Hedgecock, G. Moreno, F. Palmiotto, and J. Chao, Solar wind interaction with the earth's magnetic field, 2. The magnetohydrodynamic bow shock, J. Geophys. Res., 78, 3731, 1973b.

Greenstadt, E. W., Binary index for assessing local bow shock obliquity, J. Geophys. Res., 77, 5467, 1972.

Greenstadt, E. W., Statistics of bow shock nonuniformity, J. Geophys. Res., 78, 2331, 1973a.

Greenstadt, E. W., Oblique structure of Jupiter's bow shock, J. Geophys. Res., 78, 5813, 1973b.

Greenstadt, E. W., I. M. Green, G. T. Inouye, D. S. Colburn, J. H. Binsack, and E. F. Lyon, Dual satellite observations of the earth's bow shock, 1. The thick pulsation shock, Cosmic Electrodyn., 1, 100, 1970a.

Greenstadt, E. W., I. M. Green, G. T. Inouye, D. S. Colburn, J. H. Binsack, and E. F. Lyon, Dual satellite observations of the earth's bow shock, 3. Field-determined shock structure, Cosmic Electrodyn., 1, 316, 1970b.

Greenstadt, E. W., Dependence of shock structure at Venus and Mars on orientation of the interplanetary magnetic field, Cosmic Electrodyn., 1, 380, 1970c.

Lin, R. P., C. -I. Meng, and K. A. Anderson, 30- to 100-keV protons upstream from the earth's bow shock, J. Geophys. Res., 79, 489, 1974.

Ness, N. F., K. W. Behannon, R. P. Lepping, Y. C. Whang, and K. H. Schatten, Magnetic field observations near Venus: Preliminary results from Mariner 10, Science, 183, 1301, 1974.

Northrop, T. G., and T. J. Birmingham, On Greenstadt's binary index criterion, J. Geophys. Res., 78, 2308, 1973.

Nourry G., and T. Watanabe, Geomagnetic micropulsations and interplanetary magnetic field, Abstract, EOS, 54, 1179, 1973.

Olson, J. V., and R. E. Holzer, On the local time dependence of the bow shock wave structure, J. Geophys. Res., 79, 939, 1974.

Scarf, F. L., W. R. Fredricks, L. A. Frank, C. T. Russell, P. J. Coleman, Jr., and M. Neugebauer, Direct correlations of large amplitude waves with suprathermal protons in the upstream solar wind, J. Geophys. Res., 75, 7316, 1970.

Tidman, D. A., and N. A. Krall, Shock Waves in Collisionless Plasmas, John Wiley-Interscience, New York, 1971.

APPENDIX A

PROGRAM LISTING

```
      PROGRAM E35BXP(INPUT,TAPE5=INPUT,TAPE6,OUTPUT,TAPE7=OUTPUT,TAPE8,
     1               TAPE50)
C
C PROGRAM E35BXP - J.S. BURGESS FOR EXPLORER 35 SEQUENCE AVERAGES.
C E35BXP USES SUBROUTINE E35DRV TO MERGE THE AMES CDC EXPLORER 35
C SEQUENCE AVERAGE TAPE WITH SELECTED TIME INTERVALS AND THEN COMPUTES -
C
C       THBV - THE ANGLE THETA BV BETWEEN INTERPLANETARY FIELD BSW AND
C              THE X(SE) AXIS. (IT IS ASSUMED X IS PARALLEL TO V(SW))
C      TBVCS - THE COSINE OF THETA BV (THBV).
C     TPCBSW - THE MICROPULSATION PERIOD = 160/BSW ACCORDING TO THE
C              RUSSIAN EXPERIMENTAL RESULT.
C     TCYBSW - THE PROTON CYCLOTRON PERIOD IN THE SOLAR WIND ACCORDING
C              TO TCYBSW = TPCBSW/2.44.
C
C INTERPLANETARY FIELD HAS MAGNITUDE BSW, LATITUDE LAMBDAB = BLMB, AND
C LONGITUDE PHIB.
C
      COMMON/PLOTIN/NSECIN,NFIRST,NAFTER,ITIC
      COMMON/DATOUT/NEWDAT(26,60),IDUM
      COMMON/XHEAD/NTAPE,NFOT,NYEAR,COMENT(8)
      COMMON/XTINT/NINT,NFILE,NRECORD,NDAY1,NHOUR1,NMIN1,NDAY2,NHOUR2,
     1             NMIN2,ISTART,IEND,IERROR,NF,NR,IFEMP
      COMMON/OPTION/LISTOP,NPLOTOP,NPLTSAV
      COMMON/XTIM/IDAY(60),ITIM(60),INSTRT,INEND,LSEQSAV
      COMMON/DARRAY/INDEX,TIM(500),NSEQ(500),LDAY(500),LHRMN(500),
     1              LSEC(500),BSW(500),TPCBSW(500),TCYBSW(500),
     2              BLMB(500),PHIB(500),TBVCS(500),THBV(500),COMBAC,
     3              TOPLOT,NSEQSAV,ISGAP,ISGAPSV,MTIMSAV
      COMMON/CONS/RADEG
      LOGICAL COMBAC,TOPLOT,ISGAP,ISGAPSV
      DATA RADEG/57.2957795/
C NCODE IS THE PRINCIPAL DIRECTIVE FROM E35DRV TO E35BXP.
C NOTE - NCODE = 1 MEANS THERE IS NEW DATA FOR PROCESSING.
C      - NCODE = 2 MEANS THERE IS SOME NEW DATA FOR PROCESSING AND THE
C        END OF THE INTERVAL HAS BEEN DETECTED, SO WRAP IT UP.
C      - NCODE = 3 MEANS THERE IS NO NEW DATA FOR PROCESSING AND THE END
C        HAS BEEN DETECTED, SO WRAP IT UP (ANNOTATE, ETC.).
C      - NCODE = 4 MEANS ABNORMAL TERMINATION - EOF REACHED ON TAPE6.
C      - NCODE = 5 MEANS NORMAL TERMINATION - EOF REACHED ON TAPE5.
C
```

REPRODUCIBILITY OF THE ORIGINAL PAGE IS POOR

```
C SECTION 1 - INITIALIZATION.
C
      CALL E35DRV(1,NCODE)
      CALL BXPLST(1)
C
C SECTION 2 - BEGINNING OF A NEW TIME INTERVAL.
C
  150 CONTINUE
C DIRECT E35DRV TO READ A NEW TIME INTERVAL.
      CALL E35DRV(2,NCODE)
C IF NCODE = 5 THEN IT IS TIME FOR NORMAL TERMINATION.
      IF(NCODE.EQ.5)GO TO 2000
C WRITE TIME INTERVAL VALUES ON DATA LISTING.
      CALL BXPLST(2)
C IF IERROR = 1 THE INTERVAL WILL BE USED.
      IF(IERROR.EQ.1)GO TO 400
      NPLOTOP = 1
C IF NPLTSAV = 3 ANNOTATION IS REQUIRED ON PLOT OF PREVIOUS INTERVAL.
      IF(NPLTSAV.EQ.3)CALL BXPPLT(3)
      GO TO 150
C DIRECT E35DRV TO POSITION TAPE AND READ FIRST DATA RECORD.
  400 CONTINUE
      IF(NPLTSAV.EQ.3.AND.NPLOTOP.EQ.1)410,420
  410 CALL BXPPLT(3)
      NPLTSAV = NPLOTOP
  420 CALL E35DRV(3,NCODE)
      GO TO(500,500,150,2000)NCODE
C
C SECTION 3 - PROCESS FIRST RECORD OF GOOD DATA.
C
  500 CONTINUE
      ISGAP = .TRUE.
C IF NPLOTOP = 1 THERE WILL BE NO PLOT MADE OF THIS INTERVAL.
      IF(NPLOTOP.EQ.1)GO TO 550
C IF NPLTSAV = 3 THE PRESENT PLOT WILL CONNECT TO THE PREVIOUS PLOT.
      IF(NPLTSAV.EQ.3)510,520
  510 ISGAP = .FALSE.
      GO TO 560
C INITIALIZE PLOT AND SAVE BEGIN TIME.
  520 MTIMSAV = ISTART
      CALL BXPPLT(1)
```

REPRODUCIBILITY OF THE ORIGINAL PAGE IS POOR

```
C RESET TIME GAP CHECK (SEQUENCE NUMBER IS USED FOR THIS).
  550 NSEQSAV = NEWDAT(1,INSTRT) - 1
C RESET COUNTER FOR DATA ARRAYS.
  560 INDEX = 0
      GO TO(600,800)NCODE
C
C SECTION 4 - PROCESSING FOR NORMAL DATA FLOW (IN MIDDLE OF INTERVAL).
C
  600 CONTINUE
      CALL CALARR
C IS IT TIME TO PLOT AND/OR LIST.
      IF(TOPLOT)610,700
  610 CONTINUE
      IF(NPLOTOP.NE.1)CALL BXPPLT(2)
      IF(LISTOP.EQ.1)CALL BXPLST(3)
      INDEX = 0
C IS THERE MORE DATA TO PROCESS.
      IF(COMBAC)GO TO 600
C DIRECT E35DRV TO READ A NEW DATA RECORD.
  700 CONTINUE
      CALL E35DRV(4,NCODE)
      GO TO(600,800,900,900)NCODE
C
C SECTION 5 - PROCESS DATA AT END OF INTERVAL AND PLOT AND/OR LIST IT
C             AND WRAP UP THIS INTERVAL.
C
  800 CONTINUE
      CALL CALARR
      IF(NPLOTOP.EQ.1)GO TO 850
      CALL BXPPLT(2)
      IF(COMBAC)850,820
  820 IF(NPLOTOP.EQ.3)GO TO 850
C ANNOTATE TIME ON PLOT.
      CALL BXPPLT(3)
  850 CONTINUE
      IF(LISTOP.EQ.1)CALL BXPLST(3)
C IT IS POSSIBLE THAT THERE IS STILL MORE DATA TO PROCESS.
      IF(COMBAC)870,150
  870 INDEX = 0
      GO TO 800
C
```

REPRODUCIBILITY OF THE ORIGINAL PAGE IS POOR

```
C SECTION 6 - END OF INTERVAL AND NO NEW DATA TO PROCESS, SO PLOT AND/OR
C             LIST ANY DATA LEFT IN ARRAYS AND WRAP UP THIS INTERVAL.
C
  900 CONTINUE
      IF(NPLOTOP.EQ.1)GO TO 950
      IF(INDEX.NE.0)CALL BXPPLT(2)
      CALL BXPPLT(3)
  950 IF(LISTOP.NE.1)GO TO 970
      IF(INDEX.GT.0)CALL BXPLST(3)
C WAS EOF REACHED ON THE TAPE (TAPE6).
  970 IF(NCODE.EQ.4)GO TO 2000
      GO TO 150
C
C SECTION 7 - TERMINATION.
 2000 CONTINUE
C TERMINATE PLOT TAPE.
      CALL BXPPLT(4)
      IF(NCODE.EQ.4)2010,2020
 2010 CALL BXPLST(4)
      STOP
 2020 CALL BXPLST(5)
      STOP
      END
"
      SUBROUTINE CALARR
C
C SUBROUTINE CALARR - J.S. BURGESS FOR EXPLORER 35 CDC SEQUENCE AVE.
C CALARR CALCULATES AND FILLS ARRAYS OF DATA FOR MAIN PROGRAM E35BXP. IT
C TAKES FROM 1-60 SETS OF UNPACKED EXPLORER 35 SEQUENCES AVERAGES,
C CALCULATES NECESSARY QUANTITIES, CHECKS FOR TIME GAPS, AND DECIDES
C WHETHER IT IS TIME TO PLOT OR RETURN FOR MORE DATA.
C
      COMMON/CONS/RADEG
      COMMON/DATOUT/NEWDAT(26,60),IDUM
      COMMON/XTIM/IDAY(60),ITIM(60),INSTRT,INEND,LSEQSAV
      COMMON/OPTION/LISTOP,NPLOTOP,NPLTSAV
      COMMON/DARRAY/INDEX,TIM(500),NSEQ(500),LDAY(500),LHRMN(500),
     1              LSEC(500),BSW(500),TPCBSW(500),TCYBSW(500),
     2              BLMB(500),PHIB(500),TBVCS(500),THBV(500),COMBAC,
     3              TOPLOT,NSEQSAV,ISGAP,ISGAPSV,MTIMSAV
      LOGICAL COMBAC,TOPLOT,ISGAP,ISGAPSV
```

REPRODUCIBILITY OF THE ORIGINAL PAGE IS POOR

```
C
C SECTION 1 - PROCESS DATA.
C
C NOTE - TOPLOT = .TRUE. MEANS IT IS TIME TO PLOT EITHER BECAUSE A TIME
C        GAP IS DETECTED OR THE ARRAYS ARE FULL.
C NOTE - COMBAC = .TRUE. MEANS THAT AFTER PLOTTING CALARR MUST BE CALLED
C        AGAIN TO FINISH PROCESSING DATA REMAINING.
C NOTE - ISGAP = .TRUE. MEANS THAT THERE IS A TIME GAP AND THE PRESENT
C        SET OF DATA TO BE PLOTTED WILL NOT BE JOINED TO PREVIOUS DATA.
C NOTE - ISGAPSV SAVES VALUE OF ISGAP FOR BXPPLT.
      TOPLOT = .FALSE.
      COMBAC = .FALSE.
      DO 500 I=INSTRT,INEND
C CHECK FOR TIME GAP AND SEQUENCE RECYCLE.
      IF((NEWDAT(1,I)-NSEQSAV).EQ.1)GO TO 300
      IF(NEWDAT(1,I).EQ.1.AND.NSEQSAV.EQ.999999)GO TO 300
C MAKE SURE THAT ARRAY IS NON-EMPTY BEFORE GOING TO PLOT.
      IF(INDEX.NE.0)GO TO 700
      ISGAP = .TRUE.
C MAKE CALCULATIONS. INDEX COUNTS CONSECUTIVE DATA POINTS.
  300 INDEX = INDEX + 1
      TIM(INDEX) = ITIM(I)
      IF(LISTOP.EQ.2)GO TO 400
      NSEQ(INDEX) = NEWDAT(1,I)
      LDAY(INDEX) = IDAY(I)
      IHRMN = 100*NEWDAT(3,I) + NEWDAT(4,I)
      CALL IFILIN(4,IHRMN,LHRMN(INDEX),MXER)
      CALL IFILIN(2,NEWDAT(5,I),LSEC(INDEX),MXER)
  400 CONTINUE
      IF(NEWDAT(6,I).NE.9999.AND.NEWDAT(6,I).NE.0)GO TO 410
C SET BAD POINTS TO FLAG VALUE
      BSW(INDEX) = 5000.
      TPCBSW(INDEX) = 5000.
      TCYBSW(INDEX) = 5000.
      GO TO 415
  410 CONTINUE
      BSW(INDEX) = NEWDAT(6,I)/10.
      TPCBSW(INDEX) = 160./BSW(INDEX)
      TCYBSW(INDEX) = TPCBSW(INDEX)/2.44
  415 IF(NEWDAT(21,I).NE.9999)GO TO 420
      BLMB(INDEX) = 5000.
```

REPRODUCIBILITY OF THE ORIGINAL PAGE IS POOR

```
      GO TO 425
  420 BLMB(INDEX) = NEWDAT(21,I)/10.
  425 IF(NEWDAT(22,I).NE.9999)GO TO 430
      PHIB(INDEX) = 5000.
      GO TO 435
  430 PHIB(INDEX) = NEWDAT(22,I)/10.
  435 IF(PHIB(INDEX).LT.5000..AND.BLMB(INDEX).LT.5000.)GO TO 450
      TBVCS(INDEX) = 5000.
      THBV(INDEX) = 5000.
      GO TO 475
  450 TBVCS(INDEX) = ABS(COS(BLMB(INDEX)/RADEG)*COS(PHIB(INDEX)/RADEG))
      THBV(INDEX) = ACOS(TBVCS(INDEX))*RADEG
  475 CONTINUE
C SAVE PREVIOUS SEQUENCE NUMBER AND CHECK TO SEE IF ARRAYS ARE FULL.
      NSEQSAV = NEWDAT(1,I)
      IF(INDEX.EQ.500)GO TO 600
  500 CONTINUE
C IF IT GETS HERE IT IS TIME TO RETURN FOR MORE DATA.
      ISGAPSV = ISGAP
      RETURN
C
C SECTION 2 - MAKE PLOT AND RETURN FOR MORE PROCESSING DECISIONS.
C
C PART 1 - THE ARRAYS ARE FILLED.
  600 CONTINUE
      ISGAPSV = ISGAP
      ISGAP = .FALSE.
      IF(I.LT.INEND)COMBAC = .TRUE.
      TOPLOT = .TRUE.
      INSTRT = I+1
      RETURN
C
C PART 2 - THERE IS A TIME GAP.
  700 CONTINUE
      ISGAPSV = ISGAP
      ISGAP = .TRUE.
      COMBAC = .TRUE.
      TOPLOT = .TRUE.
      INSTRT = I
      NSEQSAV = NEWDAT(1,INSTRT) - 1
      RETURN
```

```
      END
"                                                                    "
      SUBROUTINE BXPLST(JCODE)
C
C SUBROUTINE BXPLST - J.S. BURGESS FOR EXPLORER 35 CDC SEQUENCE AVE.
C BXPLST IS A DATA LISTING SUBROUTINE FOR MAIN PROGRAM E35BXP. IT
C PROVIDES A COMPLETE DATA LISTING FOR ANY TIME INTERVAL THAT HAS THE
C LIST OPTION ON (LISTOP=1). IT ALSO PROVIDES A LIST OF ALL TIME
C INTERVALS IN A PARTICULAR RUN REGARDLESS OF THE LIST OPTION.
C
      COMMON/XHEAD/NTAPE,NFOT,NYEAR,COMENT(8)
      COMMON/XTINT/NINT,NFILE,NRECORD,NDAY1,NHOUR1,NMIN1,NDAY2,NHOUR2,
     1             NMIN2,ISTART,IEND,IERROR,NF,NR,IFEMP
      COMMON/DARRAY/INDEX,TIM(500),NSEQ(500),LDAY(500),LHRMN(500),
     1              LSEC(500),BSW(500),TPCBSW(500),TCYBSW(500),
     2              BLMB(500),PHIB(500),TBVCS(500),THBV(500),COMBAC,
     3              TOPLOT,NSEQSAV,ISGAP,ISGAPSV,MTIMSAV
      DIMENSION TITLE(4),TGP(2)
      DATA TITLE/40H*** EXPLORER 35 THETA XB, PC3 PERIOD ***/
      DATA TGP/20H***** TIME GAP *****/
      LOGICAL ISGAPSV
      GO TO(100,200,300,1000,2000)JCODE
C
C SECTION 1 - WRITE TITLE PAGE
C
  100 CONTINUE
      WRITE(8,10)TITLE,NTAPE,COMENT
   10 FORMAT(1H1////10X,4A10/10X,*TAPE NUMBER -*,I6//10X,8A10)
      RETURN
C
C SECTION 2 - WRITE TIME INTERVAL VALUES OR AN ERROR MESSAGE
C
  200 CONTINUE
      WRITE(8,20)TITLE,NINT
   20 FORMAT(1H1,4A10//25H    * TIME INTERVAL NUMBER,I4)
C NOTE - IERROR = 1 MEANS THAT EVERYTHING IS OK.
      IF(IERROR.EQ.1)GO TO 250
      WRITE(8,30)
   30 FORMAT(///10X,*THIS INTERVAL WAS SKIPPED BECAUSE OF AN ERROR.*//
     1          10X,*SEE MONITOR LISTING FOR ERROR INFORMATION.*)
      RETURN
```

```
C WRITE OUT TIME INTERVAL VALUES.
C NOTE - LINE COUNTS PRINT LINES FOR PAGE EJECT DECISION.
C NOTE - LDAYSAV SAVES THE LAST DAY USED IN DATE PRINTOUT.
  250 CONTINUE
      LINE = 100
      LDAYSAV = -100
      CALL XDATE(NDAY1,NYEAR,MTH1,JDAY1)
      CALL IFILIN(2,JDAY1,KDAY1,MXER)
      CALL XDATE(NDAY2,NYEAR,MTH2,JDAY2)
      CALL IFILIN(2,JDAY2,KDAY2,MXER)
      WRITE(8,40)MTH1,KDAY1,NYEAR,NDAY1,NHOUR1,NMIN1,
     1          MTH2,KDAY2,NYEAR,NDAY2,NHOUR2,NMIN2
   40 FORMAT(//10X,*FROM*,I3,1H/,A2,1H/,I2,* (DAY*,I4,*)  HR*,I3,*  MIN*
     1,I3/10X,*  TO*,I3,1H/,A2,1H/,I2,* (DAY*,I4,*)  HR*,I3,*  MIN*,I3)
      RETURN
C
C SECTION 3 - DATA PRINTOUT FOR LISTOP = 1. PRINT OUT THE DATA ARRAYS.
C
  300 CONTINUE
      IF(LINE.EQ.100.OR..NOT.ISGAPSV)GO TO 310
C WRITE TIME GAP LINE
      WRITE(8,45)TGP,TGP
   45 FORMAT(14X,2A10,17X,2A10)
      LINE = LINE + 1
  310 DO 400 I=1,INDEX
C CHECK TO SEE IF NEW DATE IS REQUIRED.
      IF(LDAYSAV.EQ.LDAY(I))GO TO 320
      LDAYSAV = LDAY(I)
      CALL XDATE(LDAY(I),NYEAR,MON,MDAY)
      CALL IFILIN(2,MON,LMON,MXER)
      CALL IFILIN(2,MDAY,LMDAY,MXER)
      IF(LINE.GT.36)GO TO 330
      WRITE(8,50)LMON,LMDAY,NYEAR,LDAYSAV
   50 FORMAT(/2X,A2,1H/,A2,1H/,I2,*  DAY*,I4/)
      LINE = LINE + 3
      GO TO 350
C MAKE DECISION TO EJECT PAGE AND PRINT HEADING.
  320 IF(LINE.LT.40)GO TO 350
  330 WRITE(8,60)LMON,LMDAY,NYEAR,LDAYSAV,TITLE
   60 FORMAT(1HI,1X,A2,1H/,A2,1H/,I2,*  DAY*,I4,3X,4A10//*  SEQUENCE  HR
     1MN SC       BSW   LAMBDAB    PHIB   THBVCOS   THETABV       TPCBSW   TCYC
```

```
     2BSW*/)
      LINE = 4
C PRINT ONE LINE OF DATA
  350 CONTINUE
      WRITE(8,70)NSEQ(I),LHRMN(I),LSEC(I),BSW(I),BLMB(I),PHIB(I),
     1          TBVCS(I),THBV(I),TPCBSW(I),TCYBSW(I)
   70 FORMAT(1X,I8,3X,A4,1X,A2,1X,3F8.1,F8.3,F9.1,4X,F8.1,F9.1)
      LINE = LINE + 1
  400 CONTINUE
      RETURN
C
C SECTION 4 - TERMINATION
C
 1000 CONTINUE
      WRITE(8,80)
   80 FORMAT(1H1///43H *** ABNORMAL TERMINATION - SEE MONITOR ***)
      RETURN
 2000 CONTINUE
      WRITE(8,90)
   90 FORMAT(1H1///19H *** END OF JOB ***)
      RETURN
      END
"
      SUBROUTINE BXPPLT(MCODE)
C
C SUBROUTINE BXPPLT - J.S. BURGESS FOR EXPLORER 35 SEQUENCE AVERAGES.
C BXPPLT IS THE PLOT SUBROUTINE FOR E35BXP. VALUES OF THBV, TBVCS,
C TPCBSW, AND TCYBSW (SEE E35BXP) ARE PLOTTED AS A FUNCTION OF TIME.
C BXPPLT USES THE TRW PLOT EXECUTIVE SUBROUTINE CCP FOR THE CAL-COMP.
C AT PRESENT, THIS PROGRAM WILL NOT PLOT ACROSS THE END OF THE YEAR.
C
      COMMON/XHEAD/NTAPE,NFOT,NYEAR,COMENT(8)
      COMMON/PLOTIN/NSECIN,NFIRST,NAFTER,ITIC
      COMMON/DARRAY/INDEX,TIM(500),NSEQ(500),LDAY(500),LHRMN(500),
     1              LSEC(500),BSW(500),TPCBSW(500),TCYBSW(500),
     2              BLMB(500),PHIB(500),TBVCS(500),THBV(500),COMBAC,
     3              TOPLOT,NSEQSAV,ISGAP,ISGAPSV,MTIMSAV
      DIMENSION PTITLE(3),F1(8),F2(7),F3(2),F4(1),YTIC(1500)
      LOGICAL ISGAPSV
      DATA YTHBV,DTHBV,YTBVCS,DTBVCS,YTPCSOV,DTPCSOV,YTCYBSW,DTCYBSW
     1    / 200., -20.,  -1.0,   0.2,    0.0,    20.,    0.0,    20./
```

REPRODUCIBILITY OF THE ORIGINAL PAGE IS POOR

```
      DATA PTITLE/30H* EXP 35 THETA XB - PC3 PERIOD/
      DATA F1,F2,F3,F4/6*10H           ,12H    THETA BV,
     1                  5*10H          ,12HCOS THETA BV,
     2                    10H          ,10HIPC SOVIET,
     3                                  10H  TCYCBSW /
C
C NOTE - MCODE = 1 MEANS A NEW PLOT WILL BE SET UP.
C      - MCODE = 2 MEANS GO PLOT DATA.
C      - MCODE = 3 MEANS PLOT TIC MARKS AND ANNOTATE TIME ON PLOT.
C      - MCODE = 4 MEANS TERMINATE THE PLOT TAPE (TAPE50).
C
      GO TO(100,200,300,400)MCODE
C
C SECTION 1 - MCODE=1 - SETUP FOR A NEW PLOT.
C
  100 CONTINUE
      ISECIN = NSECIN
      IFIRST = NFIRST*60
      IAFTER = NAFTER*60
      NTIC = ITIC*60
C GET START TIME (LEFT CORNER) OF PLOT FOR GIVEN TIME INTERVAL.
      CALL MOVBACT(ISECIN,MTIMSAV,ITSTART,NSET)
      XTSTART = ITSTART
      XSECIN = ISECIN
C GET SYMBOL FREQUENCY.
      NSYM = .025*XSECIN + .5
C CALL CCP SETUP ENTRANCE.
      CALL CCP(1,  2,XTSTART,XSECIN,TIM,0,4,
     1           YTHBV,  DTHBV,  4,NSYM,  THBV,
     2          YTBVCS, DTBVCS,  0,   1, TBVCS,
     3        YTPCSOV,DTPCSOV, 45,NSYM,TPCBSW,
     4        YTCYBSW,DTCYBSW,  0,   1,TCYBSW,  30,PTITLE, 0, 0,
     5        72,F1,  62,F2,  20,F3,  10,F4)
      RETURN
C
C SECTION 2 - MCODE=2 - PLOT DATA.
C
  200 CONTINUE
      ICONECT = 0
      IF(ISGAPSV)ICONECT=1
C CALL CCP DATA ENTRANCE TO PLOT.
```

REPRODUCIBILITY OF THE ORIGINAL PAGE IS POOR

```
      CALL CCP(2,INDEX,ICONECT)
C SAVE TIME OF LAST POINT PLOTTED EACH TIME.
      ITRIGHT = TIM(INDEX) + .5
      RETURN
C
C SECTION 3 - MCODE=3 - PLOT TIC MARKS AND ANNOTATE TIME FOR THE WHOLE
C             PLOT. THIS IS THE END OF THIS PLOT.
C
  300 CONTINUE
C GET TOTAL NUMBER OF TIC MARKS AND ANNOTATIONS AND ALSO GET THE RIGHT-
C    MOST TIME (ITRIGHT) ON THE PLOT FRAME.
      LTIMSUM = ITSTART + IFIRST
      ITIMSUM = ITRIGHT - LTIMSUM
      NUMBER = ITIMSUM/IAFTER
      ITRIGHT = LTIMSUM + NUMBER*IAFTER
      IF(MOD(ITIMSUM,IAFTER).NE.0)310,320
  310 NUMBER = NUMBER + 2
      ITRIGHT = ITRIGHT + IAFTER
      GO TO 330
  320 NUMBER = NUMBER + 1
  330 NUMTIC = (ITRIGHT - ITSTART)/NTIC + 1
      IF(NUMTIC.GT.1500)NUMTIC = 1500
      DO 340 J=1,NUMTIC
  340 YTIC(J) = 0.0
      XRIGHT = ITRIGHT
      XTIC = -NTIC
C CALL CCP PARAMETER REDEFINE ENTRANCE TO SET UP TIC MARK PLOT.
      CALL CCP(-1, 2,XTSTART,XSECIN,XRIGHT,XTIC,1,0.0,100.,13,1,YTIC,
     1          0,0,0,0,0,0)
      CALL CCP(2,NUMTIC,1)
C FINISH TIC MARK LINE TO LEFT CORNER IF NECESSARY.
      IF(LTIMSUM.EQ.ITSTART)GO TO 350
      XTIC = -XTIC
      CALL CCP(-1, 2,XTSTART,XSECIN,XTSTART,XTIC,1,0.0,100.,13,1,YTIC,
     1          0,0,0,0,0,0)
      CALL CCP(2,1,0)
C
C ANNOTATE TIME ON PLOT (CCP ANNOTATION ENTRANCE).
C
  350 CONTINUE
      MDAYSAV = 0
```

REPRODUCIBILITY OF THE ORIGINAL PAGE IS POOR

```
      DO 390 I=1,NUMBER
      TOTSEC = LTIMSUM - ITSTART
      IDIS = (TOTSEC/XSECIN)*100. - 26. + .5
      CALL TIMCON(3,IFER,LTIMSUM,MDAY,MHR,MIN,MSEC,MIL)
      IF(MDAYSAV.EQ.MDAY)GO TO 370
      MDAYSAV = MDAY
C GET NEW DATE.
      CALL XDATE(MDAY,NYEAR,MONTH,MDY)
      CALL IFILIN(2,MONTH,MNTH,IXER)
      CALL IFILIN(2,MDY,LDY,IXER)
      ENCODE(8,10,DATE)MNTH,LDY,NYEAR
   10 FORMAT(A2,1H/,A2,1H/,I2)
C ANNOTATE NEW DATE - MO/DA/YR.
      CALL CCP(3,IDIS,.5,.15,8,DATE)
  370 CONTINUE
      MHRMN = 100*MHR + MIN
      CALL IFILIN(4,MHRMN,KHRMN,IXER)
C ANNOTATE TIME - HRMN.
      CALL CCP(3,IDIS,30,.15,4,KHRMN)
      LTIMSUM = LTIMSUM + IAFTER
  390 CONTINUE
C CALL CCP CLEAN-UP ENTRANCE.
      CALL CCP(5,999999)
      RETURN
C
C SECTION 4 - MCODE=4 - TERMINATE PLOT TAPE.
C
  400 CONTINUE
      CALL CCP(6)
      RETURN
      END
"
      SUBROUTINE MOVBAC(ISECIN,MTIMSAV,ITSTART,NSET)
C
C SUBROUTINE MOVBAC - J.S. BURGESS FOR EXPLORER 35 SEQUENCE AVERAGES.
C MOVBAC CALCULATES THE START OF THE TIME AXIS ON THE CAL-COMP PLOT TO
C   THE NEAREST  10 MIN   IF    300.LE.ISECIN.LT. 1800 SEC/INCH,
C   THE NEAREST   1 HOUR  IF   1800.LE.ISECIN.LT.10800 SEC/INCH,
C   THE NEAREST   6 HOURS IF  10800.LE.ISECIN.LE.64800 SEC/INCH.
C IN THIS WAY THE TIME INTERVAL CAN BEGIN ANYWHERE, BUT THE PLOT WILL
C ALWAYS BEGIN ON SOME CONVENIENT MULTIPLE OF WHOLE MINUTES.
```

REPRODUCIBILITY OF THE ORIGINAL PAGE IS POOR

```
C MOVBAC IS CALLED FROM THE E35 PLOT EXECUTIVE SUBROUTINE, BXPPLT.
C
      DIMENSION LIMIT(2),NDIV(3)
      DATA LIMIT/1800,10800/
      DATA NDIV/600,3600,21600/
C FIND THE SET OF TIME INCREMENTS THAT CONTAINS ISECIN.
      DO 200 I=1,2
      IF(ISECIN.LT.LIMIT(I))GO TO 220
  200 CONTINUE
      I=3
C GET TIME OF LEFT CORNER OF PLOT (ITSTART)
  220 ITSTART = (MTIMSAV/NDIV(I))*NDIV(I)
      NSET = I
      RETURN
      END
"
      SUBROUTINE E35DRV(ICODE,NCODE)
C
C SUBROUTINE E35DRV - J.S. BURGESS FOR EXPLORER 35 CDC SEQUENCE AVE.
C E35DRV IS THE EXPLORER 35 CDC TAPE DRIVER PROGRAM. IT MERGES THE TAPE
C WITH SELECTED TIME INTERVALS. IN GENERAL IT READS A TIME INTERVAL,
C POSITIONS THE TAPE AND LOCATES THE START TIME, AND THEN RETURNS DATA
C RECORD BY RECORD TO A MAIN CALLING PROGRAM UNTIL THE INTERVAL HAS
C BEEN SATISFIED. A LIST OF RECORDS SUPPLIED FOR EACH INTERVAL IS
C RECORDED BY E35MON. CARD INPUT IS TAPE5, THE CDC TAPE IS TAPE6, AND
C THE MONITOR IS TAPE7. SEE E35DRV WRITE-UP FOR INSTRUCTIONS.
C
      COMMON/PLOTIN/NSECIN,NFIRST,NAFTER,ITIC
      COMMON/DATIN/INDATA(8,60)
      COMMON/DATOUT/NEWDAT(26,60),IDUM
      COMMON/XHEAD/NTAPE,NFOT,NYEAR,COMENT(8)
      COMMON/XTINT/NINT,NFILE,NRECORD,NDAY1,NHOUR1,NMIN1,NDAY2,NHOUR2,
     1             NMIN2,ISTART,IEND,IERROR,NF,NR,IFEMP
      COMMON/OPTION/LISTOP,NPLOTOP,NPLTSAV
      COMMON/XTIM/IDAY(60),ITIM(60),INSTRT,INEND,LSEQSAV
      DATA COMENT/8*10H**********/
      DATA LISTOP,NPLOTOP,NSECIN,NFIRST,NAFTER,ITIC/2,1,300,0,60,10/
      NAMELIST/HEADER/NTAPE,NFOT,NYEAR,COMENT
      NAMELIST/TIMINT/NINT,NFILE,NRECORD,NDAY1,NHOUR1,NMIN1,NDAY2,NHOUR2
     I               ,NMIN2,NYEAR,LISTOP,NPLOTOP,NSECIN,NFIRST,NAFTER,
     2                ITIC
```

REPRODUCIBILITY OF THE ORIGINAL PAGE IS POOR

```
C ICODE MUST BE SUPPLIED BY THE CALLING PROGRAM TO DIRECT E35DRV.
      GO TO(200,300,400,500)ICODE
C
C SECTION 1 - ICODE=1 - INITIALIZATION - READ HEADER CARD, WRITE TITLE
C             PAGE ON MONITOR, INITIALIZE RECORD AND FILE COUNTERS.
C
  200 CONTINUE
      CALL NMLEOF
      NCODE = 0
      REWIND 6
      READ(5,HEADER)
      CALL E35MON(1)
      NR = 0
      NF = 1
      RETURN
C
C SECTION 2 - ICODE=2 - READ TIME INTERVALS AND CHECK.
C
  300 CONTINUE
      NPLTSAV = NPLOTOP
      LISTOP = 2
      NPLOTOP = 1
      LSEQSAV = 0
      READ(5,TIMINT)
      IF(EOF,5)2000,320
  320 CONTINUE
      CALL INTCHK
      CALL E35MON(2)
      RETURN
C
C SECTION 3 - ICODE=3 - POSITION TAPE TO FILE AND RECORD CONTAINING
C             START OF INTERVAL AND READ FIRST GOOD RECORD(SEE SEC.4).
C
  400 CONTINUE
C FIND FILE.
      IF(NFILE.EQ.NF)GO TO 450
      CALL SKIPF(6,NFILE-NF)
      NR = 0
      NF = NFILE
  450 IFSAME = 1
      IF(NRECORD.EQ.NR)460,470
```

```
C  IF IT GETS HERE THE RECORD HAS ALREADY BEEN READ.
  460 IFSAME = 2
      GO TO 610
C  FIND RECORD.
  470 LRECORD = NRECORD - 1
      IF(LRECORD.EQ.NR)GO TO 500
      MX = LRECORD - NR
      DO 490 LX=1,MX
  490 READ(6)
      NR = LRECORD
C
C  SECTION 4 - ICODE=4 - READ NEXT DATA RECORD, UNPACK AND SCAN TIMES.
C
  500 CONTINUE
      NR = NR + 1
      READ TAPE6,INDATA
      IF(EOF,6)510,600
  510 NF = NF + 1
      IF(NF.GT.NFOT)GO TO 1000
      NR = 0
      GO TO 500
C  UNPACK DATA AND SEARCH FOR DATA TIMES CONTAINED IN INTERVAL.
  600 CONTINUE
      CALL UNPKEX
  610 CALL TIMEND(IFSAME,IFEMP,ISTART,IEND,NCODE)
      CALL E35MON(3,NCODE)
      IF(IFEMP.NE.3)GO TO 500
      RETURN
C
C  SECTION 5 - TERMINATION
C
C  NOTE - NCODE = 4 MEANS ABNORMAL TERMINATION - EOF REACHED ON TAPE6.
C         NCODE = 5 MEANS NORMAL TERMINATION - EOF REACHED ON TAPE5.
C
 1000 CONTINUE
      REWIND 6
      CALL E35MON(4)
      NCODE = 4
      RETURN
 2000 CONTINUE
      REWIND 6
```

```
      CALL E35MON(5)
      NCODE = 5
      RETURN
      END
      SUBROUTINE INTCHK
C
C SUBROUTINE INTCHK - J.S. BURGESS FOR EXPLORER 35 SEQUENCE AVE.
C INTCHK DOES ROUTINE CHECKING FO TIME INTERVAL INPUT FOR E35DRV,
C THE EXPLORER 35 CDC TAPE DRIVER SUBROUTINE. IT RETURNS THE STATUS
C OF THE INPUT DATA THROUGH THE PARAMETER IERROR. ERROR MESSAGES
C CAN BE FOUND IN THE SUBROUTINE E35MON. INTCHK ALSO CALCULATES
C START AND STOP TIMES OF THE INTERVAL IN TOTAL SECONDS.
C
      COMMON/PLOTIN/NSECIN,NFIRST,NAFTER,ITIC
      COMMON/XHEAD/NTAPE,NFOT,NYEAR,COMENT(8)
      COMMON/XTINT/NINT,NFILE,NRECORD,NDAY1,NHOUR1,NMIN1,NDAY2,NHOUR2,
     1             NMIN2,ISTART,IEND,IERROR,NF,NR,IFEMP
      COMMON/OPTION/LISTOP,NPLOTOP,NPLTSAV
C CHECK OPTION VALUES.
      IF(LISTOP.EQ.1.OR.LISTOP.EQ.2)100,120
  100 IF(NPLOTOP.GT.0.AND.NPLOTOP.LE.3)150,120
  120 IERROR = 7
      RETURN
C CHECK VALUE OF NFILE (FILE CONTAINING START TIME OF THE INTERVAL).
  150 IF(NFILE.LE.NFOT)GO TO 160
      IERROR = 6
      RETURN
C CHECK POSITION OF TAPE RELATIVE TO NFILE (NF IS CURRENT POSITION).
  160 IF(NFILE.GE.NF)GO TO 170
      IERROR = 4
      RETURN
C CHECK POSITION OF TAPE RELATIVE TO NRECORD (IF NFILE=NF).
  170 IF(NFILE.NE.NF)GO TO 180
      IF(NRECORD.GE.NR)GO TO 180
      IERROR = 5
      RETURN
C CALCULATE START AND STOP TIMES OF TIME INTERVAL IN TOTAL SECONDS.
  180 CONTINUE
      CALL TIMCON(-3,IFER,ISTART,NDAY1,NHOUR1,NMIN1,0)
      CALL TIMCON(-3,IFER,IEND,NDAY2,NHOUR2,NMIN2,0)
```

```
C MAKE SURE START TIME IS LESS THAN STOP TIME.
      IF(IEND.GT.ISTART)GO TO 190
      IERROR = 3
      RETURN
C MAKE SURE TIMES ARE IN RANGE OF YEAR.
  190 NSCINYR = 31536000
      IF(MOD(NYEAR,4).EQ.0)NSCINYR=31622400
      IF(IEND.LT.NSCINYR)GO TO 200
      IERROR = 2
      RETURN
C ARE THERE PLOT VALUES TO CHECK.
  200 IF(NPLOTOP.NE.1)GO TO 300
      NSECIN = 0
      NFIRST = 0
      NAFTER = 0
      ITIC   = 0
      GO TO 1000
  300 IF(NPLTSAV.EQ.3)GO TO 345
C CHECK RANGE OF TIME INCREMENT PER INCH VALUE.
      IF(NSECIN.GE.300.AND.NSECIN.LE.64800)GO TO 310
      IERROR = 8
      RETURN
C CHECK RANGE OF FIRST ANNOTATION INCREMENT.
  310 IF(NFIRST.GE.0.AND.NFIRST.LE.1440)GO TO 320
      IERROR = 9
      RETURN
C CHECK RANGE OF FOLLOWING ANNOTATION INCREMENT.
  320 IF(NAFTER.GE.5.AND.NAFTER.LE.25920)GO TO 330
      IERROR = 10
      RETURN
C CHECK TIC MARK INCREMENT VALUE.
  330 IF(ITIC.GT.0.AND.MOD(NAFTER,ITIC).EQ.0)GO TO 340
  335 IERROR = 11
      RETURN
  340 NSTART = ISTART
  345 ITIMTOT = IEND - NSTART + NAFTER*60
      IF(ITIMTOT/(ITIC*60).GT.1500)GO TO 335
C EVERYTHING APPEARS TO BE OK.
 1000 IERROR = 1
      RETURN
      END
```

```
      SUBROUTINE E35MON(LCODE,NCODE)
C
C SUBROUTINE E35MON - J.S. BURGESS FOR EXPLORER 35 CDC SEQUENCE AVE.
C E35MON IS A LISTING SUBROUTINE CALLED FROM E35DRV, THE EXPLORER 35
C CDC TAPE DRIVER PROGRAM. THE PRIMARY FUNCTION OF E35MON IS TO MAKE
C A LISTING OF ALL RECORDS ACCEPTED BY E35DRV AS VALID INPUT FOR THE
C CURRENT TIME INTERVAL. IT ALSO LISTS VALUES OF INTERVAL INPUT AND
C WRITES VARIOUS ERROR MESSAGES.
C
      COMMON/PLOTIN/NSECIN,NFIRST,NAFTER,ITIC
      COMMON/XHEAD/NTAPE,NFOT,NYEAR,COMENT(8)
      COMMON/XTINT/NINT,NFILE,NRECORD,NDAY1,NHOUR1,NMIN1,NDAY2,NHOUR2,
     1             NMIN2,ISTART,IEND,IERROR,NF,NR,IFEMP
      COMMON/OPTION/LISTOP,NPLOTOP,NPLTSAV
      COMMON/DATOUT/NEWDAT(26,60),IDUM
      COMMON/XTIM/IDAY(60),ITIM(60),INSTRT,INEND,LSEQSAV
      DIMENSION ERRMES(3,11),ERRIND(2),MLERR(3,2)
      DATA ERRIND/10H0**********,10H0* ERROR */
      DATA ERRMES/30H*** OK ****** OK ****** OK ***,
     1            30HTIME IS OUT OF RANGE OF YEAR. ,
     2            30HTIME 2 IS LESS THAN TIME 1.   ,
     3            30HTAPE POSITION IS PAST NFILE.  ,
     4            30HTAPE POSITION IS PAST NRECORD.,
     5            30HNFILE IS GREATER THAN NFOT.   ,
     6            30HOPTION VALUE IS OUT OF RANGE. ,
     7            30HNSECIN IS OUT OF RANGE.       ,
     8            30HNFIRST IS OUT OF RANGE.       ,
     9            30HNAFTER IS OUT OF RANGE.       ,
     A            30HITIC IS NOT ACCEPTABLE.       /
      DATA MLERR/30H***** OVERLAP OR NO TIME MATCH,
     1           30H***** RECORD HAS ALL BAD TIMES/
      GO TO(100,200,200,1000,2000)LCODE
C
C SECTION 1 - WRITE TITLE PAGE.
C
  100 CONTINUE
      WRITE(7,10)NTAPE,NFOT,NYEAR,COMENT
   10 FORMAT(1H1////10X,32H**** E35DRV MONITOR LISTING ****
     1            //15X,       *TAPE NUMBER -*,I7
     2            //15X,       *NUMBER OF FILES -*,I3
```

```
     3              //15X,        *YEAR OF DATA -*,I6//10X,8A10)
      LINE = 100
      RETURN
C
C SECTION 2 - WRITE PAGE HEADING.
C
  200 CONTINUE
      IF(LINE.LT.40)GO TO(100,300,400)LCODE
      LINE = 2
      WRITE(7,20)
   20 FORMAT(1H1,* INT FILE REC  START-SEQUENCE DAY HR MN SC  END-SEQUEN
     1CE   DAY HR MN SC NCODE     ISTART    TIME1     TIME2      IEND*/)
      GO TO(100,300,400)LCODE
C
C SECTION 3 - WRITE TIME INTERVAL VALUES AND ANY ERROR MESSAGE.
C
  300 CONTINUE
      IER = 1
      IF(IERROR.GT.1)IER = 2
      WRITE(7,30)ERRIND(IER),NINT,NFILE,NRECORD,NDAY1,NHOUR1,NMIN1,
     1           NDAY2,NHOUR2,NMIN2,NYEAR,LISTOP,NPLOTOP,NPLTSAV,
     2           (ERRMES(LM,IERROR),LM=1,3),IERROR,NSECIN,NFIRST,NAFTER,
     3           ITIC
   30 FORMAT(A10,I5,* NFILE=*,I3,* NRECORD=*,I4,1H,,I5,2I4,1X,I5,2I4,
     1       *  NYEAR=*,I5,1H,,3I3,1X,3A10,I5/16X,*NSECIN=*,I9,1H,,
     2       *  NFIRST=*,I9,1H,,*  NAFTER=*,I9,1H,,*  ITIC=*,I9)
      LINE = LINE + 3
      RETURN
C
C SECTION 4 - WRITE ONE MONITOR LINE OR ERROR MESSAGE.
C
  400 CONTINUE
      LINE = LINE + 1
      IF(IFEMP.EQ.3)GO TO 450
      WRITE(7,35)NINT,NF,NR,(MLERR(LM,IFEMP),LM=1,3)
   35 FORMAT(1X,2I4,I5,2X,3A10)
      RETURN
  450 CONTINUE
      IF(NCODE.EQ.3)GO TO 500
      WRITE(7,40)NINT,NF,NR,INSTRT,NEWDAT(1,INSTRT),IDAY(INSTRT),
     1           NEWDAT(3,INSTRT),NEWDAT(4,INSTRT),NEWDAT(5,INSTRT),
```

REPRODUCIBILITY OF THE ORIGINAL PAGE IS POOR

```
     2             INEND,NEWDAT(1,INEND),IDAY(INEND),NEWDAT(3,INEND),
     3             NEWDAT(4,INEND),NEWDAT(5,INEND),NCODE,ISTART,
     4             ITIM(INSTRT),ITIM(INEND),IEND
  40 FORMAT(1X,2I4,I5,2(*  S(*,I2,*)=*,I7,I5,3I3),I4,3X,4I10)
     RETURN
 500 CONTINUE
     WRITE(7,50)NINT,NF,NR
  50 FORMAT(1X,2I4,I5,2X,*ALL OF THIS RECORD PAST END OF INTERVAL*)
     RETURN
C
C SECTION 5 - WRITE TERMINATION MESSAGE.
C
1000 CONTINUE
     WRITE(7,60)NINT,NF
  60 FORMAT(1H1///* ABNORMAL TERMINATION*/* END OF TAPE REACHED IN INTE
    IRVAL NO.*,I4/* NF =*,I4)
     RETURN
2000 CONTINUE
     WRITE(7,70)
  70 FORMAT(1H1///* NORMAL TERMINATION*)
     RETURN
     END
"                                                                      "
     SUBROUTINE TIMFND(IFSAME,IFEMP,ISTART,IEND,NCODE)
C
C SUBROUTINE TIMFND - J.S. BURGESS FOR EXPLORER 35 SEQUENCE AVE.
C TIMFND IS CALLED FROM E35DRV TO DETERMINE THE FIRST (INSTRT) AND
C LAST (INEND) SEQUENCES (FROM A DATA RECORD OF 60 SEQUENCES) THAT ARE
C CONTAINED IN THE CURRENT TIME INTERVAL. TIMFND ALSO REMOVES OVERLAP,
C CALCULATES EACH TIME IN TOTAL SECONDS, GETS ACTUAL DAY OF YEAR, AND
C DETERMINES IF THE END OF THE TIME INTERVAL HAS BEEN REACHED.
C
     COMMON/DATOUT/NEWDAT(26,60),IDUM
     COMMON/XTIM/IDAY(60),ITIM(60),INSTRT,INEND,LSEQSAV
C NOTE - IFSAME = 1 MEANS RECORD CHECK AND TIME CALCULATIONS MUST BE
C        MADE FOR THE CURRENT DATA RECORD.
C      - IFSAME = 2 MEANS THAT A NEW TIME INTERVAL BEGINS IN THE SAME
C        RECORD JUST PROCESSED BY TIMFND, SO SKIP SECTION 1.
     GO TO(100,400)IFSAME
C
C SECTION 1 - TIME CALCULATIONS.
```

REPRODUCIBILITY OF THE
ORIGINAL PAGE IS POOR

```
C
  100 CONTINUE
C FIND LAST GOOD TIME IN RECORD.
      DO 200 I=1,60
      IF(NEWDAT(1,61-I).EQ.999999.AND.NEWDAT(5,61-I).EQ.0)GO TO 200
      GO TO 210
  200 CONTINUE
C NOTE - IFEMP = 2 MEANS NO GOOD TIMES. RETURN FOR NEW RECORD.
      IFEMP = 2
      RETURN
  210 LASTIM = 61-I
C ELIMINATE OVERLAP AT END OF RECORD.
      IF(LASTIM.LT.2)GO TO 290
      DO 250 I=2,LASTIM
      IF(NEWDAT(1,I).GT.NEWDAT(1,I-1))GO TO 250
      IF(NEWDAT(1,I).LT.1000.AND.NEWDAT(1,I-1).GT.999000)250,270
  250 CONTINUE
      GO TO 290
  270 LASTIM = I-1
  290 CONTINUE
C GET ACTUAL DAY OF YEAR AND CALCULATE SEQUENCE TIMES IN TOTAL SECONDS.
      DO 300 I=1,LASTIM
      IDAY(I) = NEWDAT(2,I) + 1
      CALL TIMCON(-3,IFER,ITIM(I),IDAY(I),NEWDAT(3,I),NEWDAT(4,I),NEWDAT
     1(5,I))
  300 CONTINUE
      GO TO 410
C
C SECTION 2 - DETERMINE INSTRT AND INEND
C
  400 CONTINUE
      IFSAME = 1
C NOTE - IFEMP = 3 MEANS EVERYTHING IS OK.
  410 IFEMP = 3
C FIND FIRST SEQUENCE TIME IN TIME INTERVAL.
      DO 500 I=1,LASTIM
      IF(NEWDAT(1,I).GT.LSEQSAV)GO TO 490
      IF(NEWDAT(1,I).LT.1000.AND.LSEQSAV.GT.999000)490,500
  490 IF(ITIM(I).GE.ISTART)GO TO 510
  500 CONTINUE
C NOTE - IFEMP = 1 MEANS ALL OF TIMES IN RECORD ARE BEFORE THE START OF
```

REPRODUCIBILITY OF THE ORIGINAL PAGE IS POOR

```
C          THE CURRENT TIME INTERVAL. RETURN FOR A NEW RECORD.
      IFEMP = 1
      RETURN
  510 INSTRT = I
      MTIMFIX = LASTIM+1-INSTRT
      ILASTIM = LASTIM+1
C FIND LAST SEQUENCE TIME IN TIME INTERVAL.
      DO 600 I=1,MTIMFIX
      IF(ITIM(ILASTIM-I).LE.IEND)GO TO 610
  600 CONTINUE
C NOTE - NCODE = 3 MEANS THAT ALL SEQUENCE TIMES ARE BEYOND THE END TIME
C          OF THE CURRENT TIME INTERVAL. THEREFORE, THE END HAS BEEN
C          REACHED AND THERE IS NO NEW DATA FOR PROCESSING.
      NCODE = 3
      RETURN
  610 INEND = ILASTIM-I
      IF(INEND.LT.LASTIM.OR.ITIM(INEND).EQ.IEND)620,630
C NOTE - NCODE = 2 MEANS THAT THE END OF THE TIME INTERVAL HAS BEEN
C          DETECTED, BUT THERE IS SOME NEW DATA FOR PROCESSING.
  620 NCODE = 2
      RETURN
C NOTE - NCODE = 1 MEANS THERE IS NEW DATA FOR PROCESSING AND THE END
C          OF THE TIME INTERVAL HAS NOT BEEN DETECTED.
  630 NCODE = 1
      LSEQSAV = NEWDAT(1,INEND)
      RETURN
      END
```

REPRODUCIBILITY OF THE ORIGINAL PAGE IS POOR

CARD COUNT 889

APPENDIX B

THE UPSTREAM ESCAPE OF ENERGIZED SOLAR WIND PROTONS FROM THE BOW SHOCK

THE UPSTREAM ESCAPE OF ENERGIZED SOLAR WIND PROTONS FROM THE BOW SHOCK

by

Eugene W. Greenstadt

Space Sciences Department
TRW Systems Group
Redondo Beach, California 90278

ABSTRACT

Protons of energies up to 100 Kev have been consistently observed traveling upwind from the bow shock in the solar wind. The conditions determined by the geometry of escape are defined and the resulting restrictions on pitch angles and total energies are computed. It is found that backstreaming protons of observed total energies are compatible with typical angles of the upstream-wave region boundary but that geometrical conditions alone do not select the boundary angle. It is also found that the high energies of 30-100 Kev, the 100 Kev cutoff, and the pitch angles of 60°-90° reported recently by Lin, Meng, and Anderson are compatible with the conditions imposed by escape geometry.

INTRODUCTION

A constellation of field and particle precursors has been identified upstream from the earth's bow shock. Backstreaming 2-7 keV protons (Asbridge et al., 1968; Scarf et al., 1970) and electrons (Anderson, 1969; Feldman et al., 1973) have been identified directly, and an association between backstreaming protons and electric and hydromagnetic precursor waves has been found emperically (Scarf et al., 1971; Fredricks et al., 1972) and explored theoretically (Fredricks et al., 1971; Barnes, 1970; Fredricks, 1974). In addition, the coincident occurrence of hydromagnetic precursors, "pulsation," or relation, shock structure, and quasi-parallel field orientation has been documented (Greenstadt et al., 1970a; Greenstadt, 1972b), and it has been concluded that the longest-period hydromagnetic precursors could not have propagated upstream from the shock, but must have been generated upstream by some other agency and swept downstream with the solar wind (Greenstadt et al., 1970b; Fairfield, 1969). Finally, it has been shown that protons reflected from the bow shock should be accelerated by the interplanetary electric field, seen in the shock frame, to energies comparable to those observed by plasma experiments (Sonnerup, 1969). These energies correspond to particles traveling along $\underset{\sim}{B}$ at velocities comparable to the rate at which locally-excited hydromagnetic precursor waves appear to progress upstream (Greenstadt et al., 1970b).

Despite the seemingly tight logic by which the foregoing results might be taken to imply that quasi-parallel geometry, reflected particles, hydromagnetic precursors, and relaxation shocks are all aspects of the same phenomenon, the circle has never been closed experimentally: for example, no report has been

published showing protons of the proper velocity component along $\underset{\sim}{B}$ being observed simultaneously with precursor waves progressing upstream at the same rate in the appropriate magnetic geometry. Even statistical data on the energies of reflected ions or the rates of precursor progression as functions of location of the point of origin on the bow shock are unreported. Recently, some difficulty in connecting upstream waves with particles has developed out of the systematic observation of backstreaming protons with parallel velocity components and total energies much too high to be associated with the usual long-period upstream waves (Lin et al., 1974). Thus, there is need for a fresh effort to examine the relationship between reverse flowing protons, upstream waves, shock structure, and reflected-particle energization.

This report sets forth an initial attack on a fairly straightforward part of the problem: To what extent does the geometry of individual particle motion alone select among reflected particles those that can escape upstream and those that cannot?

In the following paragraphs, the geometry of escape is described and some simple numerical examples are worked out for a few special cases. It is found that finite pitch angles are compatible with, and, indeed, necessary to produce experimentally-observed particle energies for protons moving along $\underset{\sim}{B}$ at typical wave generation advance rates or, equivalently, for protons appearing upstream on field lines making specified maximal angles with the local shock normal. It is found that geometrical restrictions do not select particles with any particular parallel speed and thus do not explain the observed upstream wave cutoff at field-normal angles of about 50° and, consequently, do not single out any particular group of particles responsible for upstream wave generation.

Somewhat surprisingly, protons with rather high energies and pitch angles can escape the shock at only marginally quasi-parallel field orientations (i.e., $\theta_{nB} \approx 50°$), if they have quite moderate speeds parallel to $\underset{\sim}{B}$.

Frequent reference is made in the text, for purposes of example, to the "Vela-Explorer case." By this is meant the only instance in which the upstream wave progression rate has been measured at a specific location on the shock (Greenstadt et al., 1970b).

THE GEOMETRY OF ESCAPE

Assumptions, Conventions, and Definitions

For simplicity, we place ourselves exclusively in the ecliptic plane so that we have an observation point on the ecliptic outside the shock. Solar wind velocity and field vectors $\underset{\sim}{V}_{SW}$ and $\underset{\sim}{B}_{SW}$ are assumed in the ecliptic, and we deal with the shock locally only as a plane whose unit normal lies in the ecliptic. It is convenient to work with dimensionless ratios and at the same time not unreasonable to suppose that reflected particle velocities are proportional to the solar wind velocity, so we dimension all velocities and energies by reference to V_{SW}, and adopt the convention that the projection $u_{\parallel}$ of a reflected particle's velocity on $\underset{\sim}{B}_{SW}$ is a product of some scalar p and V_{SW}, i.e., $u_{\parallel} = pV_{SW}$. Thermal velocities can also be written as a fraction of V_{SW}, should they need to be taken into account. If the particle also has a velocity $u_{\perp}$ perpendicular to $\underset{\sim}{B}_{SW}$, we shall set $u_{\perp} \equiv PV_{SW}$ and note that $u_{\parallel}$ is the guiding center velocity in the plasma frame and the particle has pitch angle $\alpha = \arctan \frac{u_{\perp}}{u_{\parallel}} = \arctan P/p$, also in the plasma (solar wind) frame.

The left side of Figure 1 defines a set of quantities to be used in this report. The curve represents the ecliptic intersection of the bow shock; $\underset{\sim}{n}$

is the local normal at a point located at angle θ_{XR} from the sun-earth line (X-axis). The shock is taken to be symmetric about the X axis and is given by $Y^2 = .331\left[(X-75.25)^2 - 3686\right]$. This is a symmetrized version of Fairfield's (1971) average shock used in an earlier paper (Greenstadt, 1972a). The right panel of Figure 1 is a plot of θ_{Xn} vs θ_{XR} for the dawn side of the given symmetric shock. It will be useful to refer to Figure 1 in reading the following analysis.

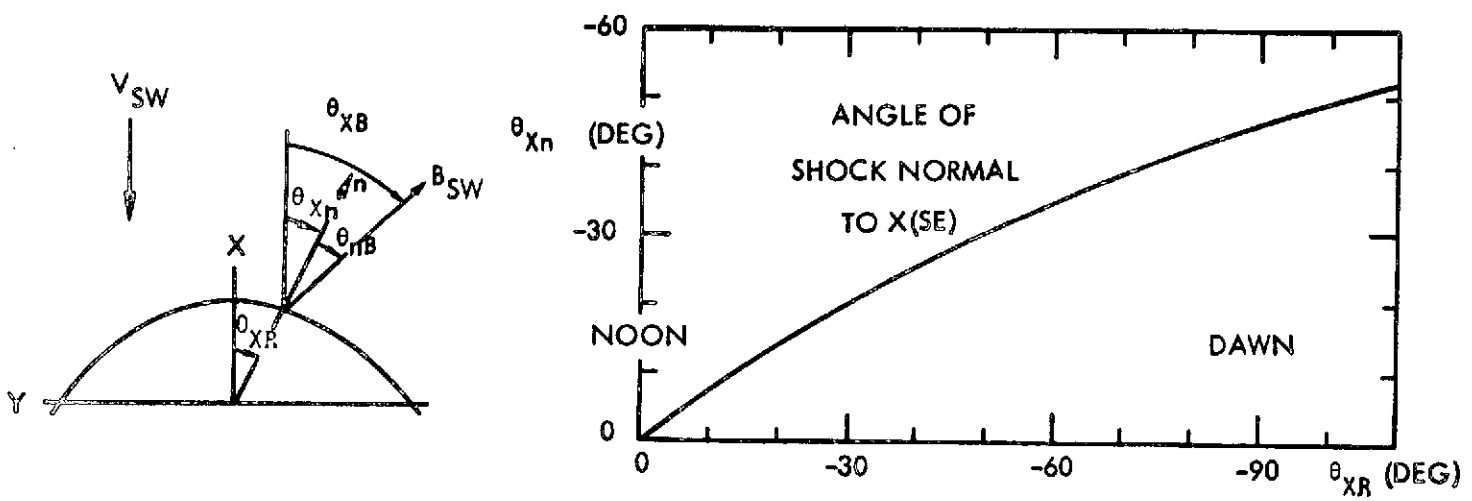

Figure 1

Negligible Pitch Angle

If a reflected proton travels in the ecliptic exactly along $\underset{\sim}{B}_{SW}$, then P = 0 and its velocity $\underset{\sim}{V}_r$ as measured by a satellite sensor in the bow shock's frame is $\underset{\sim}{V}_r = pV_{SW}\hat{\underset{\sim}{B}}_{SW} + \underset{\sim}{V}_{SW} = pV_{SW}(\cos\theta_{XB}, -\sin\theta_{XB}, 0) + V_{SW}(-1,0,0) = V_{SW}(p\cos\theta_{XB} - 1, -p\sin\theta_{XB}, 0)$. Its energy ratio is $E_r/E_{SW} = p^2 + 1 - 2p\cdot\cos\theta_{XB}$. The numerical result for the Vela-Explorer case (Greenstadt et al., 1970b) is instructive: There, at the time the upstream wave advance rate was

measured, $\theta_{XB} = 58°.5$. Figure 2 shows E_r/E_{SW} as a function of p for this angle. The value p = 1.6 found there would correspond to $E_r/E_{SW} = 1.8$ if reflected particles were responsible for the appearance of the waves. This is appreciably lower than energy ratios of backstreaming protons measured by Vela (Asbridge et al., 1968) or furnished by equation (5) of Sonnerup (1969), which gives $E_r/E_{SW} = 3.25$ when evaluated at $\psi = 58°.5$, $\phi = 21°.5$, $\delta = 1/2$, $\mu = \gamma = 0$. In the notation of this report, $\psi = \theta_{XB}$, $\phi = \theta_{Xn}$, $\psi - \phi = \theta_{nB}$.

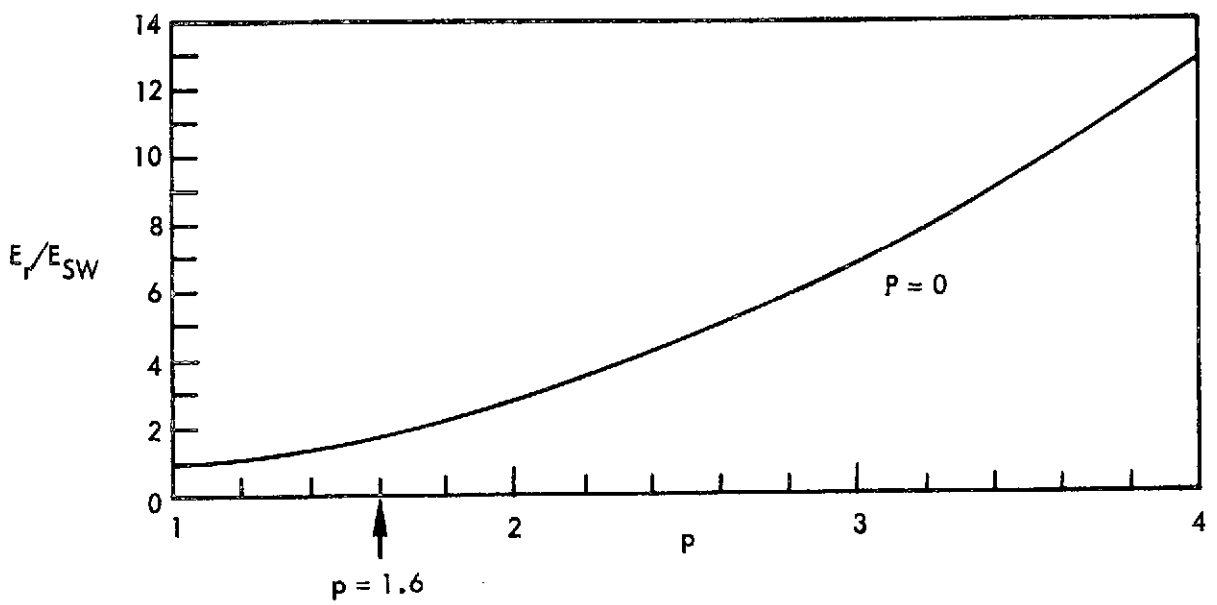

Figure 2

These comparisons suggest that P = 0 is a poor approximation to use. The relative positions of shock and satellite in the dual satellite case and the cases reported by Asbridge et al. are unknown, however, so direct comparison is impossible. Nevertheless, a simple geometric generalization confirms the indication that $P \neq 0$ if upstream waves and protons are tightly bound to each other. Figure 3 displays E_r/E_{SW} for P = 0 at various positions

along the ecliptic profile of the shock in the western hemisphere, at what, judging by statistics of upstream wave and pulsation shock geometry, should be an improbably high cutoff angle, $\theta_{nB} = 60°$. Position on the shock is designated by θ_{XR} (see Figure 1). A high cutoff angle tilts the field toward the antisolar direction, raising the total energy sensed by a sun-oriented detector for particles traveling along $\underset{\sim}{B}_{SW}$. We see in Figure 3 that not until near the dawn meridian ($\theta_{XR} = -60°$), and only with $p \gtrsim 1.9$, does E_r/E_{SW} equal 5 for $\theta_{nB} = 60°$. The morning measurements reported by Vela were taken at about this position and found $E_r/E_{SW} \approx 5$, which would be compatible with such a combination, i.e., $\theta_{XR} \approx -60°$, $\theta_{nB} = 60°$, $p = 1.9$, $P = 0$, but would be too high for any $p < 1.9$, or $\theta_{nB} < 60°$. If we assume morning-afternoon symmetry when backstreaming protons are detected in the afternoon quadrant, then one of the Vela cases, at $\theta_{XR} = 53°$, gave a value $E_r/E_{SW} \approx 6.5$ much too high for $\theta_{nB} < 60°$ or $p \lesssim 2.3$. The limited statistic on p, which has been fairly effective at correlating quasiparallel structure when $p = 1.6$, and the more extensive statistic on upstream wave cutoff, which usually occurs at $40° \lesssim \theta_{nB} \lesssim 50°$, suggest that the observed reflected proton energies were above those allowed by the calculation of Figure 3, and cannot have been produced by particles traveling parallel to $\underset{\sim}{B}_{SW}$ only. It would follow that $P \neq 0$. This suggestion is virtually certified by the recent work of Lin et al. (1974) describing backstreaming protons with high pitch angles and E_r/E_{SW} up to 100 Kev forward of the bow shock at $\theta_{nB} \approx 45°$. We shall return to this observation later.

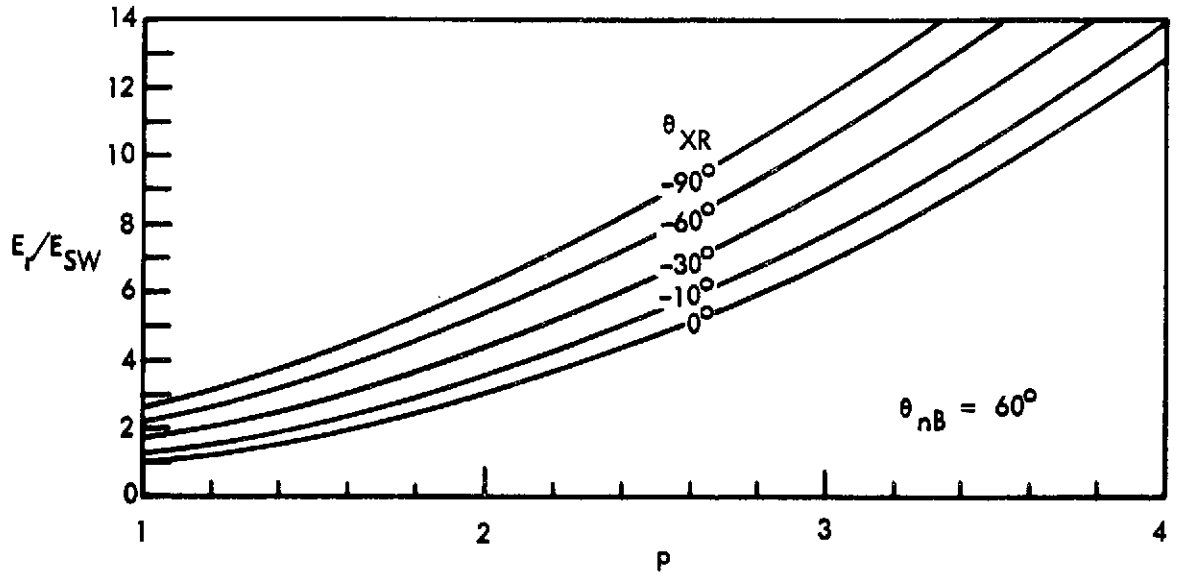

Figure 3

So far, we have simply rummaged in the available data for some empirical support for what must anyway be an intuitively incontroversial notion: reflected particles are unlikely to leave the shock exclusively at zero pitch angle in the plasma frame. The general case, $P \neq 0$, can be developed, however, by building on the geometric foundation already set forth.

Finite Pitch Angle

New terms used in the following paragraphs are defined in Figure 4. The ecliptic plane contains $\underset{\sim}{X}$, $\underset{\sim}{Y}$, $\underset{\sim}{B}$, $\underset{\sim}{B}_\perp$, and $\underset{\sim}{n}$, and $\underset{\sim}{Z}$ is the usual ecliptic pole. The solar wind impacts the shock at velocity $\underset{\sim}{V}_{SW}$ along $-\underset{\sim}{X}$. The insert shows the common $XYBB_\perp n$ plane looking down in the direction of negative $\underset{\sim}{Z}$. We are interested in a proton whose trajectory, given by the vector $\underset{\sim}{S}$ from the origin, follows a spiral along $\underset{\sim}{B}$ away from the shock, as depicted. Its guiding center has speed $u_\parallel = pV_{SW}$, and its Larmor radius is $a_c = u_\perp/\omega_c = PV_{SW}/\omega_c$. We shall enhance the clarity of the ensuing discussion by treating

the unshocked plasma as if at rest at zero temperature, so the shock, moving upward along $\underset{\sim}{n}$ at speed $V_{SW} \cos \theta_{Xn}$, encounters protons at rest, some of which are picked up by the shock, accelerated, and emitted, like our test particle, at phase ϕ and time $t = 0$. These protons spiral up $\underset{\sim}{B}_{SW}$ with the shock in pursuit. Phase angle ϕ is defined as 0 when $\underset{\sim}{u}_{\perp}$ is parallel to $\hat{\underset{\sim}{B}}_{\perp}$, i.e., when the reflected proton escapes the shock at $\underset{\sim}{S}(X,Y,Z) = (0,0,a_c)$.

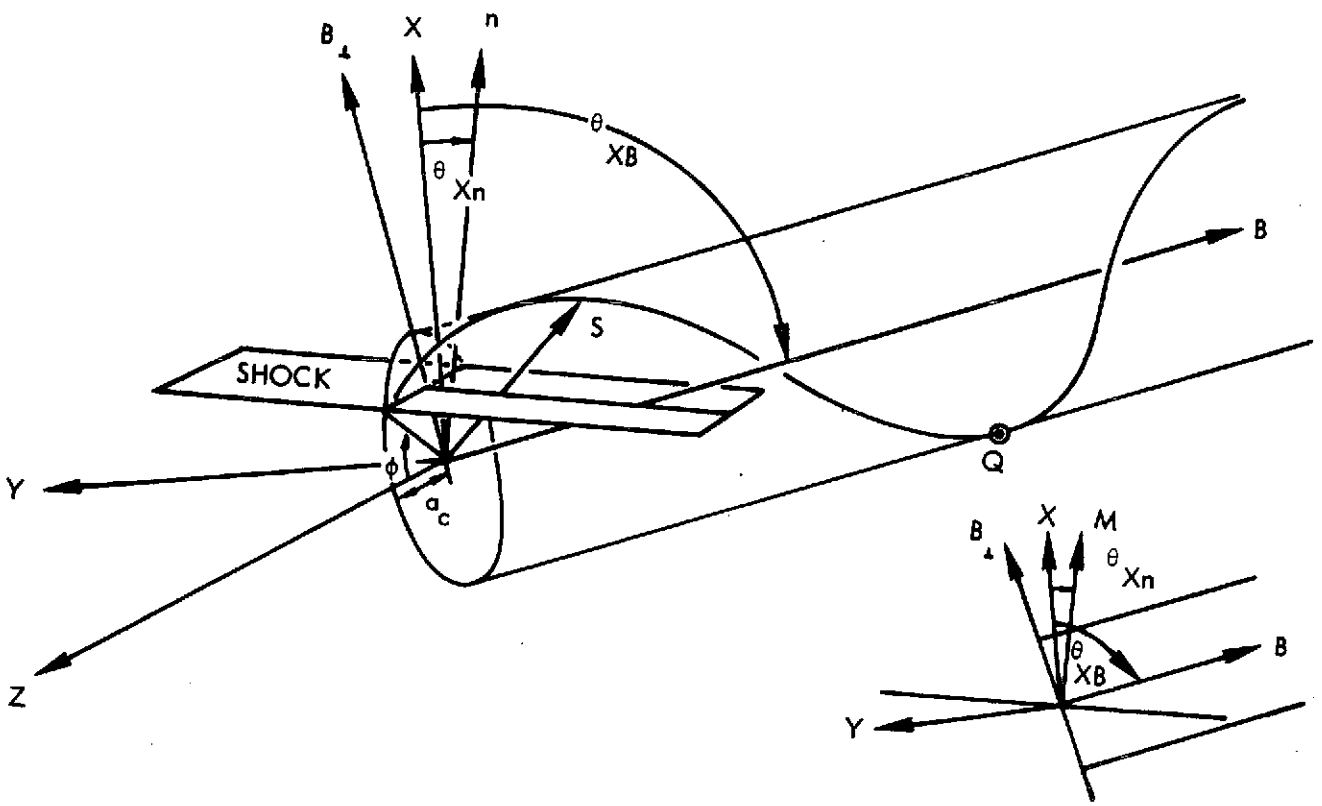

Figure 4

We are interested in those protons that are not overtaken by the shock after they begin their corkscrew journey away from it. These are the particles that will be detected far upstream and with which we continue to

assume that upstream waves are associated. The condition for "free escape" is $\underset{\sim}{S}\cdot\underset{\sim}{n} > V_{SW}t \cos \theta_{Xn}$ for all $t > 0$. Note that a proton is most vulnerable to recapture when it circles around to the "bottom" of its spiral the first time ($\phi + \omega_c t \simeq 2\pi$), shown as point Q in Figure 4. It should be intuitive that only some ratios P/p will permit free escape. It is less obvious that phase ϕ at $t = 0$ strongly influences the acceptable range of P/p. If $S_n \equiv \underset{\sim}{S}\cdot\underset{\sim}{n}$, the condition previously stated can be written $S_n(t) - S_n(0) > V_{SW}t \cos \theta_{Xn}$, which, when expanded, yields the inequality:

$$P \sin \theta_{nB} \frac{\sin (\omega_c t+\phi) - \sin \phi}{\omega_c t} + (p \cos \theta_{nB} - \cos \theta_{Xn}) > 0 \ . \qquad (1)$$

Combinations of p, P, and ϕ which satisfy this relation for all t define the free escape particles. Actually, the above expression places a maximum limit on $P/p > 0$ for each value of t, but since the inequality must be satisfied for all t, there is a least such maximum limit for any given ϕ.

NUMERICAL EXAMPLES

The Observed Case p = 1.6

To make the foregoing result more concrete, we turn again to the Vela-Explorer dual satellite example where $\theta_{nB} = 37°$, $\theta_{Xn} = 21°.5$, $\theta_{XB} = 58°.5$, and $p = 1.6$. Figure 5 shows a vector velocity diagram on a polar plot of P vs ϕ for these parameters. The length of each arrow indicates the greatest relative velocity $P = u_{\perp}/V_{SW}$ a proton may have to escape the shock if it emerges at $t = 0$ at the phase position represented by the tail end of the arrow. In the figure, we are looking backward along $\underset{\sim}{B}_{SW}$ at the projection of the proton's Larmor circle on a plane perpendicular to $\underset{\sim}{B}_{SW}$; arrows are placed at 30° phase increments.

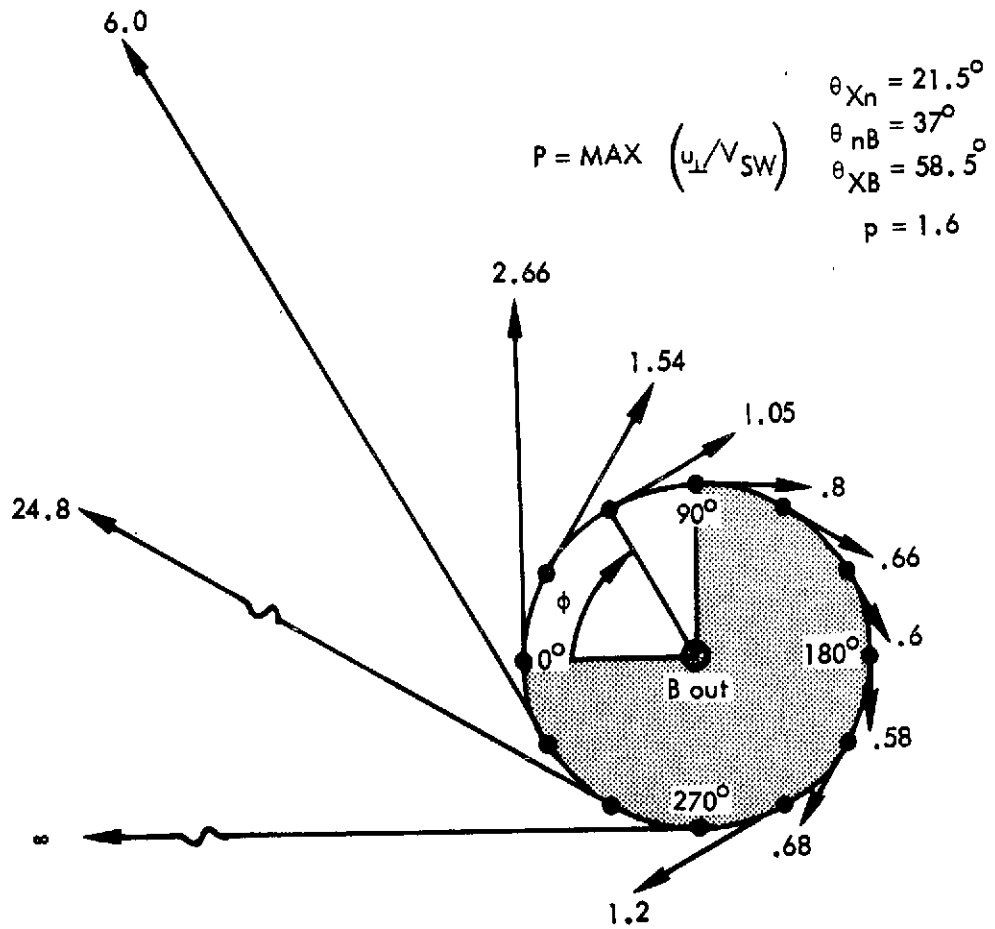

Figure 5

The computation summarized in Figure 5 allows a wide range of possible maximum P for arbitrary ϕ. The outcome can be narrowed significantly, however, by reasoning that a stationary proton, initially captured, according to assumption, by the shock at relative normal speed $V_{SW} \cos \theta_{Xn}$, will enter the shock layer at $\phi = 180°$ and emerge after one-half to one cyclotron orbit at $0° \lesssim \phi \lesssim 90°$. Subject to this argument, P would take on values up to about 2.7.

The energy ratio of a reflected proton of finite pitch angle measured by a directionally-sensitive detector, and its direction of arrival, will depend on the phase ϕ_D of the spiralling particle at its instant of detection and on the angle θ_{XB} the interplanetary field makes with the solar wind flow (along X):

$$E_r/E_{SW} = p^2 + P^2 + 1 - 2\ (p \cos \theta_{XB} + P \cos \phi_D \sin \theta_{XB}).$$

If ϕ_D is 0 when the proton is at the sunward extreme of its Larmor spiral, the highest value of E_r/E_{SW} is achieved when $\phi_D = \pi$, and the lowest when $\phi_D = 0$. Figure 6 shows the behavior of the maximum and minimum of E_r/E_{SW} vs p for $\phi_D = \pi$ and 0, respectively, when P takes on its maximum values of 2.66 and .8 at $\phi = 0°$ and 90°. The P = 0 result of Figure 2 is repeated as the dashed curve, for comparison. Obviously, introduction of the limiting P value for reflected protons raises appreciably the possible measured energy of escaping particles over that permitted when P = 0. In fact, at p = 1.6 there is no difficulty in providing backstreaming protons of energy 6 kev or more (such as those recorded by Vela) for $\phi_D = \pi$, $\phi = 0°$. One may interpolate visually to appreciate that the same is true for a range of $\phi_D < \pi$, $\phi > 0°$ as well.

The Subsolar Point

Another specialized case of considerably more general interest is illustrated in Figure 7. Here, the curves represent the maximal detectable energy ratio E_r/E_{SW} (at $\phi_D = \pi$) of protons reflected from the subsolar point of the shock ($\theta_{XR} = \theta_{Xn} = 0$) and traveling along $\underset{\sim}{B}_{SW}$ at the forward edge of the upstream particle (= wave?) region. Exit phases $\phi = 0$ and 90°, with three possible cutoff angles θ_{nB} for each phase, are shown. To clarify the interpretation of Figure 7 by specific example, suppose a satellite-borne proton detector is located in the ecliptic upstream from the bow shock, westward and

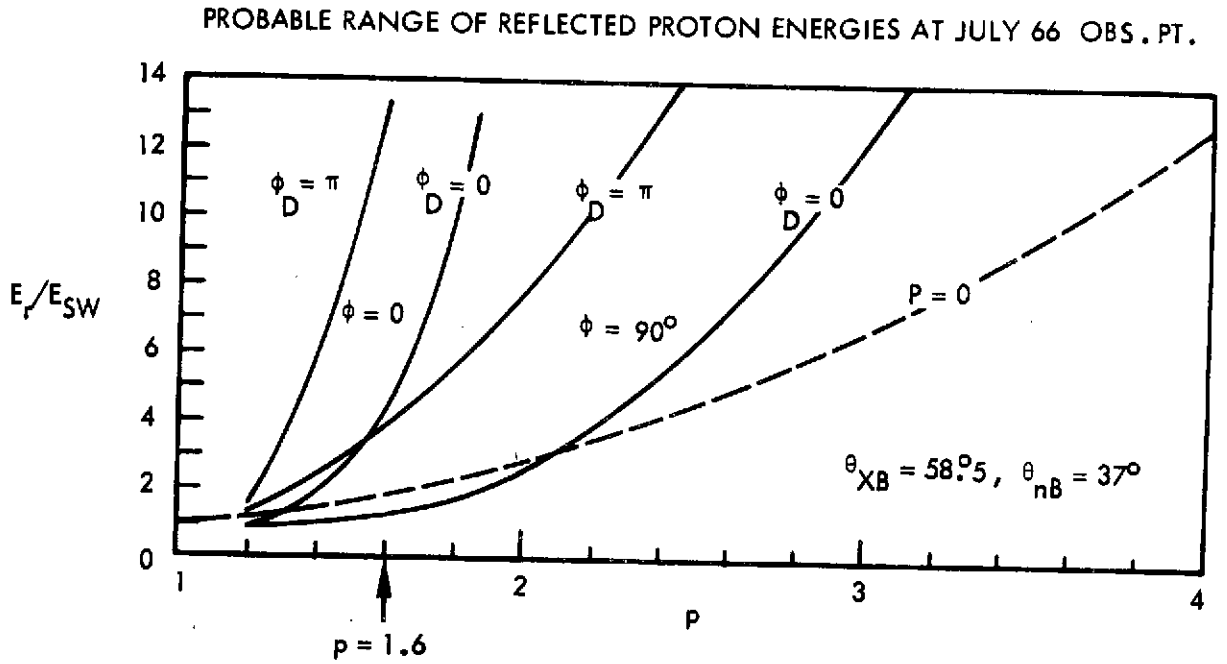

Figure 6

forward of the subsolar point, and the interplanetary field, which has been perpendicular to the solar wind flow thereby cutting off all reflected particles, rotates suddenly to a stream angle of 50°, connecting the satellite to the subsolar point. Then reflected protons barely emerging from the shock at $\phi = 90°$ with $u_{||}/V_{SW} = p = 1.6$, after completing three-quarters of a cyclotron rotation in the shock layer, will be permitted to arrive at the satellite with total energies up to $E_r = 1.6\ E_{SW}$. Alternatively, imagine the satellite moving antisunward in the same upstream region and first encountering the edge of the precursor zone when $\theta_{nB} = 50°$; at that point protons will be detected with $u_{||} = 1.6\ V_{SW}$ and $E_r/E_{SW} \leq 1.6$. It is an assumption that an accompanying magnetometer would first detect upstream waves at the same time.

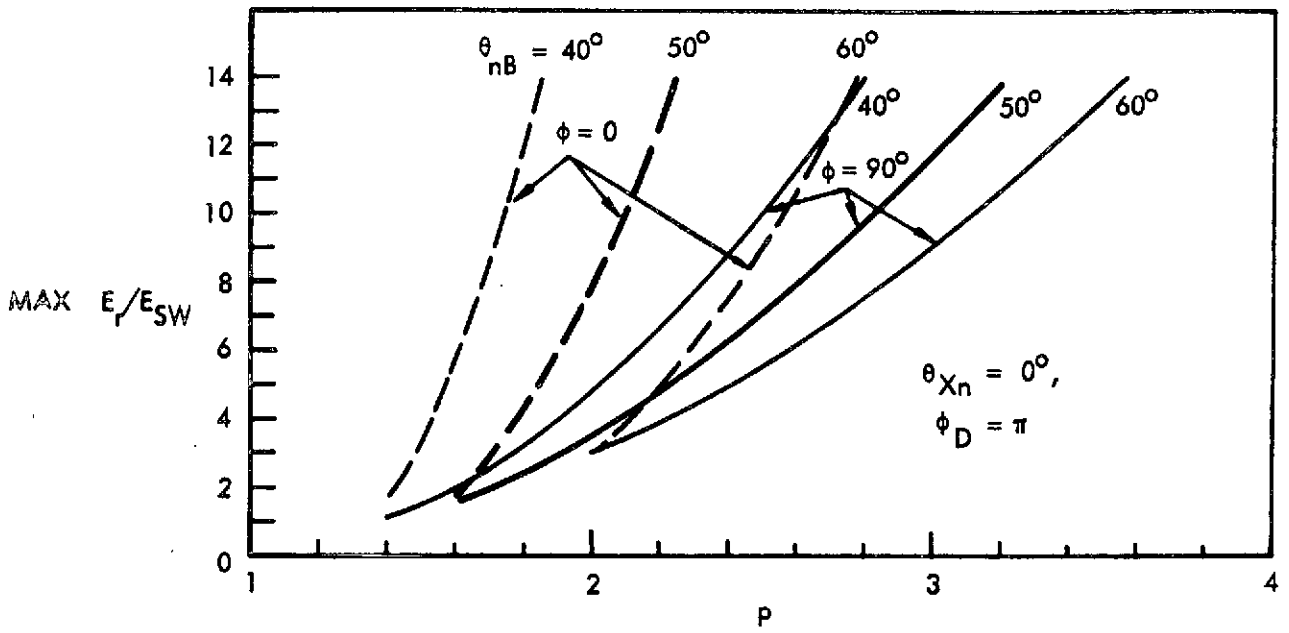

Figure 7

High Energy (30-70 KeV) Protons

Another example provides some interesting numbers. We refer to the insert at the upper left of Figure 8. Imagine a proton detector in the ecliptic upstream on the morning side of the shock at the forward edge of the precursor region (circled point), and suppose that the field angle θ_{nB} corresponding to that boundary of the forward region is 40° to 50° at the subsolar point (where the shock normal is parallel to the X axis). Then, for escape angles ϕ = 0° and 90° at the subsolar point, our formulas for P and E_r/E_{SW} give the maximal energy ratios vs p shown in the curves in the main part of Figure 8. The figure states, for example, that a proton can leave the subsolar shock at ϕ = 0°, travel along $\underset{\sim}{B}_{SW}$ at 40° to the normal, with parallel component (guiding center velocity) $u_{||} = 3\ V_{SW}$, and escape upstream with energy as high as E_r = 100 E_{SW}. A bulk velocity of the solar wind corresponding to 1 Kev would imply

E_r = 100 Kev. Such an example would provide the high energy particles found by Lin et al. (1974) without invoking any acceleration enroute. The shaded region of Figure 8 denotes the width of the 30 to 100 Kev energy channel of the Lin et al. experiment, for a 1 Kev solar wind. We see that, for p = 5, which was at the extreme of the distribution Lin et al. found, even a proton barely escaping at $\phi = 90°$ with the field at 50° to the normal could have total energy high enough to be recorded in their 30-100 Kev channel. The shapes and ranges of the curves suggest that a preference for escape angle of intermediate $\phi \approx 45°$ could easily explain both the consistency with which the 30-100 Kev channel was occupied for moderate p and the apparent absence of protons above 100 Kev even at high p.

PROBABLE MAXIMUM ENERGIES OF REFLECTED PROTONS FROM SUBSOLAR POINT

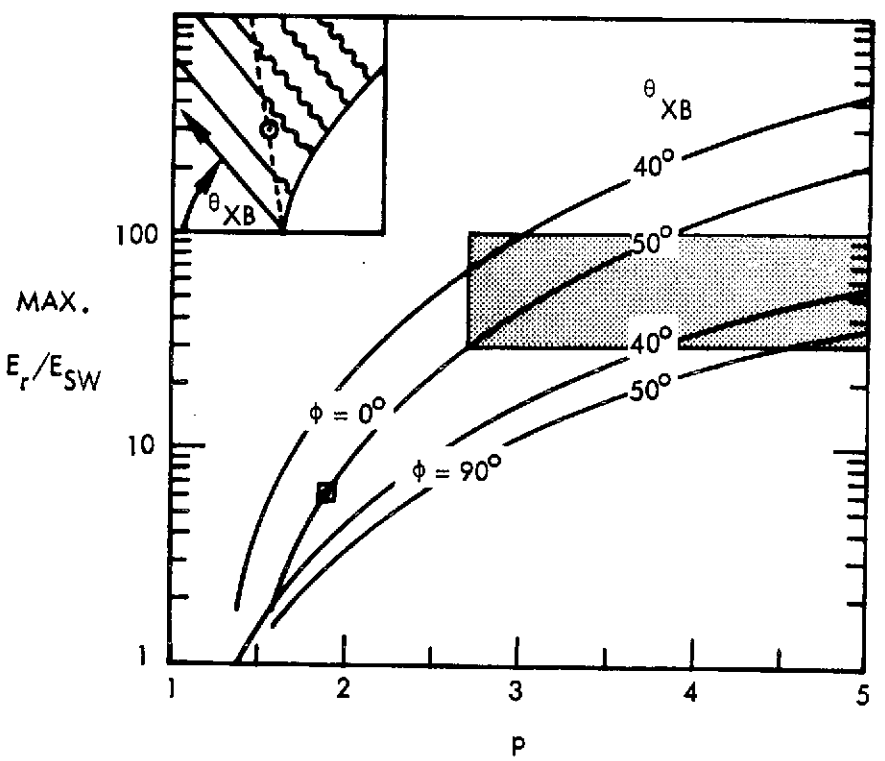

Figure 8

DISCUSSION

The geometry of escape and the numerical examples described above demonstrate that protons can leave the bow shock and travel upstream with almost arbitrary energy, given only the appropriate p, θ_{Xn}, θ_{nB}, and ϕ, and can satisfy observation with very reasonable selection of values for these parameters. However, we do not know the correct values of p or θ_{nB}, even at the subsolar point, or, in any event, do not know that we know, nor do we know the acceleration mechanism.

The foregoing calculations regarding high energy protons cannot therefore be used as evidence that such particles are produced at the bow shock, but only that, if produced, they can escape upstream with the characteristics already observed. The maximal energy ratio yielded at the subsolar point by Sonnerup's (1969) formula for protons energized by the interplanetary electric field is approximately 6.7 at $\theta_{nB} = 50°$ (setting his $\delta = 1/2$, $\mu = \gamma = 0$). In Figure 8, this would correspond, for $\phi = 90°$, to p = 1.9 (square point) and, incidentally, to $P \approx 1.9$. Clearly, if the interplanetary electric field is all there is to work with and p is about as small at the subsolar point as it is on the midmorning flank, where $p \approx 1.6$, the protons of Lin et al. cannot be explained without invoking some upstream energization process, as those authors do.

But consider the following: the entire preceding exposition has treated only cold particles encountering the shock at relative speed V_{SW} and leaving it with combinations of p, P, θ_{nB}, ϕ , etc. rendering them capable of perfect escape. But what of those that don't satisfy the inequality (1)? Are they all retained or recaptured by the shock? What happens, for instance, to a proton that emerges, say, at $\phi = 60°$ with P = 2 when p = 1.6 (see Figure 5)?

It seems reasonable that some particles will encounter the shock two or more times, accelerating each time and compounding their total energy until it reaches a high level. A proton of 30 Kev has observed velocity of only about 5.5 V_{SW} for a 1 Kev solar wind. This does not seem impossible to achieve by multiple reflection when a double reflection may multiply the original relative velocity by, say a factor of 2.56 (= 1.6^2), especially remembering the character of quasi-parallel shocks with their large amplitude pulsations and irregular boundaries. The question of whether energization by multiple reflection in quasi-parallel turbulent waves should be designated as a shock process or an upstream process may thus be only semantic. It is this author's provisional belief that most if not all of the acceleration responsible for the high energies detected by Lin et al. occurs close to the nominal shock although some may be technically "upstream." The only apparent difficulty is providing the proper ratio of $P/p \approx \sqrt{5.5} = 2.3$ for such reflected protons.

The provision of adequate P/p by the physics of shock reflection, the introduction of finite temperature, and the representation of three-dimensional reflection in the curved bow shock are left for future analysis.

CONCLUSION

The first-order calculations described in this report support three conclusions:

1. The geometry of escape does not by itself select from all possible backstreaming protons a particular group that would necessarily leave the shock at $\theta_{nB} \approx 50°$, i.e., with $u_{||} \approx 1.6\ V_{SW}$.

2. The geometry of escape does, however, permit backstreaming protons to leave the shock at $40° \lesssim \theta_{nB} \lesssim 60°$, with $1.5 \lesssim u_{\parallel}/V_{SW} \lesssim 2$ and a wide range of total energies comparable to those observed, i.e., $2 \lesssim E_r \lesssim 10$ keV.

3. The geometry of escape permits backstreaming protons of 30-100 keV to leave the subsolar region of the shock at $\theta_{nB} = 50°$ with $2 \lesssim u_{\parallel}/V_{SW} \lesssim 5$, hence with large pitch angles.

The first two conclusions above imply that the connection between upstream particles and waves should be found in the selectivity of either the shock acceleration process itself, the growth rate of the appropriate instability in the solar wind, or the dispersion characteristics of the wavemode. We close by noting that it seems intuitive that for a given θ_{nB}, the larger the shock radius of curvature, i.e., the less convex it is locally, the more likely a particle will undergo multiple reflection before free escape upstream. Higher energies should therefore be expected for particles upstream from interplanetary shocks, and from Jupiter's bow shock than from the earth's. Such particles have been observed (Armstrong et al., 1970; Simpson et al., 1974), and the acceleration of protons to relativistic energies by multiple reflection in interplanetary shocks has been developed theoretically by Sarris and Van Allen (1974).

ACKNOWLEDGMENT

The material presented in this report was funded by the National Aeronautics and Space Administration under Contract NASW-2398.

REFERENCES

Anderson, K. A., Energetic electrons of terrestrial origin behind the bow shock and upstream in the solar wind, J. Geophys. Res., 74, 95, 1969.

Armstrong, T. P., S. M. Krimigis, and K. W. Behannon, Proton fluxes at 300 keV associated with propagating interplanetary shock waves, J. Geophys. Res., 75, 5980, 1970.

Asbridge, J. R., S. J. Bame, and I. B. Strong, Outward flow of protons from the earth's bow shock, J. Geophys. Res., 73, 5777, 1968.

Barnes, A., Theory of generation of bow-shock-associated hydromagnetic waves in the upstream interplanetary medium, Cosmic Electrodyn., 1, 90, 1970.

Fairfield, D. H., Bow shock associated waves observed in the far upstream interplanetary medium, J. Geophys. Res., 74, 3541, 1969.

Feldman, W. C., J. R. Asbridge, S. J. Bame, and M. D. Montgomery, Solar wind heat transport in the vicinity of the earth's bow shock, J. Geophys. Res., 78, 3697, 1973.

Fredricks, R. W., F. L. Scarf, and L. A. Frank, Nonthermal electrons and high-frequency waves in the upstream solar wind, 2. Analysis and interpretation, J. Geophys. Res., 76, 6691, 1971.

Fredricks, R. W., F. L. Scarf, and I. M. Green, Distributions of electron plasma oscillations upstream from the earth's bow shock, J. Geophys. Res., 77, 1300, 1972.

Greenstadt, E. W., Binary index for assessing local bow shock obliquity, J. Geophys. Res., 77, 5467, 1972a.

Greenstadt, E. W., Observation of nonuniform structure of the earth's bow shock correlated with interplanetary field orientation, J. Geophys. Res., 77, 1729, 1972b.

Greenstadt, E. W., I. M. Green, G. T. Inouye, D. S. Colburn, J. H. Binsack, and E. F. Lyon, Dual satellite observation of the earth's bow shock, 1. The thick pulsation shock, Cosmic Electrodyn., 1, 160, 1970a.

Greenstadt, E. W., I. M. Green, G. T. Inouye, D. S. Colburn, J. H. Binsack, and E. F. Lyon, Dual satellite observation of the earth's bow shock, 2. Field-aligned upstream waves, Cosmic Electrodyn., 1, 279, 1970b.

Lin, R. P., C.-I. Meng, and K. A. Anderson, 30- to 100-keV protons upstream from the earth's bow shock, J. Geophys. Res., 79, 489, 1974.

Sarris, E. T., and J. A. Van Allen, Effects of interplanetary shock waves on energetic charged particles, Univ. of Iowa Report 74-4, January 1974.

Scarf, F. L., R. W. Fredricks, L. A. Frank, C. T. Russell, P. J. Coleman, Jr., and M. Neugebauer, Direct correlations of large amplitude waves with suprathermal protons in the upstream solar wind, J. Geophys. Res., 75, 7316, 1970.

Scarf, F. L., R. W. Fredricks, L. A. Frank, and M. Neugebauer, Nonthermal electrons and high-frequency waves in the upstream solar wind, 1. Observations, J. Geophys. Res., 76, 5162, 1971.

Simpson, J. A., D. Hamilton, G. Lentz, R. B. McKibben, A. Mogro-Campero, M. Perkins, K. R. Pyle, and A. J. Tuzzolino, Protons and electrons in Jupiter's magnetic field: results from the University of Chicago experiment on Pioneer 10, Science, 183, 306, 1974.

Sonnerup, B. U. O., Acceleration of particles reflected at a shock front, J. Geophys. Res., 74, 1301, 1969.

APPENDIX C

STRUCTURE OF THE TERRESTRIAL BOW SHOCK

21333-6013-RO-00

STRUCTURE OF THE TERRESTRIAL BOW SHOCK

by

Eugene W. Greenstadt

Space Sciences Department

TRW Systems Group
Redondo Beach, California 90278

May 1974

Prepared for
publication in

Proceedings of the Asilomar Solar Wind Conference

Asilomar, California
25-29 March 1974

Space Sciences Department

TRW Systems Group
One Space Park
Redondo Beach, California 90278

STRUCTURE OF THE TERRESTRIAL BOW SHOCK

Eugene W. Greenstadt

Space Sciences Department
TRW Systems Group
One Space Park
Redondo Beach, California 90278

ABSTRACT

An extensive examination of bow shock morphology has progressed to a point where distinctions in shock structure, as sensed by a variety of diagnostics, can be correlated with M, β, and θ_{nB} in the solar wind. Shock structures are now designated quasi-perpendicular or quasi-parallel, and laminar, quasi-laminar, quasi-turbulent, or turbulent, depending on the ambient parameters set. For quasi-perpendicular geometry, electromagnetic turbulence, as detected by magnetic sensors, increases with β, independent of M. Irregularity of the shock transition layer and plasma wave noise in the layer increase with M, independent of β. For quasi-parallel geometry, the shock layer broadens and breaks up, showing strongly periodic components at the lowest frequencies, limited levels of plasma wave noise, and marked precursor effects. The parallel shock produces a hybrid average ion spectrum characteristic of neither solar wind nor magnetosheath. The shock is summarized as a complex plasma system in the solar wind.

STRUCTURE OF THE TERRESTRIAL BOW SHOCK

Eugene W. Greenstadt

Space Sciences Department
TRW Systems Group
One Space Park
Redondo Beach, California 90278

INTRODUCTION

A persistent objective among researchers concerned with the solar wind-magnetosphere interaction region has been to study the intricacies of collisionless plasma shocks. Two interrelated questions are at the heart of the issues raised by shock investigations:

1. What processes limit the steepening of the waves composing the shock by dissipating flow energy, thus preventing the superposed waves from forming a discontinuity of infinite amplitude?

2. What processes heat the streaming ions, giving them a jump in temperature across the shock?

Answers to these questions are known not to be unique but to depend on various qualities of the flowing plasma in which the shock forms. The qualities most important to determination of shock processes are apparently defined by combinations of three quantities: Alfvénic or magnetosonic mach number M_A or M_{MS}, ratio of thermal to magnetic field energy β, and angle θ_{nB} between the shock normal and the magnetic field vector in the unshocked plasma flow. The importance of these quantities is illustrated, for example, by a property dependent on M: when M is very low ($\gtrsim 1$), ion heating is negligible and question 2 hardly arises, while when M is high (≈ 5), ion heating is appreciable and indeed exceeds electron heating.

For reference, these quantities are defined here as follows: $M_A = V_1/C_{A1}$, $M_{MS} = V_1/(C_{A1}^2 + C_{S1}^2)^{1/2}$, $\beta = 8\pi N_1 k(T_{i1} + T_{e1})/B_1^2$, $\theta_{nB} = \arccos(\underset{\sim}{B}_1 \cdot \underset{\sim}{n}/|B_1|)$, where C_A and C_S are Alfvénic and sonic velocities, N denotes

density, $\underline{n}$ the shock normal, $\underline{B}$ the magnetic field, T_i and T_e the ion and electron temperatures, and subscript 1 refers to the unshocked (upstream) plasma.

Isolation of the effects associated with each of these quantities is the first step in moving toward answers to the questions posed. This has been achieved in part in the laboratory, but always within certain inherent experimental limitations, such as the presence of chamber walls. The earth's bow shock parameter separation is just now becoming a reality through the use of high resolution data sampling and simultaneous measurements by two spacecraft and by groups of related diagnostics. An extensive case by case study of the bow shock based on isolation of the various parameters is in progress by V. Formisano, C. T. Russell, F. L. Scarf, M. Neugebauer, and the present author. This report synopsizes the early results of the investigation using data principally from OGO 5 and HEOS 1. The main result is successful isolation of shock structures by parameter set and correlated diagnostic behavior. We shall first modify the existing shock structural nomenclature to suit the results of spacecraft observations and to provide the terminology needed in the remainder of the paper. We then display a few examples of shock morphology for a wide range of plasma states, as seen with various diagnostics. We summarize by describing the bow shock as a system in the solar wind, note its advantages as an object of shock investigation, and close by listing a few aims of future study.

CLASSIFICATION AND NOMENCLATURE

Existing Classifications. The classification scheme for shock structures with which most workers are familiar arises out of laboratory experience (Paul, 1971) and theoretical idealization (Tidman and Krall, 1971). There are two main divisions for magnetic shocks, by which we mean those in which the flowing plasma includes a magnetic field. These divisions are Perpendicular and Oblique, as defined in Figure 1a. The Perpendicular is actually a narrowly-

defined case in which θ_{nB} is almost exactly 90°. More precisely, the restriction on this division is that the complement of $\theta_{nB} \lesssim \arctan \sqrt{\frac{m_-}{m_+}}$ which means that $\underset{\sim}{B}$ must be within 1°.3 of tangency to the shock "surface." The latter division, Oblique, is intended to include every other θ_{nB}, with the possible exception of the parallel shock when $\theta_{nB} = 0°$. The question marks designate the range of θ_{nB} essentially unexplored.

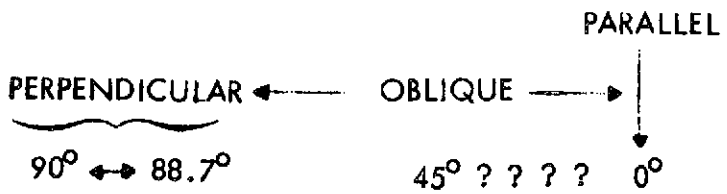

Figure 1a

Perpendicular Class. Most experimental work has dealt with perpendicular shocks, which are further subdivided into parameter ranges of β and M as shown in Figure 1b. M_c denotes a "critical" mach number which is in turn dependent on β. In low-β shocks the magnetic field dominates the internal (thermal) disorder of the plasma. At low M, resistivity and/or dispersion limit shock steepening up to M_c, and the shock has a thin ramp profile. Above M_c resistivity and/or dispersion are inadequate, and an effective viscosity is needed to provide additional dissipation. The shock then broadens, and reflected ions form a foot ahead of the main shock ramp. The resistive critical value $M_c = M_A^*$ lies roughly between 2.3 and 2.7, tending to decrease with rising β. In ultra high-β shocks, thermal disorder dominates the field, perpendicularity becomes moot, and the structural distinction between subcritical and supercritical shocks loses identity probably because of the reduction of M_c to very low values between 1.0 and 2.0 (see reference to Figure 1c below). A useful experimenter's review has been given by Paul (1969).

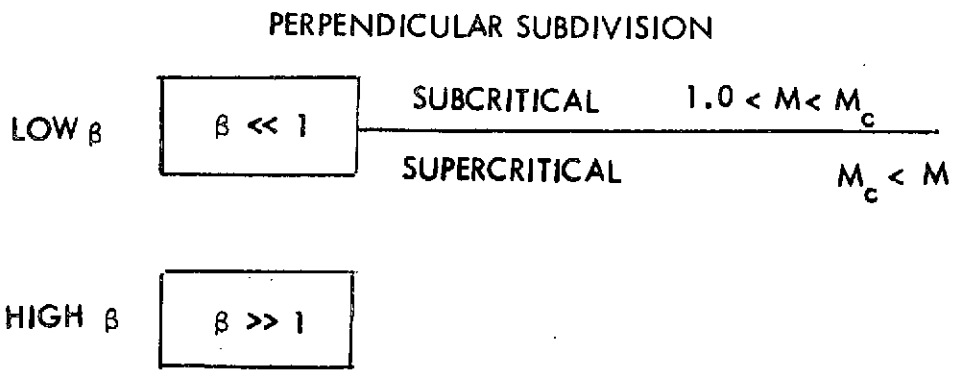

Figure 1b

Oblique Class. Experimental work with oblique shocks (Robson, 1969) has been confined almost entirely to the range $45° \lesssim \theta_{nB} \lesssim 90°$, a limitation important to the revised classification with which this paper will be concerned. In general, oblique shocks preserve the subcritical/supercritical subdivision of perpendicular shocks insofar as resistive/viscous dissipation is concerned, but add to the structure a large amplitude, damped whistler wave standing upstream from the main ramp at low M and downstream at high M while losing the supercritical "foot" of reflected ions. The ions presumably escape upstream along the field. Another feature of oblique shocks is an additional dependence of M_c on θ_{nB} as well as on β. A typical dependence has been computed from theory by Drummond and Robson (1969) and is displayed for a few parameter combinations in Figure 1c. The shaded section of the figure denotes the values of θ_{nB} incompletely studied in the laboratory. The figure shows that M_c, in this case M_A^*, diminishes with decreasing θ_{nB} and increasing β until the parameter distinction between subcritical and supercritical structure almost vanishes for parallel shocks with $\beta \gtrsim 1$, where M_A^* is close to 1.0, the minimal M for having any shock at all. In other words, at the extreme lower right of the panel virtually all structures ought to be supercritical with respect to M_A^*, with viscosity as the necessary dissipation mechanism taking over when resistivity no longer suffices. Dispersion can also limit shock steepening for $M > M_A^*$,

however, with viscosity not taking over until a higher critical value is reached. The elevation of M_c by dispersion is indicated for cold plasma (β=0) at 90° and 45° by the arrows at the left of the lower panel. The result of this elevation is to widen the "subcritical" range of M, making observation of low-M shocks easier. Wave breaking occurs at a still higher critical number.

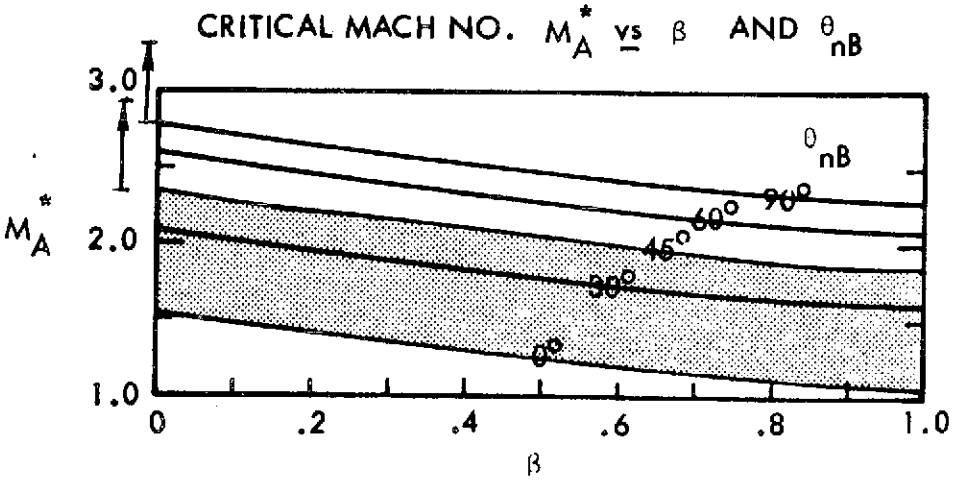

$M = M_A^*$ WHEN $V_2 = C_{S2}$

Figure 1c

The relationships depicted in Figure 1c seem to be in fair agreement with laboratory observation for $88° \gtrsim \theta_{nB} \gtrsim 45°$. Although the remaining range of θ_{nB} has been extended to about 30° at high β experimentally (Robson, 1969), it is more accessible and actually common, in the earth's bow shock.

Revised Classification. The chart of Figure 2 introduces the classification and nomenclature that will be used in this report. There are still two main divisions in this scheme. Together, they encompass the very wide range of θ_{nB} hitherto called "oblique" plus two extreme classes, perpendicular and parallel, defined as before. These last two are simply special cases observed

much less frequently in space than the others. The two principal divisions, quasi-perpendicular and quasi-parallel, memorialize the empirically-determined distinction in magnetic structure that depends on whether the upstream field in the unshocked plasma is greater or less than about 45°. Physically, the division probably separates those cases in which the upstream field prohibits or permits the shock to communicate its presence to the oncoming plasma with sufficient energy to "preoscillate" the field, "prescatter" the approaching ions and, by feedback of these effects, modify its own structure through wave amplification (McKenzie and Westphal, 1968) or other process. Note that the "quasiparallel" class covers just the range of θ_{nB} unfamiliar in the laboratory and corresponds to the "pulsation" shocks described by Greenstadt et al. (1970); its observational range of identification has been almost entirely the contribution of satellite measurements.

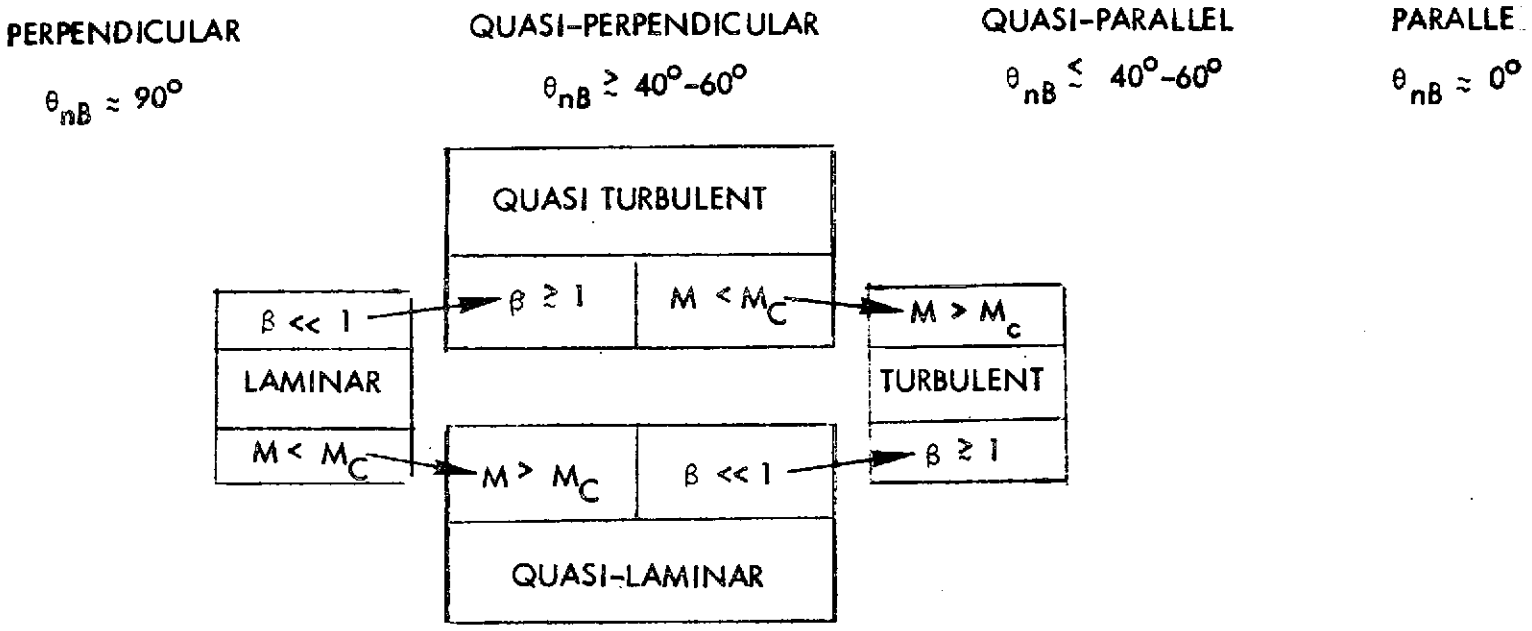

Figure 2

Each of the main classes may be subdivided according to various combinations of β and M. The subdivisions are shown in the chart under the quasi-perpendicular heading. Cold plasma at subcritical mach number is represented by the laminar designation at the left, hot plasma at supercritical mach number is represented by the turbulent designation at right. The upper and lower subclasses define two routes from simplicity to complexity of shock structure. One, called quasi-laminar, results when a cold solar wind flows supercritically; the second, called quasi-turbulent, results when a hot solar wind flows subcritically. Criticality is used here as a general term without specification of what kind. Spacecraft results so far make a distinction only of M_c less than or greater than about 3.0. The transitions in form are assumed to be smooth as far as β is concerned, there being no critical value of this quantity.

The scheme of the figure is a blend of observation and speculation, as not all designated categories have been observed in detail. It is anticipated from the M_c-β-θ_{nB} dependence of Figure 1c that the subdivisions should become increasingly indistinct or inapplicable in progressing from perpendicular to parallel geometry. Certainly they should be increasingly difficult to record as the range of subcritical M shrinks. Up to now, results have been consistent with anticipation in that the quasi-perpendicular category has provided the most complete documentation. In the sequel, it should be remembered that the chart of Figure 2 does not exhaust the ways in which shock morphology can be described. For example, the shock does communicate upstream for some angles $\theta_{nB} \gtrsim 45°$ by reflecting electrons rather than protons, creating a region of small amplitude upstream waves of frequency about 1 Hz. Also, ratios T_e/T_i or N_α/N_p may be important in differentiating certain shock structures. The possibility of overlapping classification schemes should be kept in mind.

BOW SHOCK MORPHOLOGY

Quasi-Perpendicular Structures. Figure 3 displays four multidiagnostic profiles of the quasi-perpendicular bow shock according to the scheme of Figure 2, but with specific values $M_c = 3$, $\beta = .1$ defining the subclasses at the center. These values follow the empirical divisions of Formisano and Hedgecock (1973b). We shall see that suitable plasma diagnostics follow these divisions. The left and top examples were obtained at 1.15 sec/sample, the botton and right examples at .144 sec/sample. All are from observations by OGO 5 instruments, with upstream parameters checked against HEOS measurements, and free-stream magnetosonic mach number used throughout.

The laminar shock at left is magnetically monotonic and virtually free of macroscopic and microscopic turbulence. One cycle of a very small wave, probably a standing whistler, is visible just at the foot of the ramp. The uncalibrated output of the Lockheed light ion spectrometer, below the field profile, shows the presence of thermalized protons in the sheath behind the trailing edge of the ramp. Next below, the 560 Hz channel of the TRW plasma wave detector registers electrostatic noise up to a few millivolts/meter in the ramp and just outside in the small standing wave. Below the plasma wave panel, four channels of the x-axis of the JPL/UCLA search coil, uncalibrated, show a region of magnetic noise up to about 100 Hz centered on the midramp of the shock.

When β and M are both elevated above their "laminar" values, the monotonic nature of the ramp disappears, a clear foot develops, and macroscopic turbulence is evident both ahead of and behind the principal leading gradient. All of these features are apparent at the right of Figure 3. Also, in contrast to the laminar profile, the turbulent shock at right shows numerous bursts of electromagnetic noise at frequencies up to and including 1 kHz,

with higher activity in various channels upstream and downstream. The symbol X10 indicates that the search coil data were recorded at 10 times higher sensitivity than where the symbol is absent. This noise was also present deeper in the magnetosheath. In this case, the plasma (electric) wave noise in the 560 Hz channel reaches about 50 millivolt/meter. The Lockheed spectrometer records the scattering of protons behind the outermost irreversible field gradient.

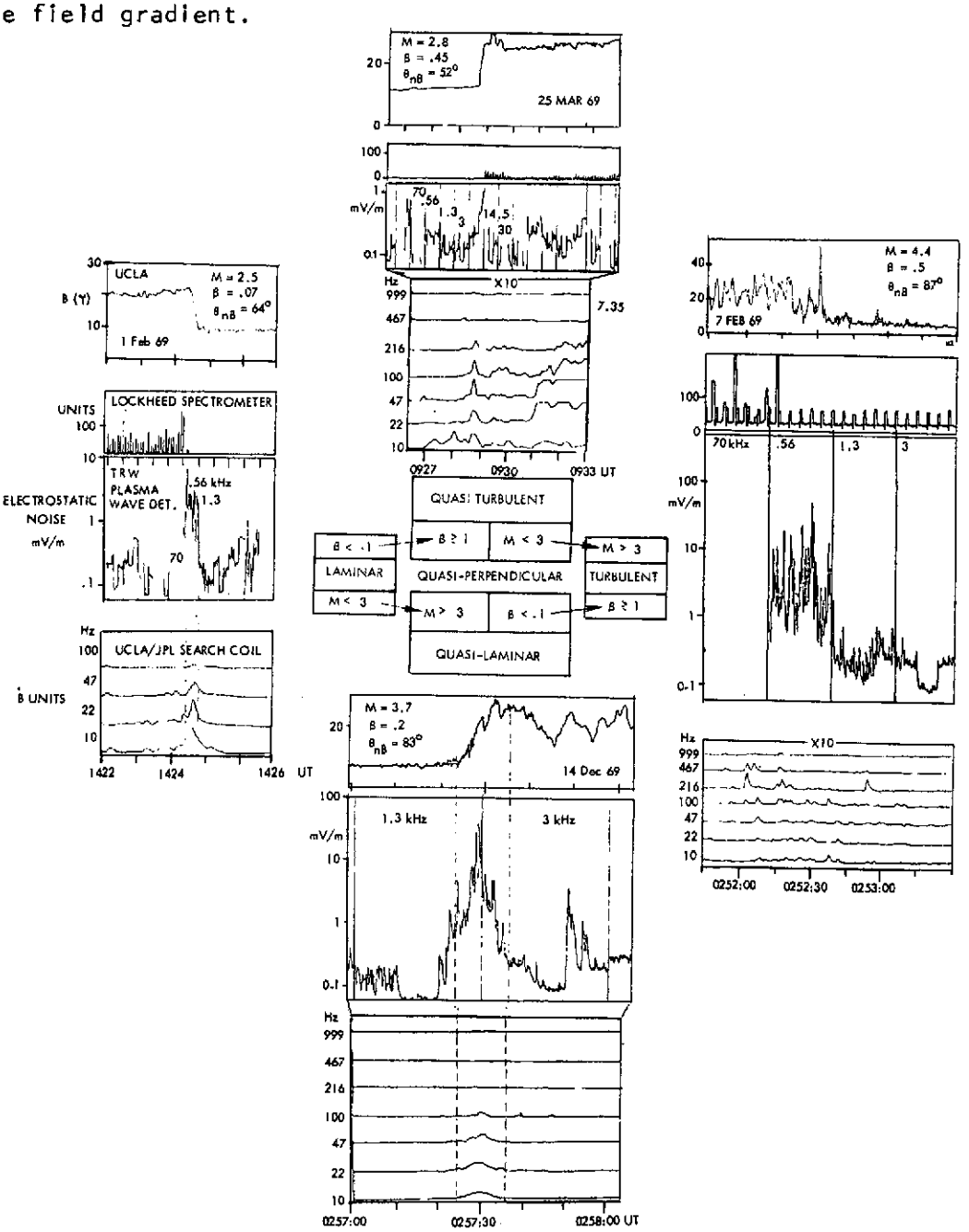

Figure 3

If β is raised, but M remains low (subcritical), the macrostructure of the shock remains largely indistinguishable from that of the laminar case. The quasi-turbulent example at top center shows a monotonic ramp and perhaps a modest increase in fluctuation level just behind the ramp. The other diagnostics applied to the quasi-turbulent case reveal a distinction from the laminar shock not apparent in the magnetic field profile. Electromagnetic noise occurs at higher frequencies and amplitudes (X10) than in the laminar case, even up to 1 kHz, and is not confined to the ramp, but remains intense downstream in the sheath. Electrostatic noise does not reach above 1 mv/m in this case. The electric wave frequency sampled, 7 kHz, is not the best frequency with which to observe the shock with this diagnostic, but the electrostatic profile is representative, anyway; such low noise levels are typical of quasi-turbulent shocks observed in any of the lower frequency channels. Proton thermalization occurs at the rear of the ramp, as in the laminar case.

We look finally at the quasi-laminar example, at the bottom center, which illustrates the result of the mach number rising above 3 while β remains low. The ramp remains monotonic but the waves created in oblique shocks by dispersion in the plasma appear downstream. The magnetic noise occurs only in and around the ramp, as in the laminar case, but intense plasma wave noise up to tens of millivolts per meter appear, as in the turbulent structure. Particle data were unavailable in this case.

The foregoing examples illustrate the dependence of shock structure interpretation on the diagnostic employed and the interleaving of similarities and differences among the various subclasses. Magnetic noise, always present up to the local ion plasma frequency, is confined to the immediate neighborhood of the shock ramp in laminar and quasi-laminar cases, but persists in the sheath in quasi-turbulent and turbulent cases. Plasma wave noise, also always present in

the ramp, remains below a few millivolts per meter in laminar and quasi-turbulent shocks, but rises an order of magnitude higher in quasi-laminar and turbulent shocks.

The physical meaning of these distinctions is clarified to some degree by consulting another diagnostic. Post-shock ion spectra in the magnetosheath were not available from OGO 5, but a statistical study of HEOS data by Formisano et al (1973) revealed that downstream proton spectra were Maxwellian when $M \lesssim 3$. while they had a high energy tail when $M \gtrsim 3$. In detailed studies of particle behavior inside the shock transition, Montgomery et al (1970) and Formisano and Hedgecock (1973a) have shown that double-peaked distributions appear within the turbulent shock structure, the second peak occurring above the solar wind bulk velocity at about 2-4 V_{sw}. The change in proton distribution through the early part of the shock reported by Montgomery et al (1970) is shown in Figure 4a. The double distributions of Formisano and Hedgecock (1973a) are shown in Figure 4b in relation to the simultaneously-measured magnetic field shock profile. The field indicated a shock encounter in which the shock retreated from the satellite (HEOS) before it was fully crossed. The solar wind spectrum at the left was obtained a few minutes before the shock was engaged; the two bimodal spectra are positioned approximately at the times they were recorded.

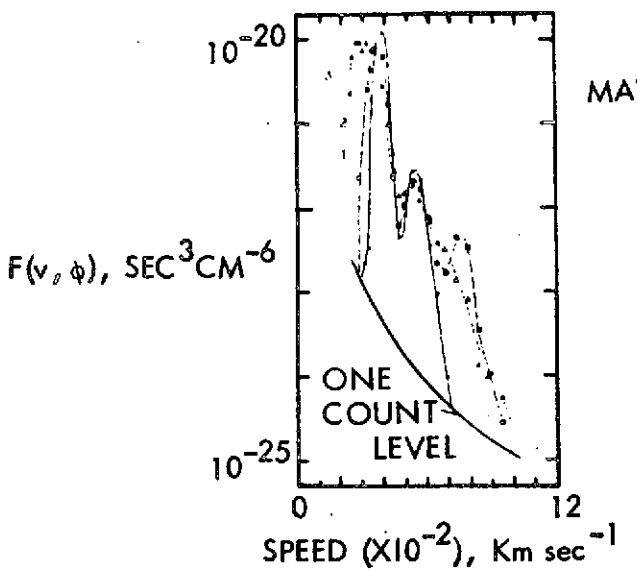

Figure 4a

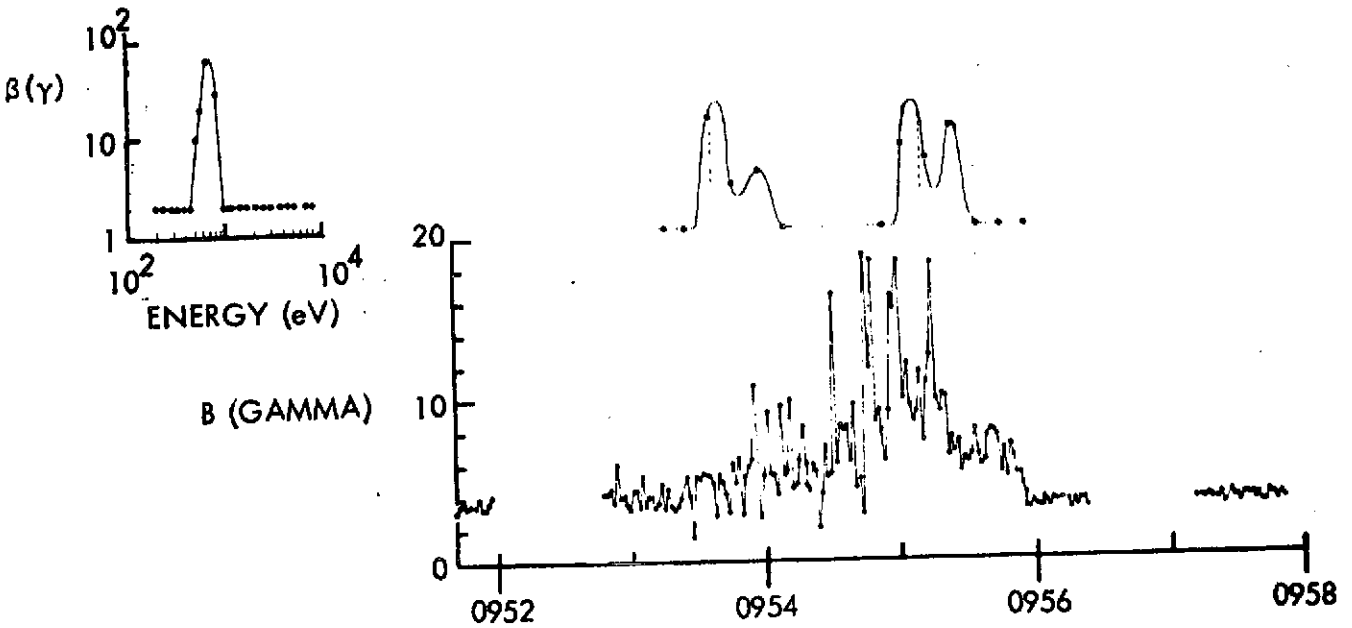

Figure 4b

The bimodal distribution immediately suggests the presence of bulk velocity protons reflected by the shock and energized by the interplanetary electric field through the process described by Sonnerup (1969). Counterstreaming protons are central to the idea that viscosity takes over to limit shock steepening above M_c where resistivity becomes inadequate. The bimodal distribution, together with the electron heating known to develop early in the ramp (Montgomery et al., 1970; Neugebauer et al., 1971), which in turn elevates T_e/T_p, provides a medium favorable to plasma instability, possibly leading to a subshock, finally resulting in high postshock proton temperature, characterized by a non-Maxwellian energy distribution with a high energy tail.

These findings round out the distinctions among the subclasses and their likely physical bases. Quasi-laminar and turbulent shocks are supercritical, in some sense, are characterized by high levels of electrostatic and electromagnetic activity, probably associated with a viscous subshock. Downstream

the bimodal distribution of the shock is smoothed to form a visibly-skewed ion spectrum. Laminar and quasi-turbulent shocks are subcritical, lack the conditions presumed to be associated with a subshock, especially high electrostatic noise, are limited by anomalous resistivity and dispersion only, and produce cool ion spectra downstream, with relatively little detectable deviation from Maxwellian distributions. The persistent magnetic noise of the quasi-turbulent shock is a feature consistently associated with its high thermal noise level and high-β plasma upstream.

Observe that in no quasi-perpendicular case are any regular, undamped, long period upstream waves present, but that very small fluctuations at about 1 Hz are visible ahead of the shock in three examples, those of 1, 7, and 14 February.

Quasi-Parallel Structures. The quasi-parallel structures collected so far have included no quasi-turbulent case. Figure 5 is therefore deficient in this subclass. Also, chance has produced only one transient laminar case. Nevertheless the laminar example at the left of the figure illustrates clearly, by comparison with Figure 4, the upstream activity produced by even borderline quasi-parallel $\theta_{nB} \approx 45°$. The monotonicity of the magnetic ramp has been destroyed, as in the irregular turbulent, quasi-perpendicular cases, but with an important difference: the precursor waves forward of the final average field elevation of 0640:30 are of appreciable amplitude and show the strong near-periodicity, in this case $T \approx 20$ sec, often observed far upstream on field lines connected to the shock (Fairfield, 1969). The regularity of the field in the sheath before 0640 UT appears to have been associated with a quasi-perpendicular upstream field orientation which became quasi-parallel at 1640.

The quasi-laminar example at bottom center of Figure 5 is formally on the borderline between quasi-laminar and turbulent as far as β is concerned,

but since β-determined changes are continuous anyway, it has been placed by virtue of its diagnostic combination in the quasi-laminar category. The alternation between large amplitude "pulsations" and upstream waves typical of quasi-parallel structures (Greenstadt et al., 1970) is evident in the figure. Observe that this example was recorded at the low resolution 1.15 sec/sample rate. The section shown is 28 minutes long in contrast to the minute-and-a-half view of the "irregular" turbulent shock of Figure 4. Moreover, this example is of a relatively subdued section taken near the solar wind end of a structure that was observed for over an hour by two satellites, one more than an earth radius behind the other. It is quite likely that this is actually an example of a parallel shock within the accuracy of estimation of θ_{nB}.

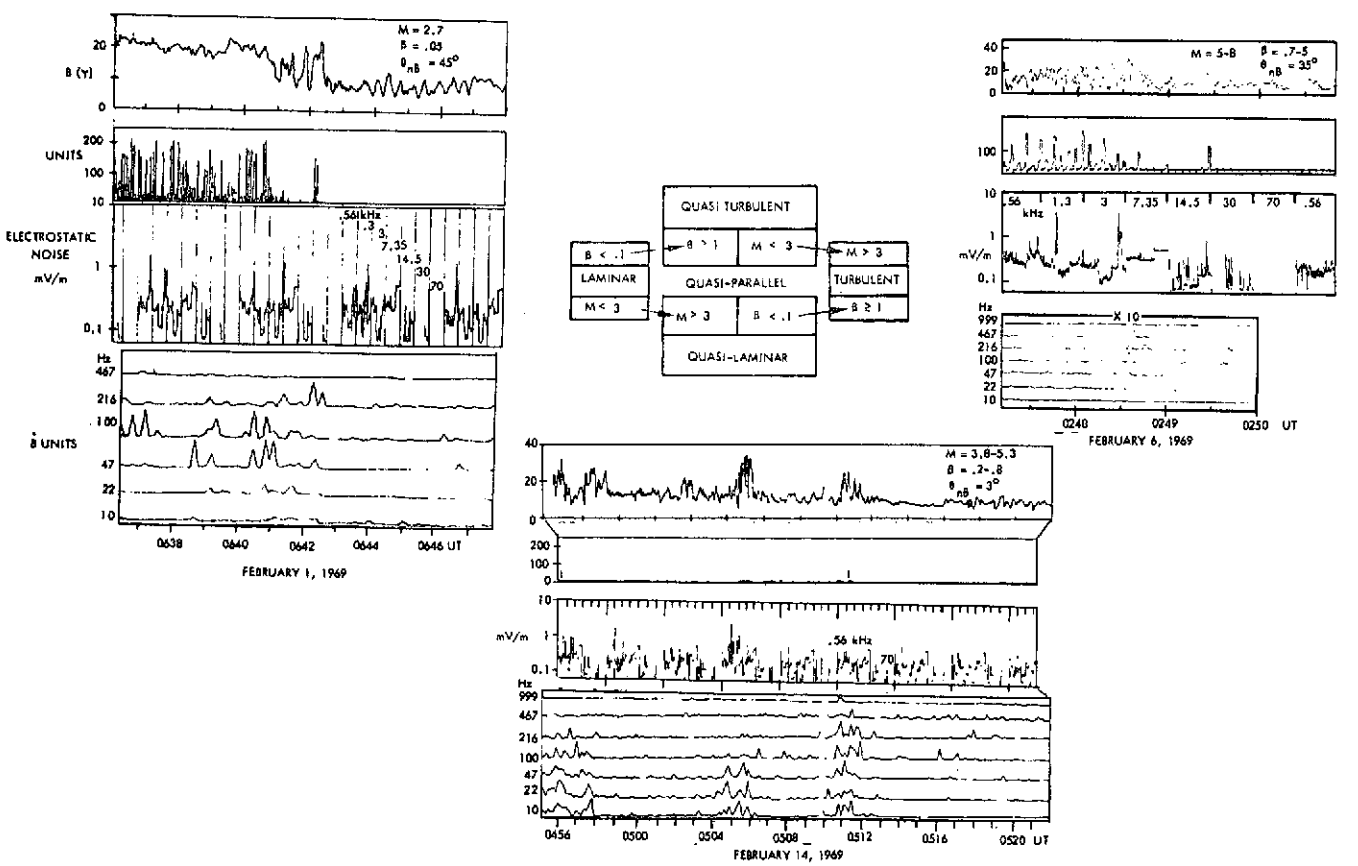

Figure 5

A shock that is definitely quasi-parallel and definitely turbulent is shown in the last example at the right in considerably greater detail. Here, at .144 sec/sample, we see the total absence of any regularity in what appears to be the shock at 0248:40. We also see both short and long period waves upstream, the latter having peak-to-peak amplitudes equal to the average field level. Bursts of damped waves appear at the leading edges of the longer-period upstream waves.

The other diagnostics displayed for the quasi-parallel shocks are informative. The figure shows the same format of electrostatic, electromagnetic, and proton scatter data used earlier. The irregularity of the magnetic profiles is clearly shared by the other measurements, but one phenomenon is particularly striking: intense electrostatic noise is absent just where it is notable in quasi-perpendicular shocks, namely in quasi-laminar and turbulent cases. Magnetic noise, as detected by the search coil, occurs at high amplitude only in the turbulent case. The expanded diagnostic picture of the quasi-parallel, turbulent shock emphatically confirms the observation that high electrostatic noise levels are absent in quasi-parallel structures. To complete the picture, we recall that the statistical analysis by Formisano et al. (1973a) gave only Maxwellian distributions in the sheath when upstream waves were detected, under presumably quasi-parallel geometry, regardless of M or β.

14 February 1969. Further examination of the essentially parallel shock of 14 February provides some evidence of conditions in a well-developed pulsation region. Figure 6 shows an overall view of the shock as seen concurrently by both HEOS 1 and OGO 5 magnetometers, when the satellites occupied the relative position seen in the figure at the top. The extremely active shock structure,

which coincided with $I_p = 1$ conditions (Greenstadt, 1972a), as shown in the small inserts above the field profiles, was at least 1 R_e thick. The figure incidentally demonstrates the difficulty of obtaining reliable upstream plasma parameters for the parallel shock, even with two spacecraft. Plasma data obtained by OGO 5 before and after the large field excursions yielded β and M associated with either the quasi-laminar or the turbulent subclass.

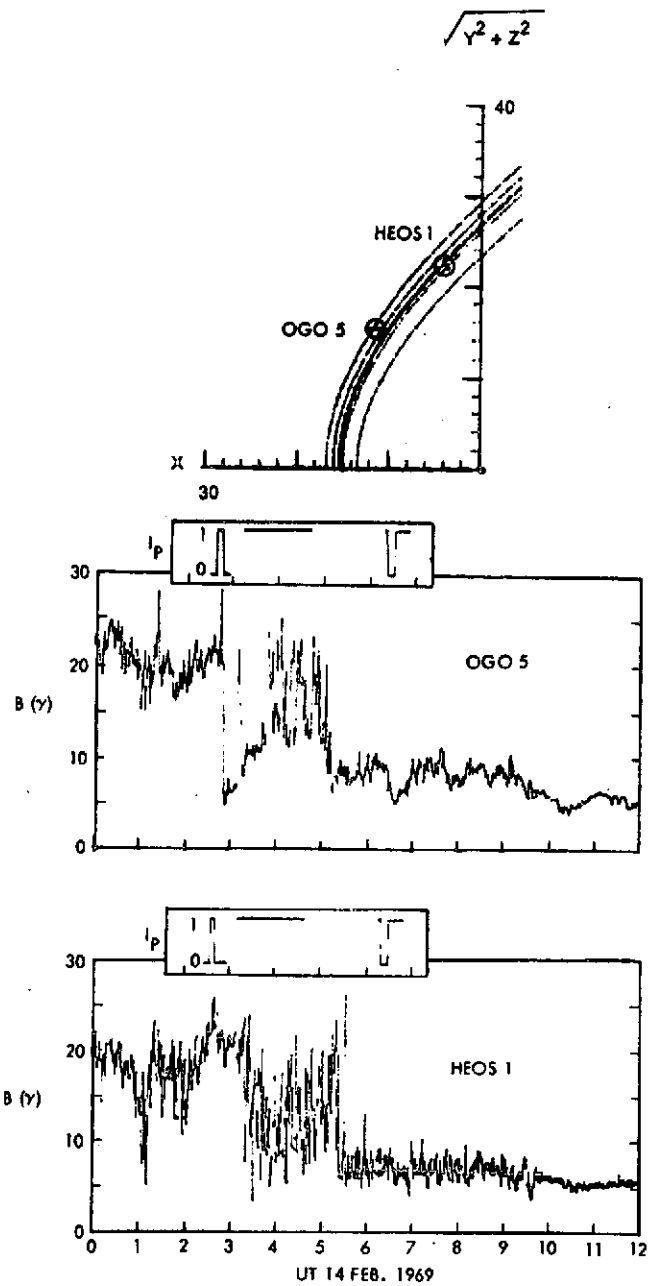

Figure 6

A detail of the magnetic field behavior at OGO obtained in the center of the pulsation structure at 1.15 sec/sample is shown in Figure 7. Above the sample are shown three contrasting ion spectra taken from HEOS 1 data. The solar wind spectrum was averaged from several distributions upstream from the shock. The magnetosheath spectrum is an average composite of several such distributions collected downstream from the shock before the quasi-parallel structure was encountered. The pulsation spectrum is the average of all distributions recorded while HEOS was in the pulsation structure. This spectrum clearly shows the plasma energy peak at the bulk energy of the solar wind but with a lower maximum and a broadened, hotter distribution. It appears, then, that the ions were severely scattered but the flow was not visibly retarded by the large amplitude magnetic waves of the parallel structure. This structure therefore offers some ambiguity as to whether it existed "upstream" or "downstream" of the "shock": it was thermally downstream, but dynamically upstream as far as slowing the bulk flow was concerned.

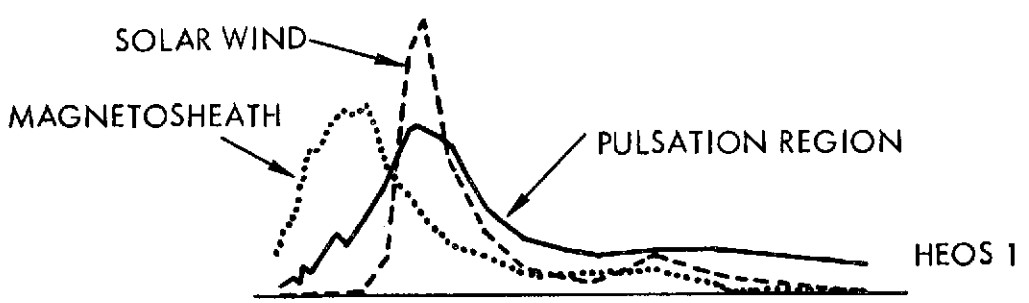

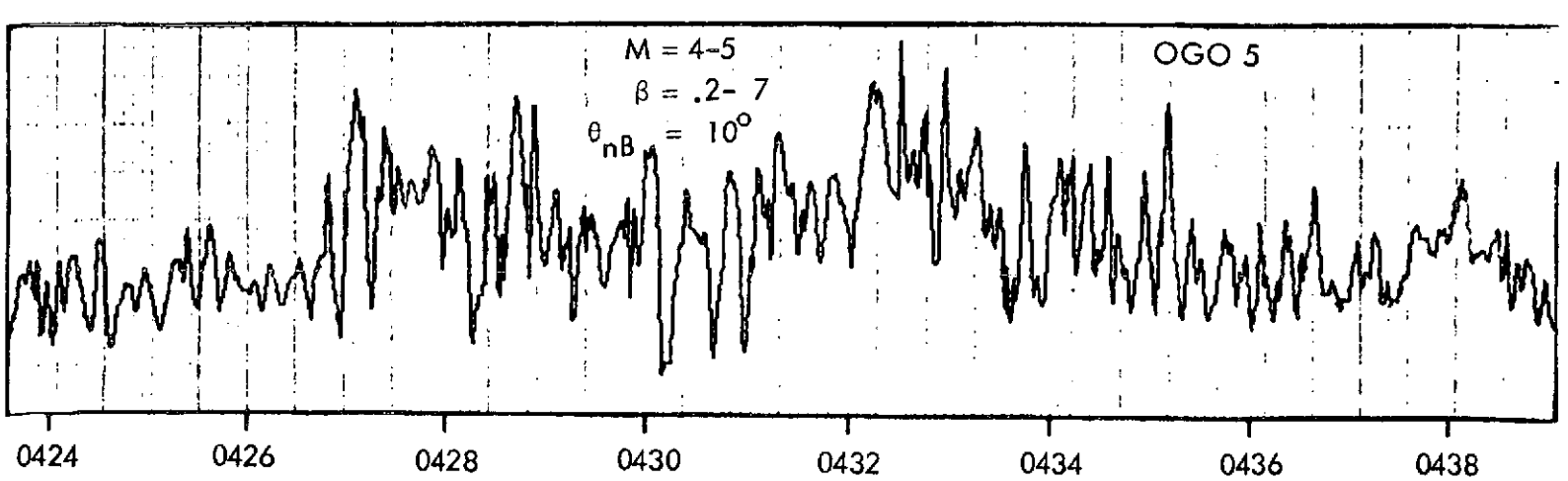

Figure 7

The foregoing result suggests the qualitative inference that to the extent that quasi-parallel structure may be regarded as upstream from some eventual average field and velocity jump, the plasma parameters delivered to the jump could be significantly different from those naively computed far upstream in the unaffected solar wind, and could put the shock in a different subclass, or in even more than one subclass simultaneously.

Venus Bow Shock. The character of Mariner 5's encounter with the Venus interaction region was interpreted earlier as consistent with the quasi-perpendicular/quasi-parallel division discussed here (Greenstadt, 1970). The fresh results from Mariner 10's recent flyby of Venus reconfirm this interpretation and the applicability of earth-derived shock analyses to neighboring planets. The characteristics associated with a thick, well-developed quasi-parallel shock, probably turbulent, are evident on early examination of the data (Ness et al., 1974), and the experimenters point out that such an interpretation is compatible with the average stream angle field direction in the ecliptic in the morning quadrant, discernible before a time gap in their Figure 4, and with the position of the Mariner crossing near the dawn meridian. It is also consistent with the quietude of the field after the time gap, when the field had apparently changed to the afternoon quadrant, preventing the familiar precursor region from reaching the spacecraft. It will be important, in further analysis, however, to bear in mind that the recorded structure could signify an ultra-high-β electrostatic shock, if the plasma temperature proves to have been very high.

DISCUSSION

Communication with the Solar Wind. The foregoing remark about an anticipated precursor region at Venus serves as a reminder that a planetary bow shock, in particular the earth's, is not an isolated, self-contained phenomenon

affecting only a tight region around the magnetosphere through which an insignificant tube of solar wind flux passes. From a space researcher's viewpoint, the bow shock must be regarded as the principal entity inside a large volume of solar wind with which it communicates. Downstream, the shock sends a heated, decelerated, and deflected solar wind it has prepared to flow around the magnetosphere. The field in this magnetosheath flow carries significant information from the shock. Its direction with respect to the magnetospheric field at the magnetopause may differ from what it had been upstream and may initiate or cancel a substorm by virtue of its refracted orientation. Large amplitude oscillations associated with quasi-parallel structure may reach the magnetopause and stimulate the magnetosphere, setting up resonant oscillations detectable at the surface as micropulsations. A model for such an excitation has been proposed by Greenstadt (1972b) and appears to be consistent with observation (Bolshakova and Troitskaya, 1968; Nourry and Watanabe, 1973). Upstream, the shock radiates waves and reflects protons and electrons of considerable enrgy (Asbridge et al., 1968; Feldman et al., 1973; Lin et al., 1974), which in turn stimulate upstream waves that forewarn the solar wind of the obstacle in its path. The low-frequency upstream wave region mapped out statistically by Fairfield (1969) is well known, and a plasma wave region has also been described (Fredricks et al., 1972). The intimate, apparently 1-for-1 association of long period upstream waves with what we here designate as quasi-parallel structure, has been documented by Greenstadt et al. (1970), and related by statistical inference to Maxwellian ion distributions downstream by Formisano et al. (1973).

The Bow Shock System. Figure 8 synopsizes the key elements of what should be regarded as the bow shock system. The shock itself is divided broadly into quasi-parallel and quasi-perpendicular regions, shown here in an ecliptic view for a nominal 45° stream angle. The precursor region is di-

$$\tan \theta_{XS\pm} = \frac{P_{\pm} \sin \theta_{XB}}{P_{\pm} \cos \theta_{XB} - 1}$$

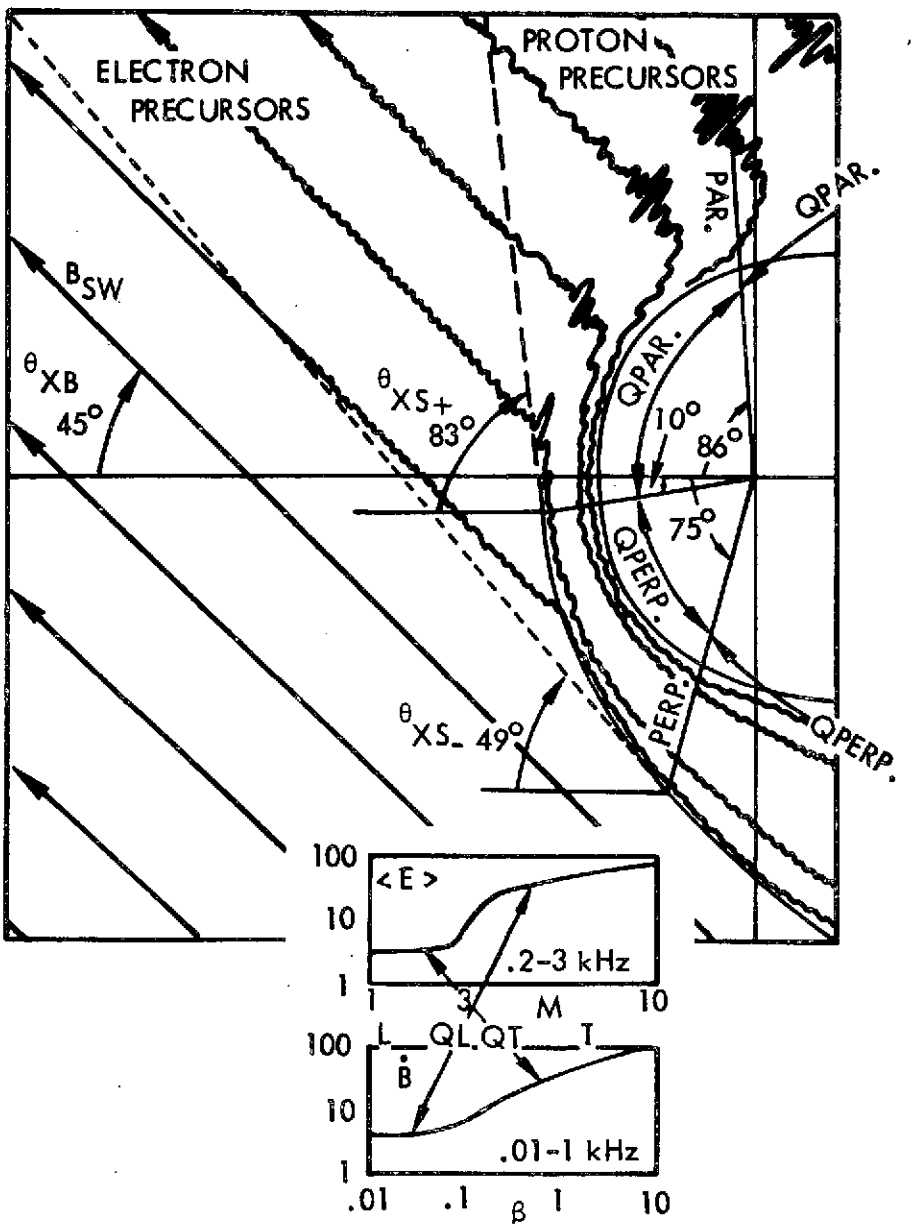

Figure 8

vided into two parts. An advance region of electron precursors consists of reflected electrons, plasma waves at the local electron plasma or upper hybrid frequency (generally in the 15-30 kHz range, Fredricks et al., 1972), accompanying magnetic waves in the same range, and very possibly small amplitude waves around 1 Hz, at least close to the shock. A less extensive region of proton precursors consists of reflected protons of energies up to as much as 100 keV, low frequency waves of tens of seconds period in a spacecraft frame, and the features of the electron precursor region as well. The formula at the top gives the means of estimating the forward boundaries of the two precursor regions, shown as dashed lines in the figure. In the equation, p represents the speed, as a multiple of V_{SW}, with which the appropriate reflected particle moves upstream along the field while the field is carried downwind. The angles indicated here, 83° and 49°, were obtained by setting $p_+ = 1.6$, a value found by the author to work well for predicting long period upstream waves and quasi-parallel structures, and $p_- = 10$, a value roughly compatible, for a 400-Km/sec solar wind, with the 4000 Km/sec ($\sim 10\ V_{SW}$) electron velocity cited in a report on reflected electrons by Feldman et al. (1973). Actually, both electrons and protons are reflected with a spectrum of velocities. Electrons, in particular, are hot and not well represented by a single velocity.

The insert at the bottom synopsizes qualitatively the empirical behavior of electric and magnetic noise in the quasi-perpendicular shock as functions of M and β. When both parameters are low, both noise levels are low and the shock is clearly laminar (L); when M rises above about 3 but β remains very low, the electric noise increases dramatically; the shock is quasi-laminar (QL). In the opposite case, when M remains low but β approaches 1, the mag-

netic noise increases in a more or less continuous fashion; the shock becomes quasi-turbulent (QT). When M and β are both high, the shock is turbulent (T); it is electrostatically and magnetically noisy and the sheath is magnetically noisy.

When similar parameter divisions are applied to the quasi-parallel structure, the shock is found to be low in electrostatic noise regardless of β or M, although the magnetic noise seems to rise with β as in quasi-perpendicular shocks.

CONCLUSION

The new data from which examples of bow shock structure were drawn for this report will be described in detail and discussed in greater depth in a series of papers now being prepared by the researchers named earlier. The overall result will be to bring the study of collisionless plasma shocks by means of spacecraft techniques up to and, in some respects, ahead of the prevailing level of laboratory and theoretical investigation. This paper is concluded therefore by outlining a few of the remaining goals to be pursued in seeking improved understanding of processes in the bow shock. These are:

1. Precise separation of structures differentiated by refined definitions of critical mach number.

2. Identification of the mechanisms responsible for the bimodal proton distribution, the viscous subshock, and thermalization of the ions.

3. Exact identification of the processes responsible for generation of the proton precursor waves.

4. Determination of the means by which reflected particles are energized and released upstream and the proportions in which they are divided into reflected and transmitted subspectra.

5. Differentiation of the roles of particle reflection, wave amplification, and wave breaking in the development of quasi-parallel structures.

Anyone interested in plasma processes can enlarge this list. The important point, however, is that none of the objectives listed seems impossible to achieve even with existing spacecraft data, and all should be reached when the HMD satellites go into operation.

ACKNOWLEDGMENT

Results described in this report were funded in part by the National Aeronautics and Space Administration under Contract NASW-2398.

REFERENCES

Asbridge, J. R., S. J. Bame, and I. B. Strong, Outward flow of protons from the earth's bow shock, J. Geophys. Res., 73, 5777, 1968.

Bol'shakova, O. V., and V. A. Troitskaya, Relation of the interplanetary magnetic field direction to the system of stable oscillations, Dokl. Akad. Nauk SSSR, 180, 4, 1968.

Drummond, Wm. E., and A. E. Robson, Oblique collisionless shock waves in plasma, DASA Report 2520, September 1969.

Fairfield, D. H., Bow shock associated waves observed in the far upstream interplanetary medium, J. Geophys. Res., 74, 3541, 1969.

Feldman, W. C., J. R. Asbridge, S. J. Bame, and M. D. Montgomary, Solar wind heat transport in the vicinity of the earth's bow shock, J. Geophys. Res., 78, 3697, 1973.

Formisano, V., and P. C. Hedgecock, On the structure of the turbulent bow shock, J. Geophys. Res., 78, 6522, 1973a.

Formisano, V., and P. C. Hedgecock, Solar wind interaction with the earth's magnetic field, 3. On the earth's bow shock structure, J. Geophys. Res., 78, 3745, 1973b.

Formisano V., G. Moreno, F. Palmiotto, and P. C. Hedgecock, Solar wind interaction with the earth's magnetic field, 1. Magnetosheath, J. Geophys. Res., 78, 3714, 1973.

Fredricks, R. W., Scarf, F. L., and Green, I. M., Distributions of electron plasma oscillations upstream from the earth's bow shock, J. Geophys. Res., 77, 1300, 1972.

Greenstadt, E. W., Binary index for assessing local bow shock obliquity, J. Geophys. Res., 77, 5467, 1972a.

Greenstadt, E. W., Field-determined oscillations in the magnetosheath as possible source of medium-period, daytime micropulsations, Proc. of Conf. on Solar Terrestrial Relations, Univ. of Calgary, 515, April 1972b.

Greenstadt, E. W., Dependence of shock structure at Venus and Mars on orientation of the interplanetary magnetic field, Cosmic Electrodyn., 1, 380, 1970.

Greenstadt, E. W., I. M. Green, G. T. Inouye, D. S. Colburn, J. H. Binsack, and E. F. Lyon, Dual satellite observation of the earth's bow shock, 1. The thick pulsation shock, Cosmic Electrodyn., 1, 160, 1970.

Lin, R. P., C. -I. Meng, and K. A. Anderson, 30- to 100-keV protons upstream from the earth's bow shock, J. Geophys. Res., 79, 489, 1974.

McKenzie, J. F., and Westphal, K. O., Interaction of linear waves with oblique shock waves, Phys. Fluids, 11, 2350, 1968.

Montgomery, M. D., J. R. Asbridge, and S. J. Bame, Vela 4 plasma observations near the earth's bow shock, J. Geophys. Res., 75, 1217, 1970.

Ness, N. F., K. W. Behannon, R. P. Lepping, Y. C. Whang, and K. H. Schatten, Magnetic field observations near Venus: Preliminary results from Mariner 10, Science, 183, 1301, 1974.

Neugebauer, M., C. T. Russell, and J. V. Olson, Correlated observations of electrons and magnetic fields at the earth's bow shock, J. Geophys. Res., 76, 4366, 1971.

Nourry, G., and T. Watanabe, Geomagnetic micropulsations and interplanetary magnetic field, Abstract, EOS, 54, 1179, 1973.

Paul, J. W. M., Collisionless shocks, Cosmic Plasma Physics, edited by K. Schindler, Plenum., New York, 1971.

Paul., J. W. M., Review of experimental studies of collisionless shocks propagating perpendicular to a magnetic field, Spec. Publ. 51, p 97, ESRO, Frascati, Italy, 1969.

Robson, A. E., Experiments on oblique shock waves, Spec. Publ. 51, p 159, ESRO Frascati, Italy, 1969.

Sonnerup, B. U. O., Acceleration of particles reflected at a shock front, J. Geophys. Res., 74, 1301, 1969.

Tidman, D. A., and N. A. Krall, Shock Waves in Collisionless Plasmas, John Wiley-Interscience., New York, 1971.

APPENDIX D

STRUCTURE OF THE QUASI-PERPENDICULAR, LAMINAR BOW SHOCK

21333-6015-RU-00

STRUCTURE OF THE QUASI-PERPENDICULAR, LAMINAR BOW SHOCK

by

E. W. Greenstadt, C. T. Russell*, F. L. Scarf,
V. Formisano†, and M. Neugebauer[1]

May 1974

*Institute of Geophysics & Planetary Physics, University of California, Los Angeles, California 90024

†CNR-LPS "Laboratorio Plasma Spazio", 00044 Frascati, Italy

[1]Jet Propulsion Laboratory, Pasadena, California 91103

Space Sciences Department
TRW Systems Group
One Space Park
Redondo Beach, California 90278

ABSTRACT

The earth's bow shock was observed several times at high resolution on 12 February 69 by an array of OGO 5 field and plasma instruments under unusual circumstances: The field was at large angle to the local shock normal, the solar wind parameters M and β were both low enough to ensure laminar shock structures, upstream parameters were verified by complementary measurements by HEOS 1, and approximate shock velocities were available by virtue of elapsed time observations obtained with the two satellites. It was found that the low $M(\lesssim 2.5)$ and $\beta(<< 1)$ and high $\theta_{nB}(\gtrsim 65°)$ produced oblique, laminar shock profiles as expected from theory, with marginal or vanishing upstream standing whistlers probably damped by drift or other plasma wave instability. The whistler mode appeared to dominate the electromagnetic spectrum. The laminar shock ramp thickness was several hundred kilometers and equal to 2-4 c/ω_{pi}. Composition of the shock as an accumulation of near-standing waves and an evidently reproducible varying flux pattern was discernible. Electron thermalization occurred early in, or just before, the magnetic ramp, while proton thermalization occurred late in the ramp. Instantaneous shock velocities derived from the standing whistler wavelength were consistent with average velocities derived from the elapsed-time estimates and were as high as 200 Km/sec.

INTRODUCTION

One of the major applications of the study of particles and fields in space is to the physics of collisionless plasmas in general, and to collisionless shocks in particular. Shock phenomena are difficult to scale in the laboratory and notoriously complex to represent in theory. A principal reason for their theoretical complexity is the number of independent parameters that can affect shock structure and shock dissipation processes. The contribution of satellite measurements to the experimental study of collisionless shocks lies in the opportunity to obtain repeated, high resolution observations of the earth's bow shock, which is constantly available for examination, for a wide range of instantaneous parameter sets.

Naturally, the most advantageous use of satellite data is in illuminating shock structures under complicated conditions least accessible to laboratory and theoretical attacks. However, spacecraft shock observations are not without their limitations too, the most blatant of which is the need for simultaneous measurements by at least two vehicles, one of which must define the parameter set under investigation through measurement upstream in the continuously-changing solar wind. A second, not much less serious, limitation is the need for reliable estimates of bow shock velocities, for the shock is seldom stationary in the spacecraft frame, and without its velocity, its dimensions may not be correctly inferred, especially when complex structure prevails. A third limitation lies in the difficulty of finding comprehensive plasma instrumentation on a single spacecraft.

In view of these restrictions, it is not inappropriate to seek first a comprehensive characterization of the bow shock in its simplest phases, which

are already fairly well understood theoretically, for cases where all or most of these limitations can be overcome. We regard this as a necessary step to more advanced analysis of the bow shock under conditions where fresh ground will have to be broken. In this report we therefore describe several observations of the bow shock in a single day, 12 February 1969, when the important parameters M and β were very low for many hours and θ_{nB} was oblique, but made a large angle with the local shock normal. The parameter combination $M \lesssim 3$, $\beta << 1$ corresponds to the so-called "laminar" shock in which "fields and particle distributions change coherently through the shock," as discussed by Tidman and Krall (1971), i.e., large scale turbulence is absent and small scale microturbulence, if it exists, "does not destroy the ordered appearance of the transition layer."

Geometrically, we describe the situation of our shocks as "quasi-perpendicular," meaning numerically that $50° \lesssim \theta_{nB} \lesssim 88°$, where θ_{nB} is the angle between solar wind field $\underset{\sim}{B}$ and the local shock normal. The term quasi-perpendicular is used to designate that range of oblique θ_{nB} in which the shock retains its essentially monotonic character and is readily identifiable in the data (Greenstadt et al., 1970; Fairfield, 1974; Greenstadt, 1974).

We define M as the magnetosonic mach number $M \equiv M_{MS} = V_{SW} \cos \theta_{xn} / (C_A^2 + C_S^2)^{1/2}$, and $\beta = 8\pi Nk(T_p+T_e)/B^2$, where V_{SW} and B are the solar wind speed and magnetic induction, θ_{xn} is the assumed angle between V_{SW} and local shock normal $\underset{\sim}{n}$ (X is the solar ecliptic X-axis), C_A and C_S are the Alfvénic and sonic velocities, N is the plasma density, and T_p and T_e are the proton and electron temperatures of the solar wind. We assume, since electron temperatures were not measured, that $T_e = 1.5 \times 10^{5°}K$. For the cases to be described here, β varied between .035 and .23, but remained below .1 in all

but one instance. Under these circumstances, M_{MS} is essentially identical to the Alfvén mach number M_A, since $C_S \ll C_A$. In our cases, $M_A \lesssim 2.4$.

This communication, then, gives the first detailed picture of the bow shock in what should be its simplest, laminar form. The shock crossings we display were the first for which velocities were estimated directly by elapsed time observations of shock motion between two satellites (Greenstadt et al., 1972), and therefore the first for which direct estimates of shock thickness could be made. We have assembled a comprehensive, although still imperfect, set of plasma diagnostics in order to discern the various stages of plasma alteration through the shock and the wave noise that accompanied them. In the following sections, we describe the data, calling attention to numerous details, some of which may assume additional importance in future analyses of laminar or other shocks, and we discuss some of the most significant characteristics of the wave structure in and around the shock transition layer. We include an analysis of the whistler precursor that leads to an independent confirmation of the elapsed-time velocities, and introduce thereby a new technique for computing instantaneous shock velocity when upstream standing waves are detected.

MEASUREMENTS

The data shown here were obtained by the TRW plasma wave detector of OGO 5, the triaxial fluxgate magnetometers of OGO 5 (UCLA) and HEOS 1 (Imperial College), and the JPL plasma analyzer, Lockheed light ion spectrometer, University of London Langmuir probe, and UCLA/JPL search coils of OGO 5. The OGO 5 instruments provided the high resolution records of the shock at sampling intervals of 1.15 and .144 sec/sample, corresponding to 1 and 8 kilobit/sec telemetry rates.

The field and particle instrumentation of OGO 5 and HEOS 1 that provided data for this report are described by Bonetti et al. (1969), Hedgecock (1970), Crook et al. (1969), Snare and Benjamin (1966), Harris and Sharp (1969), and Neugebauer (1970). In using data from the University of London Langmuir Probe, we rely here only on relative changes in the raw signature of its energy sweep.

Magnetic field measurements are direct vector recordings of ambient induction, with the HEOS-1 data used to adjust the absolute bias levels of the OGO-5 readings, the latter having been subject to intermittent spacecraft interference. Plasma wave measurements were generally represented by the field strength in a broadband channel covering the range 1 to 22 kHz, with most of the shock noise probably contributed by signals between a few hundred Hz and 2 kHz. The broadband channel was sampled for 1.15 sec every 9.216 sec, and the wave amplitude level is given in terms of the wideband electric field strength for a broad noise spectrum. Electromagnetic wave noise is represented by the equivalent level of white noise over the bandwidth of each channel of the UCLA/JPL search coils. The JPL plasma analyzer provided plasma flux readings and upstream velocity and density parameters in the solar wind. These quantities were lost once OGO entered the shock because the analyzer looked only in a fixed direction toward the sun. Proton thermalization and diversion of solar wind protons in directions away from that of normal flow were detected by the Lockheed spectrometer, after the shock was entered, since this instrument looked only in a direction across the solar wind stream. Electron behavior was monitored by noting the slope of the electron distribution registered by the London probe, in which a high energy component appeared when electrons were thermalized (scattered) by the shock process. These last two measurements are represented here by relative changes in uncalibrated telemetry units.

Measurement imprecision contributed partially to the uncertainties of numbers quoted in this communication. Raw measurements of individual magnetic field components were accurate to 0.5γ (5×10^{-6} gauss) or better, and field angles based on them to 5° or less. VLF electric field strengths were measured to within a factor of two because the wideband output of only one of the triaxial electric antennas was monitored. Another source of uncertainty of numbers quoted here lay in the separations of the various satellites from each other in space and in the uncontrolled constitution of the solar wind. It has been assumed that the solar wind was not perfectly uniform over the distances between OGO 5 and the other spacecraft and that what near-uniformity there was, was not instantaneous. The ranges of some parameter values given in the next section reflect uncertainties arising from the unknown degree of non-uniformity in the solar wind and from delays of up to 15 or 20 minutes between OGO 5 and the other spacecraft. The chief uncertainties were contributed by solar wind density and magnetic field variability. Ranges of magnetic field direction mean that the field was varying in orientation on a scale comparable to the expected intersatellite delay. It must be remembered throughout this report that neither the aberration nor the instantaneous angles of solar wind flow were taken into account in any computation, so that all quantities dependent on direction of the shock normal or the flow contain uncertainties of up to several degrees. It was decided that comparable, unrecoverable uncertainties in the shock-normal model and inherent in temporal field variation would have vitiated the "accuracy" implied by incorporating average flow direction in estimates of instantaneous quantities.

In addition to the data illustrated in this report, plasma and magnetic field parameters for the unshocked solar wind were obtained from plasma analy-

zers on HEOS 1 (Univ. of Rome) and Explorer 33 (MIT) and from the magnetometer of Explorer 35 (NASA/ARC).

OBSERVATIONS

General. The center panel of Figure 1 displays the magnitude of ambient $\underset{\sim}{B}$ recorded for 20 hours by HEOS 1 and OGO 5. Low values are for the solar wind, high values for the magnetosheath. HEOS was the more distant of the two, so as the shock moved outward and inward past the two spacecraft, HEOS was always in the solar wind outside the magnetosheath when the shock crossed OGO. The crossings numbered 1 through 4 are those for which average shock velocities were obtained in an earlier study (Greenstadt et al., 1972).

In the central panel, the HEOS field data are represented by 48-second samples, the OGO data by 1-minute averages. In the five separate panels surrounding the central one, the OGO data are represented by 1.15-sec samples. In the top four inserts, the step-like, almost noise-free appearance of the shock in the averages and at the 48-sec sample interval is seen to have been preserved at resolution 48 times higher than that of the HEOS graph at center. There are small differences between the first shock signature and the other three, namely in the presence or absence of upstream waves. These differences will be discussed later. The bottom panel in Figure 1 shows the pair of crossings 7 and 8, which were no longer strictly laminar, but turbulent and, in the case of crossing 8, perhaps multigradient as well. The shock front of crossing 7 was as sharp as those of the earlier crossings, but there was a small foot ahead of it and appreciable noise behind it. The change may have

been caused by a rise in β or in the mach number closer to the critical value, which is assumed to have been between 2.5 and 3.0. A sudden rotation of the interplanetary field toward the shock normal at 1750 was responsible for the additional complexity of crossing 8. These last two shock observations of the day serve to show the extreme simplicity of the earlier laminar shock profiles chosen for this study.

Dimensions. The upper half of Table 1 lists the salient quantities pertaining to the dimensions and local geometry of shock crossings 1 through 4. Measured dimensions are at the left, derived theoretical quantities at the right of the vertical division. Ramp thickness ΔS is the product $\overline{V}_{SS}\Delta t$, where Δt is the observed rise time of the ramp and $\overline{V}_{SS}$ is the average velocity of normal shock motion between OGO and HEOS positions in the spacecraft frame: positive indicates outward, negative inward, shock motion. V_{SH} is the velocity of the shock relative to the solar wind velocity component along the shock normal. Angle θ_{nB} is the angle between solar wind field vector B_{SW} and the local normal to the assumed rotationally-symmetric hyperbolic bow shock surface at OGO 5. The right-hand columns give M_A, proton inertial length c/ω_{pi}, and the ratio of ΔS to this last quantity. The inertial length was computed from HEOS 1 and Explorer 33 plasma data and HEOS 1 magnetometer data; the ranges of c/ω_{pi} express uncertainties in n_i.

The ramp thickness could also be related to the cyclotron radius of the bulk flow component across the field in the shock. However, the cyclotron radius was of the same order as c/ω_{pi} in the cases described here, so no useful distinction could be made by displaying it separately, and we have chosen to compare ΔS with c/ω_{pi} only.

In the θ_{nB} column, the table shows that at crossing 1, B_{SW} was 25° away from the perpendicular orientation, while at crossing 4, it was very close to perpendicular. In all but the third case, the ramp thickness was a small multiple of c/ω_{pi}, as listed. The third case is included for completeness, but we do not regard its listed velocity $\overline{V}_{SS}$ as reliable for reasons discussed below; hence, quantities derived from V_{SS} are not useful.

Details at High Resolution. Further details of the laminar shock were resolved in observations at a still higher sampling rate. Figure 2 displays the pair of crossings numbered 5 and 6, which were observed when OGO 5 was operating at its 8-kilobit telemetry rate. The magnitude and the three components of the magnetic field in spacecraft coordinates are shown. Magnetic field samples were .144-sec apart, which was adequate to provide some 67 measurement points in the ramp alone in case 6. The two shock profiles are very similar, there being only two significant distinctions between them, namely, that at the second shock a set of tiny waves is visible in the foot and some wavelike steps are more pronounced in the ramp. (In the following discussion the term "waves" is used to describe ultra low frequency electromagnetic noise measured by the magnetometer; the terms "plasma waves" or "electric field waves" are used to describe electromagnetic or electrostatic oscillations measured in various channels by the plasma wave electric field antenna.) The magnitude and all components are equally "laminar." Each of the two shock signatures exhibits a "plume" consisting of five distinct waves, or pulses, at the top of its main field jump, seen in B, and its principal component, B_y, and each has a "dome" of average field higher than was found a few tens of seconds

further downstream The domes seem to have been about one-and-a-half to two times the duration of the plumes. The waves of the plumes were evidently stationary in the respective shock frames, so they were propagating upstream in the solar wind plasma at 300 to 400 Km/sec.

The time-dimensions of the high-resolution shocks of Figure 2 are characterized in the figure by three quantities: first, the duration of the ramp, defined as the time between the first point at which the field rises above the level of small preshock maxima and the last point at which the field is below the level of small postshock minima; second, the duration of the plume; third the sum of ramp and plume. In Table 1, Δt denotes the duration of the ramp. This quantity was chosen as the only common quantity reasonably identifiable in shocks 1 through 4, where plumes would not have been resolvable, as well as in 5 and 6. Thus the Δt entered for shocks 1 through 4 in Table 1 is not the time from base to peak, but is the interval from the beginning of the steep field gradient to the level of the post-gradient minima, going in the direction from solar wind to magnetosheath.

The period of the average pulse in the plume at 1325 was 1.26 sec; the period of the average pulse in the plume at 1355 was 1.03 sec. The sums of ramp and plume duration were 10.3 seconds in both cases. The "steps" in the 1355 ramp were 1 to 1.5 seconds long, and the small oscillations in the foot averaged .4 sec. If we take the period of the average step in the ramp and pulse in the plume to be 1.2 sec, the ratios of durations of: foot wave to plume (or ramp) wave to ramp to total structure (ramp and plume) are 1/3/13/25 for the 1355 UT shock. Thus, the total structure from the base of the gradient to the end of distinguishable individual waves (the sheath end of the plume) appeared to be composed of some eight or nine waves or steps of a little over

1-second period each, half of them in the ramp and half in the plume; this was preceded by a precursor comprised of a few cycles of a damped standing wave (to be discussed later) and an eight-sec train of very small amplitude oscillations of about .4 sec average period. The small oscillations in the foot are close to the digitization level of the instrument, and form a somewhat irregular pattern in which groups of waves less than 0.14-sec period were just resolved in the raw data.

As the center panel of Figure 1 shows, there was a gap in HEOS data when the shock crossings of hour 13 (Figure 2) were observed by OGO. Consequently no average shock velocities could be determined for these events, so translation of periods and durations into thicknesses and wavelengths could not be made directly. However, we note that the ramp duration of case 4 is comparable to that of cases 5 and 6 and we reason as follows: the correct conversion of times to distances actually requires not an average shock velocity but an instantaneous velocity at the moment of crossing. Of the four measured average velocities, the last one, at 1628, is the closest to a true instantaneous velocity because the elapsed time from which it was calculated was the shortest of the four, leaving the least margin for discrepancy between average and instantaneous speeds. Also, an instantaneous velocity of some 100 Km/sec has been determined independently for the shock's crossing of HEOS at about 1627 UT as it was on its way toward OGO (Formisano et al., 1973).

If the structure of the laminar shock is assumed to have been essentially the same for crossings 4, 5, 6, and 7, then the ramp thickness for crossings 5 and 6 should have been about 2-3 c/ω_{pi}. This value is indicated in parenthesis in the last column in the lower half of Table 1. From this multiple of c/ω_{pi}, inferred values of ΔS, hypothetical V_{SH}, V_{SS}, and M_A were calculated for

cases 5, 6, and 7. These are also indicated by parentheses in Table 1. Based on the above argument that short elapsed times should reduce discrepancies between average and instantaneous shock speeds, cases 1 and 2 have good approximations to true instantaneous velocity, although not as good as case 4, while case 3's estimate is poor, which is why it was discounted in an earlier remark. The derived velocities for cases 5, 6, and 7 are therefore compatible with those of the most reliable of the first four cases of the table.

We recognize that θ_{nB} was not the same in case 4 as it was in cases 5 and 6, and that our thickness estimate could be affected. Appreciable broadening of the shock ramp may have occurred with decreasing θ_{nB}. If significant thickening had occurred, 400 Km would be an underestimate for ΔS in cases 5 and 6. Doubling ΔS, for example, would in turn raise the inferred V_{SH} in case 5 to 200 Km/sec, a speed at or above a statistical extreme found by Formisano et al. (1973). Substantial thickening was therefore not ruled out, and will be supported in a later section (Table 2). Very large ΔS, for $73° \leq \theta_{nB} \leq 80°$, would, however, have been incompatible with the value of ΔS found for case 2.

Shock broadening by field obliquity did clearly take effect when θ_n fell in the range 65°-70°. An example is illustrated by case 1. Figure 3 shows a comparison of the field and plasma wave profiles of crossings 1 and 3. At crossing 3, the shock encounter was sudden and the plasma wave noise consisted of a well defined noise peak at the field gradient; at crossing 1, a set of waves had developed ahead of the shock and the region of plasma wave noise was broadened to coincide with the waves, probably indicating preshock electron thermalization or reflection. The electric field noise appeared to increase with increasing wave amplitude as the main gradient was approached.

Still Further Details: Plasma Modifications in the Shock. The laminar structure and high resolution of the 1325-1355 shock crossings combined to offer an unusually uncluttered picture of the sequence of plasma changes across the shock gradient. These changes are shown in Figure 4. At the bottom, the field magnitude graph of Figure 3 is repeated for reference, with the range of estimated c/ω_{pi} thicknesses noted. Above the field is the plasma flux profile from the JPL Faraday Cup. Recall that this analyzer maintained a fixed view toward the sun; absence of flux inside the magnetosheath signifies deflection of flow outside the acceptance angle of the instrument, as at left and right edges, respectively, in the figure. We shall discuss the sequence of events in Figure 4 always from solar wind to magnetosheath, regardless of the actual order of observation. In the left panel, the flux underwent some small fluctuations as the shock was approached, then began a series of major oscillations just as the ramp started, and finally reappeared at a very low level behind the shock (the instrument was turned off at the top of the ramp and beginning of the plume). In the right panel, the same sequence was repeated with two exceptions: there appears to have been a gradual decline in average flux in the foot just outside the ramp, and the flux never entirely disappeared behind the ramp. The pattern of major oscillations was evidently a fixed characteristic of the laminar shock structure, as the numbered maxima and minima in the two panels elucidate. The first minimum in each case occurred before, and highest maximum after, midramp. Examination of plasma spectra indicates that the bulk solar wind velocity was still essentially unaffected at the time of the highest maximum, so this peak represents a density increase in the sheathside half of the shock ramp. The preramp, or early ramp, decrease in flux, on the other hand, was the result of a change

in flow direction. The sequence of observable flux events in the laminar shock, then, was early deflection of flow, strong variations in density, and essentially unreduced bulk velocity through most of the field ramp until the flow was redirected and the flux so diminished at the head of the ramp that plasma parameters could no longer be determined. The density variations included a rise to a density above that of the unshocked solar wind.

The third and fourth graphs from the bottom of Figure 4 illustrate the relative thermal behavior of solar wind electrons and protons, in uncalibrated telemetry units. In both panels magnetosheath electron spectra are clearly distinguishable from solar wind electron spectra by their rather flat distribution when the Langmuir probe sweep analyzed the higher electron energies (right-hand side of each sample curve). The shaded portions of the electron retardation curves indicate the difference between those spectra and the unaffected solar wind distribution measured upstream several minutes outside the shock. The electron measurements of both panels show that slight changes in electron energy distribution occurred outside the shock ahead of the ramp. The right panel shows that significant enhancement at high energy took place in the first half of the ramp; the left panel shows that full thermalization had not occurred by the end of the ramp and beginning of the plume; the right panel shows that full thermalization did occur by the end of the plume. Electron acceleration on the upstream side of the shock has previously been observed by Montgomery et al. (1970) and by Neugebauer et al. (1971) in their study of five non-laminar oblique shocks.

The Lockheed light ion spectrometer peers in a direction not aligned with the sun and is therefore a detector of thermalization and flow deflection, sensing only the protons that move in directions across the original direction

of flow. For brevity, we shall designate appearances of particles in this instrument as "heating" or "thermalization." The left panel, then, shows that by midramp no proton thermalization whatever was apparent; the right panel shows that some proton heating could have occurred after midramp; both panels show that the protons were deflected and/or thermalized by midplume. There is an ambiguity between the panels in properly associating proton heating with the flux pattern, but it appears that initial deflections of the ions occurred in conjunction with the high density spike or its forward edge.

Above the proton graph, the fifth and sixth strips depict the electric field noise recorded by the TRW plasma wave detector (PWD). The PWD, which cycled through its frequency channels at a relatively slow pace, was not in any of the more favorable channels ($\leq$ 3 kHz; Fredricks et al., 1970) during either crossing in Figure 4, as the fifth strip shows. Nevertheless, it is evident that sporadic elevated noise levels, even at 7 and 14 kHz, accompanied the shock ramp. In particular, a well-defined spike of 7 kHz noise was recorded at midramp simultaneously with the forward edge of the major density elevation in the left panel, and a noise jump at 14 kHz was detected at the analogous point of the right panel

The subcommutated PWD data in the sixth strip are somewhat more informative. We see that in both panels the 200 Hz channel recorded increases in noise level outside the ramp where the electrons were already affected by the presence of the shock, and that the 200 Hz noise was considerably elevated where partial thermalization of the electrons was taking place, both early and late, in the ramp. Noise in this channel persisted longer behind the shock in the right than in the left panel. There is no obvious association of electrostatic noise with proton effects, but this could have been easily missed with the PWD's incomplete frequency-time coverage. Special purpose, i.e., wideband, PWD data were not recorded on 12 February.

Electromagnetic Noise. The crossings of cases 5 and 6, as witnessed by one axis of the OGO 5 search coils, are shown in Figure 5, with the field magnitude profile repeated at the bottom for reference. Individual channel center-frequencies are identified in the vertical center column, between the two panels. In this figure, the very small-amplitude, damped standing waves barely discernible in front of the shock have been marked by a dottec curve near the bottom, just above the plot of B. These will be discussed further in a later paragraph.

We see that EM wave noise began upstream from the ramp (in one or more of the five lowest frequency channels) concurrently with the appearance of the tiny, standing waves ahead of the shock, and continued through the ramp. This upstream noise had an upper frequency cutoff somewhere between 216 and 467 Hz: this is the range in which the electron cyclotron frequency, f_{ce} = 252 Hz, fell at that time. We take it that the upstream data represent whistler mode noise arising in the shock and propagating at angles less than 60° to $\underset{\sim}{B}$, since the high frequency whistler cutoff is already reduced to 216 Hz and 100 Hz for propagation at 30° and 60° to $\underset{\sim}{B}$, respectively. Along the shock normal, i.e., at 75°, the cutoff was only 62 Hz. The small standing waves were simply the appropriate component of the whistler spectrum, at about 1 to 2 Hz, matching the solar wind velocity along the local normal. The steps in the ramp and the waves of the plume may then have been whistlers just below the standing wave frequency, or with decreasing $d\omega/dk$ as discussed by Tidman and Krall (1971, p 22).

Another perspective of the search coil data, in physical units, helps to clarify the EM noise behavior. Figure 6(a) shows a three-dimensional repre-

sentation of the history of one-axis magnetic wave power spectra through the shock crossing of 1355. Selected spectra, constructed from the seven-channel data of Figure 5 are shown on a common time scale with a sampled version of the field magnitude plotted obliquely on an arbitrary baseline. The entire array of spectra is 38.6 seconds long, with adjacent spectra .69 sec apart. Some spectra were omitted where they essentially duplicated those adjacent to them. The small circles designate the 100 Hz channels of the spectra as a guide to the eye in following wave behavior between $f_{ce} \cos \theta_{nB}$ and f_{ce}. Conversion to physical units of spectral density was based on assumed white noise across each frequency channel bandwidth.

As the figure shows, field noise grew rapidly just as, but definitely before, the shock ramp was approached, and decayed again rapidly behind the ramp. The pattern of 100 Hz noise illustrates well the generation of whistlers in the forward edge of the shock ramp, their propagation upstream along $\underset{\sim}{B}$, and their rapid damping in the solar wind. The 100 Hz noise reached its peak power at the foot of the ramp, suggesting propagation along the shock or, more probably, along $\underset{\sim}{B}$, which is only 15° from the tangent. The (b) insert at the lower right of the figure details the 216 and 467 Hz noise patterns through the ramp. The 216 Hz noise, just below the upstream whistler cutoff at $f_{ce} = 252$ Hz, appears within what must have been the 30° cone of propagation for that frequency. Moreover, the whistlers must have been severely damped along $\underset{\sim}{B}$, or they would have reached the detector earlier, having traveled laterally from a more distant point on the shock. The 467 Hz noise, which could not have propagated in any direction in the solar wind, peaked in the ramp behind the 216 Hz peak, only after the elevation in B raised the electron cyclotron frequency.

To summarize, we may imagine two typical "antenna patterns" of whistler mode waves propagating from the shock preferentially along $\underset{\sim}{B}$, one pattern ahead of the forward edge of the shock ramp, the other behind it. As the shock approached the satellite, the search coils moved through the various phase velocity "layers" of the upstream pattern, each frequency channel being affected as it entered the corresponding propagation cone, at $f_{ce} \cos \theta$. Behind the ramp, the satellite moved through the second pattern in reverse order, but with elevated f_{ce} affecting channels of higher frequency. The mode was effectively damped both upstream and downstream in distances on the order of the ramp thickness. Toward the rear of the ramp, changes in n, B, and T evidently allowed higher frequencies up to and above 1 kHz to propagate.

The Upstream Waves of Crossing 1. Simple geometrical properties of the standing waves can be obtained. As the OGO 5 panel in the center of Figure 1 shows, crossing number 1 into the sheath was immediately proceeded by a crossing out of the sheath. The two crossings were very similar to one another in profile, with one the reverse of the other. The field components spanning the two crossings are shown in Figure 7, in rectangular spacecraft coordinates, in which the X-Y plane approximates the shock plane. The mean interplanetary field, measured by HEOS and Explorer 35, was very steady, except for a slight shift in direction, seen just before the 0049 crossing in the X and Y components of the OGO 5 data. Angle θ_{Bn} was $\simeq 74°$ at the time of crossing; before the shift, about half a minute earlier, it was 64°-66° (Table 1).

Outstanding features of these crossings were the damped wavetrains appearing both times in the solar wind ahead of the shock. There are about six identifiable cycles associated with each crossing, the first set averaging about 8 seconds per cycle, the second about 11.5 sec per cycle. The appearance of

the waves certainly suggests that they were standing in the shock frame. The ratios of ramp duration to average wave period are .9 and 1.1 in the two cases, so the wavetrain precursor seems to have been moving with the shock. No elapsed time velocity estimate is available for the first set, but the 55 Km/sec found for the 0049 crossing (Table 1) gives an average wavelength λ of 630 Km.

In Figure 7, the wave perturbation lies in the X-Y plane, i.e., in a plane approximately parallel to the local shock surface. The polarization diagrams for the two wave sets are shown at the top of Figure 8; the senses of rotation of the two sets are opposite in the spacecraft frame. The sketch at the bottom of Figure 8 depicts the common standing wave perturbation in three dimensions relative to the local shock. The wave is polarized in the sense of a whistler propagating along the outward normal. Since it is standing in the shock frame, its phase velocity in the solar wind plasma is some 470 Km/sec.

DISCUSSION

The details of the laminar shock described above can be used to make some quantitative tests for consistency of the measurements with theory. Ideally, one would like to have high resolution proton and electron spectra through the shock transition layer, including the ramp, to define completely the behavior of the particles. Particle data of such fine resolution were unavailable, however, so our discussion is confined to some selected items involving wave behavior. Since whistler mode waves played a large role in these laminar shocks, we concentrated on these.

Standing Waves. The oblique (not necessarily laminar) shock in the laboratory and in theory is typically depicted as having a damped, standing

whistler precursor at both subcritical and supercritical mach numbers, with the last preshock cycle often of amplitude comparable to that of the final shock gradient (Robson, 1969; Tidman and Krall, 1971). Yet of the seven shock profiles shown in this paper, only three, the pair in Figure 7 (including case number 1) and number 7 of Figure 1, show any clear wavelike oscillations in the foot of the shock, and those are of small amplitude. Only one demonstrable standing wave occurred, in case 1, if we regard the prior crossing of 0045 (Figure 6) as simply another view of the same shock under the same conditions at essentially the same time. A barely-discernible example, of very small amplitude, was associated with the crossing pair of Figure 5. Thus, it appears that stationary whistler precursors are rare for quasi-perpendicular, laminar shocks and do not appear or barely appear when $\theta_{Bn} \gtrsim 70°$ (case 7 may not even have been laminar). Examination of other laminar crossings at high bit rates, not shown here, support this inference. We note that a sequence of non-laminar shocks with a particularly long whistler precursor studied by Holzer et al. (1972) revealed no waves which were phase-standing in the solar wind flow.

The marginal appearance of upstream standing precursors in these laminar shocks is explainable. A stationary whistler precursor must satisfy the following conditions to exist: 1) its phase velocity must equal the solar wind velocity; 2) its group velocity must exceed the solar wind velocity; 3) it must be stable at finite amplitude. When we use the term velocity, we always mean the component of velocity along the local shock normal. Whistler phase velocities depend on B, N, and θ_{nB}, and typically exceed the solar wind velocity for a range of frequencies, as depicted by Smith et al., 1967; and Scarf et al., 1968. Their examples for average conditions were essentially similar to the solid curves of Figure 9, in which are plotted the whistler phase velocity dependences for the

conditions that prevailed for our cases 1 and 4. The pairs of curves take into account the possible ranges of phase velocities V_ϕ allowed by the limit over which N and θ_{nB} might have occurred within measurement uncertainties. For each case the applicable velocity vs frequency curve lay somewhere between the extremes. The high frequency cutoff in each case is at $f/f_{ce} = \cos \theta_{nB}$ rather than $f = f_{ce}$, as in parallel propagation (where $\cos \theta_{nB} = 1$). The frequencies at which whistlers would stand along the shock normal occur where the phase velocity curves cross the corresponding shock velocity lines V_{SH}. There are two such crossings for each curve that has $V_\phi > V_{SH}$, but we have noted only the lower frequency crossing in each case. The circles near the apex of the curves mark the frequencies below which the group velocities V_g exceed the phase velocities; these critical frequencies are located at $f/f_{ce} = \frac{1}{2} \cos \theta_{nB}$. Hence, $V_\phi = V_{SH} < V_g$ only at the lower standing frequencies, where applicable. The algebraic relations underlying Figure 8 are outlined in Appendix 1.

The message of Figure 9 is that in case 1, whistlers can propagate upstream for a wide range of frequencies and will be stationary for some value f between 1.9×10^{-3} f_{ce} and 5×10^{-3} f_{ce}, while in case 4, values of N and θ_{nB} may have prevailed for which $V_\phi < V_{SH}$ for all frequencies, with no standing wave possible. Since case 1 (together with its companion in Figure 7) was the only one in which a significant standing wave was observed, the phase (and group) velocity criterion seems to explain the difference between the case 1 and 4 profiles.

In all the remaining cases except case 7, the phase velocity curves were similar to those of case 1. Case 7 was similar to case 4. Standing wave precursors should therefore have been the rule rather than the exception on the basis that, at some frequency, $V_\phi = V_{SH} < V_g$ in five out of seven observations. However, favorable velocity considerations do not by themselves guarantee the existence of waves of measurable amplitude nor do they provide any guidance as

to what upstream amplitudes should be. Waves of finite amplitude present finite field gradients to the upstream solar wind flow and can therefore cause finite currents large enough to generate their own signatures in the plasma, i.e., currents associated with field gradients tend to generate plasma instabilities which may in turn damp the waves.

The general criterion for development of instability is that the drift velocity responsible for the current exceed the plasma thermal velocity w_T. The threshold value at which $V_D \gtrsim w_T$ is proportional to the product of $\Delta B/B$ and either β^{-1} or $\beta^{-1/2}$, depending on the scale length involved. A convenient tabulation of several instability modes related to the bow shock has been assembled, together with suitable references, by Greenstadt and Fredricks (1973), who show that on the c/ω_{pi} scale, instabilities arise when $\Delta B/B \gtrsim A\beta^{1/2}$, where A is a constant depending on the mode invoked. The key fact is that low β is conducive to microinstability growth for a given $\Delta B/B$, and $\beta_i << .1$ on 12 February 1969. The drift instability, for example, requires $\Delta B/B \gtrsim \beta_i^{1/2}$ on the c/ω_{pi} scale length ($A \simeq 1$). For $\beta_i = .01$, $\beta_i^{1/2} = .1$, so that at the time of case 2, a wave with $\Delta B \geq .1B = .1(9) = .9\ \gamma$ would have been sufficient to trigger this mode. Formisano et al. (1971) have given values of $\beta_i = .002$ to $.004$ early on the 12th, so the drift mode requirement may have been satisfied even by tiny waves of amplitude $\simeq .5\ \gamma$. Certainly, where small standing waves of 1 to 2 γ amplitude did appear, in case 1, they were accompanied by doppler-shifted plasma wave noise of unknown frequency recorded in the broadband channel (Figure 3). In nonlaminar cases of high β examined by the authors, profiles with at least one large amplitude wave outside the shock have been noted.

In sum: in four cases, 2, 3, 4, and 6, where phase and group velocity considerations would in principal have permitted upstream standing whistler waves, the dispersive wavelength could have been less than the dissipative scale length and waves could have been damped by easily triggered plasma instabilities; in three cases, 1, 4, and 7, where the dispersive wavelength may have exceeded the dissipative scale length, only one, case 1, occurred when upstream whistler propagation was unambiguously permitted, and in that one case, only small waves appeared, which were accompanied by plasma wave noise possibly generated by the waves themselves in a condition of extremely low β_i. The present observational profiles of low mach number shocks with no standing precursors and considerable magnetic noise is substantially similar to the results of the AVCO laboratory experiment (Pugh and Patrick, 1967; Patrick and Pugh, 1969), which also obtained thicknesses of (2-4) c/ω_{pi}.

Velocity Estimates from Standing Wavelength. Since in oblique shocks, the standing whistler wavelength must necessarily be related to the shock velocity as well as to the ambient plasma parameters, it is possible to use the wavelength, L_d, to estimate the local, instantaneous shock velocity V_{SS} in the plasma frame. The procedure for doing so is described in Appendix 2. We have applied equation (4) of Appendix 2 to three cases in which standing waves were in evidence, case 1 (0049 UT), and cases 5 and 6 (1325, 1355 UT). The outline of the small waves ahead of the shock in cases 5 and 6 was indicated in Figure 5.

The results of estimating V_{SS} from L_d are shown in Table 2, along with some useful data for comparison. The first five columns of the table give the case number, time, estimated average standing wave period T_{wave} in the spacecraft frame, density N, and velocity V_{SS} in the spacecraft frame. Equation (4) (Appendix 2) was evaluated for the extremes of the density range, N = 1 and 2.

The equation is capable, of course, of yielding up to four real solutions, but only for N = 2 in case 5 did it actually do so. Only real solutions of reasonable magnitude are shown in the table. In case 5, density N = 1 gave no real solution at all. The sixth column of Table 2 repeats $\overline{V}_{SS}$ from Table 1. In case 1, the solution V_{SS} for N = 1 is very close to $\overline{V}_{SS}$, giving remarkably good agreement between the instantaneous and average velocities, estimated by entirely independent methods. It will be recalled that the crossings of cases 5 and 6 were not observed by both spacecraft, so $\overline{V}_{SS}$ (Table 1) had to be approximated in an indirect way, assuming ramp thickness as a suitable multiple of c/ω_{pi} (parentheses in the table). Nevertheless, in case 6, the lower end of the range of estimated $\overline{V}_{SS}$ is very close to V_{SS}. In case 5, the instantaneous and average velocities are not in agreement numerically, but the higher instantaneous speed is consistent with the higher estimated range of average speed.

The next two columns give the wave-derived shock ramp thickness $\Delta S_w = V_{SS}\Delta t$, computed from V_{SS}, the ramp time of Table 1, and the ratio of ΔS_w to c/ω_{pi}. The earlier inference that shock thickness is a small multiple of c/ω_{pi} is supported, although it appears that a range of 2-4 or 2-5 would be better for $\Delta S/c/\omega_{pi}$ than 2-3. The last two columns of the table display $L_d = V_{SS}T_{wave}$ and the ratio $\Delta S/T_{wave}$, showing $\Delta S \gtrsim T_{wave}$, i.e., the ramp length is on the order of the dispersive length or a little longer. It would follow that the dissipative length for the electrons ought to be less than, or about equal to, T_{wave}, and the wave noise (Figures 3, 5) and electron heating profiles (Figure 4) are compatible with such an inference.

The bottom entry in Table 2 shows the thickness and dispersion lengths for case 4, for comparison with the cases just discussed. This case had the

most reliable average velocity. Ratio $\Delta S/c/\omega_{pi}$ is reasonably compatible with the others, but $\Delta S/L_d$ is appreciably larger and perhaps even very much larger than in the other cases. Here, L_d was computed from expression (1) of Appendix 2, since no upstream waves were visible. The high values of $\Delta S/L_d$ are precisely what would be expected for the absence of detectable waves and the nearly perpendicular θ_{nB}: the standing wavetrain was swallowed up by the ramp because the wavelength exceeded the dissipation length.

Ion Acoustic Waves. An argument was given in an earlier paragraph that upstream whistlers were damped by wavemodes easily excited at low β. The drift instability was selected as an example of a suitable mode, but the ion acoustic mode might also have been chosen. We therefore show separately here that this mode was highly improbable, using the dimensions estimated in this report.

The condition for generation of ion acoustic noise is that the electron drift velocity $V_d \approx \Delta B/2\Delta S\mu_o Ne$ (mks units) exceed the sound speed $w_T = (kT_e/m_i)^{1/2}$ in the ramp, where ΔB is the jump in B over distance ΔS. In our case 1 (0049 UT), we take $\Delta B \approx 17\ \gamma$ (Figure 3), $\Delta S = 660$ Km (Table 2) at N = 1, and we assume T_e, which tends to be largely constant in the solar wind, $\approx 1.5 \times 10^{5}$°K. The measured value of T_i was about 6×10^{3}°K. Then $V_d/w_T \approx .08/35 << 1$. which falls far short of the threshold for generation of ion noise. This value, based on an assumed T_e in the solar wind, is undoubtedly too high in the ramp, because the early preferential heating of electrons (Figure 4) would have raised T_e and w_T there, thus lowering V_d/w_T. Although our value of T_e was only assumed, it is highly improbable that $V_d/w_T \geq 1$, since this would require T_e to have been less than $\left(\frac{.08}{35}\right)^2 \times 1.5 \times 10^5 = .78$°K, according to the expressions above. It therefore seems certain that ion acoustic noise was not responsible for the plasma waves surrounding the shock

in cases 1 and 3 (Figure 3), 5 and 6 (Figure 4), and the other laminar cases, not illustrated, where similar electric oscillations occurred. This improbability does not necessarily mean the drift instability was a contributor to the noise. More sophisticated apparatus, or perhaps further analysis, will be needed to distinguish the correct wavemode.

CONCLUSION

The structure of the earth's bow shock for low β, low M upwind plasma conditions in local quasi-perpendicular geometry when $65° \lesssim \theta_{nB} \lesssim 88°$ is indeed laminar in the sense that macroscopic turbulence is absent from the magnetic field profile and particle thermalizations evidently occur in an orderly way. The electrons are heated first over a relatively broad region including both precursor and ramp, and the protons are heated in a relatively narrow region somewhere between the middle and end of the magnetic ramp. The shock magnetic profile is 2-4 c/ω_{pi} thick and corresponds well to the form expected from laboratory and theoretical results for oblique shocks at low β, where upstream standing whistlers are heavily damped.

Whistler waves propagating within their frequency-dependent phase-velocity cones around B are a significant constituent of the electromagnetic spectrum in the shock and its precursor up to the local electron cyclotron frequency. Indeed the precursor itself is simply the whistler whose phase velocity equals the normal component of solar wind velocity in the shock frame. The shock (magnetic) ramp itself appears to be composed of damped whistlers near the standing wave frequency, and the times at which whistlers were detected at all observed frequencies coincided in our cases with the region in which small waves or steps were clearly visible in the magnetic record, the region consisting of precursor, ramp, and plume.

Electric plasma waves occur in the laminar shock and its precursor. In one of our cases, noise at 7 kHz was concentrated at midramp, probably where proton thermalization began and the solar wind flux underwent some fluctuations. These fluctuations of the plasma flux appeared to form a pattern characteristic of the shock, probably related to density gradients and current sheets in the shock transition layer.

The measured period of standing precursor whistlers can be used to obtain a reliable instantaneous bow shock velocity in the spacecraft frame, if the upstream plasma parameters, as well as the field, are known. The method for obtaining the shock velocity should work equally well for any quasi-perpendicular (oblique) shock, whether it is laminar or not, as long as the stationary upstream waves are discernible.

ACKNOWLEDGMENTS

Numerous discussions with R. W. Fredricks, T. G. Northrop, and A. E. Robson were valuable in preparing this report, which was funded by the National Aeroanutics and Space Administration under Contracts NASW-2398, NGR 05-007-004, NASW-2513, and NAS7-100. We thank Drs. G. Sharp, K. Harris, and K. Norman for allowing us to display and discuss their low energy proton and electron data.

REFERENCES

Bonetti, A., G. Moreno, S. Cantarano, A. Egidi, R. Marconero, F. Palutan, and G. Pizzella, Solar wind observations with ESRO satellite HEOS 1 in December 1968, Nuovo Cimento, 64B, 307, 1969.

Crook, G. M., F. L. Scarf, R. W. Fredricks, I. M. Green, and P. Lukas, The OGO 5 plasma wave detector: Instrumentation and in-flight operation, IEEE Trans. Geosci. Electron., GE-7, 120, 1969.

Fairfield, D. H., Whistler waves observed upstream from collisionless shocks, J. Geophys. Res., 79, 1368, 1974.

Formisano, V., P. C. Hedgecock, G. Moreno, J. Sear, and D. Bollea, Observations of earth's bow shock for low mach numbers, Planet. Space Sci., 19, 1519, 1971.

Formisano, V., P. C. Hedgecock, G. Moreno, F. Palmiotto, and J. Chao, Solar wind interaction with the earth's magnetic field, 2. The magnetohydrodynamic bow shock, J. Geophys. Res., 78, 3731, 1973b.

Fredricks, R. W., G. M. Crook, C. F. Kennel, I. M. Green, F. L. Scarf, P. J. Coleman, Jr., and C. T. Russell, OGO 5 observations of electrostatic turbulence in bow shock magnetic structures, J. Geophys. Res., 75, 3751, 1970.

Greenstadt, E. W., I. M. Green, G. T. Inouye, D. S. Colburn, J. H. Binsack, and E. F. Lyon, Dual satellite observation of the earth's bow shock, 1. The thick pulsation shock, Cosmic Electrodyn., 1, 160, 1970.

Greenstadt, E. W., P. C. Hedgecock, and C. T. Russell, Large-scale coherence and high velocities of the earth's bow shock on February 12, 1969, J. Geophys. Res., 77, 1116, 1972.

Greenstadt, E. W., Structure of the terrestrial bow shock, paper presented at Third Solar Wind Conference, Asilomar, March 1974.

Greenstadt, E. W., and R. W. Fredricks, Plasma instability modes related to the earth's bow shock, Magnetospheric Physics, ed. by B. M. McCormac, D. Reidel, Dordrecht, Holland, 355, 1974.

Harris, K. K., and G. W. Sharp, OGO 5 ion spectrometer, IEEE Trans. Geosci. Electron., GE-7, 93, 1969.

Hedgecock, P. C., The solar particle event of February 25, 1969, in Inter-correlated Satellite Observations Related to Solar Events, edited by V. Manno and D. E. Page, D. Reidel, Dordrecht, Netherlands, 419, 1970.

Holzer, R. E., T. G. Northrop, J. V. Olson, and C. T. Russell, Study of waves in the earth's bow shock, J. Geophys. Res., 77, 2264, 1972.

Montgomery, M. D., J. R. Asbridge, and S. J. Bame, Vela 4 plasma observations near the earth's bow shock, J. Geophys. Res., 75, 1217, 1970.

Morton, K. W., Finite-amplitude compression waves in a collision-free plasma, Phys. Fluids, 7, 1801, 1964.

Neugebauer, M., Initial deceleration of solar-wind positive ions in the earth's bow shock, J. Geophys. Res., 75, 717, 1970.

Neugebauer, M., C. T. Russell, J. V. Olson, Correlated observations of electrons and magnetic fields at the earth's bow shock, J. Geophys. Res., 76, 4366, 1971.

Patrick, R. M., and E. R. Pugh, Laboratory study of turbulence in collision-free shocks, Phys. Fluids, 12, 366, 1969

Pugh, E. R., and R. M. Patrick, Plasma wind tunnel studies of collision-free flows and shocks, Phys. Fluids, 10, 2579, 1967.

Robson, A. E., Experiments on oblique shock waves, Spec. Publ. 51, ESRO, Frascati, Italy, 159, 1969.

Scarf, F. L., G. M. Crook, I. M. Green, and P. F. Virobik, Initial results of the Pioneer 8 VLF electric field experiment, J. Geophys. Res., 73, 6665, 1968.

Smith, E. J., R. H. Holzer, M. G. McLeod, and C. T. Russell, Magnetic noise in the magnetosheath in the frequency range 3-300 Hz, J. Geophys. Res., 72, 4803-4813, 1967.

Snare, R. C., and C. R. Benjamin, Magnetic field instrument for the OGO-E spacecraft, IEEE Trans. Nucl. Sci., NS-13, 6, 1966.

Stix, T. H., The Theory of Plasma Waves, McGraw-Hill, New York, 1962.

Tidman, D. A., and N. A. Krall, Shock Waves in Collisionless Plasmas, John Wiley-Interscience, New York, 1971.

Table 1. Shock Thicknesses

Time (UT)	Δt (Sec)	$\overline{V}_{SS}$ (KM/Sec)	ΔS (Km)	n (cm^{-3})	B (γ)	V_{SH} (Km/Sec)	θ_{Bn} (Deg)	M_A	c/ω_{pi} (Km)	$\Delta S/c/\omega_{pi}$
1) 0049	13	55	720	1-2	13.5	430	64-66 74	1.5-2.1	160-230	3.1-4.5
2) 0215	4.6	-49	226	1-2.5	13.0	326	73-80	1.2-1.8	143-230	1.0-1.6
3) 0223	9.2	11	101	1-2.5	12.5	387	75-79	1.4-2.2	143-230	.4-.7
4) 1628	4	-100	400	1-2	7.5	273	84-88	1.7-2.4	160-230	1.7-2.5
5) 1325	4	-(80-120)	(320-480)	1-2	9.0	-(242-282)	75	(1.2-2.0)	160-230	(2-3)
6) 1355	5.15	(62-93)	(320-480)	1-2	9.0	(424-455)	75	(2.2-3.3)	160-230	(2-3)
7) 1741	6	(43-115)	(260-690)	1-3	7.5	(443-515)	77-85	(2.7-5.5)	130-230	(2-3)
8) 1752		No single ramp defined					47-66			

Table 2. Shock Velocities from Standing Wavelength

$$V_{SS}^4 + (2nV_{SW}\cos\theta_{Vn})V_{SS}^3 + (V_{SW}^2\cos^2\theta_{Vn} - C_A^2)V_{SS}^2 - \left(\frac{2\pi C_A}{T}\cos\theta_{Bn}\frac{c}{\omega_{pi}}\right)^2 = 0$$

$$L_d = \frac{2\pi\cos\theta_{Bn}}{\sqrt{M_A^2-1}}\quad\frac{c}{\omega_{pi}}$$

Case	Time	T_{wave} (sec)	n	V_{SS} (Km/sec)	$\overline{V}_{SS}$ (Km/sec)	ΔS_W (Km)	$\Delta S_W/\frac{c}{\omega_{pi}}$	L_d	$\Delta S/L_d$
1	0049	11.5	1	51	55	663	2.9-4.6	587	1.13
			2	23		299	1.3-2.1	265	1.13
5	1325	4.0	1	-561		2244	9.8-14.0	2244	1.0
			2	-502		2008	8.7-12.6	2008	1.0
				-217	-(80-120)	868	3.8-5.4(2-3)	868	1.0
				-30		120	.5-.75	120	1.0
6	1355	3.1	1	62.4	(62-93)	321	1.4-2(2-3)	193	1.7
			2	32.0		165	.71-1.0	100	1.7
						ΔS	$\Delta S/c/\omega_{pi}$		
4	1628				-100	400	1.7-2.5	16-110	3.6-25

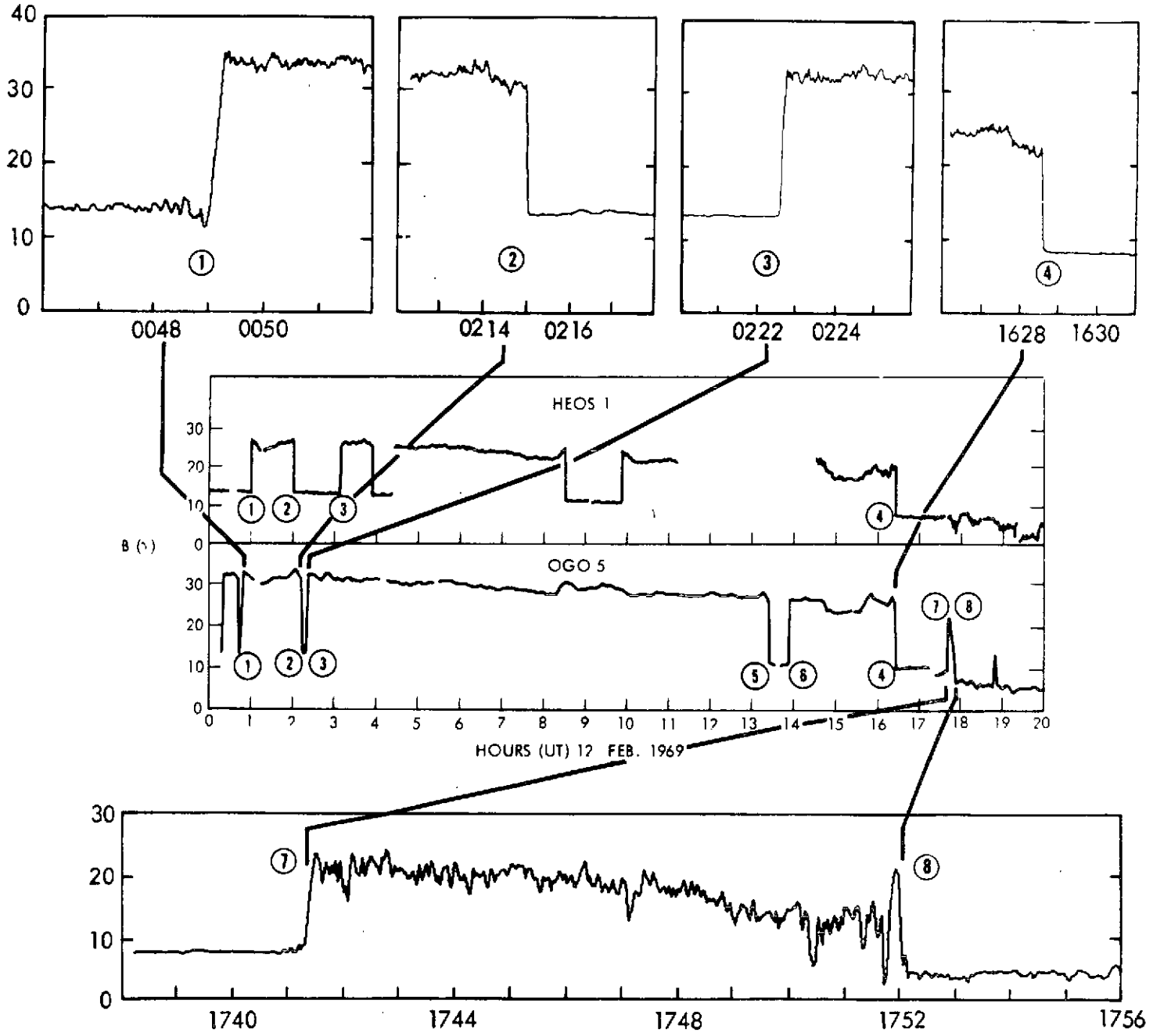

Figure 1. Summary view of the shock-crossing sequence of 12 February 1969. The circled numbers designated case numbers discussed in the text.

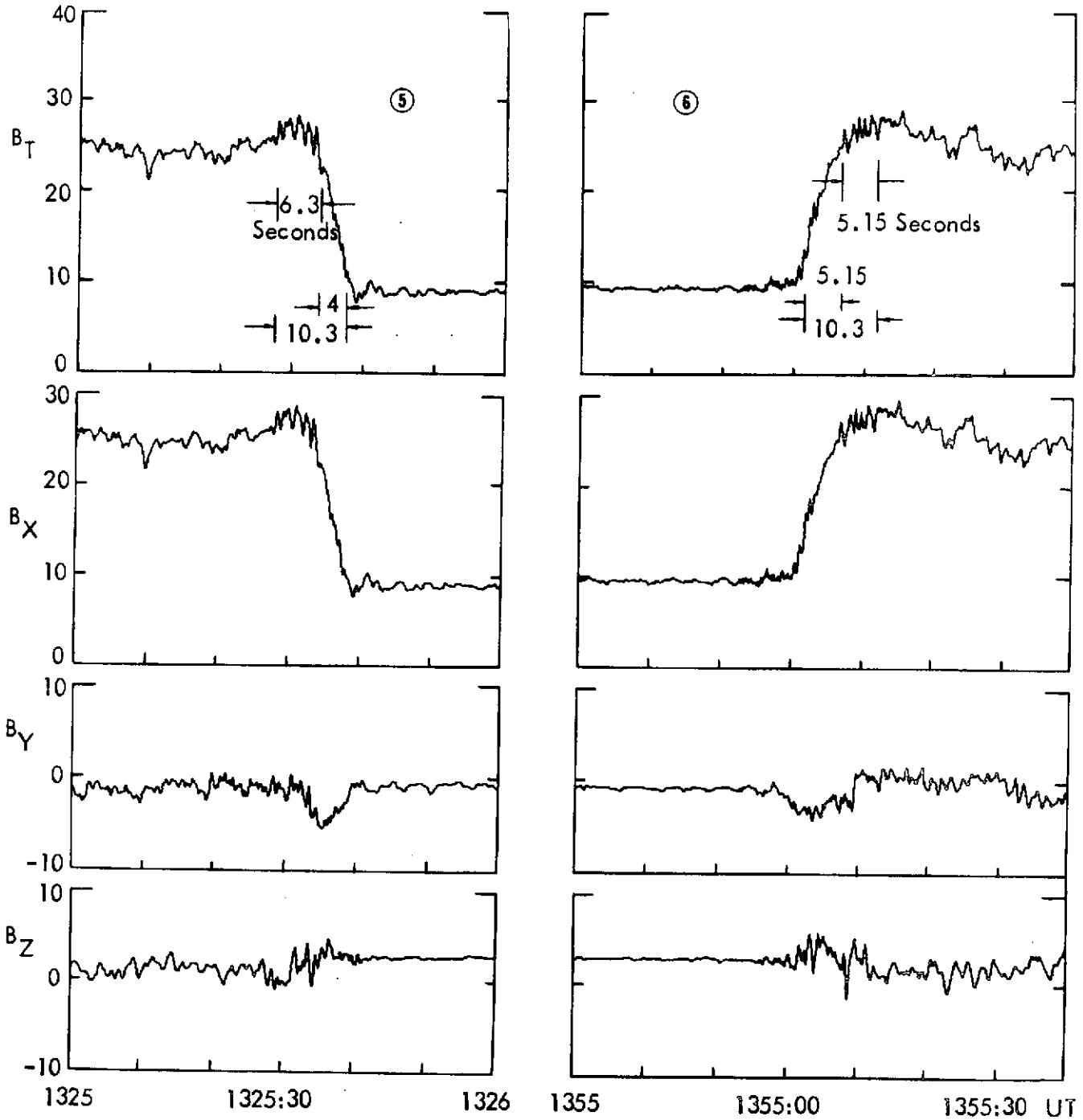

Figure 2. Two adjacent magnetic profiles of the laminar shock at high resolution: .144 sec/sample.

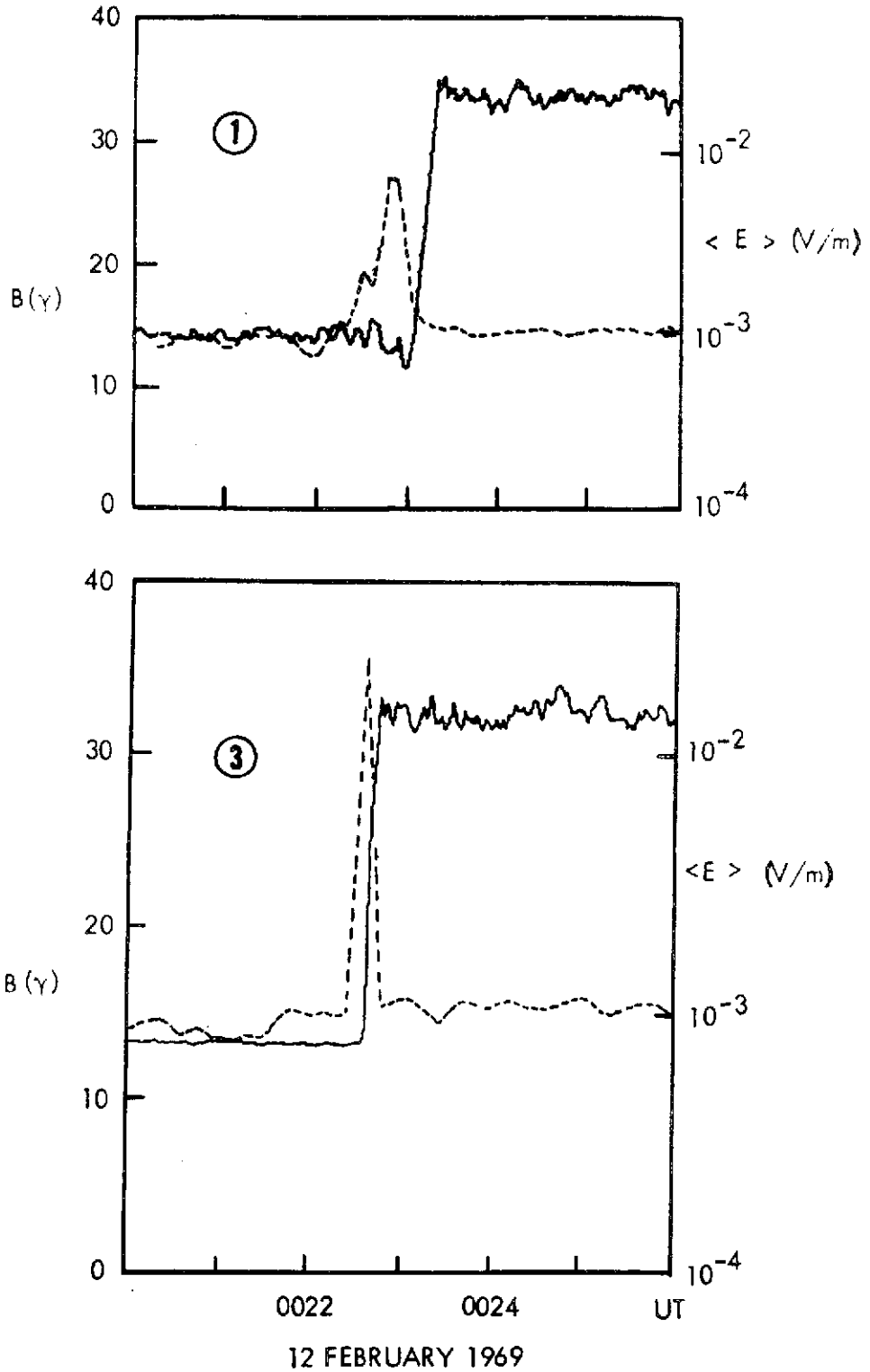

Figure 3. Two profiles of the laminar shock at a resolution of 1.15 sec/sample, with differing field-normal angle θ_{nB}. At $\theta_{nB} \approx 65°$, upper panel, the shock exhibits damped precursor oscillations, with a correspondingly broadened region of plasma wave noise (dashed curve). At $\theta_{nB} \approx 78°$, the waves vanish and the electric noise is narrowed to the shock ramp.

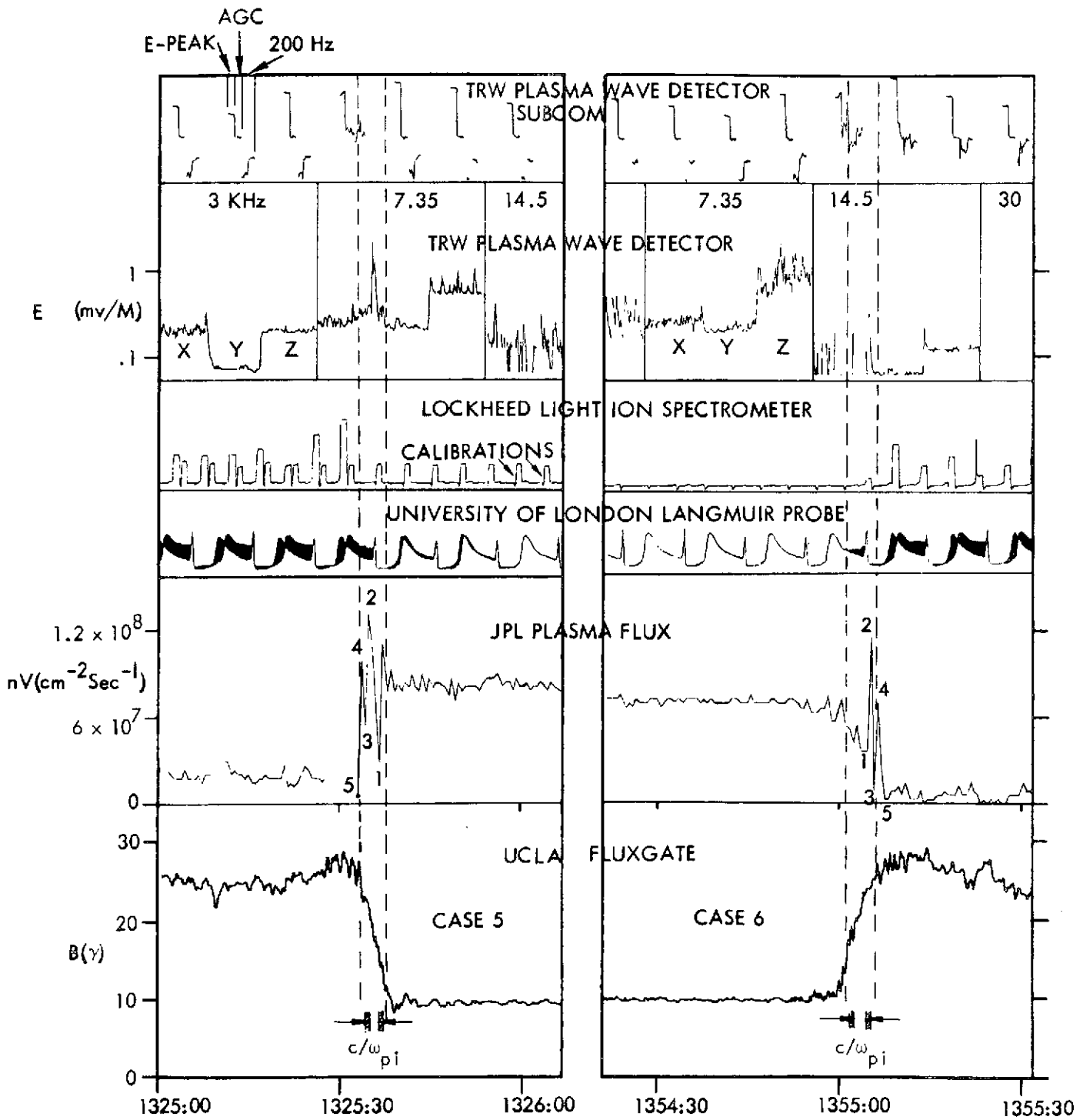

Figure 4. Multi-diagnostic view of the high-resolution crossings.

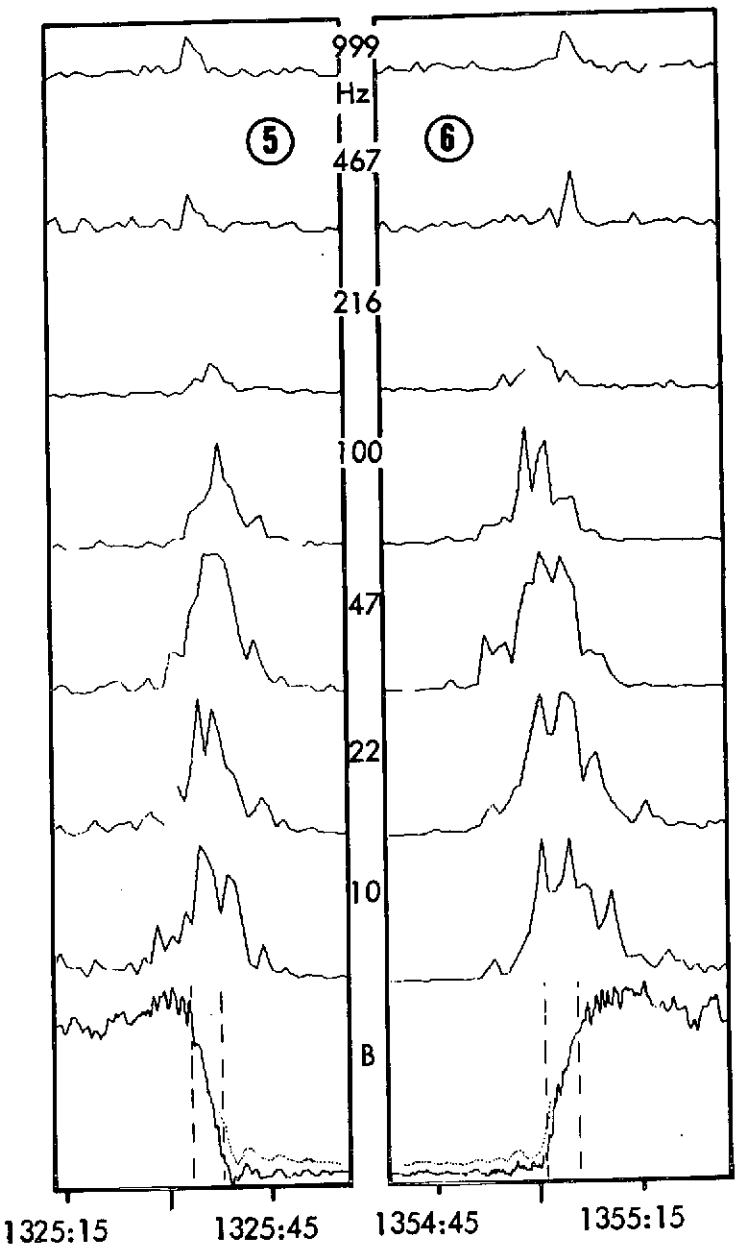

Figure 5. Multi-channel view of the high-resolution crossings as recorded by the X-axis loop of the $\dot{B}$ ELF search coils.

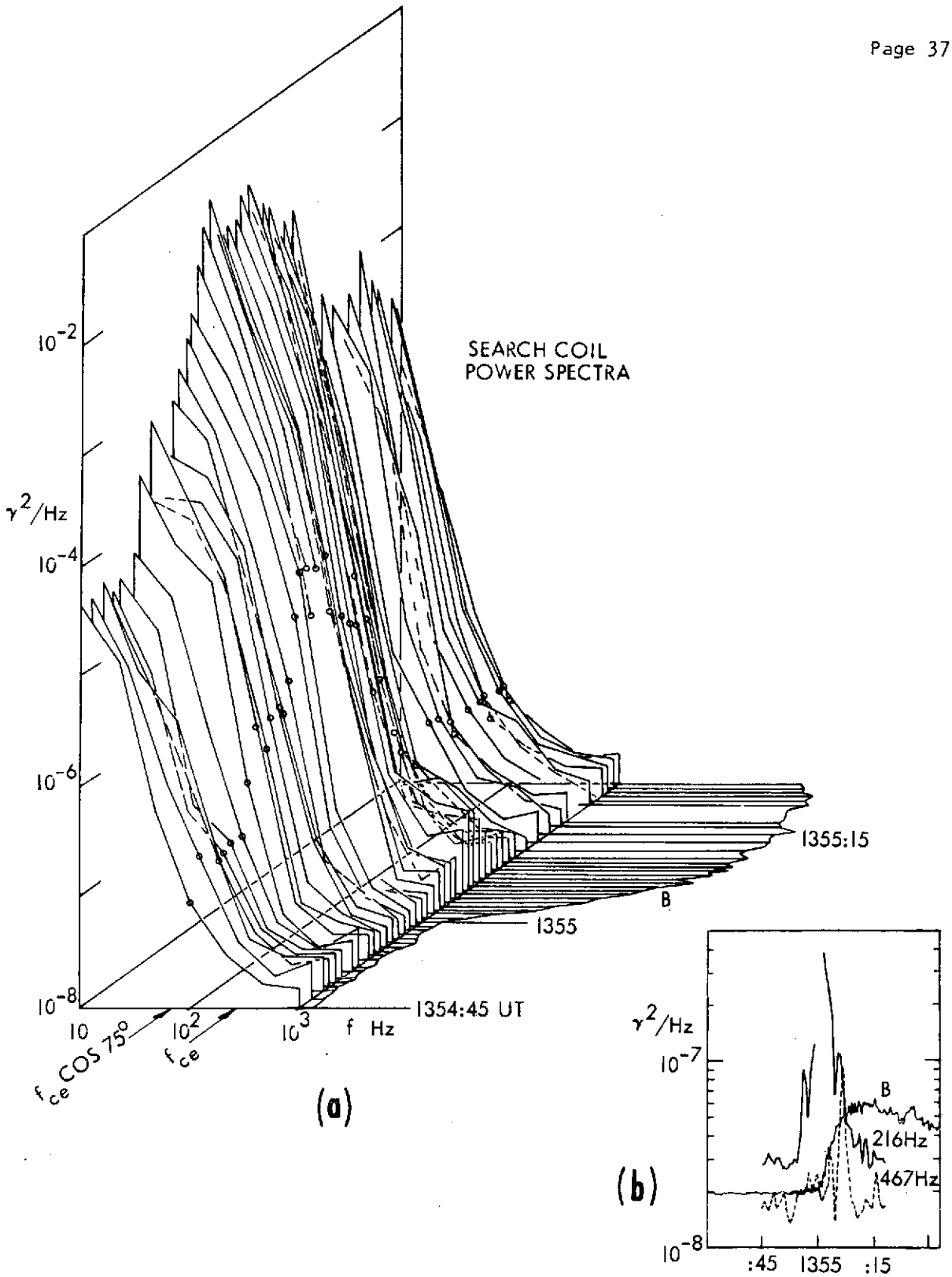

Figure 6. (a) ELF power spectra accompanying the high-resolution crossing of 1355 UT. (b) Behavior of the ELF 216 Hz channel, below, and the 467 Hz channel, above, f_{ce} in the solar wind as the ramp was crossed.

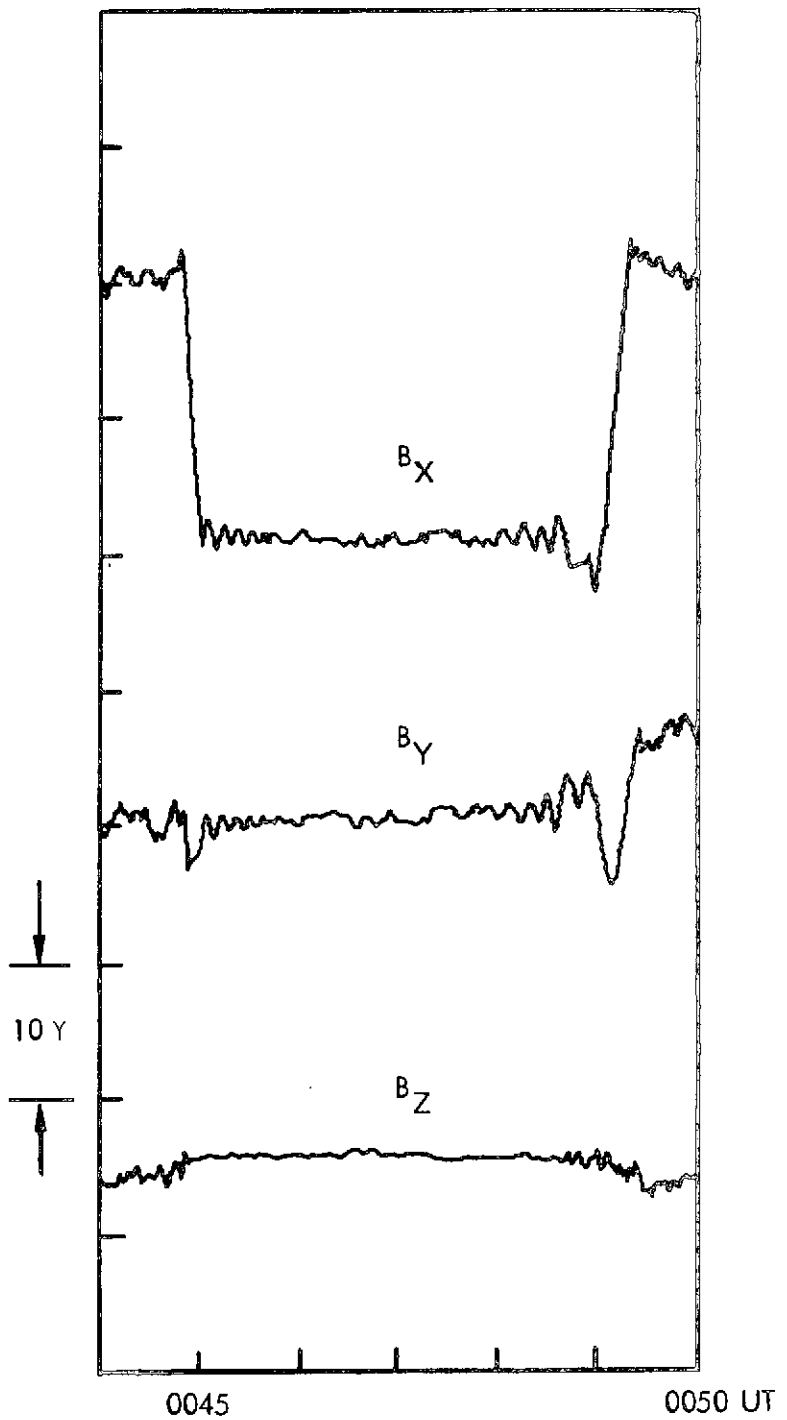

Figure 7. A pair of adjacent shock crossings showing stationary upstream wave structure.

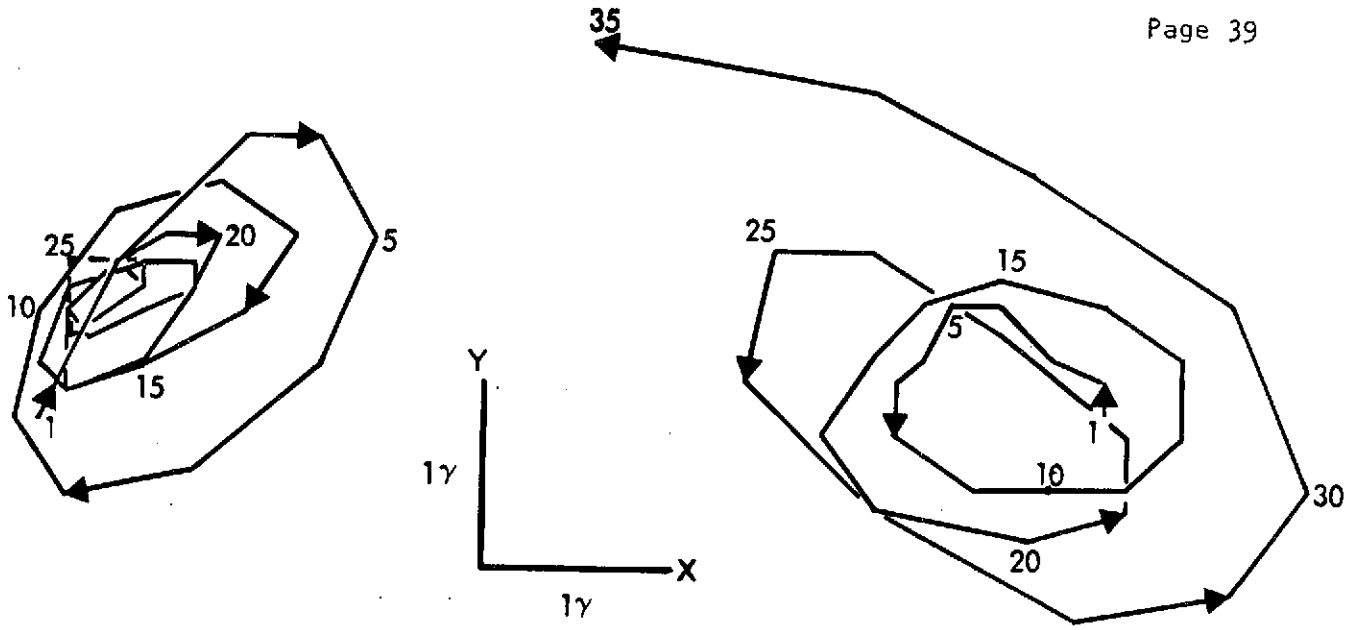

0044:50-0045:43

0047:48.5-0048:27.7

(a)

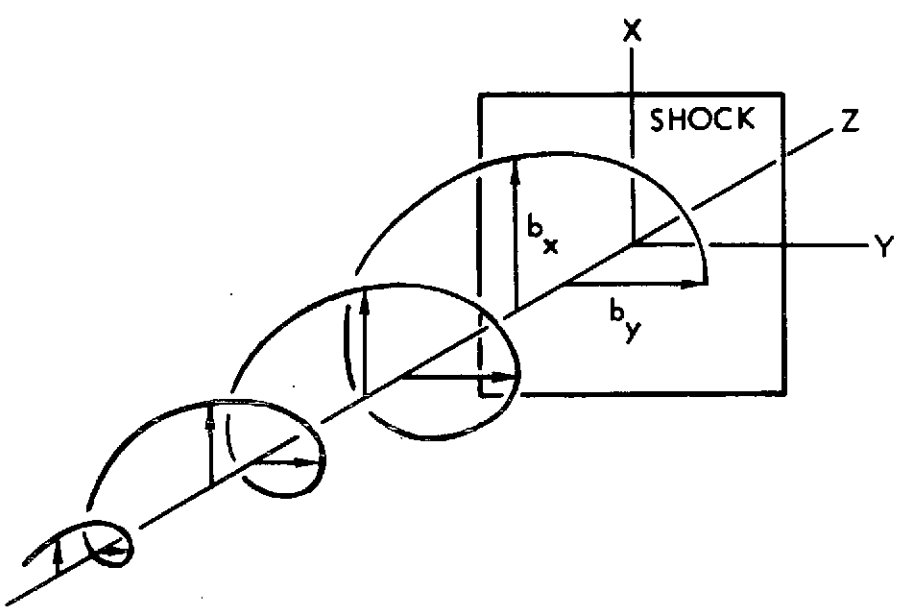

(b)

Figure 8. Whistler polarization characteristics of the stationary precursors of Figure 7; (a) individual polar diagrams of the perturbation vectors in an approximate shock plane; (b) conceptualization of the common whistler-wave polarization of the two precursors along the approximate shock normal. The average upstream field is about 25° from the shock plane, with its sensor inward.

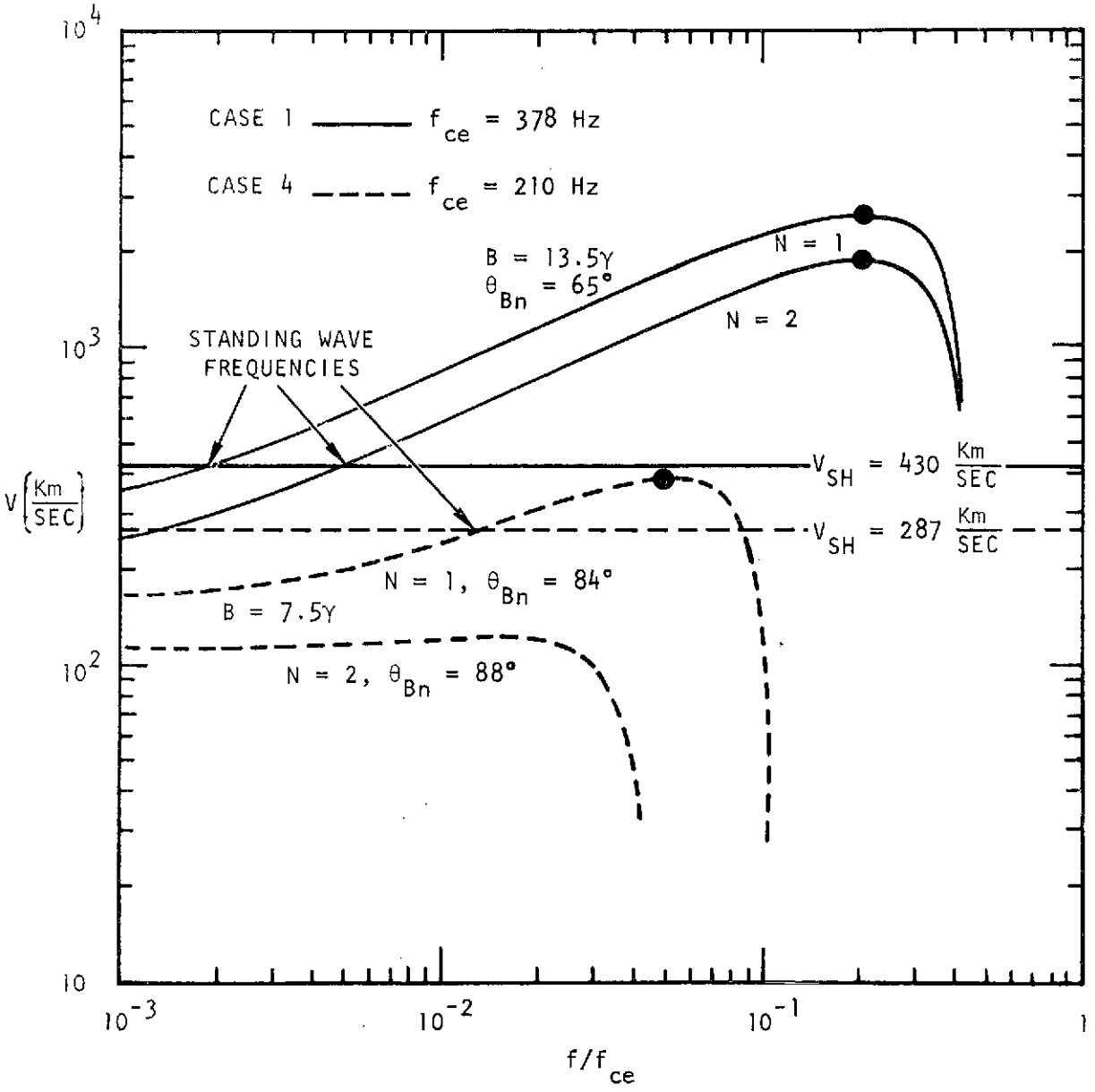

Figure 9. Phase velocity vs frequency for the whistler mode (Appleton-Hartree cold-plasma approximation) in the solar wind in cases 1 (solid curves) and 4 (dashed curves).

APPENDIX 1

WHISTLER PHASE AND GROUP VELOCITIES

The curves in Figure 8 of the text are based on the Appleton-Hartree, quasi-longitudinal dispersion relation for cold plasma, justified here by the low β_i, laminar conditions that prevailed for these observations. We refer particularly to the QL-R expression of equation (50) of Stix (1962, p 40), with the factors 1 and ω_{pi} neglected, so $\alpha = \omega_{pe}^2/\omega^2$ and

$$n^2 = \frac{k^2c^2}{\omega^2} = \frac{c^2}{u_n^2} = \frac{-\omega_{pe}^2}{\omega(\omega-\omega_{ce}\cos\theta_{nB})} = \frac{-f_{pe}^2}{f(f-f_{ce}\cos\theta_{nB})} \quad .$$

As the notation indicates, we are interested in phase velocity u_n upstream along the local shock normal at angle θ_{nB} to the interplanetary field. For any angle θ to $\underset{\sim}{B}$ the group velocity vector $\underset{\sim}{u}_g$ is given by $\underset{\sim}{u}_g \equiv \frac{d\omega}{d\underset{\sim}{k}} = \underset{\sim}{k}\frac{\partial\omega}{\partial k} + \underset{\sim}{\theta}\frac{1}{k}\frac{\partial\omega}{\partial\theta}$, but along $\underset{\sim}{n} = \underset{\sim}{k}$, $u_{gn} \equiv \underset{\sim}{u}_g \cdot \underset{\sim}{n} = \underset{\sim}{u}_g \cdot \underset{\sim}{k} = \frac{\partial\omega}{\partial k}$. When evaluated algebraically from the expression given above for $u_n \equiv \frac{\omega}{k}$, $u_{gn} = -2\,u_n \frac{f_{pe}^2 u_n}{c^2k^2f_{ce}\cos\theta_{nB}}$. Elimination of $k(= 2\pi f/u_n)$ and some algebraic excercise ultimately yield

$$u_{gn} = 2\,u_n\,(1 - f/f_{ce}\cos\theta_{nB}) \ ,$$

hence $u_{gn}/u_n > 1$ when $f < \frac{1}{2} f_{ce}\cos\theta_{nB}$, i.e., whistler mode waves can advance upstream along n only for frequencies less than half the electron cutoff frequency in the normal direction.

APPENDIX II

BOW SHOCK VELOCITY DERIVED FROM STANDING WHISTLER WAVELENGTH

For laminar, oblique shocks, the wavelength λ_d, or L_d, of the whistler wave standing upstream in the unshocked plasma is given by the formula

$$L_d = \frac{2\pi \cos \theta_{Bn}}{\sqrt{M_A^2 - 1}} \frac{c}{\omega_{pi}}, \tag{1}$$

where L_d is measured along the shock normal (Morton, 1964). If V_{SS} is the shock speed in the spacecraft frame, the apparent period of the standing wave as it moves with the shock along the shock normal is

$$T_d = L_d / V_{SS} . \tag{2}$$

If spacecraft motion, seldom more than about 1 Km/sec along the bow shock normal, is neglected, then the local velocity V_{SH} of the shock with respect to the ambient plasma is

$$V_{SH} = V_{SW} \cos \theta_{vn} + V_{SS}, \tag{3}$$

where θ_{vn} is the angle between the local normal and solar velocity V_{SW}, and V_{SS} is defined as positive outward from the earth, i.e., positive when it increases the velocity of the shock relative to the solar wind. The local Alfvén mach number is given by

$$M_A = V_{SH} / C_A,$$

where C_A is the upstream Alfvén velocity. Combination of all the above expressions yields the 4th degree equation in V_{SS},

$$V_{SS}^4 + (2V_{SW}\cos\theta_{vn})V_{SS}^3 + (V_{SW}^2\cos^2\theta_{vn} - C_A^2)V_{SS}^2 - \left(\frac{2\pi C_A \cos\theta_{nB}}{T_d}\frac{c}{\omega_{pi}}\right)^2 = 0 \quad (4)$$

This equation may have more than one real root, necessitating some independent criterion for selecting the one most probably correct. The measurements necessary to obtain V_{SS} are $\underset{\sim}{B}_{SW}$ (for B and θ_{Bn}), N_{SW}, and V_{SW}, all upstream. In addition, a local normal $\underset{\sim}{n}$ must be estimated from a model shock surface to obtain θ_{nB}.

TRW

TRW #21333.000
1780.4.74.14-185
1 July 1974

NASA Headquarters
Attn: Director, Physics &
Astronomy Programs
Code SG
Washington, D. C. 20546

Subject: Contract NASW-2398
Final Report

Provided herewith are thirty copies of the Final Report, "Study of the Relation Between Pc 3 Micropulsations and Magnetosheath Fluctuations and for the Multisatellite Multimeasurement Investigation of Earth's Bow Shock." This report is submitted in accordance with Article IX of the subject contract.

TRW INC.

W. H. Simmons
Contracts Manager for Science and
Applications Satellite Systems
Space Vehicles Division
TRW Systems Group

WHS:slg

Encl: as stated

cc: NASA Scientific & Technical Information Facility (1 repro + 2 cys)
NASA Headquarters, New Technology Rep (1 cy)
NASA Headquarters, Contracts Administration